From Transcription to Tubulogenesis: Insights from the *Drosophila* Ovary

Nathaniel Clement Peters

A dissertation submitted in partial fulfillment of the requirements for the degree of

Doctor of Philosophy

University of Washington

2015

Reading Committee:

Celeste A. Berg, Chair

David W. Raible

Barbara T. Wakimoto

Program Authorized to Offer Degree:

Molecular and Cellular Biology

University of Washington
Graduate School

University of Washington

Abstract

From Transcription to Tubulogenesis:

Insights from the *Drosophila* Ovary

Nathaniel Clement Peters

Chair of the Supervisory Committee:

Dr. Celeste A. Berg, Professor

Department of Genome Sciences

During *Drosophila melanogaster* oogenesis, subsets of the epithelial cells that surround each developing egg chamber undergo morphogenesis to form epithelial tubes, and the lumens of these tubes serve as molds for the dorsal appendage (DA) filaments of the mature eggshell. This process is a simple and tractable system for identifying and characterizing the cellular events and molecular mechanisms required for epithelial tube morphogenesis, or tubulogenesis. The work presented in this dissertation provides insight both into the upstream gene regulatory elements that set the stage and maintain control, and into the downstream molecular effectors that govern cell shape, order, and movement, throughout DA tubulogenesis. In Chapter I, I highlight the fundamental importance of cellular tubes and the intimate relationship between tube morphology and function, explain what we do and do not know about the cellular and molecular mechanisms

that drive tubulogenesis, provide a detailed description of the process of DA tubulogenesis, and emphasize the advantages of DA tubulogenesis as a model for epithelial tubulogenesis. In Chapter II, I establish regulatory links, specifically in regard to DA tubulogenesis, between upstream transcription factors, such as Tramtrack69 and Mirror, and downstream effectors, such as Paxillin and Dynamin. In Chapter III, I focus specifically on the role of Dynamin and Dynamin-mediated endocytosis in DA tubulogenesis. I identify and characterize novel roles for Dynamin in epithelial tube closure, cell intercalation, and biased apical-luminal expansion. Furthermore, I provide evidence that Dynamin is regulating the levels and behavior of both E-Cadherin and Integrin-based cellular adhesions, and propose that Dynamin facilitates the aforementioned cellular, tubulogenic processes by regulating the turnover of cellular adhesions. Finally, in Chapter IV, I summarize the results of my graduate research, discuss how these results fit with and augment our current knowledge of epithelial tubulogenesis, and propose future experiments that would further delve into the specific roles and mechanisms by which conserved, downstream, tubulogenic effectors, such as Dynamin and Paxillin, drive epithelial tubulogenesis.

Table of Contents

List of Figures

Figure:

List of Tables

Table:

Acknowledgements

I would like to thank: Rob Hall and Kurt Hardesty at the UW Center for Array Technologies for help with microarrays and analysis, Brigham Meecham for additional analysis, Greg Martin at the UW Keck Microscopy Center for frequent and fruitful imaging discussions, Sandra Zimmerman for protocol optimization and statistical consultation, Faith Hassinger for construct analysis, Robert Matlock for egg-processing, Kelsey Kaeding for *in situ* contributions, and Kamsi Odinammadu for performing *br[69B08]-GAL4* and *A90-GAL4* experiments.

I would like to acknowledge funding sources that supported this research: NIH R01-GM079433, UW Provost Bridge Funds, NSF Graduate Research Fellowship DGE-0718124.

I would like to thank Anne Sustar, Dan Kiehart, David Bilder, Denise Montell, Hannele Ruohola-Baker, Gabrielle Boulianne, Helen McNeil, Kendall Broadie, Leo Pallanck, Mani Ramaswami, Miriam Osterfield, Sally Horne-Badinovac, Stanislav Shvarstman, Stefano De Renzis, Steven Hou, Susan Parkhurst, Trudi Schüpbach, the Bloomington Stock Center, the Developmental Studies Hybridoma Bank, NIG-Fly (Kyoto), and the Vienna *Drosophila* Resourch Center for fly strains and reagents.

I would like to thank my PI, Dr. Celeste Berg, for her continual support, patience, and guidance over the years. I would also like to thank all past and present members of the Berg lab.

I would like to thank past and present members of the MCB Program Staff, including David Raible, Michael Emerman, MaryEllin Robinson, Terry Duffey, Diane Darling, Milli Morris, Michele Karantsavelos, Maia Low, Nomi Odano, and Maria Sanders.

Finally, I would like to thank my friends and family for their continual support. In particular, I would like to thank my fiancé, Anna Sczaniecka, for being the best and most honest companion I could ever have hoped for.

I would like to dedicate this dissertation to my grandparents:

Robert and June Peters

Clifford and Prudence Bedell

All that is gold does not glitter,

Not all those who wander are lost

-J.R.R. Tolkien

It seems to me that the natural world is the greatest source of excitement; the greatest source of visual beauty; the greatest source of intellectual interest. It is the greatest source of so much in life that makes life worth living.

-Sir David Attenborough

Chapter I
Introduction

The fundamental importance of tubes

Could multicellular life exist in the absence of tubes? The answer, perhaps indisputably, is no. Even the simplest of known metazoans (*i.e.,* animals), the four-celled *Tetrabaena socialis*, requires cytoplasmic, tubular bridges between cells to exist as an integrated, multicellular organism (Arakaki *et al*., 2013). In complex metazoans, tubes do exist within single cells, but tubes are more often multicellular structures that serve key roles in embryonic development and as the infrastructure for mature organs and tissues.

To illustrate the critical importance of tubes during embryogenesis, I proffer the examples of metazoan gastrulation and vertebrate neurulation. Gastrulation (Greek: *gaster* – gut) is one of the earliest coordinated, multicellular processes in metazoan development, and its purpose is to specify and separate the three primary germ layers (*e.g.,* endoderm, mesoderm, and ectoderm) and, as its name implies, form a gut. By orienting with respect to previously specified embryonic axes (*e.g.,* **A**nterior-**P**osterior, **D**orsal-**V**entral, **L**eft-**R**ight), and by employing 4 evolutionarily conserved cell movements (*e.g.,* emboly, epiboly, convergence, and extension), gastrulation is able to transform a relatively amorphous ball or sheet of cells into a basic, asymmetric body plan with an internalized, tubular gut, or tissues that will give rise to the gut (Stern 2004; Solnica-Krezel and Sepich, 2012). Lewis Wolpert aptly articulated the importance of gastrulation when he stated, "It is not birth, marriage, or death, but gastrulation which is truly the most important time in your life" (Lewis Wolpert, 1986). Since the cell movements of gastrulation either directly create, or allow the subsequent creation of, a tubular gut, I would take

Wolpert's words one step further and argue that the most important thing we do in life is make a tube.

A classic example of the intimate relationship between gastrulation and tubes is the process of sea urchin gastrulation, which includes the internalization (*i.e*., emboly) of mesoderm and the invagination, extension, and fusion of an endodermal, epithelial tube called the archenteron, which subsequently becomes the gut (Fig 1.1; reviewed in Kominami and Takata, 2004). *Drosophila* gastrulation also includes invagination, but of a mesoderm-based, transient epithelial tube called the ventral furrow that runs along the ventral midline of the embryo. The endoderm is internalized separately in a process called posterior midgut invagination (Sweeton *et al.,* 1991). Though the ventral furrow tube is transient, an end-on, transverse view of a mid-gastrulation *Drosophila* embryo closely resembles a mid-gastrulation sea urchin embryo in morphology (middle image in Fig 1.1; Solnica-Krezel and Sepich, 2012). In vertebrates, the principles of mesoderm and endoderm internalization during gastrulation are conserved, but they accomplish this internalization through involution movements (*e.g*., *Xenopus*), ingression movements (*e.g*., chick, mouse), or combinations of both (*e.g*., zebrafish; Solnica-Krezel and Sepich, 2012). These movements do not directly form tubes, but they do involve the internalization of endoderm to eventually form a gut, and as we can all appreciate, the gut is one of the most important of metazoan tubes.

Vertebrate neurulation is another exquisite example of the integral role that tubes play during embryonic development. Neurulation is the first step in developing a vertebrate central nervous system, and invariably results in the formation of an epithelial neural tube (Fig 1.2). This tube then serves as the precursor for the brain and spinal cord of the adult organism. Although the morphogenetic movements, cellular behaviors, and molecular mechanisms that

Figure 1.1. Sea urchin gastrulation

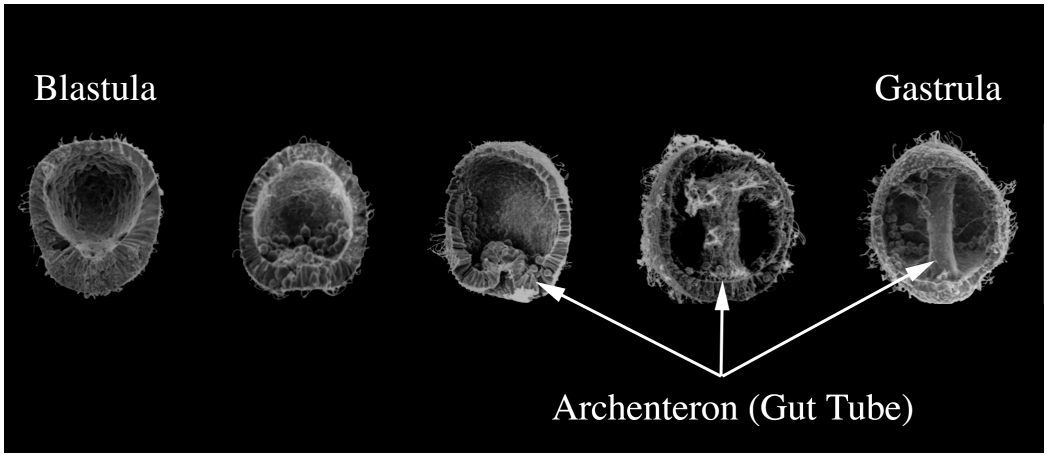

Fig 1.1. In sea urchin, gastrulation involves internalization of skeletal mesoderm and gut-forming endoderm, leaving the ectoderm to cover the outer surface. First (left diagram), at the vegetal pole (bottom) of the blastula, the vegetal plate, containing the presumptive mesoderm and endoderm, thickens. Second (left of center diagram), the mesoderm cells undergo an epithelial to mesenchymal transition (EMT), move inside the blastula, and become the primary mesenchyme. The vegetal endoderm initiates apical constriction and begins to invaginate, or bend inward. Third (center diagram), accompanying the invagination of the endoderm, secondary mesenchyme cells appear at the tip of the invaginating tube, now called the archenteron, and begin to send long filopodia towards the animal pole (top). Fourth (right of center diagram), the archenteron reaches its terminal length, turns, and contacts the ectoderm. Finally (right diagram), a completed gastrula forms when the archenteron fuses with the ectoderm and opens to form the mouth of the gut, with the anus at the original site of invagination. Mesenchymal cells secrete the larval skeleton, and further differentiation eventually produces a pluteus larva. This image was adapted Wolpert *et al.,* 2010).

drive neurulation vary widely across vertebrates (Fig 1.2), a fact that raises questions about which models are best for comparison to humans, the product of vertebrate neurulation is most certainly an epithelial tube (Harrington *et al.,* 2009). In humans, gross defects in neurulation result in embryonic lethality, but even minor errors in neural tube closure can lead to neural tube birth defects such as spina bifida. These defects are commonly detected with an estimated 0.5-2/1000 pregnancies worldwide (Greene and Copp, 2009). By identifying and characterizing the cellular and molecular mechanisms needed for neural tube closure, it may be possible to develop better tools and practices for assessing risk of, preventing, or even treating, neural tube defects in humans.

In later stages of embryonic, larval, and adult development, when tubes attain their terminal morphologies (*i.e.,* shapes), they can effectuate a multitude of essential functions. If one takes a moment to think about all the various functional tubes in one's own body, one will appreciate how much one's life depends on tubes. Not only is this diversity of metazoan terminal tube morphologies tremendous, but this diversity is essential for specific functions in the vascular, respiratory, digestive, excretory, and reproductive systems, essentially allowing organisms to live and reproduce.

Tubes vary in whether they are formed within cells or by sheets of cells. The smallest of tubes may form within single cells (*e.g*., the smallest capillary tubes of vertebrate vasculature (Kamei *et al.,* 2006; Lenard *et al.,* 2013), the excretory system of *C. elegans* (Buechner 2002); the terminal tracheal tip cells in *Drosophila* (JayaNandanan *et al.,* 2014)). Most multicellular tubes are epithelial in origin, meaning that they form from sheets of cells, and so they are referred to as epithelial tubes. Other multicellular tubes do not form from epithelia, but they require the core features of epithelia (*i.e.,* polarity and adhesion), and they establish these

Figure 1.2. Examples of different modes of vertebrate neurulation

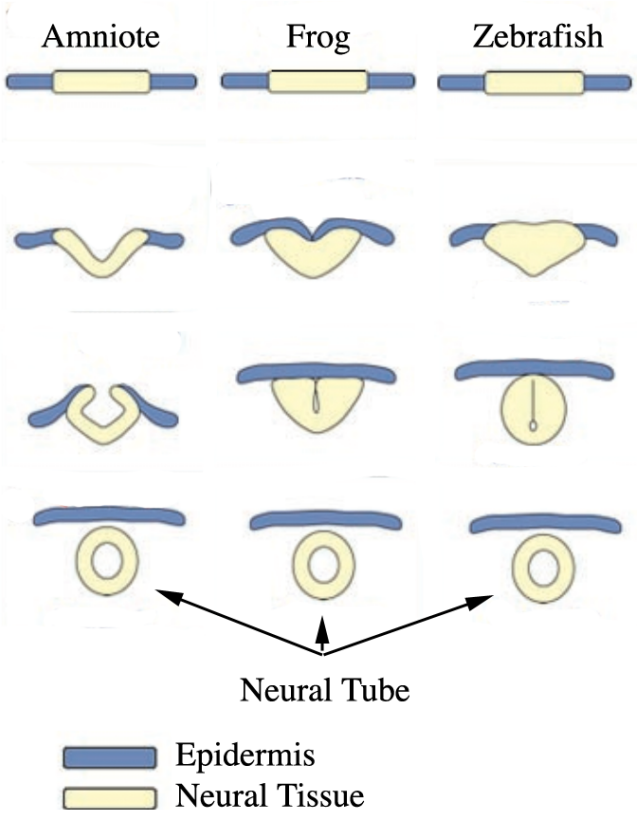

Fig 1.2. There is significant morphological variation in vertebrate neurulation, but the product of neurulation is a morphologically and functionally similar neural tube. Primary amniote neurulation (left) involves the invagination of an existing neural plate to form a neural groove. Wrapping movements then create neural folds and bring together adjacent, non-neural ectoderm from each side to fuse. *Xenopus* (Frog) neurulation (middle) morphologically resembles amniote primary neurulation (*i.e.*, folding of a pre-existing neural plate). Zebrafish neurulation (right) involves a pre-existing neural plate, but has features of amniote secondary neurulation: no obvious neural groove or folds, neural tube hollowed by cavitation. (Adapted from Harrington *et al.,* 2009).

features during tube lumen formation. Though there is great diversity in tube morphology across metazoans, the cellular mechanisms and behaviors used to create these morphologies during development are relatively few and highly conserved. Thus, the goal for tubular developmental biologists now is to understand the genetic and molecular mechanisms that underlie these cellular mechanisms and behaviors.

In the following sections of the Introduction, I will provide background on epithelia and epithelial tubes and discuss the features of epithelia that are important for tube function. Then I will explain the concept of morphogenesis (Greek: *morpho* – shape, *genesis* – beginning) during development and outline what we currently know about the cellular, genetic, and molecular mechanisms that underlie tube morphogenesis, or tubulogenesis (*i.e.,* the creation of tubes). Finally, I will discuss the contributions that my own graduate research makes to the field of developmental tubulogenesis.

The epithelium

The **epithelium** is one of the most ancient and fundamentally important structures for multicellular life and is essential for organizing and supporting a multicellular body plan. The structure first arose in the most primitive, Precambrian metazoans ~600 million years ago (Nelson, 2009). The meaning of the word "epithelium" is somewhat odd, because it literally means "above the nipple" (Latin: *epi* – above; Greek: *thele* – nipple), but when the word was first coined in the 18th century, it was simply meant to refer to the skin, or everything on the outside of the body that was in addition to the nipple. In its modern use, the word epithelium does not just refer to skin, but refers to a sheet of cells that possesses two key properties: **polarity** and **adhesion** (Andrew and Ewald, 2010). In terms of polarity, this means that the

individual cells of a sheet have asymmetric molecular and morphological properties, so that the sheet of cells is different on one side than the other, or is different across the plane of the epithelium. When considering one face of the sheet versus the other, one face is referred to as "**apical**," which is defined within individual cells by the **apical junctional complex (AJC)**, and which is the primary site of secretion, exchange with the outer environment, and cell-cell adhesion. The specialized, molecular adhesions and junctions of the AJC separate the apical membrane from the rest of the membrane and allow epithelial cells to both communicate and exchange with one another and with the external environment and to act as a functional sheet or barrier. The other face of the sheet, referred to as "**basal**," contacts and adheres to an extracellular matrix (ECM, also known as basal lamina) and regulates interactions with the internal environment (Fig 1.3; Nelson, 2009; Fig 1.4; Andrew and Ewald, 2010; St. Johnston and Ahringer, 2010; Rozario and DeSimone, 2010; Guillot and Lecuit, 2013). In addition to apico-basal polarity, epithelia often possess polarity across the plane of the epithelium. This polarity is controlled by either the overall **AP/DV polarity** of the sheet, and in many cases, is regulated by the conserved **Frizzled/planar cell polarity (PCP) pathway** (Zallen, 2007). Together, the features of cell polarity and cell adhesion allow epithelial cells to function as a polarized, uniform sheet.

One of the primary functions of a polarized epithelium is to act as a selective barrier. In the earliest and simplest metazoans, epithelia served primarily to separate the outside environment from the inside of the organism. As metazoans became more complex and developed different tissues and organs, they used epithelia to form selective boundaries between and within these structures, and they evolved many different types of epithelia for different functions (Fig 1.4; Andrew and Ewald, 2010). Polarized epithelia allow for the regulated

Figure 1.3 Functional and structural organization of polarized epithelial cells.

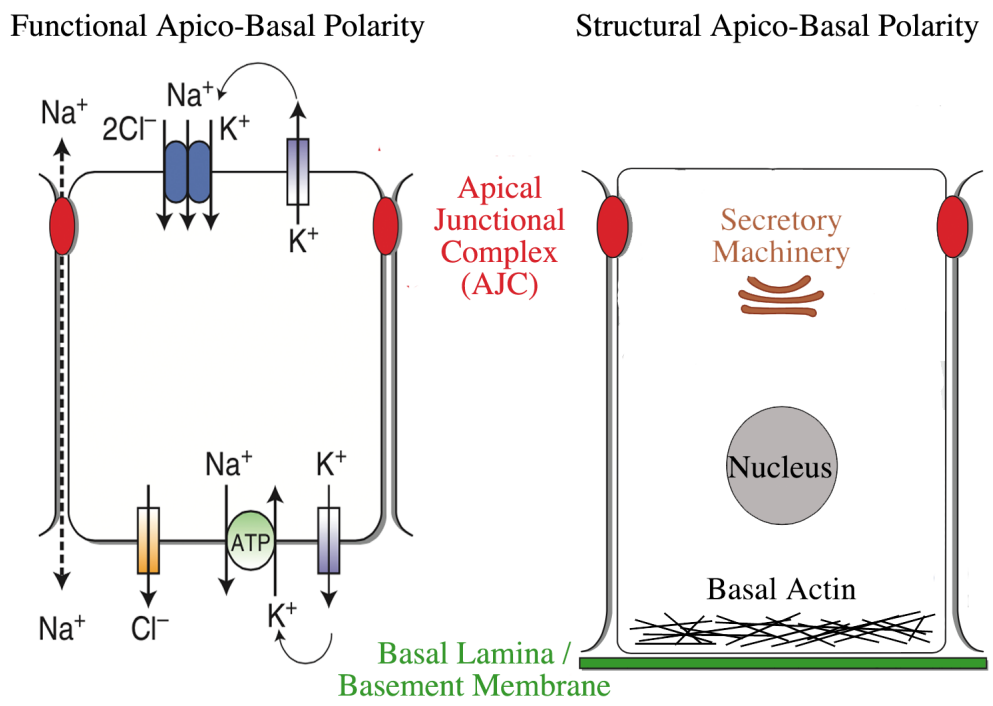

Fig 1.3. (**A**) Functionally, apico-basal polarity allows for selective, polarized distribution of ion channels and pumps within the membrane. In this example, portraying conserved function between mammalian kidney tubules and crab gill cuticles,, a polarized channels create a sodium-potassium gradient to provide energy for regulated transport of other ions and solutes across the epithelium. (**B**) Structurally, apico-basal polarity organizes distinct plasma membrane domains, the apical junctional complex (AJC), the centrosome/basal body, the microtubule cytoskeleton and primary cilium, the Golgi-based secretory pathway, and even the nucleus. (Adapted from Nelson, 2009).

Figure 1.4 General features of polarized epithelial cells and the morphological diversity of epithelia.

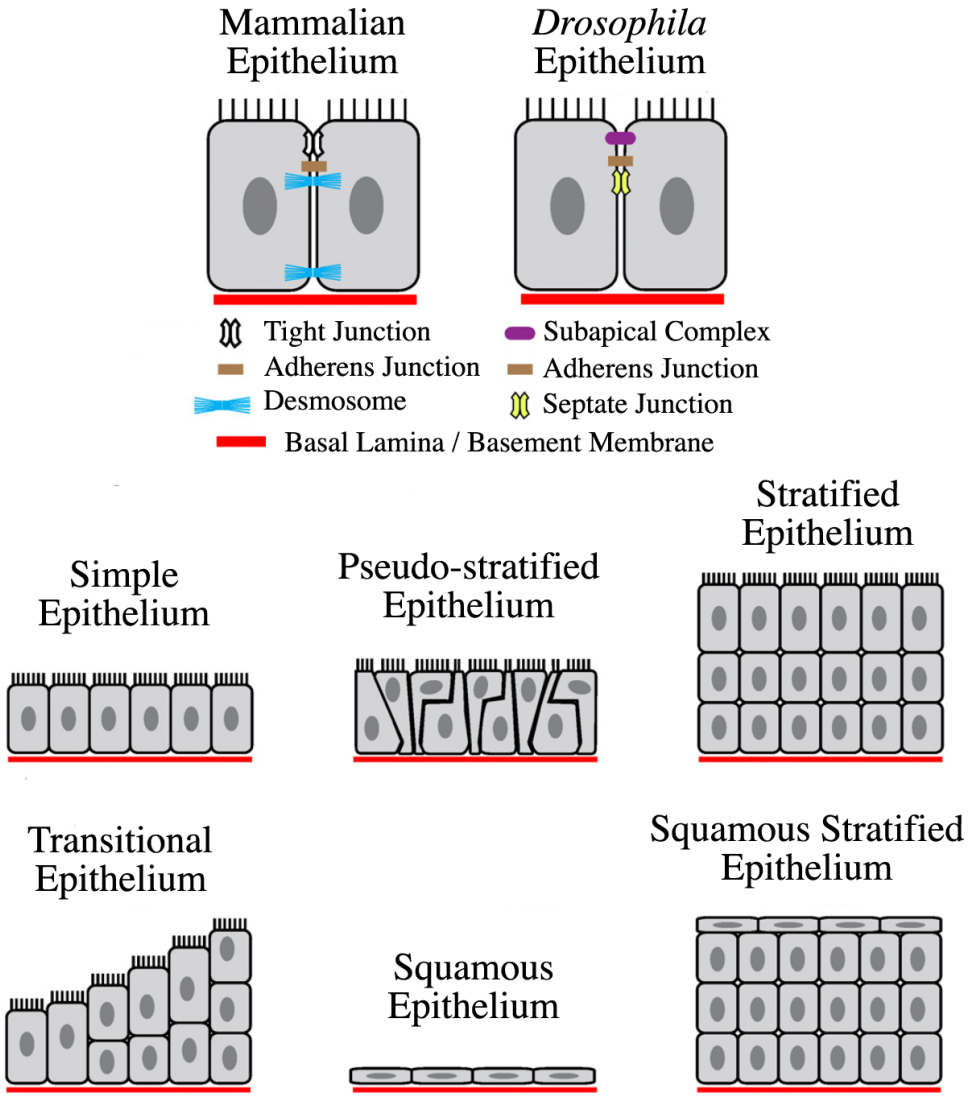

Fig 1.4. Epithelial cells possess apico-basal polarity, and differentially localized adhesive (red, brown) and junctional (blue, yellow, magenta) complexes. Many types of epithelia have evolved for specific functions, including single-cell-layered epithelia and stacked epithelia, but the general features of polarity and adhesion are maintained. (Adapted from Andrew and Ewald, 2010).

exchange of nutrients and wastes, both within internal compartments and with the external environment. Within epithelial cells, polarized distribution of membrane-associated ion channels and pumps lets cells regulate the movement of ions and solutes and allows for the creation of gradients across the epithelium (Fig 1.3; Nelson, 2009). To establish these distinct apical and basolateral surfaces, there is polarized sorting and retention of membrane proteins to apical and basolateral domains using the exocytic pathway, the endocytic pathway, the microtubule network, and the AJCs (Fig 1.3; Nelson, 2009). Despite obvious morphological and practical differences that exist between metazoan epithelia, the core features that have been highly evolutionarily conserved include: apico-basal polarity, cell-cell/cell-matrix adhesion, and the functional properties that they afford.

Epithelial adhesion

Cell-cell adhesion in epithelial cells is mediated by a number of adhesive complexes that compose the AJC. The AJC is mainly composed of the cadherin-based **adherens junctions (AJs)**, which are the primary cell-cell adhesion complexes and interact with the actin cytoskeleton, and the **tight junctions (TJs; in *Drosophila,* septate junctions (SJs))**, which hold adjacent cell membranes close enough to effectively seal the epithelium and keep "inside" in and "outside" out. These junctions also act as a molecular fence to prevent the apico-basal diffusion of membrane-associated proteins. In vertebrates, the TJ is more apical to the AJ, and there is sometimes a more basal, cadherin-based adhesive complex called the desmosome that is not found in all epithelia, is particularly strong, and interacts with intermediate filaments. In *Drosophila*, the AJ is more apical than the SJ, and there are no desmosomes, but the overall

functions and interactions of the AJs and SJs are similar to their counterparts in vertebrates (Nelson, 2009; Fig 1.4; Andrew and Ewald, 2010; Oda and Takeichi, 2011).

Of the cell-cell adhesion complexes, the AJ is the most evolutionarily conserved junctional complex, can be a stable or transient structure, and is considered to be the universal adhesive complex for metazoans (Fig 1.4; Andrew and Ewald, 2010). The primary adhesive components of AJs are classical cadherins (Ca^{2+}-dependent adhesion proteins) such as E-Cadherin, which are transmembrane, homophilic, adhesion molecules. These cadherins possess long, extracellular cadherin tails that adhere to similar extracellular cadherin tails presented by adjacent cells. Their intracellular domains bind to p120-catenin, which stabilizes the cadherin molecule in the membrane, and β-catenin (Armadillo in *Drosophila*), which associates with the actin cytoskeleton through the adaptor α-catenin. The superfamily of cadherins, which contain both classical and non-classical cadherins, are capable of both homophilic and heterophilic interactions, and facilitate both adhesion and signaling (Oda and Takeichi, 2011).

The TJ, or SJ in *Drosophila*, is the most important junctional complex for maintaining the barrier function of an epithelium, and selectively regulates ion passage between neighboring cells (Anderson and Itallie, 2009; Fig 1.4; Andrew and Ewald, 2010). This complex completely encircles epithelial cells and is the most complicated of the cell-cell adhesion complexes, containing over 40 proteins. The defining feature of the complex is the presence of transmembrane, claudin-family proteins (Latin: *claudere* – to close). Other important proteins in TJs include occludin, tricellulin, and the cytoplasmic plaque proteins ZO-1, ZO-2, and ZO-3, which contain PDZ (PSD-95, Discs large, ZO-1) domains for protein-protein interactions, and are of the MAGUK (Membrane-Associated GUanylate Kinase) family (Furuse, 2010). Aside

from sealing the epithelium and regulating ion passage, in *Drosophila* the SJs regulate epithelial tube size in the larval trachea (Paul *et al.,* 2003; Wu and Beitel, 2004; Nelson *et al.,* 2010).

Desmosomes are not found in all epithelia but are the strongest of the cell-cell adhesions that assemble in distinct locations (not circumferential bands like the TJs), and they effectively "rivet" neighboring cells together (Fig 1.4; Andrew and Ewald, 2010). These cadherin-based adhesions link to strong, keratin-based intermediate filaments (not present in *Drosophila*) within epithelial cells, and are found in tissues that are subject to intense mechanical stress, such as the epidermis and myocardium. Desmosomes can switch between high and low adhesive states to facilitate morphogenesis and wound healing, in a protein kinase C-dependent manner (Garrod and Chidgey, 2007; Delva *et al.,* 2009).

In addition to cell-cell adhesions, epithelial cells also form and regulate basal cell-ECM adhesions. These adhesions are particularly important for the movement, or migration, of epithelial cells. The most well characterized cell-ECM adhesions are **integrin-based adhesions**, and consist of transmembrane α-β integrin heterodimers, which link the ECM to a complex of intracellular proteins that associate with the actin cytoskeleton and relay signals to and from the ECM. These complexes are called focal adhesions, and they contain a multitude of proteins including actin-associated proteins (*e.g.,* talin, vinculin, α-actinin, and zyxin) and signaling/adaptor proteins (*e.g.,* Src, focal adhesion kinase (FAK), paxillin, and integrin-linked kinase (Ilk). These focal adhesions dynamically form and turn over during cell migration, providing physical traction with the ECM and migratory signaling (Huttenlocher and Horwitz, 2011). Integrin-based adhesions are some of the most important components of cell migration in metazoans.

Another important class of cell-ECM adhesions is Dystroglycan-based, which consist of an extracellular α-subunit, which binds to the ECM, and an intracellular β-subunit, which connects to the actin cytoskeleton. These adhesions act as major signaling centers in muscle, particularly at costameres (*i.e.,* connections between contracting sarcomeres and the cell membrane) but they are also found in other cell types at focal adhesions and podosomes. At all of these sites they regulate ERK (MAP kinase) signaling and the actin cytoskeleton, but the scope of their function is not as well understood as for integrin-based adhesions (Moore and Winder, 2010). Additionally, studies in *Drosophila* indicate that Dystroglycan can also regulate apico-basal and AP polarity (Deng *et al.,* 2003; Schneider *et al.,* 2006; Mirouse *et al.,* 2009).

Epithelial polarity

Apico-basal polarity in epithelial cells is established and maintained by the interactions between, and the resulting polarized localization of, three conserved, core polarity complexes (PAR, Crumbs, and Scribble) as well as the kinase Par1 (Fig 1.5; St. Johnston and Ahringer, 2010). The PAR complex is composed of atypical protein kinase 3 (aPKC; Tabuse *et al.,* 1998) and the PDZ-domain-containing proteins Par3 (Etemad-Moghadam *et al.,* 1995; Bazooka in *Drosophila*) and Par6 (Hung and Kemphues, 1999). The Crumbs complex is composed of the transmembrane protein Crumbs (Crb; Jürgens *et al.,* 1984), and the PDZ-containing proteins Patj (Discs lost (Dlt) in *Drosophila*; Bhat *et al.,* 1999; Pielage *et al.,* 2003) and Pals1 (Stardust (Sdt) in *Drosophila*; Tepass and Knust, 1993; Knust *et al.,* 1993), which is also a MAGUK family member. Finally, the Scribble complex is composed of the LAP (Lucine-rich-repeat And PDZ)-family member Scribble (Scrib; Bilder and Perrimon, 2000), the PDZ-domain-containing, MAGUK-family member and tumor suppressor, Discs Large (Dlg; Woods and Bryant, 1991;

Bilder *et al.,* 2000), and the WD (Tryptophan(W)-Aspartate(D))-repeat-containing, tumor suppressor, Lethal giant larvae (Lgl; Mechler *et al.,* 1985; Bilder *et al.,* 2000; Lutzelschwab *et al.,* 1987), which associates with the plasma membrane through a conserved polybasic motif (Hong *et al.,* 2015). The kinase Par1 is not stably bound to any of the three core polarity complexes but plays an important role in establishing polarity (Guo and Kemphues, 1995). In terms of apico-basal localization, the PAR and Crumbs complexes localize apically, defining the apical domain, and the Scribble complex and Par1 localize basolaterally (Margolis and Borg, 2005, Suzuki and Ohno, 2006, Assemat *et al.,* 2008; St. Johnston and Ahringer, 2010). The apical PAR and Crumbs complexes and the Scribble complex and Par1 mutually antagonize one another, via phosphorylation of specific targets within the complexes, and these antagonistic interactions drive the polarity complexes to their respective apical and basolateral domains. The AJCs then form at the apical-basolateral interface, and their presence allows for the structural and functional organization of an epithelial cell along the apico-basal axis (Fig 1.3; Nelson, 2009; Fig 1.5; St. Johnston and Ahringer, 2010).

Planar polarity in epithelial cells can be established by two mechanisms: through anterior-posterior (AP) gene expression patterns and through non-canonical Wnt signaling via Frizzled, also called the planar cell polarity (PCP) pathway (Zallen, 2007). AP patterning of gene expression along the body axis has the ability to polarize the distribution of cytoskeletal and junctional proteins (*e.g.,* E-Cadherin, Armadillo (β-catenin), Bazooka (PAR3)) within epithelial cells, and the AP-polarized distribution of adhesion proteins facilitates embryonic axis elongation in *Drosophila* (Irvine and Wieschaus, 1994; Zallen and Wieschaus, 2004; Blankenship *et al.,* 2006). This system also is employed during axis elongation in *Xenopus*, but these cells are mesenchymal and do not have defined AJs (Keller *et al.,* 2000; Ninomiya *et al*.,

Figure 1.5 Molecular interactions that define epithelial polarity are highly conserved between *Drosophila* and mammals

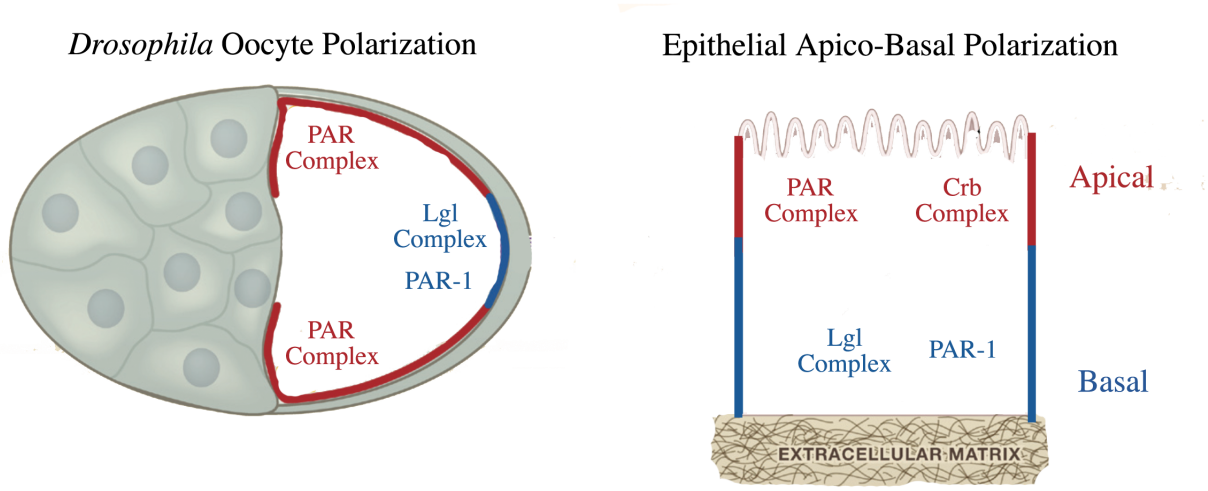

Fig 1.5. The same polarity proteins, and the same interactions between these proteins, establish and maintain polarity in *Drosophila* and mammals. In the *Drosophila* oocyte, a large polarized cell, antagonistic interactions between the PAR complex and both Par1 and the Scribble complex, which contains Lgl, allow for the polarized localization of *bicoid* and *oskar* mRNA within the oocyte. The same interactions exist in polarized epithelial cells in *Drosophila*, with the addition of the transmembrane protein Crumbs, which organizes the Crumbs complex in apical regions. In mammalian epithelial cells, the apical Crumbs and PAR complexes antagonize the basolateral Scribble complex and Par1, and vice versa, just as in *Drosophila*. (Adapted from St. Johnston and Ahringer, 2010).

Figure 1.6 The planar cell polarity (PCP) pathway in *Drosophila*

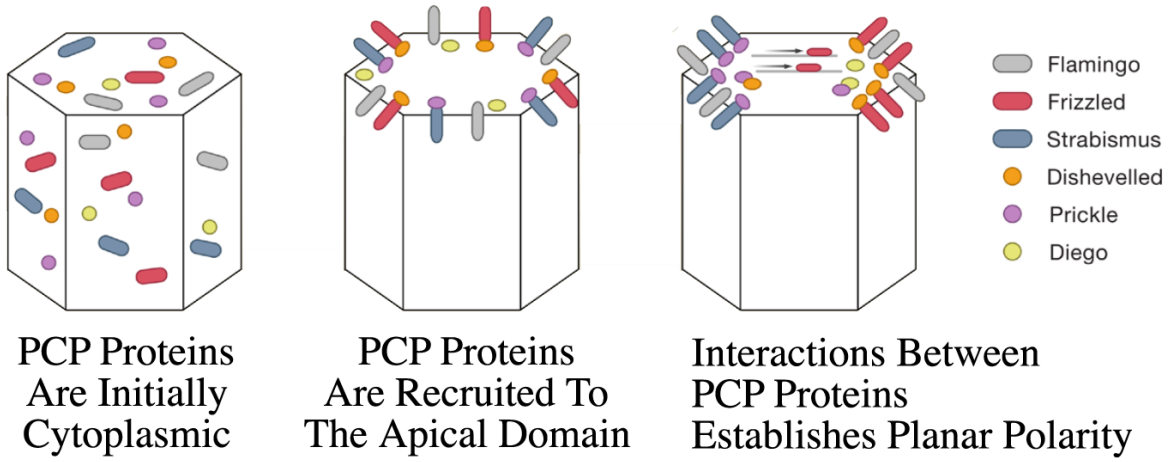

Fig 1.6. Also known as the non-canonical Wnt signaling pathway, the PCP pathway in *Drosophila* polarizes cells across the plane of the epithelium and is employed primarily in stable epithelia of the adult, such as the wing and cuticle. Initially, PCP proteins are cytoplasmic. Frizzled and Strabismus are brought to the apical surface by Flamingo, where Frizzled recruits Dishevelled and Strabismus recruits Diego. Interactions between these proteins at the apical surface, driven initially by the activity of Frizzled, localize Flamingo, Strabismus, and Prickle to the proximal surface (left) and localize Frizzled, Dishevelled, and Diego to the distal surface (right). (Adapted from Zallen, 2007).

2004; Hyodo-Miura *et al.,* 2006). The Frizzled/PCP pathway is more commonly employed in stable epithelia, such as the adult *Drosophila* wing or mammalian skin, because it involves the polarized, microtubule-based sorting of proteins within an individual cell such that that cell can signal to its neighbor, and to its neighbor, and so on across the epithelium. This pathway was initially worked out in *Drosophila*, although it is conserved in vertebrates, and it involves proteins at the cell surface, such as Frizzled, Strabismus (van Gogh), and Flamingo (Starry night), and cytoplasmic proteins, such as Dishevelled, Prickle, and Diego (Fig 1.6; Zallen, 2007). Of these proteins, Frizzled appears to be the most important for establishing the direction of planar polarity (Adler *et al.,* 1997). In *Xenopus*, components of the PCP pathway are used in intercalating cells to organize the fibronectin-rich ECM, but they do not appear to polarize within cells as they do in stable epithelia (Goto *et al.,* 2005). In summary, there are conserved mechanisms for establishing planar polarity across both stable and moving groups of cells, but there are distinct differences between how this polarity is generated in vertebrates and invertebrates (Zallen, 2007).

Morphogenesis and epithelial morphogenesis

The process by which cells create multicellular shapes (*e.g.,* tissues, organs, body plans) during development is referred to as **morphogenesis**. The question of how this process is regulated and facilitated has intrigued, baffled, and inspired developmental biologists since the field's infancy. The earliest embryologists of the Entwicklungsmechanik (developmental mechanics) movement attempted to use basic physical and mechanical properties of individual cells to explain morphogenesis, but they lacked sufficient understanding of cell biology and behavior to explain how these movements could be coordinated on a tissue and organismal level

(Keller, 2012). The concepts of selective affinity and differential adhesion between cell surface molecules (Holtfreter, 1939; Townes and Holtfreter, 1955; Steinberg, 1970; Steinberg, 1978) highlighted the importance of cell adhesion in morphogenesis and inspired biologists to identify and characterize the many different classes of cell adhesion molecules. Time-lapse imaging demonstrated that cells undergoing morphogenesis had directionality, and could integrate behaviors and forces through mechanical integration between cells (Gustafson and Wolpert, 1963). Further observations made by cell behaviorists (Bellairs *et al.,* 1982; Trinkaus, 1984) coupled with discoveries made by cell biologists regarding the cytoskeleton, motors, and receptors that could mediate adhesion and signaling, shed light on how cells with regulated, specialized behaviors could exert forces on groups of cells and tissues (Keller, 2012). Combining experimental observations and manipulations with computational modeling provided sufficient explanations for how localized cell shape changes could account for organized tissue movements during morphogenesis (Jacobson and Gordon, 1976; Odell *et al.,* 1981; Hardin and Cheng, 1986). Dramatic advances in our understanding of the molecular, biochemical, and physical properties of cells, and in imaging, force-measuring, computational, and genetic-manipulation technologies, have equipped developmental biologists with the arsenal of tools necessary to dissect and explain the mass movements of morphogenesis through the properties and behaviors of individual cells.

The regulated interplay between the stability and plasticity of tissues and epithelia lies at the heart of morphogenesis (Lecuit and Lenne, 2007). There are many behaviors of epithelial cells that can be regulated to either maintain a stable, epithelial morphology, or to change the morphology of an epithelium through **epithelial morphogenesis**. These behaviors include cell shape change, rearrangement, migration, division, and death, and these processes can be

employed alone or in combination for a tremendous variety of morphogenetic outcomes. For the purposes of this dissertation, I will focus on how cell shape change, rearrangement, and migration can act as drivers of epithelial morphogenesis since these are the processes that contribute DA tube formation.

The actin cytoskeleton is primarily responsible for regulating **cell shape**, and remodeling of that actin cytoskeleton is needed for a cell to change its shape. Actin remodeling requires a plethora of actin-associated proteins, with some of the most well known being the conserved Rho GTPases: Rac, Rho, and Cdc42 (Hall, 2005). Myosin motors can act on the actin cytoskeleton to produce cortical tension and induce contractility, and when the actin cytoskeleton is linked to cell membranes through adhesive, junctional complexes, such as the AJs, this contractility can deform the cell membranes and cause cells to change their shape. If epithelial cells change their shape through flattening, columnarization, or planar lengthening and shortening, the epithelium will become respectively thinner, thicker, or wider, but will remain a flat sheet. Conversely, if either the apical or the basal surfaces of epithelial cells constrict, the epithelium will respectively invaginate or evaginate, and bending will occur (Fig 1.7; Lecuit and Lenne, 2007). Apical constriction is one of the best-characterized cell shape changes, and, by driving epithelial bending, it is responsible for endoderm formation in *C. elegans*, *Drosophila*, sea urchins, and amphibians, as well as mesoderm formation in *Drosophila*, and neurulation in vertebrates (Lecuit and Lenne, 2007, Martin *et al.,* 2009; Sawyer *et al.,* 2010; Martin and Goldstein, 2014). Indeed, apical constriction appears to be one of the most conserved and important modes of cell shape change during metazoan morphogenesis.

Cell rearrangement can be a powerful driver of morphogenesis, and this process lies at the heart of a conserved driver of tissue elongation, convergent extension (Elul *et al.,* 1997;

Keller *et al.,* 2000, Keller, 2002; Wallingford *et al.,* 2002; Keller, 2006; Tada and Heisenberg, 2012; Guillot and Lecuit, 2013; Walck-Shannon and Hardin, 2014). CE underlies the elongation of the mouse visceral endoderm, the *Xenopus* and chick neural tube, and the *Drosophila* germ band. In order for cells to rearrange, they have to be able to modulate their cell-cell adhesions, and they have to be able to transmit forces across groups of cells. E-Cadherin-based AJs are the primary junctions used to transmit forces generated by the actomyosin network to the cell cortex, and they mechanically couple cells in an epithelium (Guillot and Lecuit, 2013). When cells rearrange, they remove old junctions, bring four or more cells together into transient tetrads or rosettes, and form new junctions in an orthogonal orientation to the junctions that were removed (Blankenship *et al.,* 2006; Guillot and Lecuit, 2013; Harding *et al.,* 2014). When this behavior is coordinated in a planar fashion across an epithelium, it can drive the extension and elongation of the epithelium (Guillot and Lecuit, 2013).

Cell migration is a highly regulated process required both for the dramatic reorganizations that take place during embryonic morphogenesis, such as gastrulation, and for homeostatic processes in the adult organism, such as immunity. In order for cells to migrate, they must be able to polarize towards, or away from, a migratory signal, regulate their actin cytoskeleton to extend membrane in an intended direction so that it can adhere to a migratory substrate, release adhesions at the trailing edge, and finally contract to drag their bodies along. The conserved Rho GTPases are particularly important for cell migration, regulating different features of the actin cytoskeleton and facilitating different aspects and modes of cell migration (Fig 1.9; Pocha and Montell, 2014). Typically, Rac functions at the leading edge of migrating cells and stimulates the production of lamellipodia, which spread forward to establish new adhesions. Cdc42, on the other hand, typically regulates the production of thin filopodia, which

Figure 1.7 Polarized, localized cell shape change, via apical constriction, leads to the bending, or invagination, of an epithelium

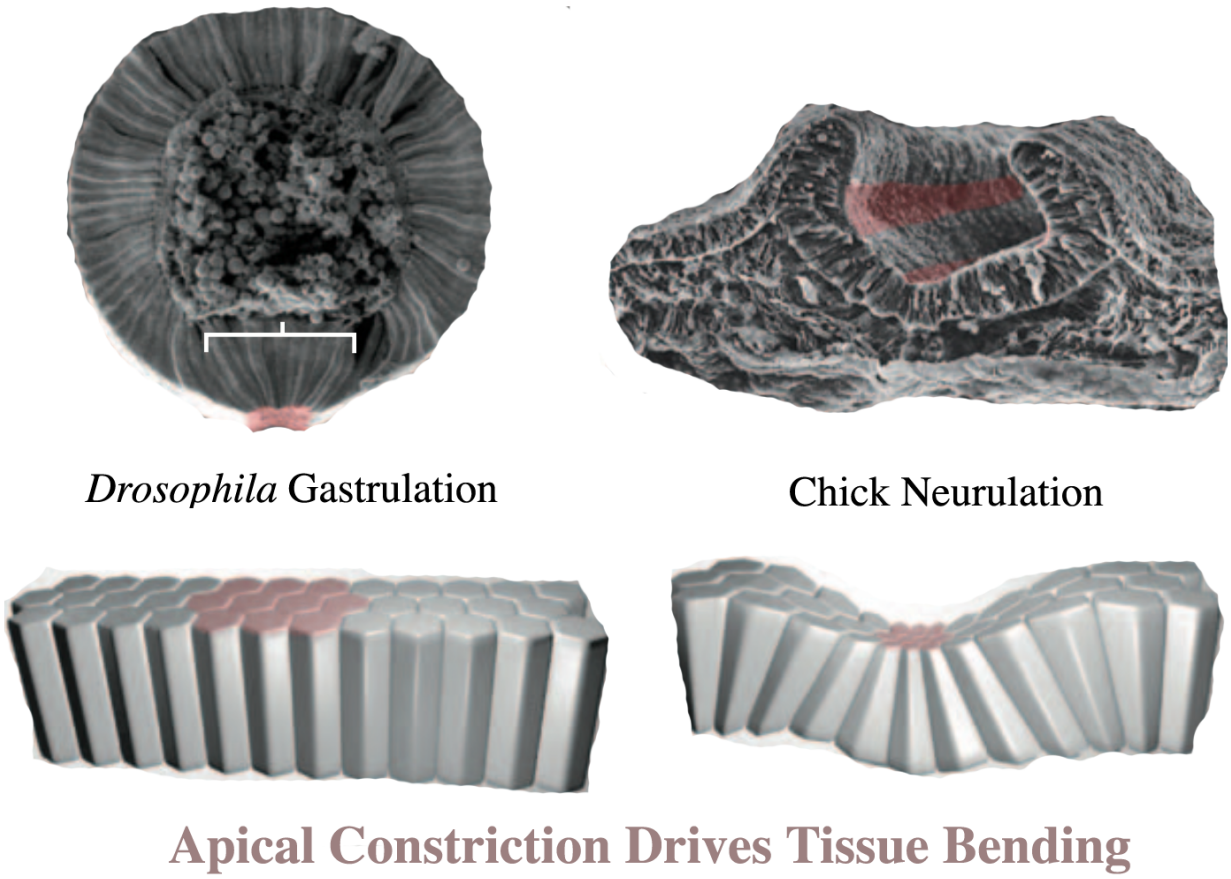

Fig 1.7. In the *Drosophila* embryo, apical constriction (red) leads to the bending and invagination of the ventral mesoderm during gastrulation. Likewise, in the chick embryo, apical constriction in defined regions (red) of the neuro-epithelium facilitates neurulation. In epithelial cells, localized apical constriction (red) can take a uniform epithelium and cause it to invaginate and bend at the site of apical constriction. (Adapted from Lecuit and Lenne, 2007).

Figure 1.8 Cell intercalation can drive epithelial elongation

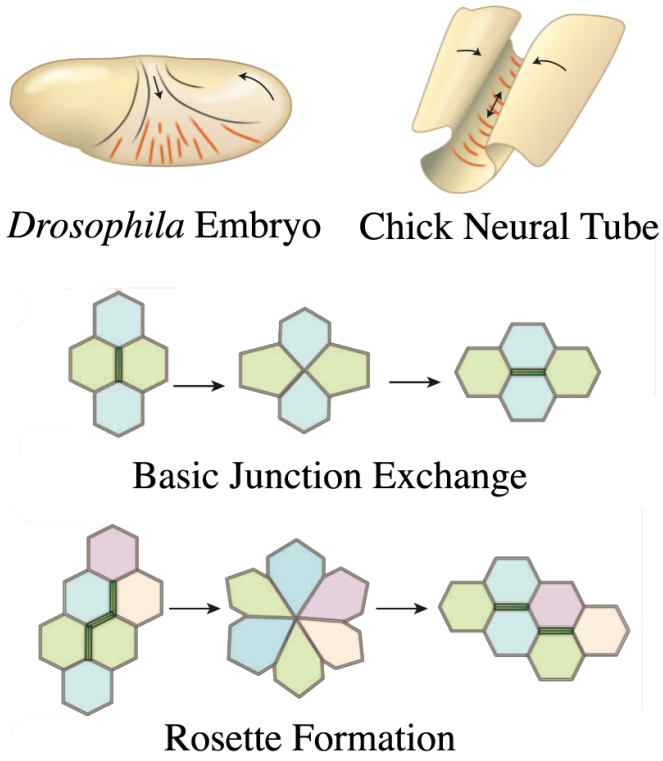

Fig 1.8. Both elongation of the *Drosophila* germband in the embryo and elongation of the neural tube in chick are driven by cell intercalation. In basic junction exchange, polarized tension between two vertical junctions can promote the formation of a tetrad and allow for junctional exchange and horizontal-junction formation. When tension is applied across more than two vertical junctions, through a multicellular actomyosin cable, a multicellular rosette can form and cause an even more dramatic horizontal junctional remodeling event. Indeed, the role of rosette formation in cell intercalation and tissue elongation has only recently been appreciated but appears to be a powerful and conserved driver of this process across metazoans (Blankenship *et al.,* 2006; Harding *et al.,* 2014). (Adapted from Guillot and Lecuit, 2013).

sense guidance cues and help polarize the migrating cell. Rho primarily functions in the cell body and lagging edge to promote actomyosin contractility (Hall, 2005, Jaffe and Hall, 2005). Cell-ECM adhesions, which form at the leading edges of migrating cells, must be removed and recycled from the lagging edges of these cells, and this process requires endocytosis. At the most basic level, cells can migrate individually, where they have front-back polarity as opposed to apico-basal polarity, and release all stable cell-cell adhesions. On the other extreme, cells can migrate as organized, epithelial sheets, where apico-basal polarity and cell-cell adhesion is maintained, and cells use planar cues across the epithelium to direct their coordinated migration. Cells can also migrate as small clusters or collectives, where they must integrate and balance the polarity and adhesive features of both individual cells and stable groups of cells (Fig 1.9; Pocha and Montell, 2014).

Epithelial tubulogenesis

In order for tubes to adopt a terminal morphology that can support the intended function, they must accomplish three fundamental events during their morphogenesis: tube patterning, tube formation, and tube elongation or elaboration (Lubarsky and Krasnow, 2003; Andrew and Ewald, 2010; Iruela-Arispe and Beitel, 2014). Tube patterning requires changes in gene expression within groups of cells so that cells take on a tube fate and behave differently from their neighbors. Tube formation involves the formation of a tube lumen, which can be a multicellular or unicellular process. Finally, tube elongation and elaboration alters the tube from a basic to a terminal morphology. Just as there is tremendous diversity in the terminal morphologies of metazoan tubes, there is tremendous diversity in metazoan tubulogenesis. This being said, the cellular behaviors that facilitate tubulogenesis are highly conserved (Lubarsky

Figure 1.9 Different modes of cell migration in *Drosophila* employ conserved regulators of the actin cytoskeleton and balance different modes of epithelial polarity

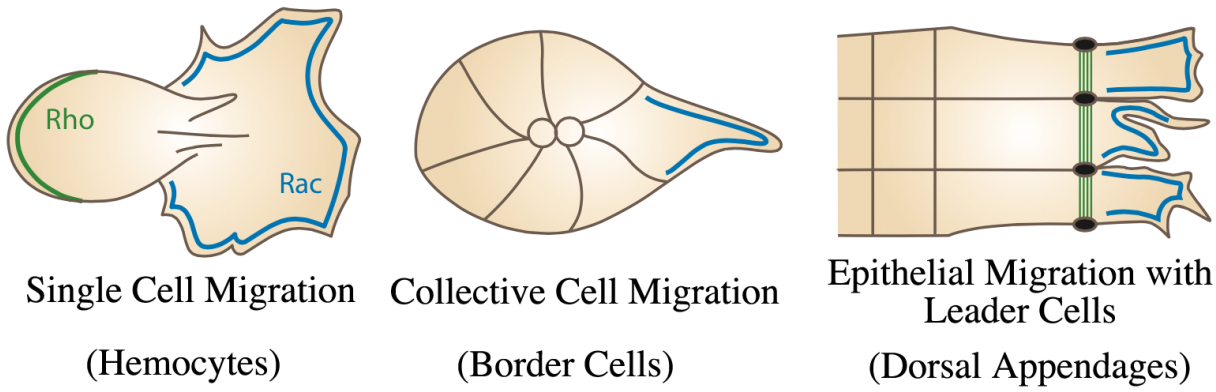

Fig 1.9. In individual migrating hemocytes, Rac functions at the leading edge to induce cell spreading and lamellipodia formation. Rho functions in the cell body and at the lagging edge to promote actomyosin contractility and drag the cell body along. These cells possess front-back polarity and do not have apico-basal polarity. In migrating border cells, Rac is also used in the lead cell to promote forward migration. The overall cluster possesses front-back polarity, but apico-basal polarity must also be maintained to hold the cluster together. During dorsal closure, the leading edge of the epithelium uses localized Rac and Rho to promote directed cell migration. In this context, planar-polarity cues direct the migration, and apico-basal polarity is maintained within the epithelium. (Adapted from Pocha and Montell, 2014).

and Krasnow, 2003; Andrew and Ewald, 2010; Iruela-Arispe and Beitel, 2014), and so it appears that it is the way in which those behaviors are employed, in vastly varied combinations, that produces the incredible diversity of tubes. Since the subject of this dissertation is epithelial tubulogenesis, I will now focus specifically on the morphogenesis of multicellular, epithelial tubes.

The basic structure of any tube relies on the essential features of epithelia: polarity and adhesion. Multicellular tubes consist of a polarized epithelium around a central lumen, such that the apical surfaces of the cells face inward towards the lumen, and the basal surfaces face outward and interact with the surrounding environment (Fig 1.4A; Andrew and Ewald, 2010). Adhesive junctions allow the cells to adhere to one another and maintain an intact lumen. Sometimes, the precursors of epithelial tubes are themselves polarized epithelia, and sometimes they are groups of cells that become polarized. If the tubular precursor is an epithelium, then it can either undergo wrapping and fusion to form a tube parallel to the epithelium (Fig 1.10A; Andrew and Ewald, 2010; *e.g.,* vertebrate neurulation, *Drosophila* gastrulation), or it can undergo budding, which forms a tube perpendicular to the epithelium while remaining contiguous with that epithelium (Fig 1.10B; Andrew and Ewald, 2010; *e.g.,* sea urchin gastrulation, *Drosophila* salivary gland or tracheal tubulogenesis). Coordinated cell shape changes, such as apical constriction, are important drivers of both wrapping and budding tubulogenesis. Groups of cells can also form a lumen between each other through cord hollowing tubulogenesis (Fig 1.10 C; Andrew and Ewald, 2010), or they can program interior cells to die through cavitation tubulogenesis (Fig 1.10E; Andrew and Ewald, 2010). In these cases, the cells create a polarized epithelial sheet during the process of tube formation. These

modes of tubulogenesis, individually or in combination, can explain the formation of almost any multicellular, tubular lumen.

Once an epithelial tube forms, it can elongate and elaborate through a variety of cellular mechanisms and behaviors. Non-proliferating tube cells can undergo coordinated cell shape changes or rearrangements to elongate a tube without changing cell number (*e.g.*, *Drosophila* leg imaginal discs; Fristrom and Fristrom, 1975; *Drosophila* salivary glands; Maruyama and Andrew, 2012; *Drosophila* tracheal branches; Caussinus *et al.,* 2008; Fig 1.11 A, B; Andrew and Ewald, 2010). Interestingly, in many of these cases, lumen size and morphology are limited mainly by the apical shape and size, and to a lesser extent by the number, of the tube cells (Fankhauser, 1945; Beitel and Krasnow, 2000). Tube cells that are capable of proliferating can localize or generalize that proliferation to extend or expand the tube almost indefinitely, and this mode is particularly important when the tube must be dramatically elaborated (*e.g.,* Müllerian duct elongation in birds (Guoili *et al.,* 2007) and mammals (Orvis and Behringer, 2007); mammary duct branching in mammals (Watson and Khaled, 2008); Fig 1.11 C, D; Andrew and Ewald, 2010). Tube cells can also recruit new cells to become tube cells, increasing the range of possible tube sizes and morphologies than can be achieved (*e.g.*, *Drosophila* Malpighian tubules (Denholm *et al.,* 2003); Fig 1.11 E; Andrew and Ewald, 2010). Cell migration can also drive tube elongation, often with the use of single or multiple lead cells (*e.g.*, lead roof and floor cells in *Drosophila* dorsal appendage tubes (Boyle *et al.,* 2010); tip cells in the *Drosophila* tracheal branches (Cabernard and Affolter, 2005); and mammalian kidney buds (Shakya *et al.,* 2005); Andrew and Ewald, 2010). Tubes can remain unelaborated, and exist as a simple lumen (*e.g.*, *Drosophila* DA tubes or salivary glands), or they can bifurcate, branch, or cleft to form more complicated lumens in either a programmed (*e.g.*, mammalian lung (Metzger *et al.,* 2008)) or

Figure 1.10 Mechanisms of tube lumen formation

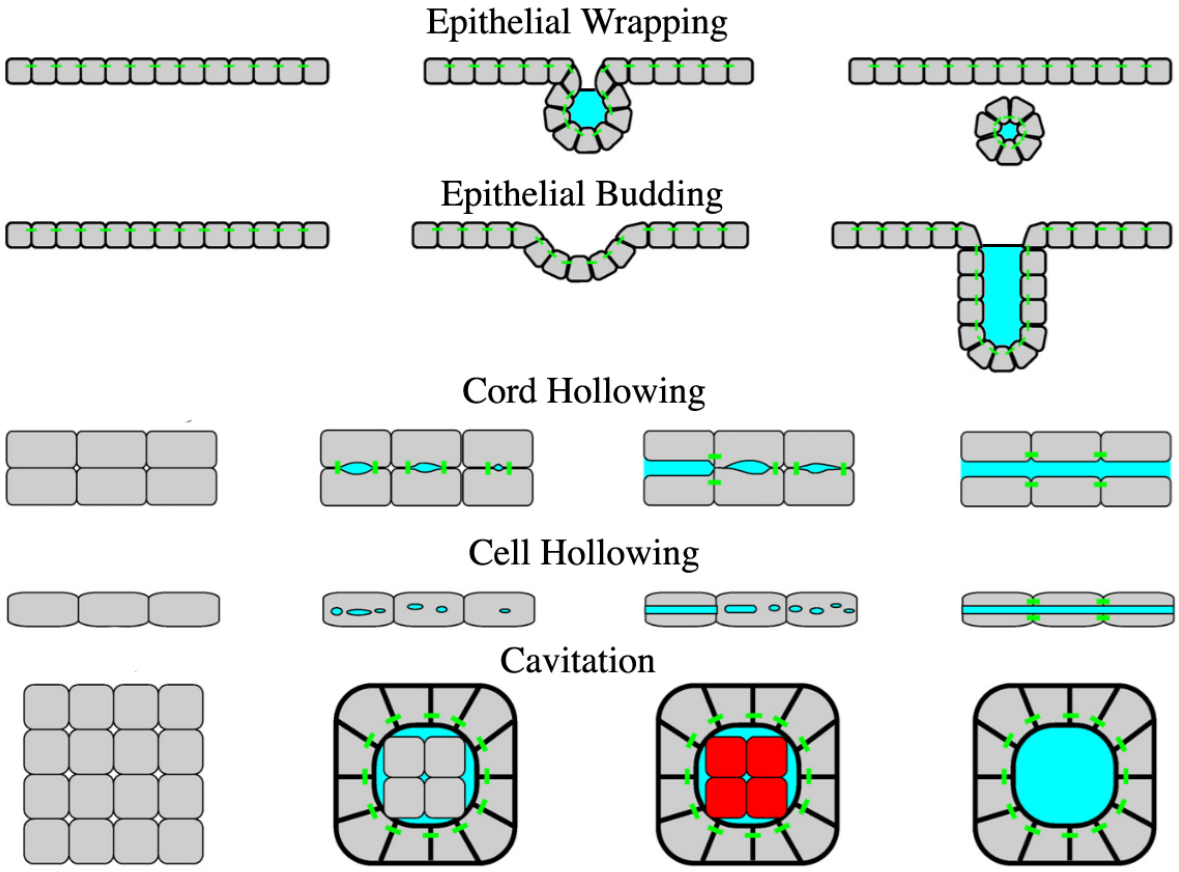

Fig 1.10. In wrapping tubulogenesis, the tube forms parallel to the epithelium, and lumen formation requires fusion along the length of the tube. In budding tubulogenesis, the tube forms perpendicular to the epithelium and remains contiguous with the epithelium. In cord-hollowing tubulogenesis, groups of cells polarize and remodel their junctions to create a lumen and become an epithelium around it. In cell-hollowing tubulogenesis, individual cells create intracellular lumens through coordinated, localized vesicle fusion. In cavitation tubulogenesis, cells within a group of cells are programmed to die and are cleared, and a polarized epithelium forms around the cavity to create a lumen. Green = intercellular junctions; cyan = lumen; red = dying cell. (Adapted from Andrew and Ewald, 2010).

Figure 1.11 Mechanisms of tube lumen elongation

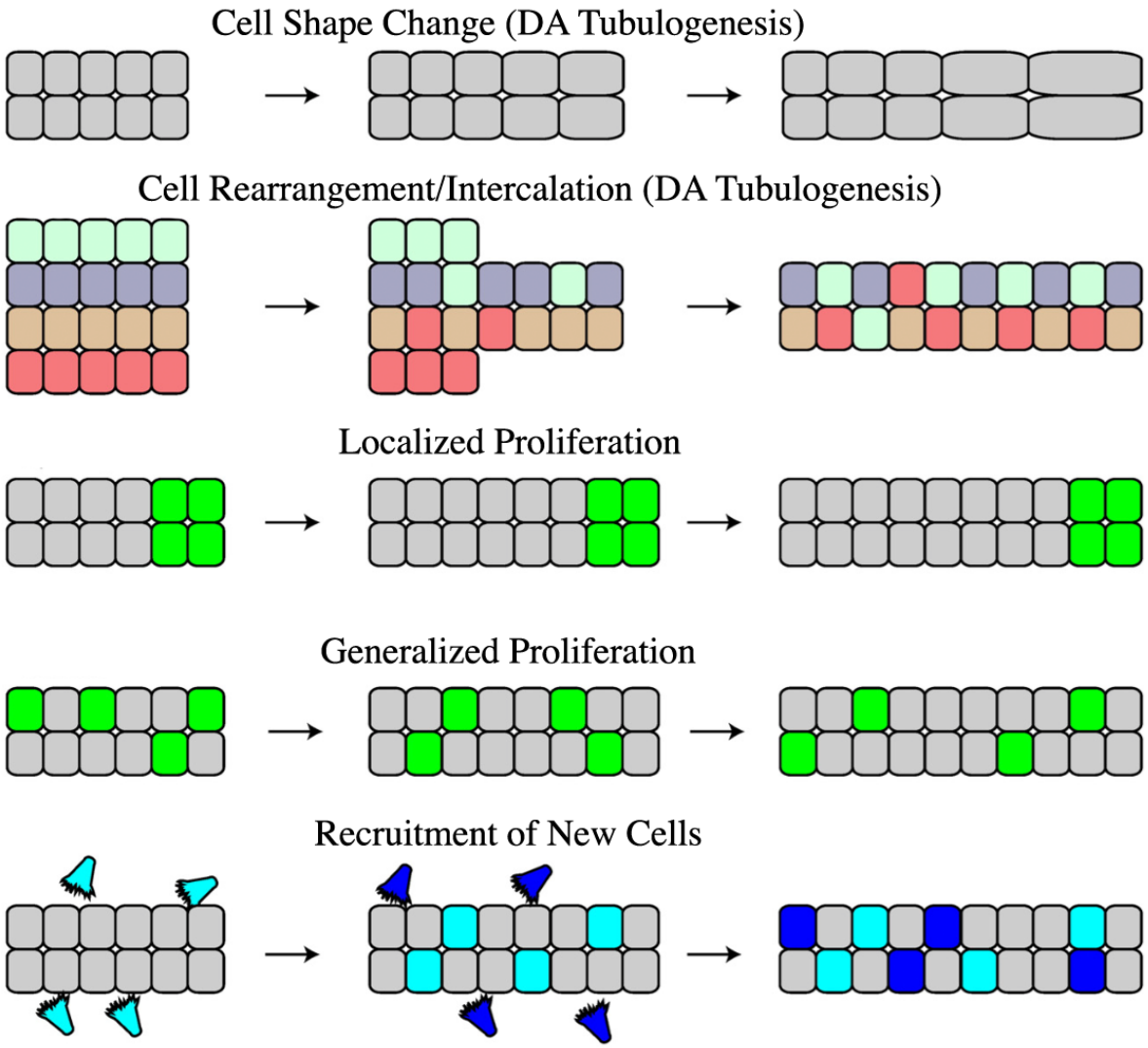

Fig 1.11. Coordinated cell shape change, or cell rearrangement, can drive tube elongation, but the number and dimensions of these cells limits terminal tube size and morphology. In contrast, spatially restricted proliferation, or generalized proliferation, can extend and elaborate tubes potentially indefinitely, but require additional regulation of cell division. Tubes can also recruit new cells to become part of the tube. (Adapted from Andrew and Ewald, 2010).

stochastic fashion (*e.g.,* mammalian mammary glands (Watson and Khaled, 2008); Fig 1.12; Andrew and Ewald, 2010). Even fluid flow within a tube lumen can, in some cases, affect the morphology of the tube (*e.g.,* loss of the ability to sense flow in the mammalian kidney can result in the expanded lumens of polycystic kidney disease; Wilson and Goilav, 2007; Iruela-Arispe and Beitel, 2014). By employing various combinations of these cellular mechanisms and behaviors, multicellular tubes can attain almost any terminal morphology.

Drosophila oogenesis

The purpose of the *Drosophila* ovary is to produce egg chambers and, eventually, eggs. These egg chambers are composed of a germline syncytium of 16 cells, one of which is the oocyte. The syncytium is surrounded by a somatic, monolayer epithelium of follicle cells (King, 1970; Spradling, 1993). The follicular epithelium, which is the subject of my graduate research, functions to pattern and nourish the oocyte and to secrete the eggshell during the final stages of oogenesis. As part of this eggshell synthesis process, different groups of follicle cells produce specialized secondary structures, and the morphologies of these structures reflect the morphologies of the cell groups that created them. In particular, two groups of dorsal, anterior follicle cells secrete oar-shaped filaments called dorsal appendages (DAs), which facilitate gas exchange in the embryo (Hinton, 1959; Hinton, 1960; Hinton, 1969). Therefore, *Drosophila* eggshells, which can be easily collected in large quantities outside of the adult without harming the adult, are akin to footprints or fossils in that they can tell a story, to an attentive observer, of morphogenesis that took place previously inside the body of the adult. Once I have explained the structure and development of the egg chambers, I will elaborate on how studying the

Figure 1.12 Different modes of tube elaboration.

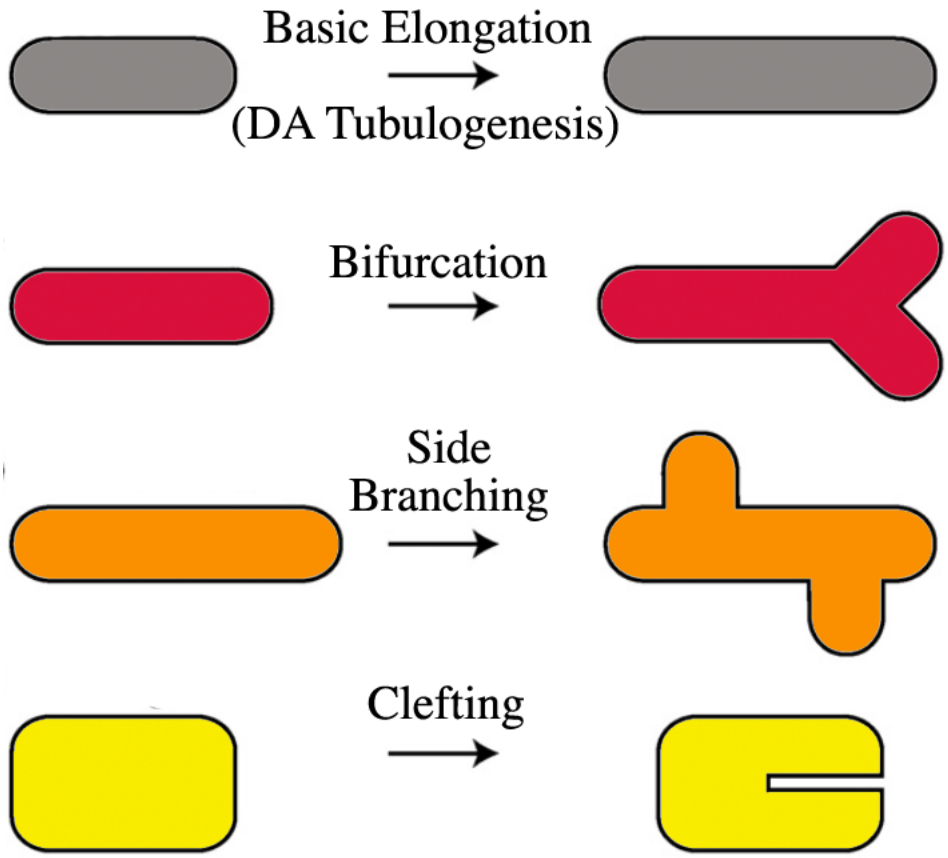

Fig 1.12. Tube elongation can be simple (e.g., DA tubulogenesis) or elaborate. (Adapted from Andrew and Ewald, 2010).

development of *Drosophila* eggshells can inform our understanding of epithelial morphogenesis and tubulogenesis.

In the adult female fruit fly, each ovary consists of a bundle of parallel egg-chamber assembly lines called ovarioles. The number of active ovarioles in an ovary varies, depending on nutrition and female health, but in robust stocks each ovary contains ~15 ovarioles, each of which can produce ~ two eggs per day. Thus, a well-fed adult female can produce over 60 eggs per day, which is approximately half of her body mass.

Egg chambers are "born" in the distal tip of each ovariole in a structure called the germarium, which houses both the germline- and follicle-cell stem cells. Each germline stem cell division renews the germline stem cell and produces a cystoblast that undergoes four incomplete divisions to produce a 16-cell germline cyst. Since these divisions are incomplete, actin-rich ring canals remain between these germline cells and allow for the passage of cytoplasm and materials between the cells (Mahajan-Miklos and Cooley, 1994). One of the two germline cells that retain four ring-canal connections to its siblings becomes the oocyte, and this cell moves to the posterior of the egg chamber through a mechanism dependent on differential E-cadherin adhesion (Godt and Tepass, 1998); the rest of the cells become nurse cells, which support the oocyte. These nurse cells produce mRNAs, proteins, and organelles, which are eventually loaded into the oocyte to prepare it for embryogenesis. As the germline cyst is created, while it is still in the germarium, the follicle stem cells produce follicle cell precursors, and about 80 of these cells encapsulate the cyst, producing a rudimentary egg chamber (Horne-Badinovac and Bilder, 2005).

Once formed, the egg chamber proceeds through 14 stages of development (King, 1970; Spradling, 1993; Fig 1.13; Horne-Badinovac and Bilder, 2005). In stages 1-6, the follicle cells

proliferate through mitotic divisions until there are ~650 cells in the epithelium. Interestingly, like the germline cell divisions, many of the follicle cell divisions are also incomplete and leave behind ring canals between mitotically related cells; these cytoplasmic bridges selectively allow proteins to equilibrate between interconnected groups of epithelial follicle cells (McLean and Cooley, 2013). Throughout these early stages the egg chamber is round, the follicle cells are cuboidal in shape, cell shape is uniform throughout the epithelium, and the epithelium is morphogenetically quiescent. The follicular epithelium is oriented such that the apical surface faces inward, contacting the germline, and the basal surface faces outward, and contacts an ECM/basement membrane that surrounds each egg chamber (Fig 1.14; Horne-Badinovac and Bilder, 2005).

During the middle stages of oogenesis (S6-10), the follicle cells undergo endoreplication, followed by selective amplification of chorion genes (during S10B-14) so that massive quantities of eggshell proteins can be produced for secretion at the end of oogenesis. During S6-10, the epithelium begins to become morphogenetically active, as AP patterning is established and the egg chambers begin to elongate along this axis through rotation (Haigo and Bilder, 2011) and pulsed contractions of the basal actomyosin network (He *et al.,* 2010; Gates, 2012). The anterior polar cells and their immediate neighbors are specified as border cells, detach from the epithelium, and migrate in between the nurse cells to reach the oocyte, and eventually help form the micropyle (*i.e.,* fertilization tube) of the mature eggshell (Montell, 2001). The remaining anterior follicle cells over the nurse cells take on a squamous morphology and become the stretch cells. The follicle cells over the oocyte become densely packed and elongate apico-basally, taking on a columnar morphology. This columnar epithelium then undergoes dorso-anterior patterning through the intersection of EGF (TGFα) and DPP (TGFβ/BMP) signaling (reviewed

Figure 1.13 Structure of a *Drosophila* ovariole and the stages of oogenesis

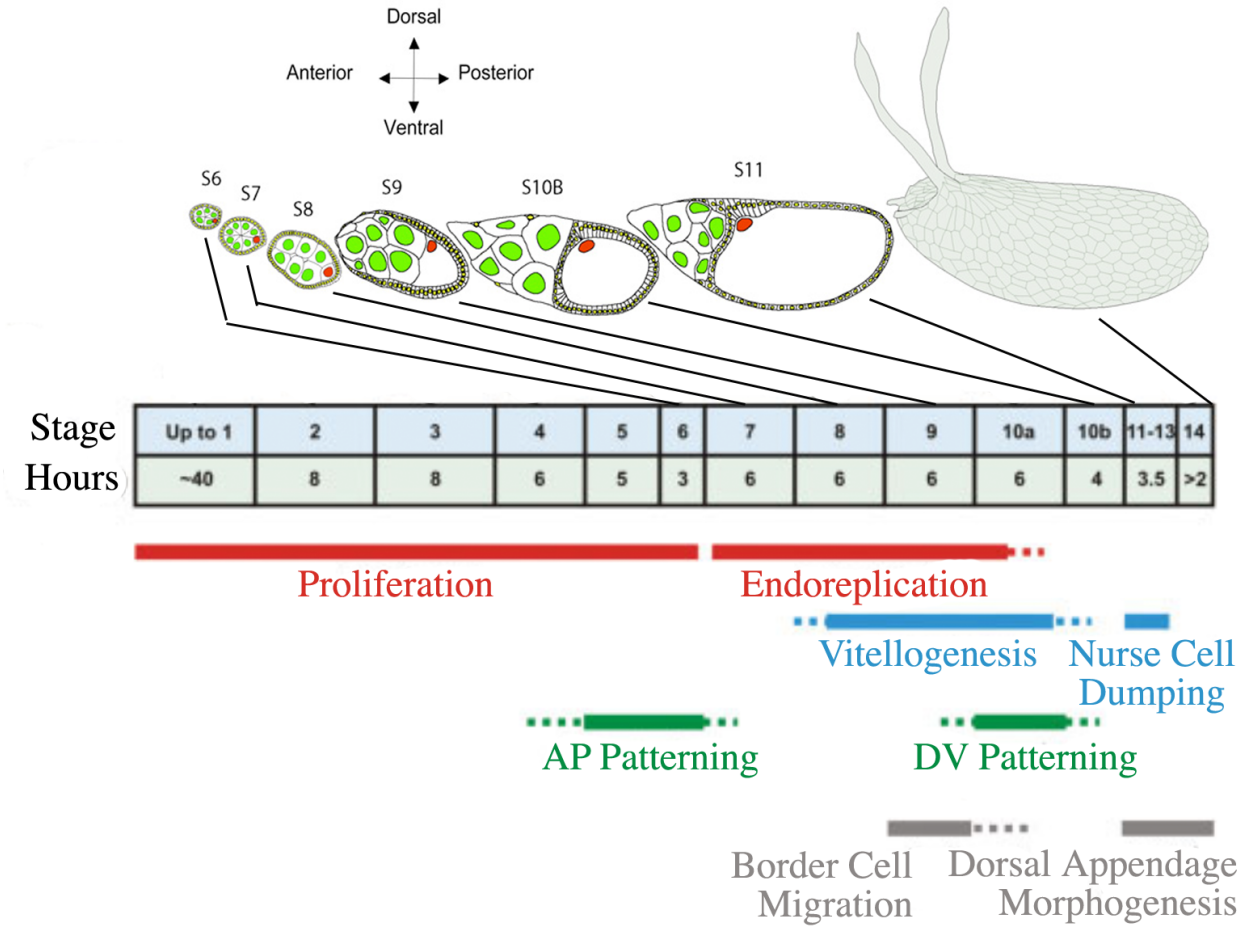

Fig 1.13. In the ovariole schematic, anterior is to the left, the oocyte is blue, the nurse cells are grey-blue, polar cells/border cells are green, and epithelial follicle cells are yellow. The table of stages under the schematic indicates the approximate time, in hours, for each of the defined stages of oogenesis (S1-S14; King 1970; Spradling 1993). Under the table, in positions corresponding to the stages in the table, are the main events of oogenesis. **Red bars** are cell or DNA replication events. **Green bars** are patterning events. **Blue bars** are germline events. **Grey** bars are morphogenetic events. (Adapted from Horne-Badinovac and Bilder, 2005 and Zartman *et al.*, 2011).

Figure 1.14 Organization of the epithelial follicle cells of the *Drosophila* egg chamber

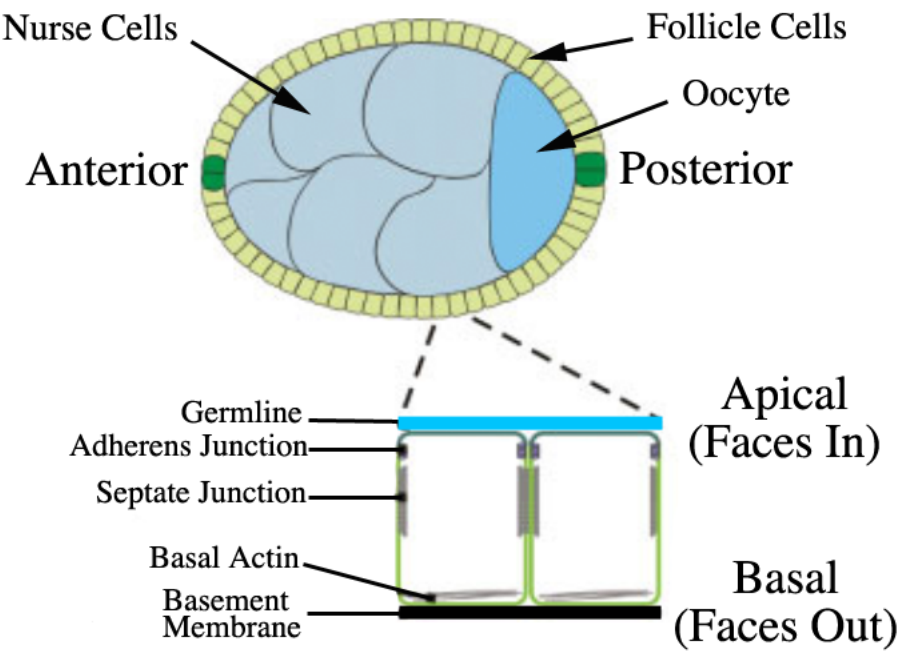

Fig 1.14. The follicular epithelium (yellow) is oriented such that the apical surface of each cell faces inward towards the germline nurse cells (grey-blue) and oocyte (blue), and the basal surface faces outward and contacts the ECM, or basement membrane. Thus, E-Cadherin-based cell-cell adhesions form at the zonula adherens, adjacent to the germline, septate junctions form on lateral surfaces, and integrin-based cell-matrix adhesions form on the outer surface of the epithelium, where they can contact the basement membrane. (Adapted from Horne-Badinovac and Bilder, 2005).

in Yakoby *et al.,* 2008), and prepares to secrete the eggshell and pattern the embryo (Berg, 2005; Horne-Badinovac and Bilder, 2005).

The late stages of oogenesis (S11-14) are marked by a series of massive, coordinated morphogenetic movements involving the germline and different populations of columnar follicle cells. In a process called dumping, the nurse cells empty all of their cytoplasm into the oocyte through the ring canals, the oocyte swells to its terminal size, and the nurse cell remains are engulfed by the stretch cells (Cummings and King, 1970; Nezis *et al.,* 2000; Tran and Berg, 2003; Jenkins *et al.,* 2013). Two groups of dorso-anterior, columnar follicle cells (*i.e.,* dorsal appendage cells), which have been precisely patterned during S10, undergo tubulogenesis to form a pair of epithelial tubes that expand and migrate over the stretch cells and dying nurse cells, eventually reaching the anterior tip of the egg chamber. During tube formation and elongation, the dorsal appendage cells secrete eggshell proteins into the lumens of the tubes they have formed, creating the respiratory filaments of the mature eggshell. Follicle cells between (*i.e.,* midline cells) and anterior (*i.e.,* centripetal cells) to the dorsal appendage cells migrate to surround the anterior end of the oocyte, separating it from the dying nurse cells, and form the operculum of the mature eggshell, through which the larva will eventually hatch. Once these various morphogenetic processes have concluded and the eggshell and secondary eggshell structures have been patterned and formed, the follicle cells die and are sloughed off as the egg chamber proceeds through the oviduct. The egg chamber matures into an egg, is then fertilized and laid, and the process of oogenesis is complete (Horne-Badinovac and Bilder, 2005).

The *Drosophila* follicular epithelium is a truly formidable developmental model, particularly for one interested in morphogenesis. The massive scale and rapid nature of egg chamber production in an adult female provides a wealth of easily accessible material for

analysis. The toolbox of genetic and molecular tools available in *Drosophila* can be readily employed in the somatic follicular epithelium. *Drosophila* egg chambers are transparent, facilitating structural analyses, and they are readily amenable to *in situ* hybridization, immunostaining, and live culturing (Dorman *et al.,* 2004; Zimmerman *et al.,* 2013). The orientation of the epithelium provides advantages for studying events at the basal surface of epithelial cells. There are a multitude of distinct, morphogenetic events that take place within the epithelium, and, as mentioned previously, the mature eggshell reflects the fidelity of these events, facilitating rapid and efficient screening for the effectors of these processes. These advantages, and more, make the *Drosophila* follicular epithelium a fascinating and rewarding subject for the developmental biologist.

Dorsal appendage tubulogenesis

The dorsal respiratory appendages (DAs) are secondary structures of the mature *Drosophila* eggshell. They are created by a pair of dorsal, epithelial, follicle cell tubes that undergo wrapping tubulogenesis and elongation during the late stages of oogenesis (S10-14) and subsequently secrete eggshell proteins into their tube lumens. As a model system for epithelial tubulogenesis, DA tubulogenesis has numerous advantages, including its relative simplicity, genetic tractability, accessibility, and amenability to both fixed and live microscopy. Well fed fruit flies produce eggs on a massive scale, and since the eggshell is the terminal product of oogenesis, analyzing DA morphology does not require closely-timed collections, as would analysis of specific features of embryogenesis. DA morphology has no direct affect on viability, although the patterning cues that fate the DA tubes are themselves required for embryogenesis, and therefore DA tubulogenesis can often be readily perturbed without affecting viability. As a result, DA morphology is also quite sensitive to perturbation, and the presence, absence, position

of, and morphology of the DAs can be used to determine whether a given phenotype reflects a defect in patterning, DA-tube formation, DA-tube elongation, or DA-tube guidance. (Berg, 2005; Berg, 2008). Finally, DA tubulogenesis displays both conservation and extensive variability between different species of *Drosophila*, and we are only beginning to realize, appreciate, and take advantage of the potential benefits of comparative analysis between respective *Drosophilid* executions of DA tubulogenesis (Fig 1.15; Throckmorton, 1962; Peri *et al.*, 1999; James and Berg, 2003; Nakamura and Matsuno, 2003; Nakamura *et al.,* 2007; Kagesawa *et al.,* 2008; Niepielko *et al.*, 2011; Niepielko *et al.,* 2012; Niepielko *et al.,* 2014a; Niepielko *et al.,* 2014b; Osterfield *et al.,* 2015).

The patterning events that determine the fate of the two dorsal, anterior groups of tube cells involve integration of spatial cues from both the EGF and DPP pathways (Schüpbach, 1987; Neuman-Silberberg and Schüpbach, 1993; Brand and Perrimon, 1994; Gillespie and Berg, 1995; Roth *et al.,* 1995; Gonzalez-Reyes *et al.,* 1995; Schnorr and Berg, 1996; Twombly *et al.,* 1996; Wasserman and Freeman, 1998; Ghiglione *et al.,* 1999; reviewed by Nilson and Shüpbach, 1999; Reich *et al.,*1999; Tzolovsky *et al.,* 1999; Peri and Roth 2000; Jordan *et al.,* 2000; Zhao *et al.,* 2000; James *et al.,* 2002; Berg, 2005, 2008; Ward and Berg, 2005; Jordan *et al.,* 2005; Atkey *et al.,* 2006; Chen and Shüpbach, 2006; Lembong *et al.,* 2008; Yakoby *et al.,* 2008a; Yakoby *et al.,* 2008b; Boslair Lachance *et al.,* 2009; Lembong *et al.,* 2009; Zartman *et al.,* 2009; Boyle and Berg, 2009; Yan *et al.,* 2009; Zartman *et al.,* 2011; Andreu *et al.,* 2012; Fuchs *et al.,* 2012; Fregoso Lomas *et al.,* 2013; Marmion *et al.,* 2013; Cheung *et al.,* 2011; Simakov *et al.,* 2012). These patterning events, in conjunction with Notch signaling (Ward et al. 2006), define two cell types within each DA tube that are spatially and morphogenetically distinct (Fig 1.16; roof and floor; Dorman *et al.,* 2004; Ward and Berg, 2005). By stage 10B, each DA-tube primordium

Figure 1.15 Eggshell and dorsal appendage (DA) diversity amongst the *Drosophilids*

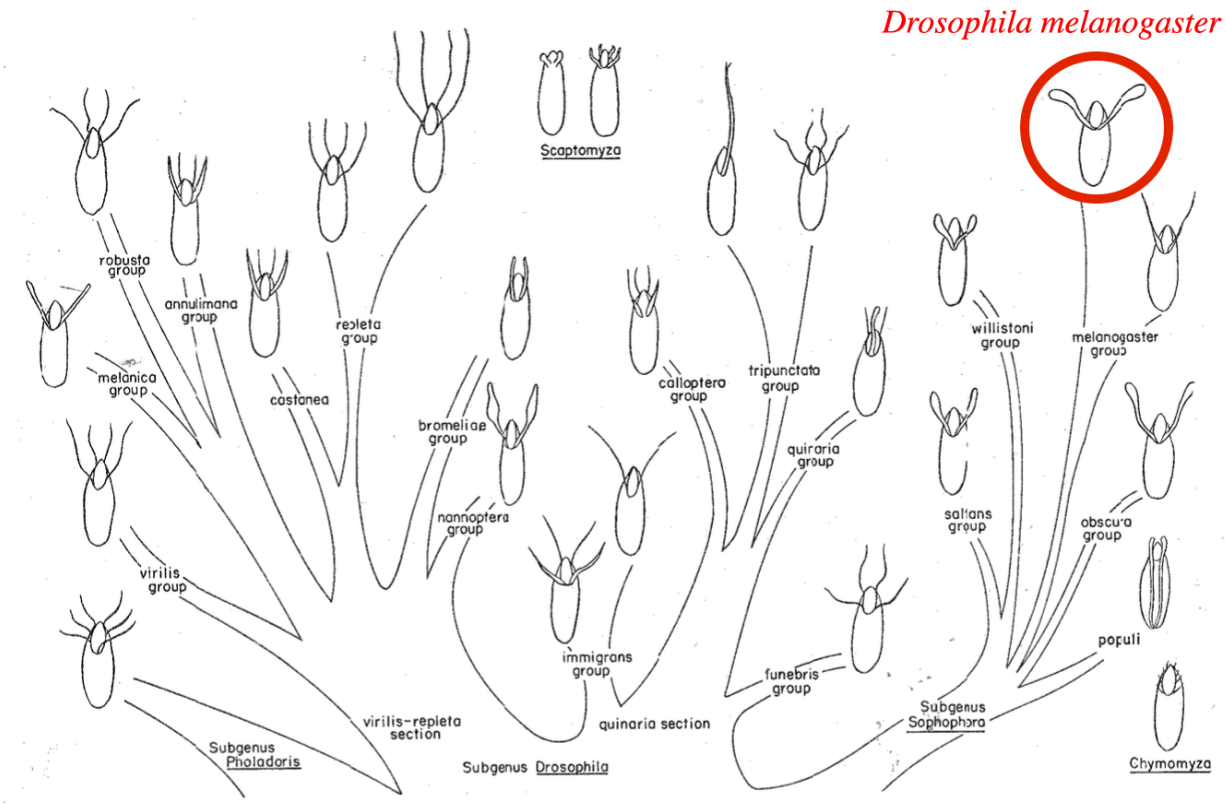

Figure 1.15 Eggshell and dorsal appendage (DA) diversity amongst the *Drosophilids*. All species of *Drosophila* have DAs, but the number, size, shape, orientation, and arrangement of these DAs vary between species, possibly correlating with oviposition preference (*i.e.,* egg-laying behavior) and food resources. **Drosophila melanogaster** possesses two dorsal, hockey stick-shaped DAs. (Adapted from Throckmorton, 1962).

contains a patch of ~65 cells (Dorman *et al.,* 2004, Ward and Berg, 2005; Peters and Berg, submitted) that express the transcription factor Broad (Deng and Bownes, 1997) and will form the outward facing roof of each DA tube. Adjacent to each patch of Broad-expressing cells, on the anterior and medial sides, is a single line of cells that express the protease Rhomboid (Ruohola-Baker *et al.,* 1993; Sapir *et al.,* 1998); these cells can be easily visualized with the *rhomboid-lacZ* marker, and they will form the inward facing floor of each DA tube. Once the fates and boundaries of these roof and floor cells have been established, all subsequent tube morphogenesis proceeds without cell division or apoptosis, and is driven exclusively by cell shape change, cell rearrangement, and cell migration.

During the transition between stages S10B and S11 of oogenesis, when the nurse cells begin to dump their cytoplasmic contents into the oocyte, the DA-tube cells thicken into a placode, initiate wrapping tubulogenesis, and create a rudimentary tube lumen. The relationship between DA-tube patterning and morphogenesis as well as the specific cell behaviors that drive DA-tube formation were first described in detail by Dorman and colleagues and have now been elaborated upon and mathematically modeled by Osterfield and colleagues (Fig 1.16; Dorman *et al.,* 2004; Fig 1.17; Osterfield *et al.,* 2013). The non-classical cadherin, Cad74A, also acts as a mediator of DA-tube patterning and morphogenesis (Zartman *et al.,* 2008). During DA-tube formation, the roof cells undergo apical constriction and bend the epithelium outward, as is quite common in invaginating, tube-forming epithelia (Dorman *et al.,* 2004). At the same time, the floor cells appear to experience high tension along their leading edge (anterior and medial), causing that edge to buckle and flip underneath. This process inverts the floor cells in terms of their apico-basal polarity and allows them to make new junctional contacts with each other and to seal off the DA-tube from underneath, much like vertebrate neurulation (Fig 1.17; Osterfield

et al., 2013). Though it has yet to be experimentally validated, precise characterization and computational modeling of floor cell behavior suggests that the floor cells may be the primary drivers of DA-tube formation (Osterfield *et al.,* 2013).

Once the DA-tube has formed, it elongates, turns, and widens during stages 12-14 until it reaches the anterior tip of the egg chamber and takes on a morphology resembling a hockey stick (Fig 1.16; Dorman *et al.,* 2004). This elongation of the DA-tube is driven by cell rearrangement, cell shape change, and cell migration. First, the roof cells intercalate and rearrange, converging toward the dorsal midline and extending anteriorly toward the nurse cells (Dorman *et al.,* 2004; Ward and Berg, 2005; see Chapter III). Second, the apices of the roof cells, which maintained equal AP/DV proportions throughout apical constriction, dramatically expand, but do so with a distinct AP bias so that they become much longer than they are wide. The anterior tube cell apices expand to a greater degree than posterior apices, creating the flattened, anterior paddle of the DA (see Chapter III). Finally, cell migration acts as a major driving force in DA tube elongation (Dorman *et al.,* 2004; see Chapter III). Even if apical expansion is perturbed, the basal surfaces of DA-tube cells migrate towards the anterior of the egg chamber (Boyle and Berg 2009). Additionally, the leading row of roof cells and the adjacent floor cells, particularly near the bend in the floor cell hinge, act as leaders during DA-tube elongation, and this function relies on trimeric G-protein signaling (Boyle *et al.,* 2010). Furthermore, the stretch cells, over which the DA-tube cells migrate, are important mediators of tubulogenic signals that emanate from the germline (Rittenhouse and Berg, 1995), acting through the non-receptor tyrosine kinases Shark and Src42A (Tran and Berg, 2003), and appear to be required for DA-tube guidance (Zimmerman *et al.,* in preparation). In summary, DA-tube elongation requires both autonomous inputs from DA-tube cells and non-autonomous inputs from the migratory substrate, and it is an

Fig 1.16. These schematics depict the relative positions and movements of roof cells (blue), floor cells (red), stretch cells (green), nurse cells (purple) and the oocyte (yellow) throughout DA tubulogenesis (stages 10B, early 11, late 11, late 12, 13, and 14). By the end of S10B, the roof and floor cells of each DA-tube primordium are distinct cell types and have thickened into a placode. In early S11, as the nurse cells initiate dumping, the roof cells initiate apical constriction and the floor cells begin to flip orientation and dive under the roof cells. By the end of S11, the roof cell apices are at their most constricted state, and the floor cells have zippered together and sealed off the floor of the DA tube, creating a rudimentary lumen. In S12, when the nurse cells have finished dumping, the roof cells intercalate in a manner similar to convergent extension, their apices begin to expand with an AP bias (see Chapter III), and the DA-tube lumen elongates along the AP axis. In S13, DA-tube elongation continues, the DA-tube bends to form the hockey stick shape, and the DA-tube cells reach the anterior of the egg chamber. Finally, in S14, the DA-tube paddle widens and flattens while elongation terminates. Throughout S11 — S14, roof cells secrete chorion proteins into the DA-tube lumen, forming the mature DA. (Reproduced from Dorman *et al.,* 2004).

Figure 1.16 Schematic representations of DA tubulogenesis in *Drosophila melanogaster*.

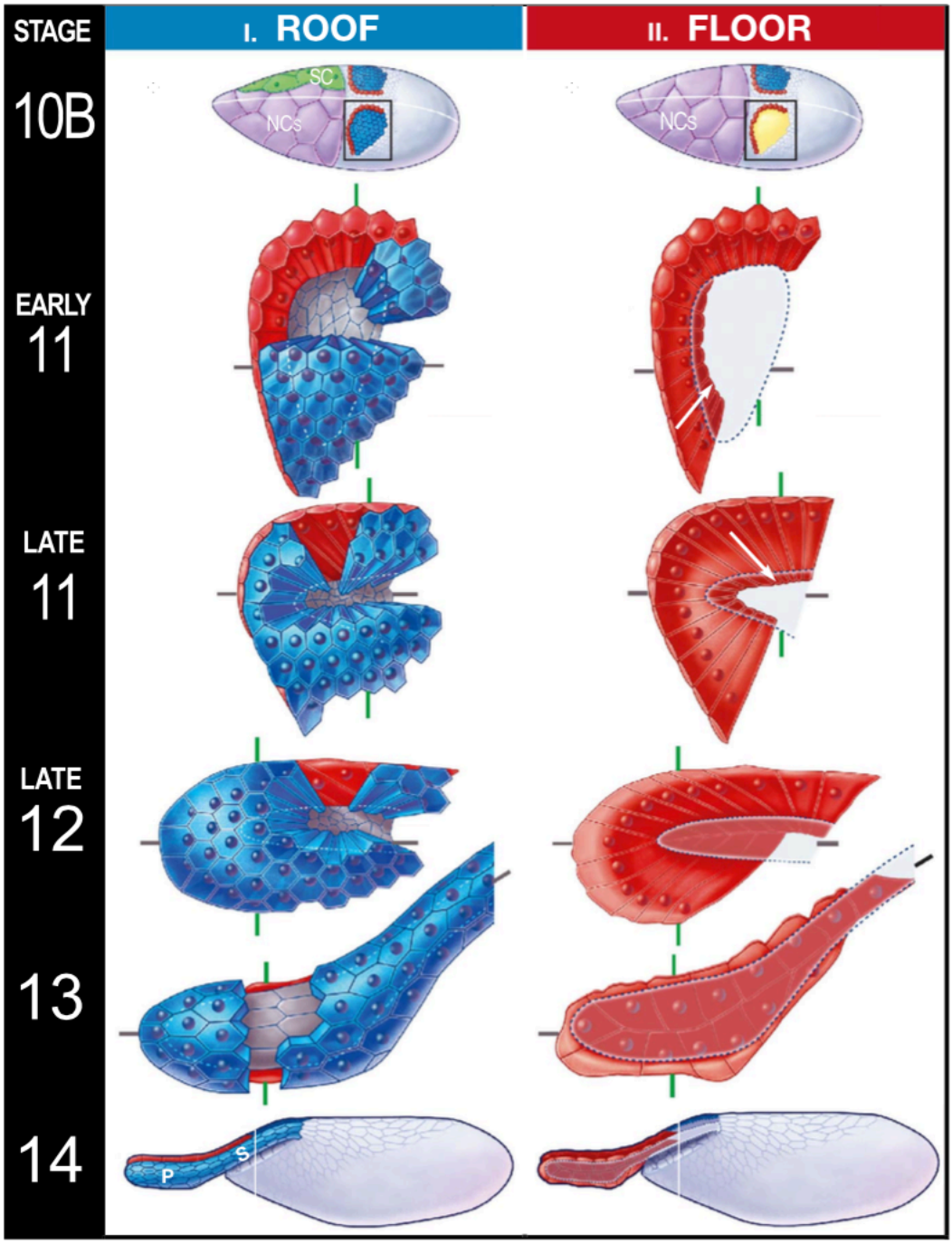

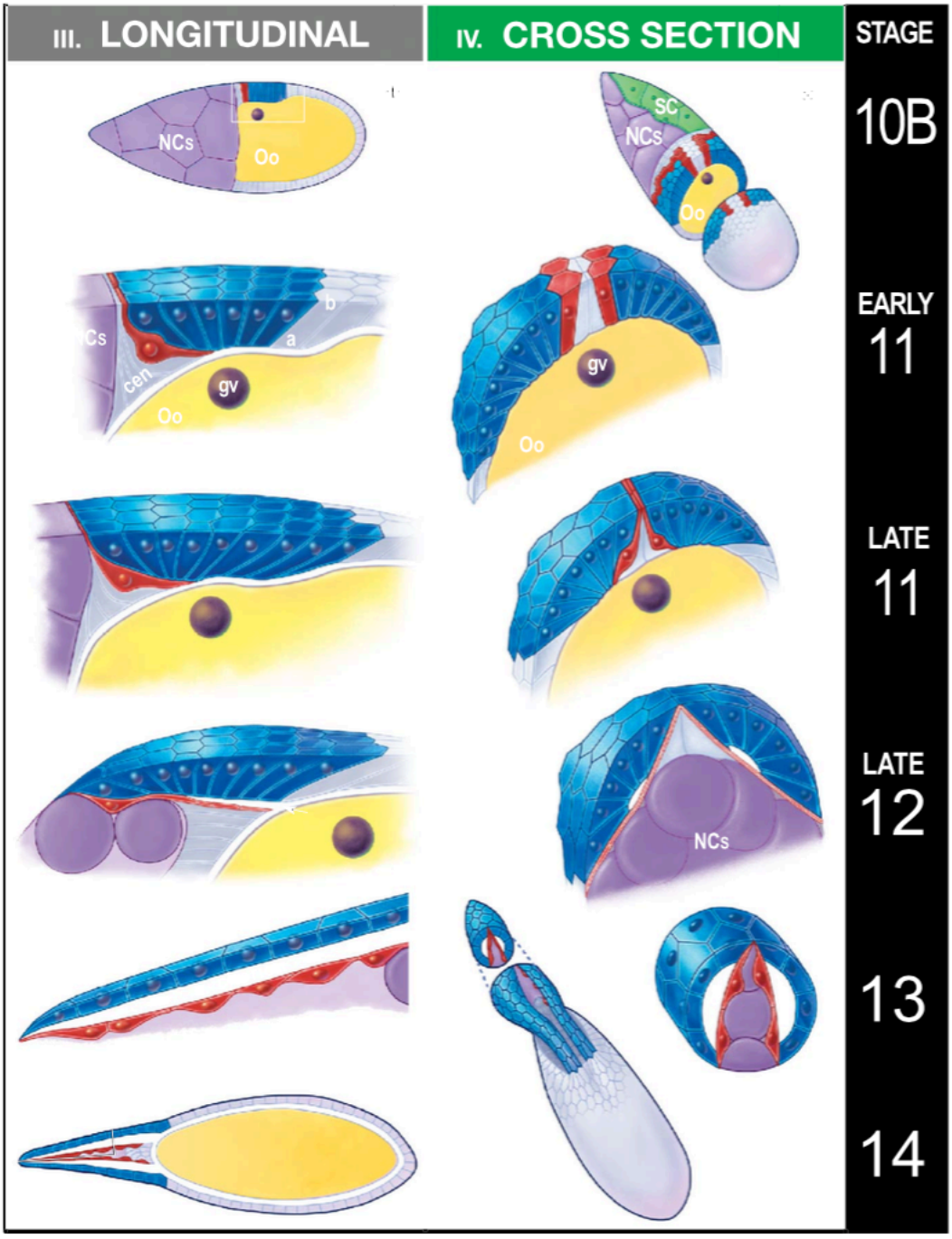
III. LONGITUDINAL
IV. CROSS SECTION
STAGE
10B
EARLY
11
LATE
11
LATE
12
13
14
NCs
Oo
SC
NCs
Oo
b
a
cen
gv
Oo
gv
Oo
NCs

Figure 1.17 Tension along the leading edge of the floor cells appears to be a major driver in the deformation of the follicular epithelium and, therefore, in DA-tube formation

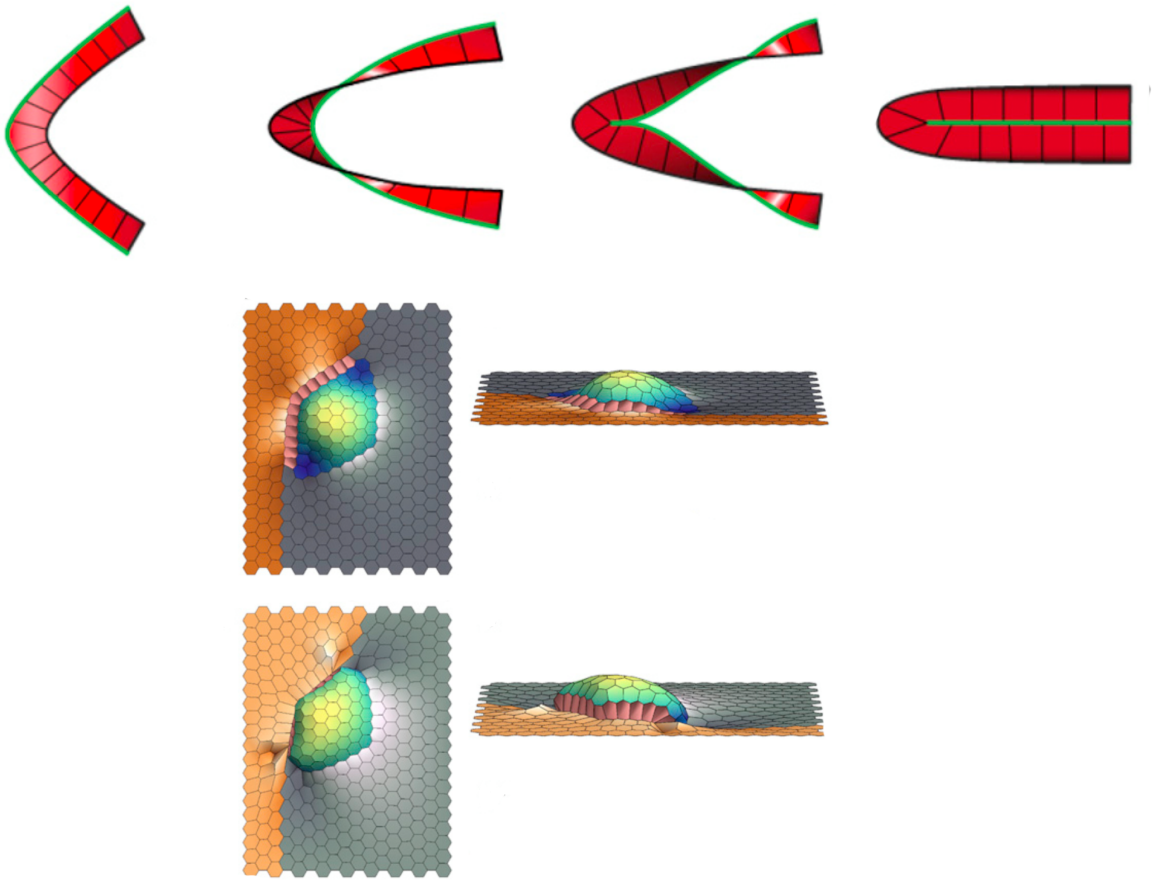

Fig 1.17. (Top panels) Increased tension along the leading edge (green) of the floor cells (red) causes the hinge to buckle and flip underneath the roof cells (not shown), so that apico-basal orientation of the floor cells is inverted, floor cells exchange contacts with adjacent follicle cells for other floor cells, and floor cells zipper together to seal the DA tube. (Bottom panels) 3D

modeling of this process supports the claim that that leading-edge tension in the floor cells is sufficient to deform the epithelial plane. (Adapted from Osterfield *et al.,* 2013).
exquisite model for understanding the contributions of cell shape change, rearrangement, and migration to epithelial tube elongation. For these reasons, and those listed above, I have made this process the focus of my graduate research.

From transcription to tubes

An overarching question in developmental biology is how regulated gene expression can poise and empower groups of cells to undertake and successfully negotiate the labyrinth that is morphogenesis. Understanding the morphogenesis of tubes is but a facet of understanding morphogenesis. Nevertheless, tubes, in all of their resplendent diversity, are essential to multicellular life, and they are absolutely worth the attention. Despite considerable functional differences, all tube functions rely on specific tube morphologies; therefore, understanding the journey from tube cells to tubulogenesis to terminal tube morphology is fundamental for understanding how multicellular life can exist. Where this tubulogenic journey begins is a bit of a "Chicken or the egg?" question, but let us say for now that this journey begins with signals that instruct certain groups of cells to become tubes. These signals, acting through conserved signaling pathways, regulate the activity of transcription factors, which go on to regulate the expression of genes. The resultant, specific patterns of gene expression equip cells with the molecular implements of tubulogenesis, implements that the cells then employ to execute the cell behaviors required for tubulogenesis. Although these transcription factors that equip cells for tubulogenesis may not be evolutionarily conserved for these precise purposes (they are

conserved in general), their downstream molecular effectors are sure to be, and so far have been required in diverse processes.

As discussed previously, many of the upstream signaling pathways that regulate and facilitate tubulogenesis are known, as well as their relationships to transcription factors that facilitate tubulogenesis. Understanding this portion of the tubulogenic program is far from complete, but comparatively, there has been far more research on cell-fate determining mechanisms than morphogenetic mechanisms (*e.g.,* dorsal appendage tubulogenesis, refer to previous section), and the relationship between transcription factors, molecular mechanisms, and cell behaviors is far less clear. Thus, I dedicated my graduate research to illuminating this "downstream" tenebrosity of tubulogenesis.

In *Drosophila melanogaster*, several transcription factors are associated with actually effectuating tubulogenesis, not just patterning tube-forming cells (*e.g.,* Twist (a bHLH or basic helix-loop-helix transcription factor) and Snail (a Zinc finger transcription factor) in ventral furrow formation in the fly embryo (Leptin and Grunewald, 1990), Broad (a Zinc finger transcription factor) in DA-tube formation (Tzolovosky *et al.*, 1999)). Forkhead (a FOX or Forkhead Box transcription factor) is required for apical constriction and salivary gland internalization (Myat and Andrew, 2000). Huckebein (a Zinc finger transcription factor) and Ribbon (a Pipsqueak domain transcription factor) regulate the cell-shape change that underlies larval salivary gland elongation (Bradley and Andrew, 2001; Myat and Andrew, 2002; Cheshire *et al.,* 2008; Kerman *et al.,* 2008) through promoting the expression of Crumbs, which is needed for apical membrane expansion in *Drosophila* and vertebrates (Knust, 1994; Gosens *et al.,* 2008). In the embryonic hindgut, STAT92E (a coiled coil transcription factor), an effector of the JAK/STAT pathway, regulates the cell rearrangement that drives epithelial tube elongation

(Johansen *et al.,* 2003). Trachealess (a BLH-PAS trancription factor) is required for apical constriction, enriching F-actin at the apical surface, and functions during tracheal cell invagination (Isaac and Andrew, 1996; Wilk et al., 1996; Llimargas and Casanova, 1999). Knirps and Knirps-related (both Zinc finger trancription factors) control cell migration and branching morphogenesis in the larval trachea (Chen *et al.,* 1998). Finally, Tramtrack69 (a Zinc finger transcription factor) regulates tube size in both the larval trachea and the dorsal appendages of the egg chamber (French *et al.,* 2003; Araujo *et al.,* 2007; Boyle and Berg, 2009; Boyle *et al.,* 2010; Rotstein *et al.,* 2011). If the downstream effectors of these *Drosophilid* tubulogenic transcription factors can be identified and validated, they could be compared to effector profiles from other metazoans transcription factors with tubulogenic roles (*e.g.,* GATA5 in zebrafish (Reiter *et al.,* 2001); Pitx1 in *Xenopus* (Chung *et al.,* 2010); TTF1, FOXA1, FOXA2 in the mouse lung (Maeda *et al.,* 2007)), our understanding of tubulogenesis and morphogenesis would be invaluably informed.

My personal tubulogenic adventure began with the *Drosophila* Zinc-finger transcription factor Tramtrack69, which is required for DA tubulogenesis (French *et al.,* 2003). Shortly after I began my graduate research, further work in our laboratory suggested that the role of Tramtrack69 during DA tubulogenesis was to regulate apical membrane expansion, a relatively understudied cell behavior (Boyle and Berg, 2009). With this knowledge in hand, I felt that seeking to understand what Tramtrack69 was doing in the ovary to promote DA tubulogenesis was a very enticing proposition. Thus, in the first stage of my graduate research, I employed microarrays, an ovary-specific *tramtrack69* mutant, *in situ* hybridization, and tissue-specific RNAi to identify and characterize downstream effectors of Tramtrack69 required for DA tube elongation (Peters *et al.,* 2013; see Chapter II). These efforts 1) identified a network of

Tramtrack69 tubulogenic effectors, including the homeobox transcription factor Mirror (which had previously been implicated only in DV patterning and not morphogenesis), the focal adhesion scaffold Paxillin, and the endocytic scissor Dynamin, and 2) identified regulatory interactions between several of these effectors (Peters *et al.,* 2013; see Chapter II). My work implicated novel effectors of tubulogenesis and laid the foundation for the second part of my graduate research.

"Following the tracks" (Peters *et al.,* 2013) laid by my prior graduate research led me to study the function of Dynamin and endocytosis in DA tubulogenesis, and these topics have been the focus of the latter years of my graduate research. These efforts have both identified novel roles, and expanded upon existing roles, for Dynamin in tubulogenesis (see Chapter III; Peters and Berg, submitted). I show that Dynamin is required for DA-tube closure, DA-tube cell intercalation, and biased apical-luminal expansion. I also show that Dynamin drives these processes through facilitating endocytosis of cell-cell and cell-matrix adhesions, and that the precise levels and localizations of these adhesions are critical for DA tubulogenesis. Dynamin-mediated endocytosis is implicated in a number of morphogenetic and tubulogenic processes from *Drosophila* (*e.g.*, salivary gland tubulogenesis (Pirraglia *et al.,* 2006; Pirraglia *et al.,* 2010); embryonic cellularization (Fabrowski *et al.,* 2013); stretch cell morphogenesis (Gomez *et al.,* 2012); DA tubulogenesis (Peters *et al.,* 2013); Peters and Berg, submitted; see **Chapters II and III**) to vertebrates (*e.g.*, zebrafish gut morphogenesis and gastrulation (Rodriguez-Fraticelli *et al.,* 2014; Lepage *et al.,* 2014); *Xenopus* gastrulation (Lee and Harland, 2010; Ogata *et al.,* 2007); mouse retinal morphogenesis and angiogenesis (Bogdanovic *et al.,* 2012; Lee *et al.,* 2014); rat dendrite morphogenesis (Gray *et al.,* 2005)), suggesting that its morphogenetic-tubulogenic functions are likely conserved.

In this dissertation, I emphasize the important role that transcription factors can play during active morphogenesis, beyond patterning and cell fate decisions. First, I functionally link two upstream, *Drosophilid*, tubulogenic transcription factors to a cohort of downstream, tubulogenic effectors, several of which had no previously documented tubulogenic function. Second, through characterization of the tubulogenic function of Dynamin in the *Drosophila* ovary, I support, and expand upon, previously demonstrated functions for Dynamin in the modulation of cell adhesion during metazoan morphogenesis. These efforts considerably augment our understanding of how regulated molecular interactions translate into coordinated cell shape changes and movements during epithelial tubulogenesis in the *Drosophila* ovary.

Chapter II

Following the "tracks": Tramtrack69 regulates epithelial tube expansion in the *Drosophila* ovary through Paxillin, Dynamin, and the homeobox protein Mirror.

– Summary –

Epithelial tubes are the infrastructure for organs and tissues, and tube morphogenesis requires precise orchestration of cell signaling, shape, migration, and adhesion. Follicle cells in the *Drosophila* ovary form a pair of epithelial tubes whose lumens act as molds for the eggshell respiratory filaments, or dorsal appendages (DAs). DA formation is a robust and accessible model for studying the patterning, formation, and expansion of epithelial tubes. Tramtrack69 (TTK69), a transcription factor that exhibits a variable embryonic DNA-binding preference, controls DA lumen volume and shape by promoting tube expansion; the *tramtrack* mutation *twin peaks* (ttk^{twk}) reduces TTK69 levels late in oogenesis, inhibiting this expansion. Microarray analysis of wild type and ttk^{twk} ovaries, followed by *in situ* hybridization and RNAi of candidate genes, identified the Phospholipase B-like protein Lamina ancestor (LAMA), the scaffold protein Paxillin, the endocytotic regulator Shibire (Dynamin), and the homeodomain transcription factor Mirror, as TTK69 effectors of DA-tube expansion. These genes displayed enriched expression in DA-tube cells, except *lama*, which was expressed in all follicle cells. All four genes showed reduced expression in ttk^{twk} mutants and exhibited RNAi phenotypes that were enhanced in a ttk^{twk}/+ background, indicating ttk^{twk} genetic interactions. Although previous studies show that

Mirror patterns the follicular epithelium prior to DA tubulogenesis, I show that Mirror has an independent, novel role in tube expansion, involving positive regulation of *Paxillin*. Thus, characterization of ttk^{twk}-differentially expressed genes expands the network of TTK69 effectors, identifies novel epithelial tube-expansion regulators, and significantly advances our understanding of this vital developmental process.

– Introduction –

Epithelial tubes are essential structures in metazoan organs and tissues and thus, errors during tube morphogenesis can have profound developmental consequences. Failure of gastrulation will arrest development and defects in neural tube closure may result in spina bifida or anencephaly (Botto *et al.,* 1999; Davidoff *et al.,* 2002; Wallingford, 2005; Ray and Niswander, 2012). Gaining insight into the molecular and cellular requirements of tubulogenesis will augment our understanding of this developmental process and illuminate underlying causes of developmental tube defects, leading to better diagnostics and treatments.

To create an epithelial tube, cells must adopt a tube fate distinct from neighboring cells, coordinate their movements to form rudimentary tubes, and expand those tubes into a terminal morphology (Andrew and Ewald, 2010). Tube-forming events involving epithelial sheets share common molecular and cellular mechanisms (patterning, adhesion, polarity, guidance, morphogenetic movements), but the network of effectors and pathways that coordinate these mechanisms, from cell fate to terminal tube morphology, is not well defined. To advance our understanding of these networks, I have identified and characterized downstream effectors of a key transcription factor that regulates tube morphogenesis in the *Drosophila* ovary.

My model for epithelial tubulogenesis resembles vertebrate neural tube formation and involves the synthesis of the dorsal appendages [DAs], respiratory structures of the eggshell (Dorman *et al.,* 2004). During oogenesis, egg chambers develop in an assembly-line fashion through 14 stages (S1-S14); a single layer of somatic, epithelial, follicle cells (FCs) envelops the developing germline (oocyte and nurse cells), undergoes coordinated morphogenesis to give shape to the egg, and secretes the eggshell (Spradling, 1993). This epithelium is polarized such that the apical surface contacts the germline and the basal surface faces outward. During stages

S10B through S14, when growth and cell division have ceased, two dorsal anterior groups of FCs become patterned through EGF, BMP, and Notch signaling, form tubes through apical constriction and zippering, and elongate the tubes by migrating anteriorly, expanding apices, and intercalating through convergence and extension (Fig 2.1A; Berg, 2005). The apical lumens of these tubes act as molds for the DAs of the mature eggshell, so although the FCs slough off during oviposition, the number, position, and morphology of the DA structures on laid eggs provide physical evidence for the efficacy of tube patterning and morphogenesis during oogenesis. Furthermore, since ovaries from well-nourished females contain all stages of egg chamber development, and since egg chambers can be dissected and cultured outside of the ovary, this system is ideal for investigating epithelial tube patterning, formation, and expansion (Berg, 2005).

The female sterile *tramtrack69 (ttk69)* mutant *twin peaks* (ttk^{twk}) produces eggs with severely stunted DAs and weak eggshells that cannot support fertilization. These defects are separable, the former resulting from a tube expansion defect (French *et al.,* 2003). In ttk^{twk} mutants, DA-tube cells undergo proper patterning and tube formation but fail to change shape and move during tube elongation. These cells retain some migratory ability and stretch along a correct, anterior path, but the DA tube itself fails to expand (Fig 2.1A; French *et al.,* 2003; Boyle and Berg, 2009).

What is the underlying mechanism of this failure in tube expansion? The ttk^{twk} mutation is an unusual, hypomorphic allele of the *tramtrack69* gene that does not influence viability or development; the ttk^{twk} *P*-element insertion disrupts a promoter required for late-oogenic *ttk69* expression, inducing visible defects only in the DAs and eggshell (French *et al.,* 2003).

TTK69 is a zinc-finger transcription factor originally identified as a repressor in

embryogenesis (Harrison and Travers, 1990; Brown *et al.,* 1991; Read *et al.,* 1992); it is also a founding member of the BTB protein family that shares a Bric-á-brac—Tramtrack—Broad protein-protein interaction domain (Godt *et al.,* 1993; Zollman *et al.,* 1994). Best known for its role downstream of Notch in repressing neural cell fates (Guo *et al.,* 1995), TTK69 also regulates diverse processes during fly development, from cell-cycle regulation to tracheal tubulogenesis (Baonza *et al.,* 1992; Araújo *et al.,* 2007). Genome-wide expression profiling in S2 cells (Reddy *et al.,* 2010) identified broad classes of TTK69-regulated genes: protein folding, mRNA splicing, cell proliferation, phagocytosis, tracheal development, and axon guidance. Microarray profiling of embryonic trachea (Rotstein *et al.,* 2011) indicated that TTK69 interacts with known pathways (*e.g., Notch*), and is upstream of known tracheal-tube size genes (*e.g.,* chitin metabolism, septate junction, polarity proteins), corroborating previous observations.

To define TTK69's regulatory role during epithelial tubulogenesis and to identify novel effectors, I exploited the unique *ttk69* allele, ttk^{twk}. I compared wild type and ttk^{twk} expression profiles via microarrays to identify direct and indirect targets of TTK69, and worked in collaboration with Nathaniel Thayer and Martin Tompa to evaluate the utility of TTK69-binding motifs as predictive tools. I then ascertained which TTK69-regulated genes are required for DA-tube expansion through *in situ* hybridization (ISH) and tissue-specific RNAi. These studies revealed regulatory links between TTK69 and known or novel tubulogenesis effectors, showed that TTK69-binding preference is highly variable, and demonstrated that *ttk69*'s influence extends beyond tubulogenesis.

– Materials and Methods –

Drosophila strains

For microarrays and *in situ* analyses, I compared *Canton S* wild type to homozygous *ry*^{506} *P{PZ}07223=P{ry+t7.2, PlacZ}ttk*^{twk} mutants (French *et al.,* 2003). For RNAi, I used *UAS-RNAi* transgenic strains from *Drosophila* stock centers (Table 2.1). *UAS-mirror* was a gift from Helen McNeill (McNeill *et al.,* 1997) and *UAS-Paxillin* (*UAS-GFP::Paxillin*) was a gift from Denise Montell (He *et al.,* 2010). *GAL4* driver strains were *w*; CY2-GAL4; ry*^{506} *ttk*^{twk}*/TM3* (Queenan *et al.,* 1997) and *w*; Vm26Aa-GAL4; ry*^{506} *ttk*^{twk}*/TM3*. To characterize *GAL4* expression (Fig 2.7A), I crossed *GAL4* lines to *UAS-GFP::moesin* (Bloor and Kiehart, 2001). To visualize floor cells, I used *y* w *; P{w+mC=Rho(ve)-lacZ.0.7}* (Ip *et al.,* 1992).

Vm26Aa-GAL4

To facilitate transcript production of *GAL4* (Furger *et al.,* 2002), Faith Hassinger added an intron into the *pGaTB GAL4* expression vector (Brand and Perrimon, 1993) to create *pF-GAL4*; she inserted a 150-bp fragment, containing splice donor, intron, and splice acceptor sequences from the *Cp36* gene, into the *hsp70* sequences that reside upstream of the Gal4 translational start site. To generate a *GAL4* driver specific to late-stage egg chambers, Scott Kerr used this modified *GAL4* vector to create *pVm26Aa-F-GAL4*. He inserted a 1047-bp PCR product from the *Vm26Aa* regulatory region, including ~950 bp of upstream sequences, the transcription start site, and the 5' UTR, upstream of the *Cp36* sequences. After verifying the construct by Sanger sequencing, he sent plasmid DNA to Rainbow Transgenics, who created >100 random insertion lines. Scott and Faith screened several hundred lines and selected the best expressing lines on X, 2 (used here), and 3. The *Vm26Aa* fragment was sufficient to direct

gene expression in columnar FCs from S10 onward (Jin and Petri, 1993). The complete *pVm26Aa-F-GAL4* plasmid sequence is available at NCBI (BankIt1606792 Seq1 KC664779).

Microarrays

Canton S and ttk^{twk} ovaries came from 36-hr-old females; for each sample (3 biological replicates for each condition), I dissected 50 ovary pairs into RNA*later*® (Life Technologies) and processed in <20 min to minimize experimental effects on gene expression. I extracted total RNA via the RNAqueous® Kit (Ambion), and Kurt Hardesty processed the RNA and microarrays at the UW Center for Array Technologies: they evaluated RNA quality via BioAnalyzer (Agilent); they used 100 ηg of total RNA to generate labeled probes via the Affymetrix GeneChip®3' IVT Express Kit (2008), and following fragmentation, they hybridized 10 μg labelled antisense RNA for 16hr at 45°C to GeneChip® *Drosophila* Genome 2.0 Arrays (>18,500 transcripts). They washed the arrays and stained in an Affymetrix Fluidics Station FS450 and scanned using an Affymetrix GeneChip® Scanner 3000 7G. Rob Hall then analyzed the data using GeneChip® Operating Software (GCOS) and the Microarray Suite version 5.0 (MAS 5.0) algorithm, and he used Expression Console (Affymetrix) for robust multi-chip analysis (RMA) normalization. I subsequently identified ttk^{twk}-differentially expressed genes via SAM (Significance Analysis of Microarrays), $q \leq 0.05$.

TTK69 Binding Preference

Using modENCODE data from 0-12-hr embryos (the modENCODE consortium *et al.*, 2012), Nathaniel Thayer and Martin Tompa used ChIP-Seq sequences from 384 TTK69-bound sites to generate a 21-bp TTK69-preferred motif (E-value = 2.2e-8) by employing the MEME-

ChIP algorithm (MEME-Suite; Bailey *et al*., 2009). They used TOMTOM (MEME-Suite) to search for similarities with published motifs, and FIMO (MEME-Suite) to examine motif-incidence within ttk^{twk}-differentially-expressed-gene promoters (including 2 kb upstream and 1 kb downstream).

In situ hybridization and immunostaining

Ariel Altaras and I worked closely with Sandra Zimmerman to optimize colorimetric and fluorescence, tyramide-amplified (Lecuyer *et al*., 2007) *in situ* hybridization (ISH) protocols for the ovary, and we formulated a protocol for dual immunostaining:FISH in the ovary (Zimmerman *et al*., 2013). For work described specifically in this dissertation, I generated probes from sequenced cDNA clones (Table 1; DGRC) with three exceptions: *ttk69*, *mirr*, and *Rac2*. For these genes, I amplified sequences unique to each gene from w^{1118} genomic DNA, cloned the sequences into TOPO-TA vectors (Invitrogen), and verified the clones by sequencing. For *ttk69*, I amplified 792 bp from the 3'-UTR of *ttk*, using sequence specific to the *ttk69* isoform (*ttk69*-FW: 5'-CGCTCTTCGGGATTTAGTTG-3'; *ttk69*-RV: 5'-GTTGGTTTTTGAGGGTGTGG-3'). For *mirr*, I amplified 419 bp from the *mirr* 3'-UTR, a region that is *mirr*-specific and shared by all *mirr* transcripts (*mirr*-FW: 5'-GCCGTAGTCACTCCCAGTTT-3'; *mirr*-RV: 5'-GCGTCGAATTGTTTGCATCT-3'). For *Rac2,* I amplified 389 bp (unique) from the *Rac2* 5'-UTR to corroborate full-length *Rac2* probe results that could reflect non-specific Rho-GTPase expression (*Rac2*-FW: 5'-TCTCTGTACGCGATTGCTTG-3'; *Rac2*-RV: 5'-GCAGAGGGTTTTTCAGTGGA-3'). To generate plots of late oogenesis expression (Figs 2.3, 2.4), I scored relative germline and FC expression in 7-50 egg chambers for each stage using a 0-2 scoring system (0 = weak/no

expression, 1 = moderate expression, 2 = strong expression). Each point represented the average score for a given stage, tissue type, and background. Kelsey Kaeding, one of the summer undergraduate students that I mentored, made a small but notable contribution to this scoring. Asterisks indicated significant differences (* = $p<0.05$, ** = $p<0.001$) calculated by Chi-square analysis. Table 2 includes qualitative descriptions of spatial expression. Ovary immunostaining was as described (Ward and Berg, 2005; Zimmerman *et al.,* 2013), using rabbit anti-β-galactosidase (preabsorbed-1:2000; Cappel), mouse anti-GFP (1:200, Molecular Probes/Invitrogen), mouse anti-BR-core (1:500, 25E9.D7-concentrate, DSHB; Emery *et al.,* 1994), mouse anti-α-Spectrin (1:50, 3A9-concentrate, DSHB; Dubreuil *et al.,* 1987), and goat anti-mouse Alexafluor 488-, 555-, and 647-conjugated antibodies (1:500, Molecular Probes/Invitrogen). Imaging was performed on a Zeiss 510 scanning confocal microscope or a Nikon Microphot FXA. Images were processed using Photoshop CS (Adobe), Helicon Focus (Helicon Soft Ltd.) and FIJI (ImageJ-based, NIH; Schindelin *et al.,* 2012).

Tissue-specific expression: GAL4-UAS

For RNAi assays, I crossed *GAL4*-bearing virgin females to *UAS-RNAi*-bearing (Table 2.1) males at 25°C; I mated female progeny of the desired genotype to w^{1118} males at 30°C in the presence of wet yeast, to optimize *GAL4* expression and egg production. After >24 hr at 30°C, I collected eggs over successive 8-12-hr periods on grape juice/agar plates, then rinsed, pooled, and mounted the eggs in Hoyer's medium (van der Meer, 1977). Robert Matlock, and undergraduate whom I mentored, assisted me for a small portion of this egg collection and preparation. For over-expression assays (*UAS-mirr* and *UAS-Pax*), I performed assays at 30°C and 25°C, to compare the effects of stronger and weaker *GAL4* expression, respectively. I

evaluated DAs using a 0-2 scoring system (0 = no DA defect, 1 = moderate DA defect, 2 = severe DA defect) and calculated an average score to facilitate comparison between strains. Moderate defects included rough/feathered DA shape, difference in DA length within the DA pair, wide DA paddles, wide DA shafts, and short DAs that extended past the micropyle. Severe DA defects included short and/or wide DAs not extending past the micropyle, fused DAs, or a combination of 2 or more category-1 criteria. Table 1 includes qualitative descriptions of DA morphology. I performed viability assays at 30°C as follows: after 8 hr of egg laying, I counted laid eggs; I then incubated plates at 25°C for an additional 30 hr, after which I counted unhatched eggs.

Accession Numbers

The microarray data discussed in this publication was deposited in NCBI's Gene Expression Omnibus (Edgar *et al*., 2002) and is accessible through GEO Series accession number GSE42758 (http://www.ncbi.nlm.nih.gov/geo/query/acc.cgi?acc=GSE42758).

– Results –

Microarray analysis of *twin peaks* (*ttk*^{twk}), a female-sterile *tramtrack69* mutant, reveals downstream genes during oogenesis

To identify TTK69 effectors in the ovary, I compared expression profiles between wild type and *ttk*^{twk} using microarrays (Fig 2.1B). This approach has been effective with whole ovaries (Jordan *et al*., 2005), staged egg chambers (Yakoby *et al*., 2008; Tootle *et al*., 2011), and purified follicle cells (Bryant *et al*., 1999; Wang *et al*., 2006). Although only a subset of FCs require TTK69 for DA-tube expansion (Boyle *et al*., 2010), I chose to analyze whole ovaries because this approach can identify differential gene expression associated with restricted FC-patterns (Jordan *et al*., 2005), the *ttk*^{twk} mutation is specific, affecting TTK69 production only during late oogenesis (French *et al*., 2003), and germline TTK69 expression is not required for DA-tube expansion (Boyle and Berg, 2009). To increase the likelihood of identifying gene-expression differences relevant to DA-tube expansion, I dissected wild-type and *ttk*^{twk} ovaries from ~36-hour-old females to ensure comparable distributions of late-stage (S10-S14) egg chambers. Using Affymetrix *Drosophila* 2.0 whole-genome arrays and Significance Analysis of Microarrays (SAM), I identified ~1000 differentially expressed transcripts in *ttk*^{twk} ovaries ($q \leq 0.05$), 251 of which displayed more than a 2-fold change in expression (Fig 2.1C; Gene Expression Omnibus: GSE42758).

As preliminary validation of array efficacy, I examined the expression data for expected features. I observed down-regulation of *ttk69* transcripts in *ttk*^{twk}, but transcripts from *ttk88*, a *tramtrack* isoform with no apparent ovarian function (French *et al*., 2003), remained low. *Chorion protein 16* (*Cp16*) transcripts were also reduced in *ttk*^{twk} (Table 2.1), corroborating

Fig 2.1. (**A**) WT vs. *ttk*^{twk} DA tubulogenesis, dorsal view. All subsequent images will be shown with the anterior facing left. S10B-S14 = late stages of oogenesis, DM = Dorsal Midline. Blue = DA-roof cells. Red = DA-floor cells. The roof cells above the dorsal midline in S11-S14 are transparent to show the underlying DA-tube lumen (black). From S10B-S12, *ttk*^{twk} resembles WT. During S13-S14, WT DA tubes expand but *ttk*^{twk} DA tubes do not (indicated by orange). (**B**) Experimental pipeline. (**C**) Genes with significant differential expression in *ttk*^{twk} ($q \leq 0.05$), plotted using mean log2-expression values for WT and *ttk*^{twk}. Colors represent degree of raw fold change. *ttk*^{twk}-down-regulated genes are above the dotted line (0-fold change) and *ttk*^{twk}-up-regulated genes are below. (**D**) Subset of *ttk*^{twk}-differentially expressed genes (*i.e.*, panel C) with FIMO motif incidence >1. Colors indicate number of TTK69 motif instances in a gene's promoter. (E) Subset of *ttk*^{twk}-differentially expressed genes selected for subsequent analysis.

Fig 2.1. ***twin peaks (ttk^{twk})*** **a female sterile** ***tramtrack69*** **mutation, affects gene expression during late oogenesis.**

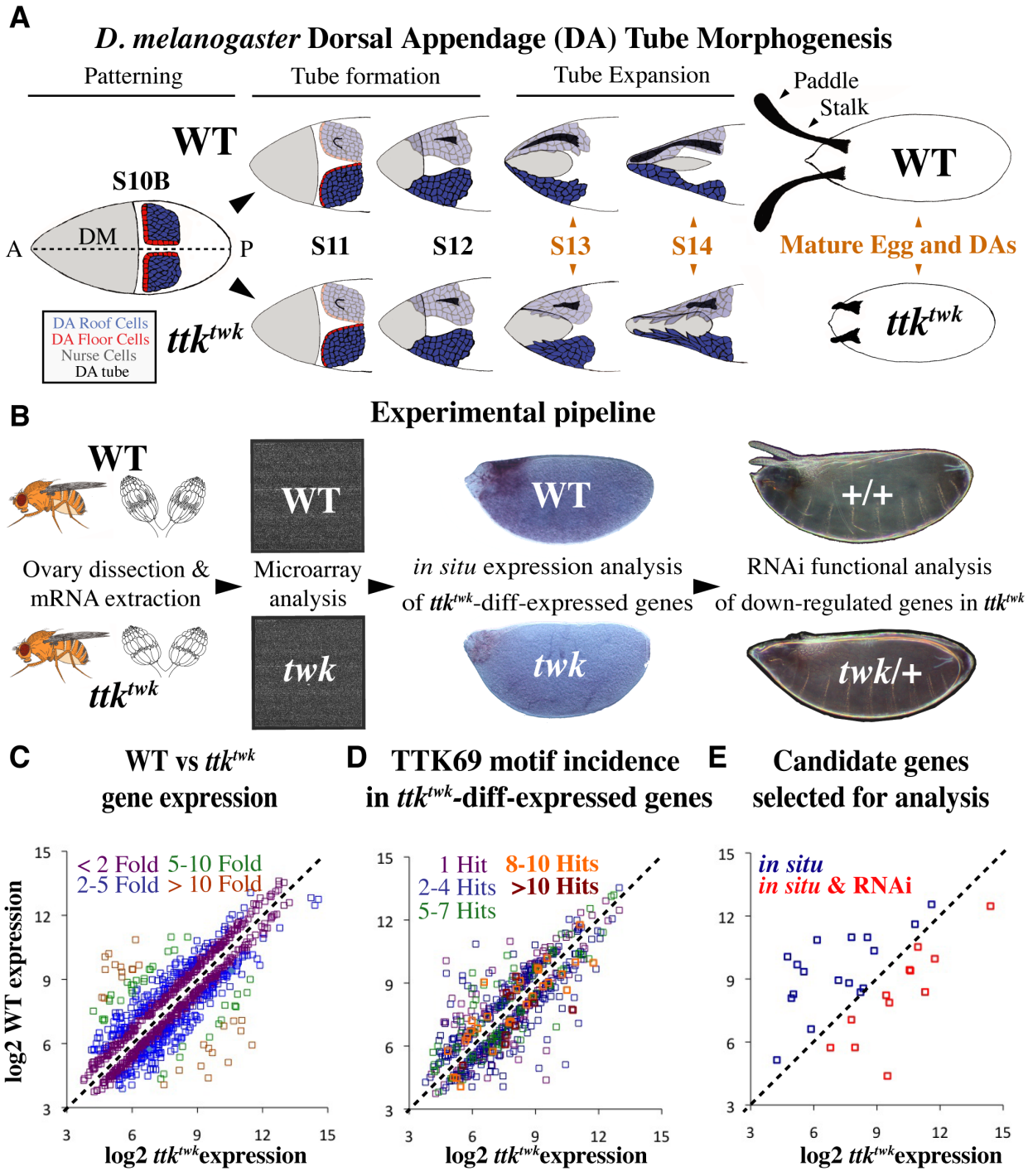

previous northern blot analysis (French *et al*., 2003). Consistent with *ttk*^{twk}'s fragile eggshell phenotype, I noted decreased transcript levels for other eggshell genes (*Cp18*, *Cp19*, *Cp7fa, CG15570,* and *CG15571*) and for an upstream regulator of eggshell gene expression, *Cytochrome P450-18a1* (*Cyp18a1;* Tootle *et al*., 2011). These data validate my whole-ovary microarray approach.

In addition to eggshell genes, *ttk*^{twk} altered expression of genes involved in metabolism, response to stress, DNA repair, ion transport, cell-cycle regulation, or phagocytosis; ~42% of differentially expressed genes had no known function. The most enriched gene ontology terms were associated with mitochondrial functions (e.g., oxidoreductase, electron acceptor, heme), eggshell synthesis (chorion), or the cytoskeleton (actin). These results were consistent with genome-wide proteomic analyses in S2 cells that show that TTK69 is present in a complex with the mitochondrial transcription factor TFAM (Guruharsha *et al*., 2011) and substantiate TTK69's role in eggshell and cytoskeletal regulation.

modENCODE data provide insight into TTK69-binding preference

To understand the relationship between TTK69 binding and the ~1000 genes that were differentially expressed in *ttk*^{twk}, and to potentially make predictions about direct vs. indirect TTK69 interactions, Nathaniel Thayer and Martin Tompa utilized MEME SUITE software components MEME-ChIP, TOMTOM, and FIMO (Bailey *et al*., 2009) to analyze modENCODE ChIP-Seq TTK69-binding data from 0-12hr embryos (384 bound sites; The modENCODE Consortium *et al*., 2010). They generated a preferred binding motif for TTK69 with MEME-ChIP (Multiple Em for Motif Elicitation, ChIP-optimized; Fig 2.2A). TOMTOM, a motif-database scanning algorithm, showed that this motif partially matched another proposed

Tramtrack motif generated by meta-analysis of experimental data (Kulakovskiy and Makeev, 2009). They then searched for the modENCODE motif within promoters of *ttk*^{twk}-differentially expressed genes using FIMO (Find Individual Motif Occurrences). 54% of *ttk*^{twk}-differentially expressed genes possessed ≥1 FIMO promoter hit, with 120 genes possessing ≥5 hits and 16 genes possessing ≥10 hits (Fig 2.1D; Table S1). These data suggested that TTK69 both directly and indirectly regulated the expression of target genes. With the caveats that the modENCODE motif was derived from sites identified in embryos, and the MEME analysis indicated that TTK69-binding preference was variable, I considered these FIMO results when selecting candidates for further analysis.

Figure 2.2. TTK69 preferred embryonic binding motif

A

MEME-ChIP
TTK69 binding motif
(modENCODE data)

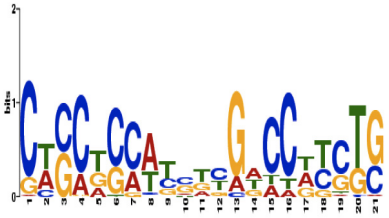

E-value = 2.2e-8

Fig 2.2. (**A**) This DNA-binding motif was generated from modENCODE ChIP-Seq data generated from 1-12-hr-old embryos, using MEME-ChIP software. Horizontal values represent nucleotide position and font height represents nucleotide preference.

Table 2.1. Down-regulated (top) and up-regulated (bottom) genes are listed alphabetically. cDNA clones are from the *Drosophila* Genomics Resource Center (DGRC) except where indicated (*; see Methods). Letters preceding RNAi stock ID indicate origin (V=VDRC, B=Bloomington, N=NIG-Fly).

Table 2.1. *ttk*^{twk}-differentially expressed genes selected for expression and functional analyses

Gene	Gene Symbol	Gene ontology (biological process)	Probed Transcript	Raw fold change in ttk^{twk}	TTK69 motif incidence	cDNA clone ID	RNAi stock ID
Activity-regulated cytoskeleton associated protein 1	*Arc1*	behavioral response to starvation; muscle system process	CG12505-RA	-3.43	9	LD41905	V 109141
CG31918	*CG31918*	proteolysis	CG31918-RA	-4.63	3	LD31822	V 12276
Chorion protein 16	*Cp16*	eggshell chorion assembly	CG6533-RA	-3.81	2	NA	V 104999
Cytochrome P450-12d1-d1	*Cyp12d1-d*	oxidation reduction process	CG18240-RA	-32.67	0	LD34576	V 109256
Cytochrome P450-18a1	*Cyp18a1*	chorion-containing eggshell formation; pupation; metamorphosis; imaginal disc-derived leg morphogenesis; ecdysteroid catabolic process; prepupal development	CG6816-RB	-3.29	5	RE70470	V 104180
Glutathione S transferase E1	*Gst-E1*	response to heat; glutathione metabolic process	CG5164-RA	-7.52	4	GH14654	V 110529
katanin 80	*kat80*	microtubule severing; microtubule-based process	CG13956-RB	-2.19	12	LD44201	V 105822
lamina ancestor	*lama*	inter-male aggressive behavior; imaginal disc development	CG10645-RC	-1.35	0	LD13253	V 107629
mirror	*mirr*	smoothened signaling pathway; embryonic development via the syncytial blastoderm; equator specification; negative regulation of transcription from RNA polymerase II promoter; imaginal disc-derived wing morphogenesis; dorsal appendage formation; compound eye morphogenesis; peripheral nervous system development	CG10601-RA	-2.08	2	* see methods	B 31907 V 22841 V 22843 V 50133 V 50134
Paxillin	*Pax*	wing disc development; regulation of Rho GTPase activity; leg disc development; regulation of autophagy	CG31794-RC	-2.31	2	SD04793	N 18061R-2
Rac2	*Rac2*	morphogenesis of an epithelium; phagocytosis	CG8556-RA	-2.30	1	GM13874 & * see methods	V 50349
scramblase2	*scramb2*	synaptic transmission; phospholipid scrambling	CG1893-RA	-7.73	11	CH10494	V 104627
shibire (dynamin)	*shi*	biological regulation; localization; learning or memory; cellular component organization or biogenesis; mating; synaptic transmission; open tracheal system development; associative learning; courtship behavior; multicellular organism reproduction	CG18102-RC	-1.66	1	LD21622	V 105971
centaurin beta 1A	*cenB1A*	cell morphogenesis; phagocytosis, engulfment	CG6742-RA	1.74	1	GM06875	
CG12560	*CG12560*	unknown	CG12560-RA	13.93	1	IP09321	
CG1824	*CG1824*	transmembrane transport	CG1824-RA	1.15	0	GH19726	
CG31673	*CG31673*	oxidation-reduction process	CG31673-RA	5.39	1	LD14730	
CG7997	*CG7997*	carbohydrate metabolic process	CG7997-RB	9.13	2	LD13649	
Cytochrome P450-9b2	*Cyp9b2*	oxidation-reduction process	CG4486-RA	25.99	1	GH08116	
huckebein	*hkb*	central nervous system development; tube morphogenesis; glial cell differentiation; lateral inhibition; cellular membrane organization; negative regulation of transcription from RNA polymerase II promoter; germ cell migration; endoderm development; salivary gland morphogenesis	CG9768-RA	1.88	4	RE60512	
nervana3	*nrv3*	potassium ion transport; ATP metabolic process; sodium ion transport	CG8663-RA	9.19	0	RH24769	
plexin B	*plexB*	axon guidance	CG32010-RA	8.88	0	RE22882	
Rab40	*Rab40*	intracellular signaling, regulation of cell shape	CG1900-RA	36.25	1	LD16331	
rolled (MAPK)	*rl*	biological regulation; response to stimulus; cellular component organization or biogenesis; post-embryonic organ morphogenesis; response to stress; cellular process; appendage development; response to organic substance; instar larval or pupal morphogenesis; response to DNA damage stimulus; positive regulation of cell proliferation; cellular response to metal ion; cellular response to arsenic-containing substance	CG40190-RA	1.93	0	RE08694	
roughest	*rst*	homophilic cell adhesion; compound eye development; lateral inhibition; regulation of striated muscle tissue development; compound eye morphogenesis	CG4125-RA	2.75	0	RE01586	
kin of irre	*kirre*	myoblast fusion; nephrocyte filtration; homophilic cell adhesion; larval visceral muscle development; heterophilic cell-cell adhesion; regulation of striated muscle tissue development; garland nephrocyte differentiation; nephrocyte diaphragm assembly; compound eye morphogenesis	CG3653-RB	3.36	8	LD21513	
SRPK	*SRPK*	protein phosphorylation	CG8174-RA	1.09	0	AT02510	
Beadex	*Bx*	imaginal disc-derived leg segmentation; inter-male aggressive behavior; leg disc development; locomotor rhythm; imaginal disc-derived wing morphogenesis; response to cocaine; phagocytosis, engulfment	CG6500-RA	2.04	0	GM05069	
CG18628	*CG18628*	unknown	CG18628-RA	22.32	3	GH08251	
βv integrin	*βInt-v*	olfactory behavior; melanotic encapsulation of foreign target; muscle cell homeostasis; imaginal disc-derived wing morphogenesis	CG1762-RA	1.68	1	LD09848	

TTK69 positively and negatively regulates FC gene-expression

To confirm that my array data reflected actual gene-expression differences during oogenesis, I selected candidate genes and used *in situ* hybridization (ISH) to compare transcript levels between wild-type and *ttk*^{twk} ovaries. Using gene ontologies and the literature, I identified genes with functions relevant to tube expansion (cytoskeletal regulation, cell adhesion, migration, vesicle trafficking; Lubarsky and Krasnow, 2003). I selected genes with a wide range of expression changes, reasoning that large differences would be more readily discernable by ISH, and that small differences could also be relevant, since mRNA differences in DA-tube-forming cells might be subtle relative to total mRNA from whole ovaries. To provide additional diversity to my candidate pool, I selected both up- and down-regulated genes, genes with a range of FIMO-motif hits, and un-annotated genes (Fig 2.1E; Table 2.1).

I compared transcript abundance and localization for 29 genes in wild type and *ttk*^{twk} ovaries by colorimetric ISH, and for FC-expressing genes, also by fluorescent ISH (FISH), noting the expressing tissue (germline, FC, both) and any spatially restricted expression (Figs. 2.1E, 2.3, 2.4; Tables 1, 2). I generated expression timelines by assessing relative expression at each late-oogenic stage (Fig 2.3C, F, I, L; Fig 2.4A"-L"). For most transcripts (24/29), I observed *ttk*^{twk}-differential gene expression as predicted by the arrays. Some transcripts exhibited subtle changes, but none contradicted the array results (Table 2; Figs. 2.3, 2.4). In addition to FC expression, I discovered that TTK69 influences gene expression in the germline. Indeed, more than half (18/29) of the tested genes displayed germline expression, with 12 appearing to express strictly in the germline (Table 2; Fig 2.4). Since germline *ttk*^{twk} clones do not result in DA defects (Boyle and Berg, 2009), however, and since TTK69 is required specifically in FCs for DA-tube expansion (Boyle *et al.,* 2010), I focused my attention on the most relevant genes, those

with FC expression (15/29; Figs. 2.3, 2.4; Table 2).

Of the 24 genes for which I observed *ttk*^{twk}-differential gene expression, 8 genes displayed uniform FC expression and/or mixed FC-germline expression. I observed expression in all FCs for three genes: *lamina ancestor (lama)*, *Cyp18a1*, and *Cyp9b2*. *lama* and *Cyp18a1* transcripts were substantially reduced in *ttk*^{twk} (Fig 2.3A-C; Fig 2.4D-D"), whereas *Cyp9b2* expression increased in *ttk*^{twk} (Fig 2.4B-B"). Interestingly, late wild-type *Cyp9b2* transcripts were enriched in anterior FCs relative to other FCs, while in *ttk*^{twk} this pattern was reversed. One gene, *rolled (rl*; MAPK) was detected in all cell types, FC and germline, and expression increased slightly in *ttk*^{twk} (Table 2). Four genes displayed late FC-expression in anterior FCs (including DA-tube cells) and germline expression at earlier stages: *shibire* (*shi*; dynamin*)*; *huckebein* (*hkb*), *Rab40*, and (*centaurin beta 1A* (*cenB1A*). The level of *shi* transcripts was reduced in *ttk*^{twk}, particularly in anterior FCs (Fig 2.3D-F), whereas levels increased uniformly for *hkb*, *Rab40,* and *cenB1A* (Table 2).

Notably, 7 genes displayed expression in specific FC-types: *CG7997*, *nervana 3* (*nrv3*), *Cytochrome P450-12d1* (*Cyp12d1*), *Glutathione S transferase E1* (*GstE1*), *Rac2*, *Paxillin* (*Pax*), and *mirror* (*mirr*). *CG7997* transcripts were restricted to the squamous stretch FCs that envelop the nurse cells, while *nrv3* transcripts were restricted to the columnar FCs covering the oocyte; in *ttk*^{twk}, both *CG7997* and *nrv3* mRNA levels were higher than in wild type (Fig 2.4A-A"; Table 2). *Cyp12d1* transcripts were present in anterior FCs during late oogenesis (S13+), and were absent in *ttk*^{twk} (Fig 2.4C-C"). *GstE1* expression began in all columnar FCs at S10, later appeared in small patches of anterior FCs (Fig 2.4E), and was absent in *ttk*^{twk} (Fig 2.4E'-E"). *Rac2* transcripts were visible in stretch FCs from S10-12, and in DA-tube cells at S12 (Fig 2.4K; inset, white arrowheads); levels were slightly reduced in *ttk*^{twk} (Fig 2.4K-K"; black arrowhead).

Table 2.2. ISH analysis of *ttk*^{twk}-differentially expressed genes

Gene Symbol	ISH Rxn. Time (min., for 1:500 dilution)	Expressing Tissue	FISH?	Relative wild-type expression	Relative ttk^{twk} expression	*in situ*-verified differential *ttk*^{twk} Expression	Validates
Arc1	50	germline		strong, germline	weak, germline	decrease	yes
CG31918	200	germline		weak, germline	weak, germline	decrease	yes
Cyp12d1-d	45	anterior FCs	X	strong, anterior FC	no visible expression	decrease	yes
Cyp18a1	35	all FCs	X	strong, all FC	moderate, all FCs	decrease	yes
Gst-E1	40	all FCs	X	moderate, all FC,	no visible expression	decrease	yes
kat80	45	germline	X	strong, germline	weak, germline	decrease	yes
lama	45	all FCs	X	strong, all FC	moderate, all FCs	decrease	yes
mirr	40	dorsal FC 'saddle'	X	strong, FC 'saddle' at S10, DA-tube cells from S13-14	moderate, FC 'saddle', no late expression	decrease	yes
Pax	40	DA tube FCs	X	weak, all FC, strong, DA FCs	very weak, DA tube FCs	decrease	yes
Rac2	60	stretch FCs and DA tube FCs	X*	strong, stretch FC and DA FC	moderate, stretch FC and DA FC	decrease	yes
scramb2	60	germline		strong, germline	no visible expression	decrease	yes
shi	45	germline and FCs	X	strong, germline, moderate, anterior FC	moderate, germline, weak, anterior FC	decrease	yes
cenB1a	70	germline and FCs		moderate, germline, strong, all FC	moderate, germline, very strong, all FC	increase	yes
CG12560	65	germline		no visible expression	moderate, germline	increase	yes
CG1824	65	germline		no visible expression	moderate, germline	increase	yes

Gene Symbol	ISH Rxn. Time (min., for 1:500 dilution)	Expressing Tissue	FISH?	Relative wild-type expression	Relative ttk^{twk} expression	*in situ*-verified differential ttk^{twk} Expression	Validates
CG31673	120	germline		no visible expression	moderate, germline	increase	yes
CG7997	60	stretch FCs	X	weak, stretch FC	strong, stretch FC	increase	yes
Cyp9b2	35	all FCs	X	strong, all FC, very strong, anterior RC	very strong, all FC	increase	yes
hkb	45	germline and anterior FCs		strong, germline, strong, anterior FC	very strong, germline, very strong, anterior FC	increase	yes
nrv3	200	columnar FCs		very weak, columnar FC	moderate, columnar FC	increase	yes
plexB	45	germline		moderate, germline	strong, germline	increase	yes
Rab40	70	germline and anterior FCs		strong germline, strong, anterior FC	very strong germline, very strong, anterior FC	increase	yes
rl	80	germline and FCs		moderate, germline, FC	strong, germline, FC	increase	yes
rst	45	germline		strong, germline	very strong, germline	increase	yes
kirre	120	germline puncta		moderate, germline	moderate, germline	no visible diff. expression	no
SRPK	40	germline		strong, germline	strong, germline	no visible diff. expression	no
Bx	40	germline		strong, germline	strong, germline	no visible diff. expression	no
CG18628	O/N	?		no visible signal	no visible signal	NA	no
βInt-v	O/N	?		no visible signal	no visible signal	NA	no

Table 2.2. Down-regulated genes (top), up-regulated genes (middle), and genes with inconclusive ISH results (bottom) are listed alphabetically.

Fig 2.3. WT (**A,D,G,J**) vs. *ttk*^{twk} (**B,E,H,K**) mRNA expression for *lamina ancestor (lama)*, *shibire (shi)*, *Paxillin (Pax)*, and *mirror (mirr)*. (**A-K'**) All images are oriented with anterior to the left. Dotted lines indicate the dorsal midline and insets indicate egg chamber orientation and stage. Scale bar = 50 μm. (**C,F,I,L**) Plots generated using a 0-2 scoring system (0 = weak/no expression, 1 = moderate expression, 2 = strong expression); asterisks indicate significant differences (see Methods); blue solid lines = WT, red dashed lines = *ttk*^{twk}. (**A-C**) From S10A-S12, *lamina ancestor* mRNA is visible in all FCs and is reduced in *ttk*^{twk}. (**D-F**) From S11-13, *shibire* (dynamin) mRNA is visible in anterior FCs and nurse cells and is reduced in *ttk*^{twk}. (**G-I**) From S10B-S13, *Paxillin* mRNA is enriched in DA-tube cells, and expression is almost absent in *ttk*^{twk}. (**J-L**) Previous studies show that *mirror* is expressed in a dorsal anterior saddle at S10B. I find new expression at S13 in DA-tube cells. In *ttk*^{twk}, *mirr* mRNA expression is significantly reduced at S10B and is absent at S13-14.

Figure 2.3. FISH demonstrates FC *ttk*^{twk} differential gene expression and reveals patterns relevant to DA-tube expansion.

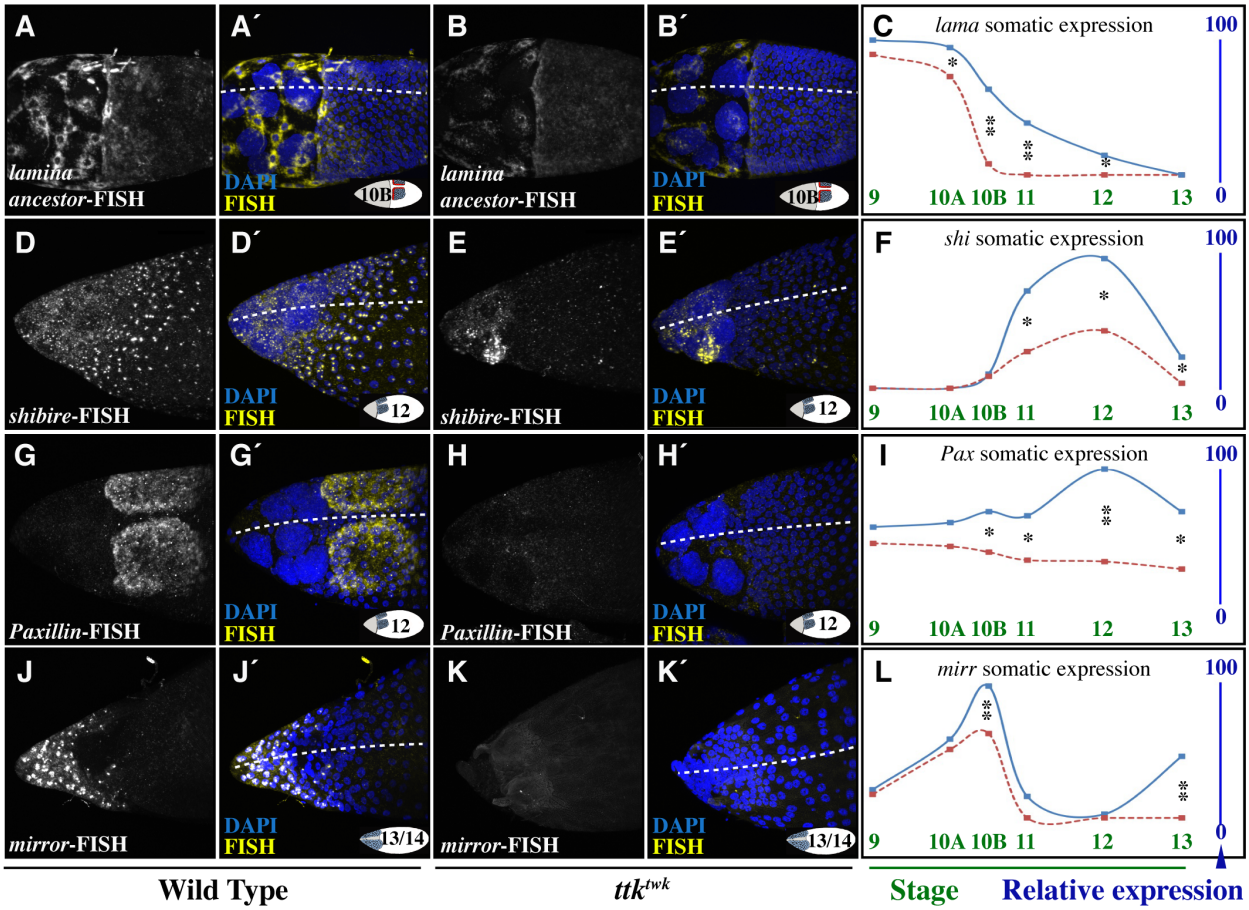

Fig 2.4. WT vs. *ttk*^{twk} gene expression for *ttk*^{twk}-differentially expressed genes, shown by FISH (**A-F''**) and colorimetric ISH (ISH; **G-L''**). Plots generated from ISH data, asterisks indicate significant differences (see Methods). (**A-A''**) *CG7997* expression in stretch FCs increases in *ttk*^{twk}. (**B-B''**) *Cyp9b2* expression in anterior FCs is absent in *ttk*^{twk}, and high in *ttk*^{twk}-main body FCs. (**C-C''**) *Cyp12d1* expression in anterior FCs is absent in *ttk*^{twk}. (**D-D''**) *Cyp18a1* expression in all FCs is reduced in *ttk*^{twk}. (**E-E''**) *Gst-E1* expression in stretch FCs and anterior FCs, with sporadic expression in DA floor cells (yellow arrowhead), is reduced in *ttk*^{twk}. (**F-F''**) *kat80* germline expression is reduced in *ttk*^{twk}. (**G-G''**, **J-J''**, **L-L''**) *Arc1*, *CG31918*, and *scramb2* germline expression is reduced in *ttk*^{twk}. (**H-H''**, **I-I''**) *CG12560* and *CG31673* germline expression is visible in *ttk*^{twk}, but not in WT. (**K-K''**) *Rac2* expresses in DA-tube FCs (**K**, *inset, white arrowheads [*Rac2*-full length probe]) and stretch FCs. Rac2-specific probe confirms DA-tube FC-expression (**K**, black arrowhead) and indicates slight reduction in *ttk*^{twk} (**K'**, black arrowhead). In plots, blue solid lines and red dashed lines represent WT and *ttk*^{twk}, respectively. Scale bars, 50 μm.

Figure 2.4. FISH/ISH demonstrates *ttk*^{twk} differential gene expression.

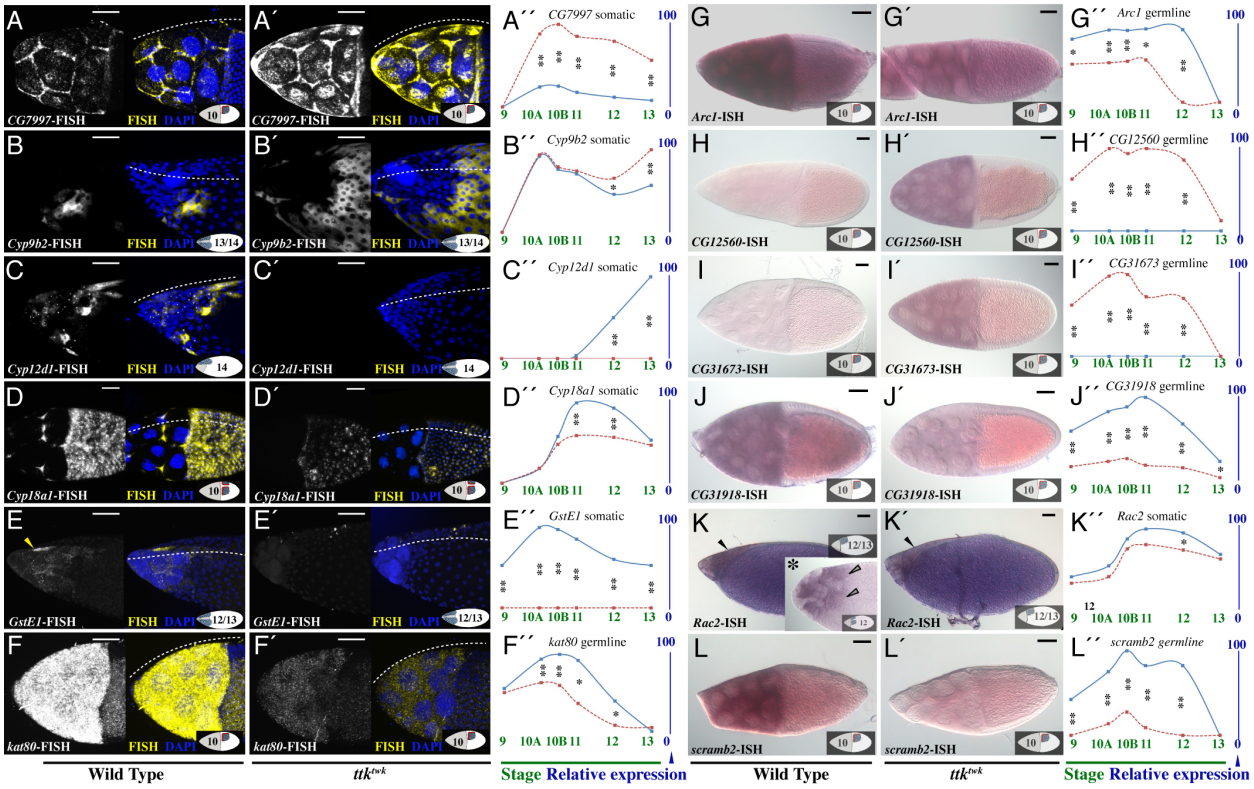

Fig 2.5. Timeline of *Pax* expression during late oogenesis (S10B-S14), visualized by dual immunostaining:FISH. (**A**-**F**) DAPI nuclear stains reveal stage. (**A'**-**F'**) *rhomboid-lacZ*, visualized by anti-βGal immunostaining, marks DA floor cells; α-Spectrin protein immunostain distinguishes cell membranes. (**A''**-**F''**) *Pax* mRNA levels in the DA-tube cells are dynamic, peaking at S12 prior to DA tube expansion. (**A'''**-**F'''**) *Pax* mRNA expresses in floor cells (*rhomboid-lacZ*) and overlying roof cells. Dotted lines = dorsal midlines; insets = egg chamber orientation and stage; scale bar = 50 μm.

Figure 2.5. *Paxillin* expression in DA-tube cells peaks immediately prior to tube expansion.

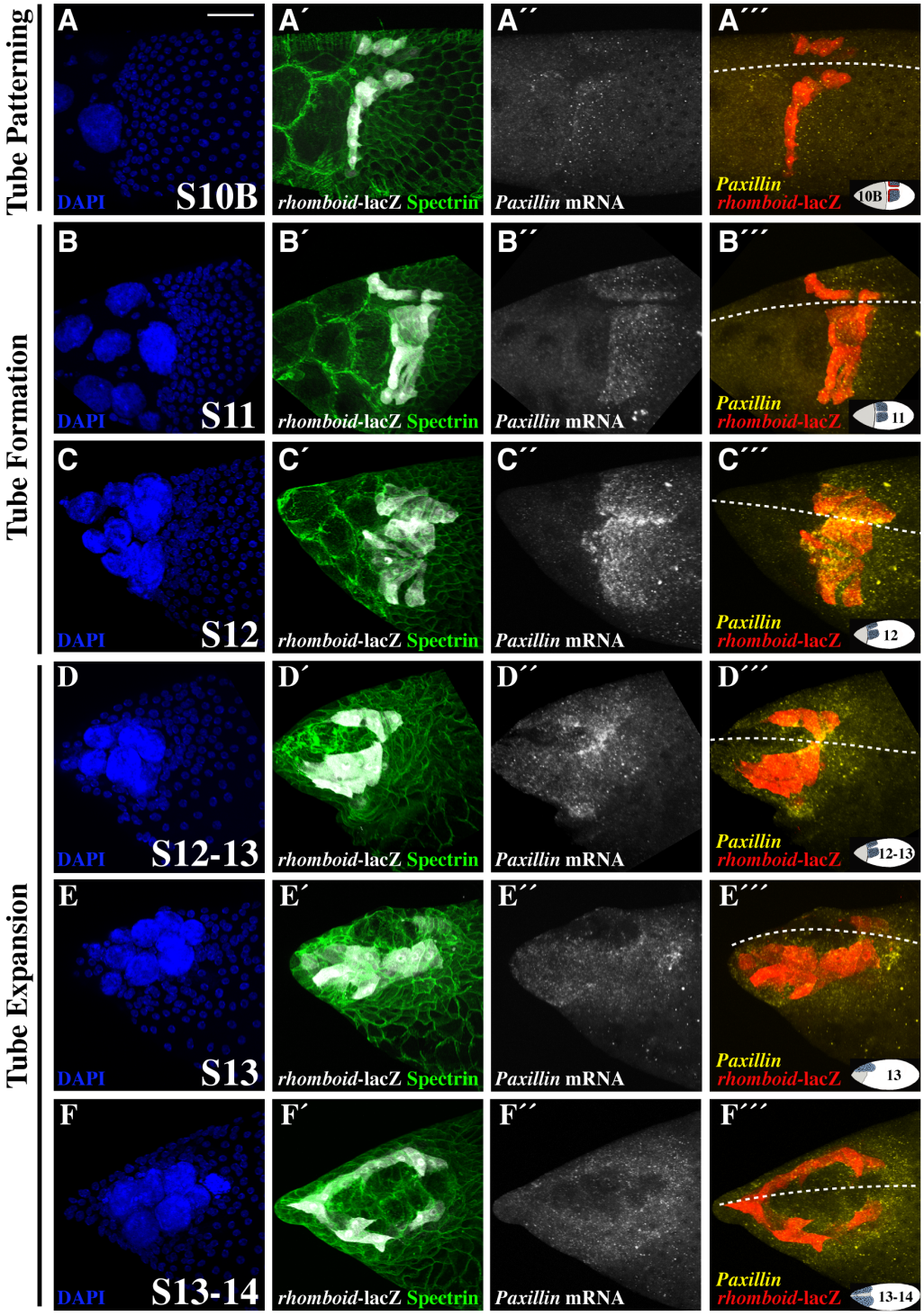

Both *Pax* and *mirr* transcripts localized primarily to DA-tube cells and therefore merited special attention, as discussed below.

In addition to the previously reported expression in migrating border cells (Chen *et al.,* 2005), *Pax* transcripts were highly enriched in DA-tube cells (Fig 2.3G-G') and substantially reduced in ttk^{twk} (Fig 2.3H-I). Dual immunostaining:FISH revealed that *Pax* expression is dynamic during late oogenesis specifically in DA-tube cells (Fig 2.5). Visualization of nuclear morphology (DAPI; Fig 2.5A-F) and cell shape (Spectrin protein; Fig 2.5A'-F') along with *Pax* mRNA (Fig 2.5A''-F'') indicated that peak transcript levels corresponded precisely to the initiation of DA-tube expansion (S12-13; Fig 2.5C''-D''). Co-staining for a DA-tube-cell reporter (*rhomboid-lacZ*; Fig 2.5A'-F') showed conclusively that high *Pax* expression is contained within *rhomboid*-expressing floor cells (Fig 2.5A'''- F''') and the adjacent roof cells (see below). *Pax* encodes a focal adhesion scaffold protein with important roles in cell migration, adhesion, and signaling (Turner et al. 1990; Brown and Turner, 2004), but a role during tubulogenesis had not been described previously.

mirr encodes a homeodomain transcription factor with dorsoventral (DV) patterning roles in the eye and ovary (McNeill *et al.,* 1997; Jordan *et al.,* 2000; Zhao *et al.,* 2000). Expression of *mirr* at S10 in a dorsal anterior FC 'saddle' helps define the DV axis of the eggshell and embryo and determines the placement of the DAs (Nakamura *et al.,* 2007; Lachance *et al.,* 2009; Fuchs *et al.,* 2012). I confirmed this reported S10 *mirr* mRNA expression (Fig 2.3L; 2.6C-C'), and noted a previously unreported, second wave of *mirr* mRNA expression in DA-tube cells during S13-14 (Fig 2.3J-J'). This observation was intriguing since Mirror's known DV patterning function is accomplished by the conclusion of S10. Analysis of *mirr* mRNA expression in ttk^{twk} revealed two important differences from wild type: the S10B expression of *mirr* mRNA in ttk^{twk}

Fig 2.6. Spatial and temporal comparison of *ttk69*, *mirr*, and *Pax* mRNA expression, visualized by FISH (**A-X**) and DAPI staining (**A'-X'**). At S10B (**A-F'**), all columnar FCs uniformly express *ttk69* mRNA (**A-A'**); a dorsal saddle and ventral belt of FCs express *mirr* mRNA (**C-C'**); and the DA-floor cells are the first to express *Pax* mRNA (**E-E'**; arrowheads). *ttk69* mRNA and *Pax* mRNA are absent in ttk^{twk} (**B-B'**; **F-F'**), and expression of *mirr* mRNA is reduced (**D-D'**). At S11 (**G-L'**), leading DA-tube cells and, to a lesser degree, midline columnar FCs, express *ttk69* mRNA (**G-G'**); several cells at the leading tip of each DA-tube express *mirr* mRNA (**I-I'**; arrowheads); and both DA-floor cells (highest levels) and DA-roof cells express *Pax* mRNA (**K-K'**). Transcripts from *ttk69* and *mirr* are absent in ttk^{twk} (**H-H'**; **J-J'**), and *Pax* mRNA expression is greatly reduced (**L-L'**). At S12 (**M-R'**), only leading DA-tube cells express *ttk69* mRNA (M-M'); no FCs express *mirr* mRNA (O-O'); and all DA-tube cells express high levels of *Pax* mRNA (**Q-Q'**). In ttk^{twk}, *ttk69* mRNA and *mirr* mRNA are absent (**N-N'**; **P-P'**) and *Pax* mRNA expression is greatly reduced (**R-R'**). At S13 (**S-X'**), a few weak puncta of *ttk69* mRNA are visible (**S-S'**); DA-tube cells begin to express high levels of *mirr* mRNA again (**U-U'**); and DA-tube cells continue to express *Pax* mRNA (**W-W'**). In ttk^{twk}, a few weak puncta of *ttk69* mRNA are visible; no *mirr* mRNA is visible (**V-V'**); and a low level of *Pax* mRNA is detectable around the dying nurse cells and stretch FCs (**X-X'**). Dotted lines = dorsal midlines; scale bar = 50 μm.

Figure 2.6. Expression of *tramtrack69*, *mirror*, and *Paxillin* mRNA during late oogenesis.

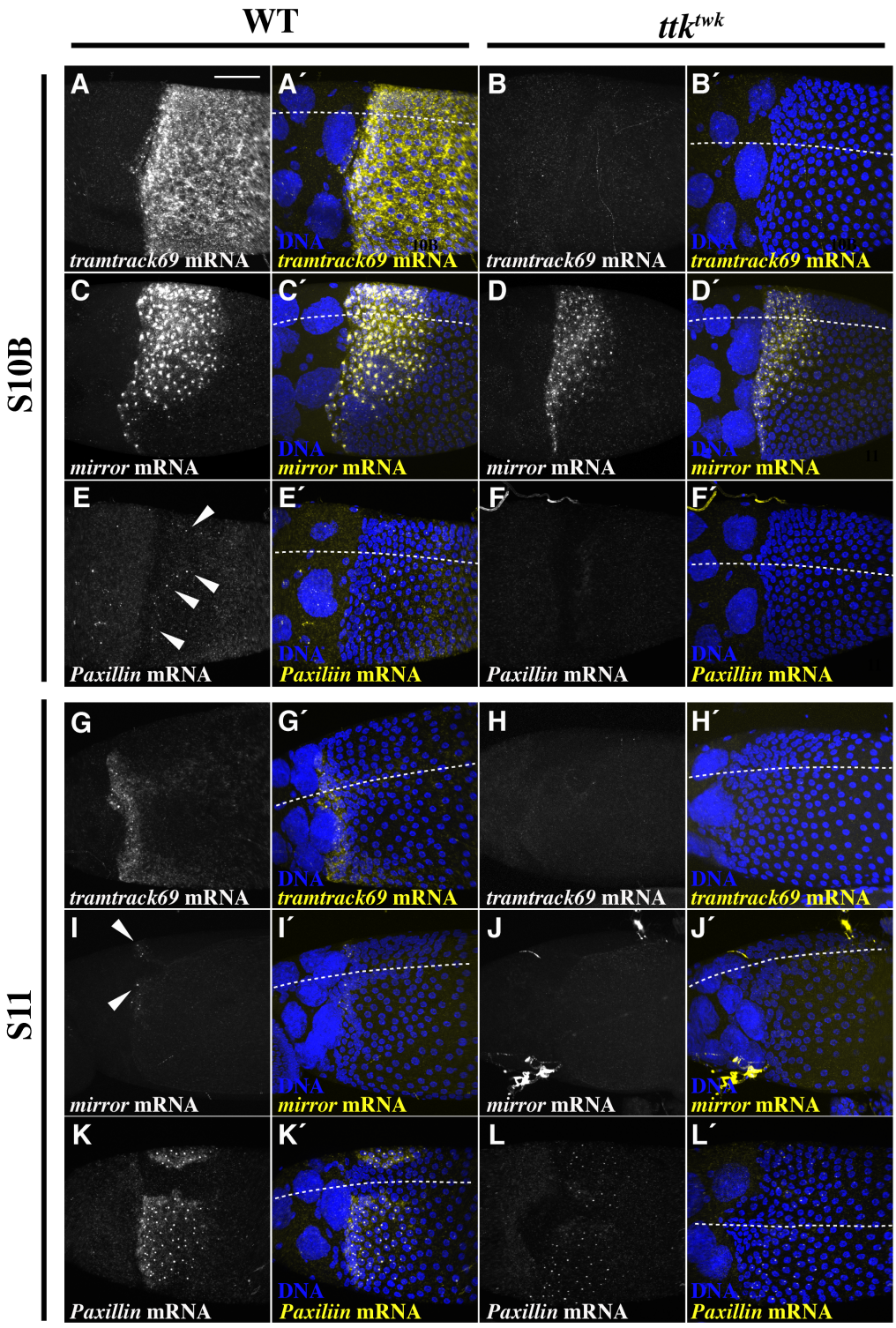

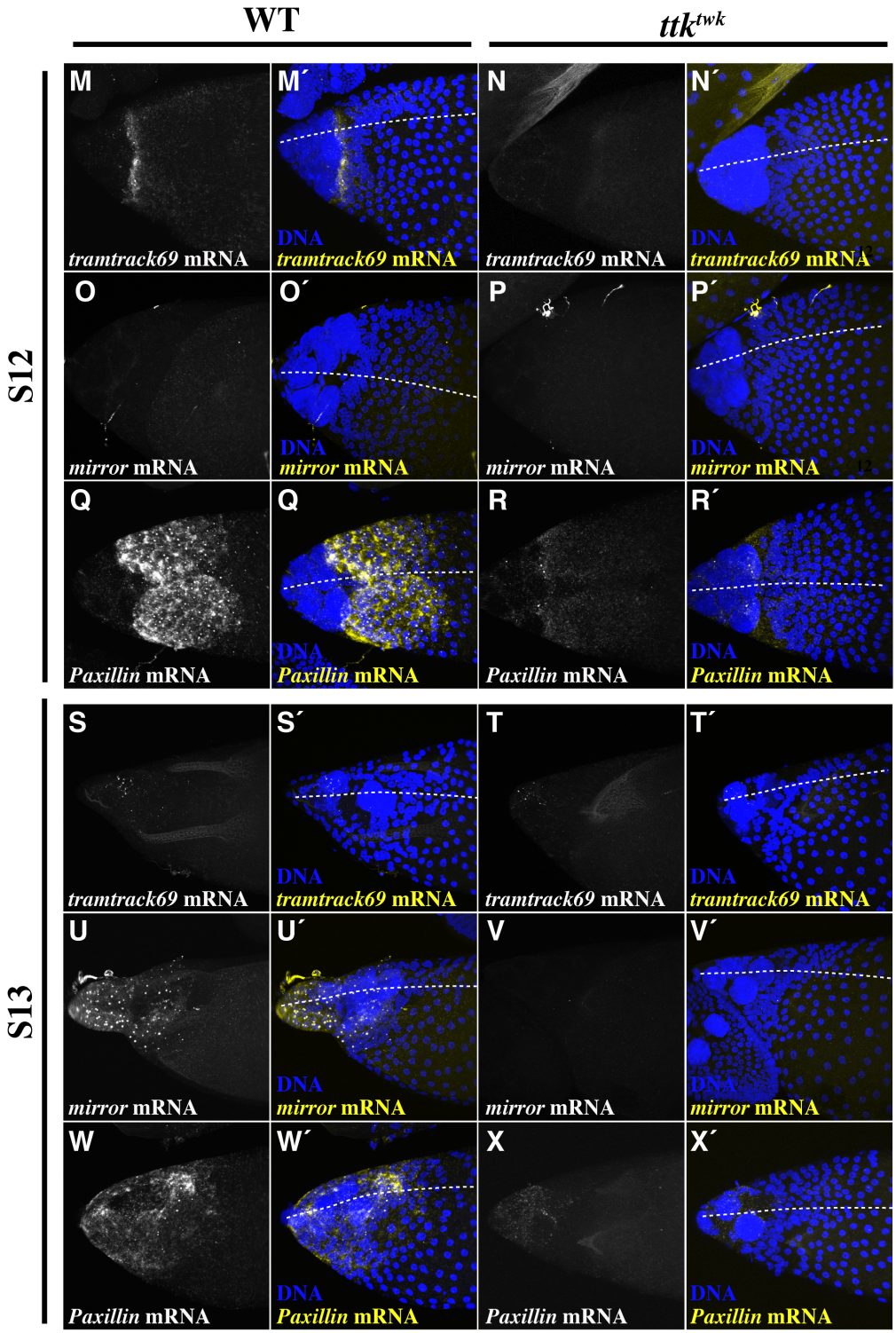
WT
ttk^twk
S12
S13
M
M´
N
N´
O
O´
P
P´
Q
Q
R
R´
S
S´
T
T´
U
U´
V
V´
W
W´
X
X´
tramtrack69 mRNA
mirror mRNA
Paxillin mRNA
DNA
tramtrack69 mRNA
mirror mRNA
Paxillin mRNA

was reduced (Fig 2.3L, 2.6D-D'), and the late wave of *mirr* mRNA expression was absent (Fig 2.3K-L, 2.6V-V'). It was shown previously that patterning is normal in ttk^{twk} (French *et al*., 2003), so I reasoned that reduced *mirr* mRNA expression at S10B must still be sufficient for patterning in ttk^{twk}. I hypothesized, however, that this reduced *mirr* mRNA expression at S10B and the lack of *mirr* mRNA expression at S13-14 could contribute to the defect in DA-tube expansion in ttk^{twk}.

To understand how the patterns of *ttk69*, *mirr*, and *Pax* mRNA expression relate to each other and to DA-tube expansion, and how mRNA expression is affected in ttk^{twk}, I compared the spatial and temporal patterns of mRNA expression for these genes in wild type and ttk^{twk} during DV patterning (S10B), DA-tube formation (S11), and at the initiation (S12) and conclusion (S13) of DA-tube expansion (Fig 2.6). At S10B, *ttk69* transcripts were present at high levels in all wild-type columnar FCs and were absent in ttk^{twk} at this stage (Fig 2.6A-B') and all subsequent stages (Fig 2.6H-H', N-N', T-T'). At this time, high levels of *mirr* transcripts were present in a dorsal saddle (Fig 2.6C-C'); both the level and posterior extent of *mirr* expression were reduced in ttk^{twk} (Fig 2.6D-D'). *Pax* transcripts were present throughout the tissue at low levels and punctate expression was just becoming visible within the nuclei of the DA-floor cells (Fig 2.6E-E', arrowheads); this expression was not detectable in ttk^{twk} (Fig 2.6F-F').

At S11, *ttk69* transcripts were still present in anterior and midline FCs but were reduced in more posterior FCs (Fig 2.6G-G'). Transcripts of *mirr* were detectable only in a few cells at the leading tip of each DA tube (Fig 2.6I-I'; arrowheads) and this expression was variably present in ttk^{twk} (Fig 2.6J-J'). *Pax* transcript levels increased notably during S11 in wild-type DA-tube cells (Fig 2.6K-K'), while in ttk^{twk}, relatively little *Pax* mRNA expression was visible in these cells (Fig 2.6L-L'). I noted that at S11, *Pax* mRNA expression was increasing in cells that

had been expressing high levels of *mirr* mRNA at S10B, suggesting that Mirror, as well as TTK69, could play a role in regulating *Pax* mRNA expression.

At S12, when DA-tube expansion initiates, *ttk69* transcript expression was restricted to the anterior-most, leading cells of the DA tube (Fig 2.6M-M'), consistent with a previously demonstrated requirement for TTK69 within those cells (Boyle *et al.,* 2010). Transcripts of *mirr* were not detectable at S12 in either wild-type or ttk^{twk} FCs (Fig 2.6O-P'). *Pax* transcript levels were dramatically elevated during S12 specifically in DA-tube cells, and this expression was greatly reduced in ttk^{twk} (Fig 2.6Q-R').

At the end of S13, *ttk69* transcripts were barely detectable in leading DA-tube-FCs (Fig 2.6S-S'). By S13 *mirr* transcription had re-initiated within the DA-tube FCs (Fig 2.6U-U'), and this late wave of *mirr* expression was dependent on TTK69 (Fig 2.6V-V'). *Pax* transcripts were present at high levels during this stage in DA-tube FCs, although not to the degree observed at S12 (Fig 4W-W'); this expression was barely detectable in ttk^{twk} (Fig 2.6X-X'). These mRNA expression data were consistent with the reduced TTK69 protein expression observed in ttk^{twk} (French *et al.,* 2003; Boyle and Berg, 2009), confirmed that TTK69 regulates both *mirr* and *Pax* expression, and demonstrated that *ttk69*, *mirr*, and *Pax* could interact with one another because their mRNAs are expressed in overlapping domains. Furthermore, this analysis confirmed that the late expression of *mirr* in DA-tube cells was distinct from the earlier *mirr* expression required for DV patterning.

Following this ISH-based expression analysis, which effectively validated my arrays and distinguished genes with spatially and temporally relevant FC expression, I sought to address gene function within the FCs. To this end, I employed a FC-specific, RNAi-based analysis of candidate-gene function during DA tubulogenesis.

FC-specific RNAi against *ttk^{twk}*-differentially expressed transcripts identifies genes with functional roles in tubulogenesis and genetic interactions with *ttk^{twk}*

To assess potential function in DA tubulogenesis (S10-14), I expressed RNAi constructs specifically in the FCs through the *GAL4-UAS* system (Brand and Perrimon, 1993; Dietzl *et al.,* 2007), and assayed DA morphology in laid eggs. Defects specific to DA-tube expansion manifested as properly located and formed, but abnormally shortened or misshapen, DAs, as in *ttk^{twk}* (Fig 2.1A). To create a spatiotemporally specific *GAL4* driver, Scott Kerr cloned the *Vitelline membrane 26Aa* (*Vm26Aa*) regulatory region upstream of *GAL4*; this construct expressed at moderate levels from S10B-S14 in columnar FCs and in no other developmental context (Fig 2.7A; Popodi *et al.,* 1988). I also employed an enhancer trap line, *CY2-GAL4*, which drives strong expression in all FCs from S8 onward, but infrequently causes lethality due to expression in other tissues (Fig 2.7A; Queenan *et al.,* 1997). FC-specific expression of *ttk*-RNAi by either driver resulted in fully penetrant, DA and eggshell defects similar to *ttk^{twk}*, providing a robust positive control (Fig 2.7B; Table 1). As negative controls for each driver I expressed GFP (Fig 2.7C-C"; Table 2.3).

In addition to *Pax* and *mirr*, which showed particularly striking expression patterns, I concentrated my functional analysis on the 11 other down-regulated candidates from the *in situ* analysis that displayed relevant FC-expression (e.g., *shibire*, *Rac2*). I chose genes with reduced expression in *ttk^{twk}* because mimicking *ttk^{twk}*-down-regulation is simpler than expressing RNAi in a *ttk^{twk}* homozygous background to suppress the *ttk^{twk}* phenotype. Additionally, this approach let me compare the effects of FC-RNAi in both wild type (+/+) and *ttk^{twk}* heterozygous (*ttk^{twk}*/+) backgrounds, providing a sensitized background and a tool for identifying *ttk^{twk}* genetic

Table 2.3. RNAi against *ttk*^{twk}-down-regulated genes reveals DA tubulogenesis functions.

Genetic Background	UAS Expressed Construct	vm26Aa-GAL4						CY2-GAL4					
		% Normal	% Moderate	% Severe	n	Weighted Score (0-2)	Description of DA defect	% Normal	% Moderate	% Severe	n	Weighted Score (0-2)	Description of DA Defect
+/+	GFP	91	9	0	106	0.09	rough DAs	81	19	1	177	0.20	rough DAs
	lamina ancestor RNAi	76	23	1	205	0.25	rough paddles	50	49	1	101	0.50	broad DAs
	CG31918 RNAi	63	36	1	103	0.38	broad DAs	55	43	2	130	0.48	broad DAs
	katanin 80 RNAi	60	31	9	167	0.49	rough, broad paddles	43	52	5	122	0.62	rough, broad paddles
	Cp16 RNAi	68	31	1	90	0.33	narrow DA paddles	66	32	2	105	0.36	narrow DA paddles
	Paxillin RNAi	79	15	6	96	0.27	rough DAs	52	48	0	145	0.48	short DAs
	Rac2 RNAi	36	56	8	146	0.73	rough DAs	52	36	11	105	0.59	wide-based DAs
	shibire RNAi	72	27	1	101	0.29	broad DAs	61	37	2	110	0.41	short, rough DAs
	mirror RNAi	7	31	62	143	1.24	short, smooth DAs	0	0	100	185	2.00	no DAs present
	tramtrack RNAi	0	0	100	224	2.00	stunted, rough DAs	0	0	100	178	2.00	stunted, rough DAs
ttk^{twk}/+	GFP	73	27	0	117	0.27	rough DAs	68	30	2	210	0.34	rough DAs
	lamina ancestor RNAi	71	29	0	116	0.29	broad, rough paddles	29	71	0	190	0.71	broad, short DAs
	CG31918 RNAi	42	57	2	65	0.60	broad DAs	29	68	3	154	0.74	broad DAs
	katanin 80 RNAi	44	53	3	182	0.59	rough, broad paddles	28	71	2	189	0.74	rough, broad paddles
	Cp16 RNAi	36	56	8	95	0.73	narrow DA paddles	31	66	2	217	0.71	narrow DAs paddles
	Paxillin RNAi	44	51	4	90	0.60	rough DAs	24	70	5	115	0.81	short, broad, DAs
	Rac2 RNAi	16	79	5	154	0.88	wide-based DAs	25	66	9	136	0.84	wide-based DAs
	shibire RNAi	6	74	19	124	1.13	broad DAs	0	70	30	138	1.30	short, broad DAs
	mirror RNAi	1	9	90	161	1.89	short, smooth DAs	0	0	100	118	2.00	no DAs present
	tramtrack RNAi	0	0	100	197	2.00	stunted, rough DAs	0	0	100	201	2.00	stunted, rough DAs

Table 2.3. GFP and *ttk*-RNAi expression serve as negative and positive controls, respectively. Weighted scores represent the average DA defect observed for a given condition (0 = 100% normal DAs, 1 = 100% moderate DA defects, 2 = 100% severe DA defects).

Fig 2.7. At 30°C, FC-RNAi against *lama*, *shi*, *Pax*, or *mirr* produces DA-tube defects. (**A**) *GAL4*-driven *UAS-GFP::moesin* expression. Left panel: *Vm26Aa-GAL4* expresses only in columnar FCs from S10-S14. Right panel: *CY2-GAL4* expresses in all FCs from S8-S14. (**B-G''**) Laid eggs from *GAL4-UAS* females in +/+ or ttk^{twk}/+ genetic backgrounds. Numbers indicate percentages of normal (N), moderate (M), and severe (S) DAs; yellow numbers indicate the category of egg being shown. White arrowheads indicate the 8 abdominal ventral denticle belts visible on near-hatching larvae. (**B**) *Vm26Aa*-driven *ttk*-RNAi (positive control) disrupts DA-tube expansion and eggshell secretion. (**C-C''**) GFP expression (negative control) indicates baseline DA-defect frequency for each genetic background. (**D-G**) *Vm26Aa*-driven RNAi causes subtle DA defects, with the exception of *mirr*-RNAi. (**D'-G'**) *CY2*-driven RNAi causes more frequent and severe DA defects for all conditions shown. (**D''-G''**) DA defects were enhanced in ttk^{twk}/+, and, for *shi*-RNAi and *Pax*-RNAi, were frequently accompanied by short, round eggs. Scale bars = 50 μm.

Figure 2.7. RNAi demonstrates DA tubulogenesis function and *ttk*^{twk} interactions

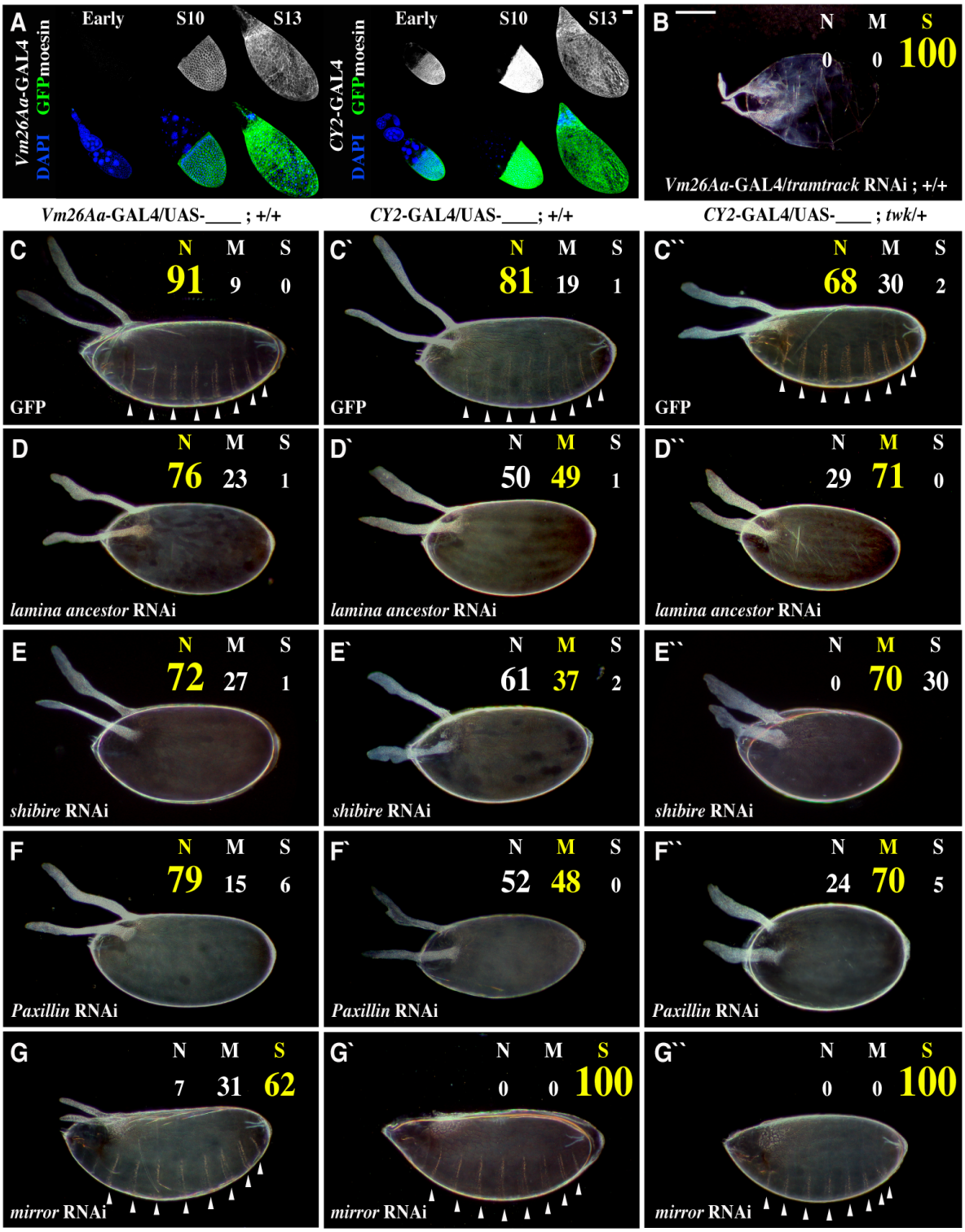

interactions. I also examined the effects of *Cp16* RNAi, since *Cp16* is expressed in dorsal anterior FCs (Parks and Spradling, 1987) and expression is reduced in ttk^{twk} (French *et al.,* 2003).

RNAi against 8 ttk^{twk}-down-regulated genes resulted in DA defects (Table 2.3; Fig 2.7D-G"). In general, these defects were more severe with the stronger *CY2-GAL4* driver (Table 2.3; Fig 2.7D'-G') and were exacerbated in the ttk^{twk}/+ background (Table 2.3; Fig 2.7D"-G"). For genes such as *lama, CG31918*, *Cp16*, and *kat80,* RNAi knockdown primarily affected DA shape as opposed to length (Fig 2.7D-D"; Table 2.3). RNAi against *shi* resulted in short, wide DAs, a defect that was greatly enhanced in ttk^{twk}/+, indicating a strong ttk^{twk} interaction (Fig 2.7E-E"; Table 1). Similar but less pronounced DA defects occurred following *Pax*-RNAi; the phenotype was significantly enhanced in ttk^{twk}/+ (Fig 2.7F-F"; Table 2.3). In contrast, *Rac2*-RNAi produced DAs with wide bases, a defect that was not significantly enhanced in ttk^{twk}/+ (Table 2.3). Finally, *mirr*-RNAi caused some unexpected phenotypes, described in detail below. These results revealed potential roles for ttk^{twk}-differentially expressed genes in DA tubulogenesis, and provided evidence for *ttk69* genetic interactions.

Mirror regulates DA tubulogenesis and *Paxillin* expression separately from DV patterning

RNAi against *mirr* produced a profound and penetrant DA defect with both *GAL4* drivers (Fig 2.7G-G"; Table 2.3). Four additional *mirr*-RNAi constructs produced similar effects (not shown) and these effects could be ameliorated by ectopic *mirr* expression (Fig 2.8; Table 2.4), indicating that the effects of *mirr*-RNAi are specific. Fine-tuning *mirr*-RNAi activity by reducing the assay temperature reduced the severity of the observed DA defects compared with controls, indicating that the level, not just the presence, of *mirr* mRNA expression influences

Table 2.4. Over-expression of *mirror* or *Paxillin* can ameliorate the effects of *mirror*-RNAi.

Genotype of mother	Eggs with normal DAs	Eggs with moderate DA defects	Eggs with severe DA defects	Total eggs scored	% Normal	% Moderate	% Severe
30 degrees							
*w**; *Vm26Aa*-GAL4 / + ; *Ly* / TM3	235	23	5	263	89	9	2
*w**; *Vm26Aa*-GAL4 / +; UAS-*mirr* / *Ly*	0	36	118	154	0	23	77
*w**; *Vm26Aa*-GAL4 / +; UAS-*mirr*RNAi / TM3	3	70	129	202	1	35	64
*w**; *Vm26Aa*-GAL4 / +; UAS-*mirr*RNAi / UAS-*mirr*	10	18	168	196	5	9	86
25 degrees							
*w**; *Vm26Aa*-GAL4 / + ; *Ly* / TM3	127	4	1	132	96	3	1
*w**; *Vm26Aa*-GAL4 / +; UAS-*mirr* / *Ly*	0	12	124	136	0	9	91
*w**; *Vm26Aa*-GAL4 / +; UAS-*mirr*RNAi / TM3	21	71	42	134	16	53	31
*w**; *Vm26Aa*-GAL4 / +; UAS-*mirr*RNAi / UAS-*mirr*	76	84	86	246	31	34	35
30 degrees							
*w**; *Vm26Aa*-GAL4 / Sp; + / TM6	108	15	10	133	81	11	8
*w**; *Vm26Aa*-GAL4 / UAS-*Pax*; + / TM6	80	29	8	117	68	25	7
*w**; *Vm26Aa*-GAL4 / +; UAS-*mirr*RNAi / +	0	150	337	487	0	31	69
*w**; *Vm26Aa*-GAL4 / UAS-*Pax*; UAS-*mirr*RNAi / +	7	292	239	538	1	54	44
25 degrees							
*w**; *Vm26Aa*-GAL4 / Sp; + / TM6	119	7	0	126	94	6	0
*w**; *Vm26Aa*-GAL4 / UAS-*Pax*; + / TM6	107	21	5	133	80	16	4
*w**; *Vm26Aa*-GAL4 / +; UAS-*mirr*RNAi / +	76	273	113	462	16	59	24
*w**; *Vm26Aa*-GAL4 / UAS-*Pax*; UAS-*mirr*RNAi / +	127	273	107	507	25	54	21

Fig 2.8. The effects of *Vm26Aa*-driven *mirr*-RNAi are reversible through ectopic expression of *UAS-mirr*. At 30°C (**A-D**), the *GAL4-UAS* system is stronger than at 25°C (**A'-D'**), but causes more background defects. (**A-A'**) Control eggs (*GAL4* driver only) have no DA defects. (**B-B'**) *Vm26Aa*-driven *mirr*-RNAi causes severe, highly penetrant DA defects. (**C-C'**) *Vm26Aa*-driven, ectopic *mirr* expression causes severe defects throughout the egg. (**D-D'**) *Vm26Aa*-driven *mirr* expression can suppress the DA defects of *Vm26Aa*-driven *mirr*-RNAi. Scale bar = 50 μm.

Figure 2.8. The degree of DA-tube expansion depends on the levels of Mirror

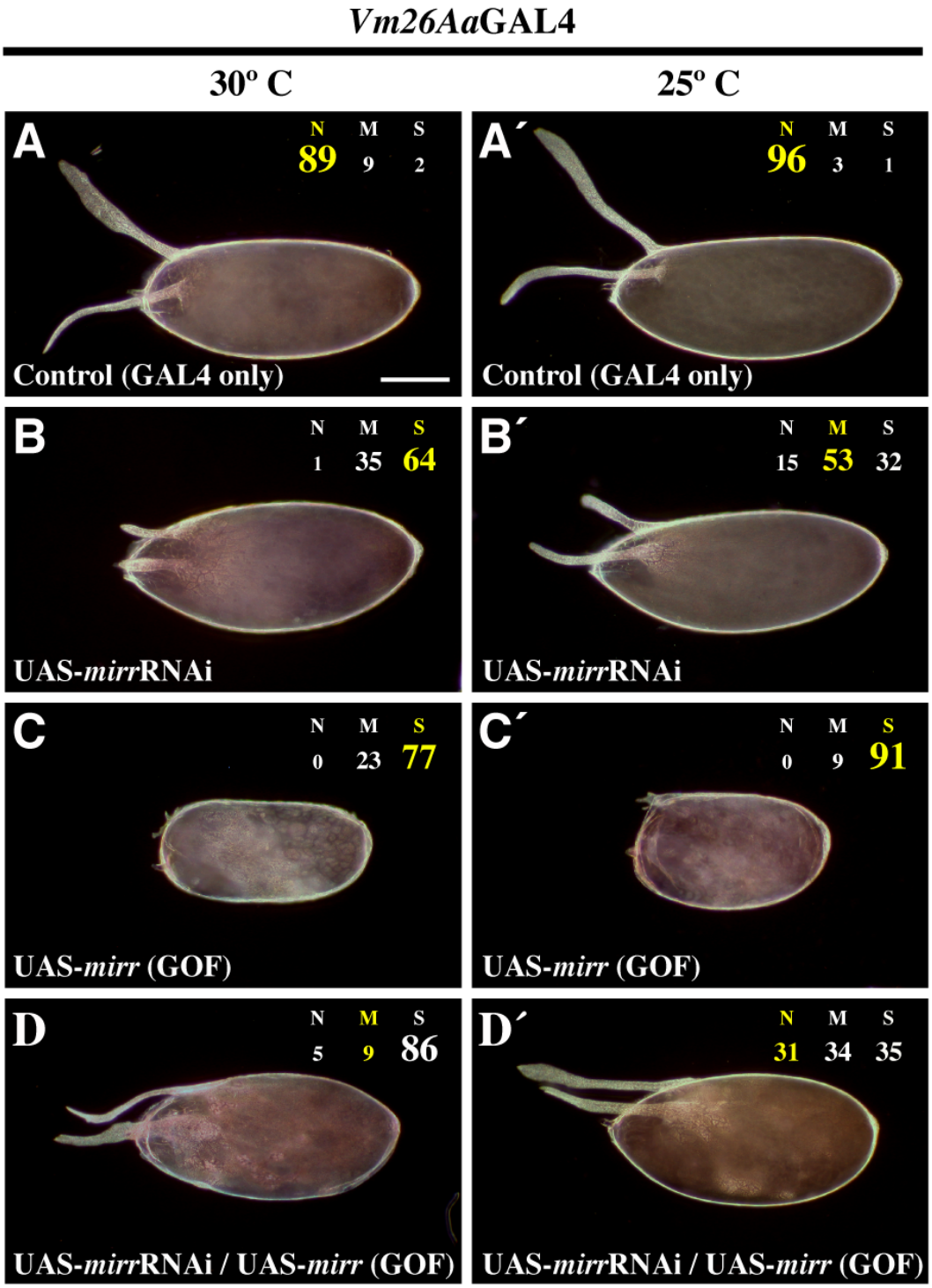

DA-tube expansion (30°C to 25°C; Fig 2.8A-B'). Ectopic *mirr* expression, representing a gain of function due to expression throughout the follicular epithelium, had a profound effect on eggshell morphology, making it difficult to interpret the DA-tube expansion defects (Fig 2.8C-C'). Nevertheless, co-expression of *mirr*-RNAi and ectopic *mirr* produced DAs of an intermediate length (Fig 2.8D-D'), occasionally producing DAs of a length comparable to controls. These results confirmed that *mirr*-RNAi does indeed disrupt *mirr* expression and indicated that the precise level of *mirr* expression dictates the degree of DA-tube expansion.

DA defects following *mirr*-RNAi resembled phenotypes produced by $mirr^{[null]}$ clones (Jordan *et al*., 2000; Zhao *et al*., 2000; Lachance *et al*., 2009; Fuchs et al. 2012), yet other features of these eggs differed significantly. *mirr*-RNAi eggs lacked DAs, yet DV polarity was unaffected: the dorsal surface of the egg was flat and the ventral surface was curved (Fig 2.7G-G"; Lachance *et al*., 2009), and the embryos developing within these eggshells exhibited the normal pattern of ventral denticle belts (Fig 2.7G-G", arrowheads). Embryonic viability assays revealed marginal differences in hatch rates compared to V*m26Aa-GAL4* controls; the small increase in lethality with *CY2-GAL4* was likely due to earlier RNAi expression (Table 2.5). These data suggested that late-oogenic *mirr*-RNAi did not significantly affect DV patterning, and that *mirr* had a novel role in DA-tube expansion.

To test this hypothesis, I examined the expression of Broad, a DA-tube cell-fate marker. DV patterning begins by localized Gurken (EGF) signaling (Schüpbach, 1987), which activates *mirr* transcription in a dorsal 'saddle' at S10 (Fig 2.6C-C'; Jordan *et al*., 2000; Zhao *et al*., 2000). Mirror helps establish DA-tube cell fate by dorsally activating *broad* and repressing *pipe* (Fuchs *et al*., 2012; Andreu *et al*., 2012). Broad protein remains high in DA-roof cells and is a terminal readout for dorsal FC fate (Tzolovsky *et al*., 1999; Dorman *et al*., 2004). Reducing *mirr*

levels via *Vm26Aa-GAL4*-driven RNAi resulted in normal Broad protein levels at S11-S12 (N=10/10; Fig 2.9A'-D'), yet laid eggs exhibited short, stubby DAs (Figs. 2.7G; 2.8B; 2.9F).

Since *mirr* and *Pax* share spatial expression domains (Fig 2.6) and high *mirr* mRNA expression at S10B precedes high *Pax* mRNA expression at S11-12, I then asked whether *mirr* acts upstream of *Pax* in DA-tube cells. V*m26Aa*-driven *mirr*-RNAi caused a reduction in *Pax* mRNA expression (N=7/10; Fig 2.9A"-D"). Simultaneous assessment of Broad protein and *Pax* mRNA using dual immunostaining:FISH confirmed that *Pax* mRNA expression is high in DA-roof cells (Fig 2.9A''', C''') and indicated that *Vm26Aa*-driven *mirr*-RNAi affects *Pax* expression without disrupting DV patterning (Broad protein; Fig 2.9B''', D'''). Interestingly, puncta of Broad protein, indicating sites of high DNA occupancy, co-localized with puncta of *Pax* mRNA, indicating nascent *Pax* transcripts (Fig 2.9A''', arrowheads).

If *Pax* were indeed downstream of *mirr*, as implicated by the reduced *Pax* mRNA expression following *mirr*-RNAi, then I reasoned that over-expression of *Pax* might be able to reverse the effects of *mirr*-RNAi. To test this hypothesis, I compared DA morphology at 30°C (Fig 2.9E-H; Table 2.4) following RNAi against *mirr* alone (Fig 2.9F), *Pax* alone (Fig 2.9G), and co-expression of *mirr*-RNAi and *Pax*-RNAi (Fig 2.9H). As observed previously (Figs. 2.7G; 2.8B), *mirr*-RNAi produced short, stubby DAs compared to driver controls (Fig 2.9E-F). Over-expression of *Pax* resulted in some moderate DA defects, but the majority of eggs bore normal DAs (Fig 2.9G). Importantly, expression of *Pax* in a *mirr*-RNAi background partially suppressed the *mirr*-RNAi DA defects, producing eggs with narrow DAs that often extended well beyond the anterior of the egg (Fig 2.9H). I observed this effect to a lesser degree at 25°C (Table 2.4). These results suggested that Mirror regulates DA-tube expansion at least in part through positive regulation of *Pax*. Given the co-localization of Broad with nascent *Pax*

transcripts, Broad could also contribute to this regulation. These data supported my hypothesis that Mirror has an additional function in tubulogenesis separate from its role in DV patterning and suggested that Mirror and Paxillin function in a similar pathway downstream of TTK69 to promote DA-tube expansion.

Table 2.5. Effects of maternal *Vm26Aa*-driven *mirr-RNAi* on embryonic viability.

Genotype of mother	Total laid eggs	Total unhatched	% lethality
w^{1118}	474	66	14
*w** ; *Vm26Aa*-GAL4 / UAS-GFP	597	58	10
*w** ; *Vm26Aa*-GAL4 ; UAS-*mirr*RNAi	818	141	17
*w** ; *CY2*-GAL4 / UAS-GFP	325	43	13
*w** ; *CY2*-GAL4 ; UAS-*mirr*RNAi	518	149	29

Fig 2.9. Dual immunostaining:FISH indicates that *Vm26Aa*-driven *mirr*-RNAi disrupts DA tubulogenesis without affecting DV patterning (**A-D'''**), and over-expression of *Pax* can suppress the *mirr*-RNAi phenotype (**E-H**). At S11 (**A-B'''**) and S12 (**C-D'''**), egg chambers expressing GFP (**A-A'''**, **C-C'''**) and *mirr*-RNAi (**B-B'''**, **D-D'''**) display relatively normal Broad protein expression. *Pax* mRNA expression in DA-tube cells is reduced following *mirr*-RNAi (compare **A"** to **B"** and **C"** to **D"**). (**A'''**) Arrowheads indicate co-localization of Broad protein and nascent *Pax* transcripts. At 30°C, eggs from females expressing the *Vm26Aa-GAL4* driver alone have normal DAs (**E**) and *Vm26Aa-GAL4*-driven *mirr*-RNAi causes severe, highly penetrant DA defects (**F**). *Vm26Aa-GAL4*-driven, ectopic *Pax* expression alone causes only minor DA defects (**G**), but can partially suppress the DA defects of *Vm26Aa*-driven *mirr*-RNAi when co-expressed (**H**). Dotted lines = dorsal midlines; insets = egg chamber orientation and stage. Scale bars = 50 μm.

Figure 2.9. Mirror regulates DA tubulogenesis and *Paxillin* expression, independently of DV patterning.

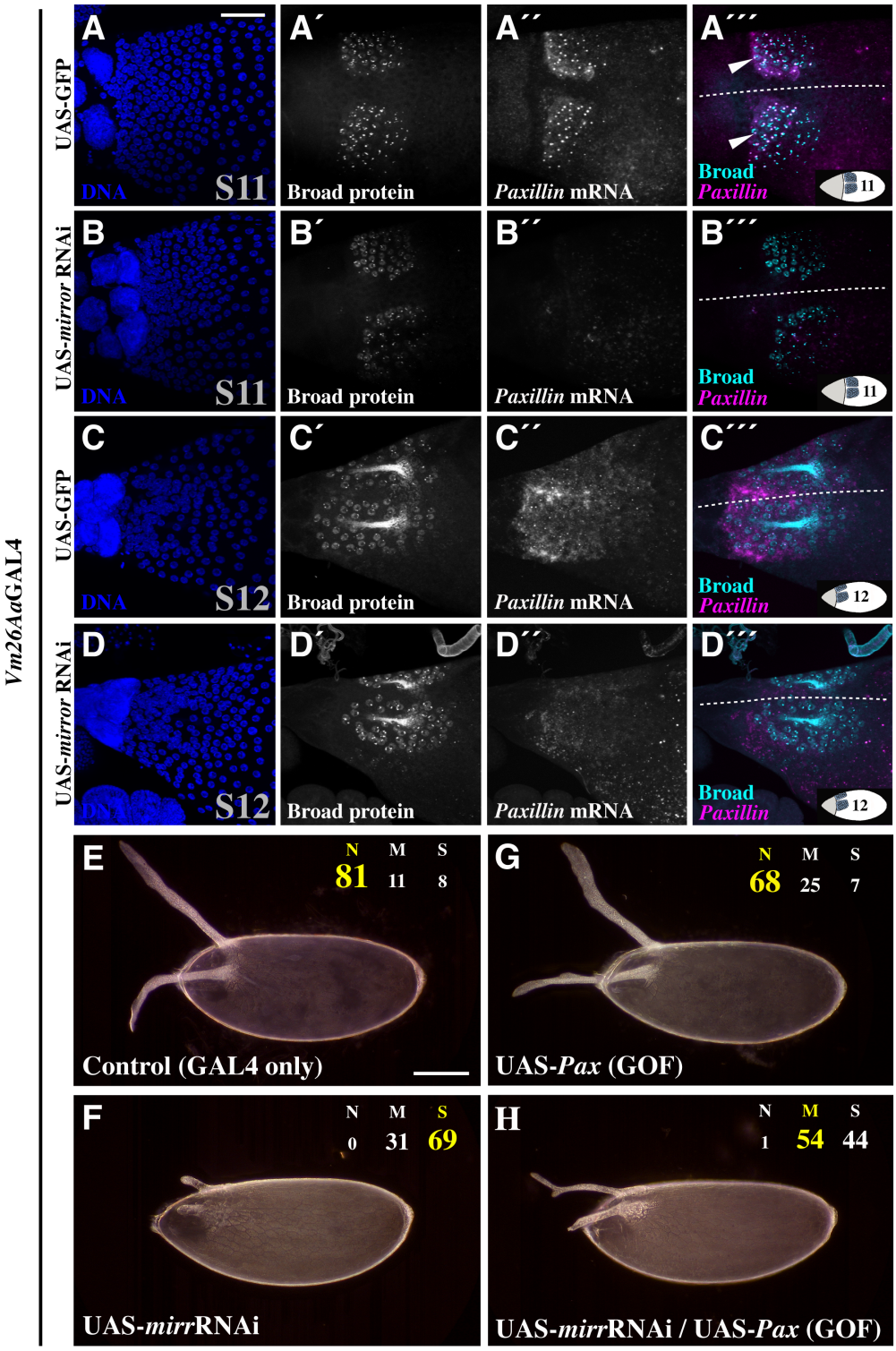

– Discussion –

Here I significantly advanced our understanding of TTK69 by characterizing its regulatory role during late oogenesis (Fig 2.10) through analysis of the unique *ttk69* allele, ttk^{twk}. I identified differentially expressed genes in ttk^{twk}, demonstrated that TTK69 effectors facilitate tube expansion and interact with one another, and elucidated novel roles for known proteins such as the homeobox transcription factor Mirror. Analysis of data for TTK69 binding during embryogenesis allowed me to speculate about direct binding of TTK69 to ttk^{twk}-differentially expressed genes, but also raised concerns about using a TTK69 motif as a predictive tool. Finally, my data substantiated TTK69's role in eggshell synthesis and indicated that TTK69's regulatory influence during oogenesis extends into the germline.

TTK69 regulates FC gene expression required for epithelial tube expansion

The ttk^{twk} mutation disrupts TTK69 expression late in oogenesis, resulting in eggshell and DA defects (French *et al.,* 2003; Boyle and Berg, 2009). My microarray analyses corroborated these results by identifying differentially expressed eggshell and tube expansion genes in ttk^{twk}. Analysis of expression by *in situ* hybridization distinguished genes whose FC expression was consistent with roles in DA-tube expansion, and tissue-specific RNAi analysis revealed functional roles in this process as well as ttk^{twk} interactions. Of the 14 ttk^{twk}-down-regulated genes knocked down by FC-specific RNAi, 8 produced measureable DA defects ranging widely in severity and penetrance.

For *lama*, *CG31918*, *Cp16*, and *kat80*, the RNAi defects were subtle or moderately penetrant, affecting DA shape. *lama* encodes a Phospholipase B-like protein that is conserved from human to *Dictyostelium*, with roles in *Drosophila* neural and imaginal-disc differentiation

(Perez and Steller, 1996; Klebes *et al.,* 2005). In *Drosophila*, *lama* has not previously been implicated in morphogenesis, but rather, is associated with undifferentiated cell types. In yeast, however, phospholipase B-like proteins regulate membrane bending during spore formation (Maier *et al.,* 2008), and a role in regulating membrane dynamics would fit with the apical expansion required for DA-tube elongation. Since *lama* mRNA is expressed in all FCs, however, its precise role is DA tubulogenesis is unclear. CP16 is an extracellular matrix protein, a minor constituent of the eggshell that is synthesized late in oogenesis (Griffin-Shea *et al.,* 1982). Consistent with this structural role, *Cp16*-RNAi produced narrow DA paddles. CG31918 is a predicted metalloendopeptidase, which could regulate the extracellular matrix during tube elongation, and *kat80* encodes a predicted microtubule-severing protein, suggesting a regulatory role in microtubule dynamics/transport. Although these proteins could affect tube morphology by controlling DA-tube cell behaviors, the majority of *CG31918* and *kat80* mRNA expression is in the germline and/or overlying stretch FCs, suggesting that the products of these genes could function outside of DA-tube cells. Indeed, the Berg lab has shown that germline and stretch FC-expressed genes also regulate DA-tube expansion (Rittenhouse and Berg, 1995; Tran *et al.,* 2003). Nevertheless, RNAi against *CG31918* and *kat80* showed enhanced defects in ttk^{twk} heterozygotes, suggesting they do play a role in DA-tube expansion, but that their specific mechanisms of action are unclear.

For the other genes identified and characterized as tube-expansion effectors in this study, I can make more educated predictions about mechanism. *Rac2*, and Rho-GTPases in general, regulate the actin cytoskeleton, cell adhesion, and cell migration (Hall 2005). Although the difference between wild-type and ttk^{twk} *Rac2* expression was small, *Rac2* was noteworthy. *Rac2*

Fig 2.10. Mirror's regulation of DVpatterning (left) is distinct from its TTK69-influenced regulation of DA-tube expansion (middle). Previously known interactions are indicated by black arrows; *in situ*-verified regulation of expression is indicated by purple arrows; RNAi-verified, functional interactions are indicated by red arrows; potential interactions are indicated by grey dashed arrows. Line weight indicates relative strength of an interaction, based on my observations.

Figure 2.10. Model for TTK69 function during late oogenesis

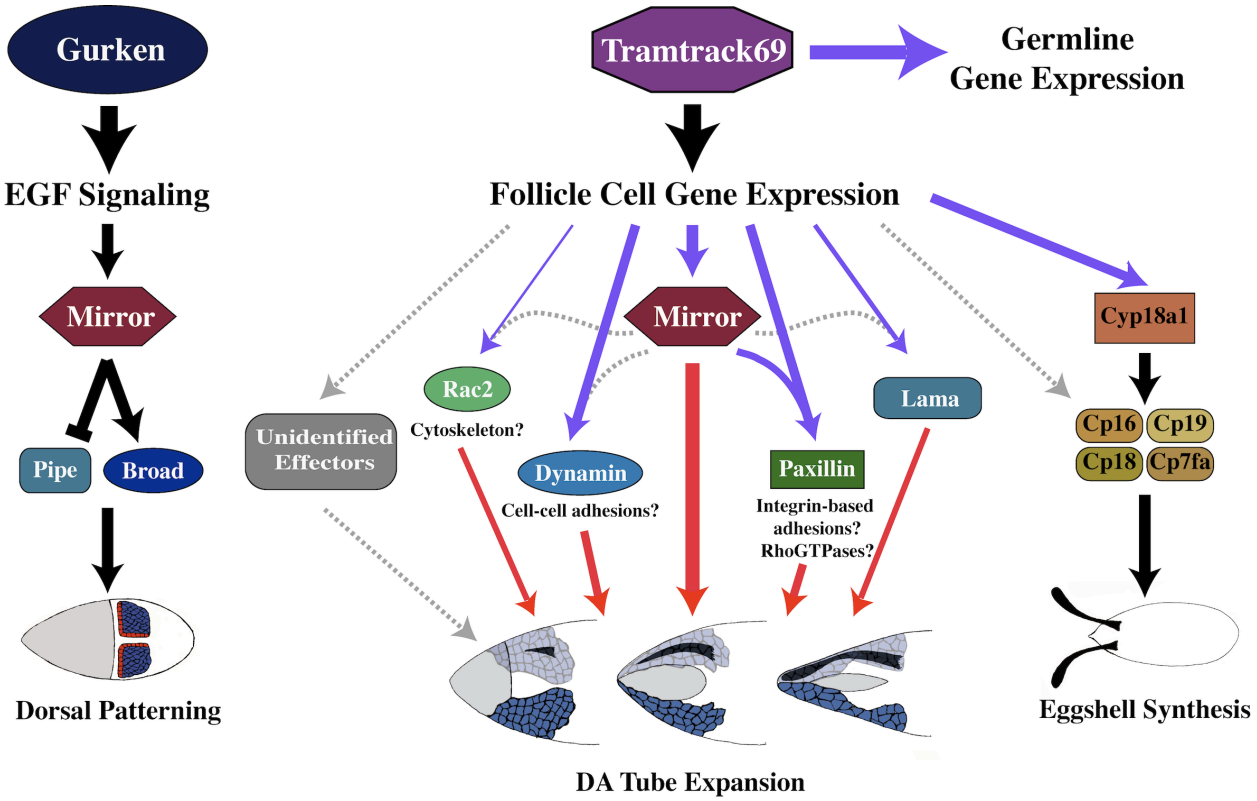

expression was enriched in DA-tube cells relative to other columnar FCs and *Rac2* RNAi produced wide, often short, DAs. Also, Rho-GTPases such as *Rac2* interact with two other tube-expansion genes identified here: *Pax* and *shi*. Paxillin's role in *Drosophila* development was first characterized through regulation of Rho and Rac signaling (Chen *et al*., 2005), and *shi* acts downstream of *Rac* during salivary gland morphogenesis, regulating E-cadherin levels via endocytosis (Pirraglia *et al*., 2006). These functions in other tissues support a role for *Rac2* in DA tubulogenesis.

shi, which encodes *Drosophila* Dynamin, regulates endocytosis throughout development. Dynamin is required during cell migration and morphogenesis events, including border cell migration, salivary gland morphogenesis, and tracheal morphogenesis (Medioni and Noselli, 2005; Pirraglia *et al*., 2006, Hsouna *et al*., 2007). Dynamin may promote DA-tube expansion by facilitating apical cell-membrane turnover following DA-tube formation, as in the salivary gland, or by regulating basement membrane features, as in the border cells.

Pax encodes a molecular scaffold that localizes to focal adhesions, regulates Rho and Rac activity, modulates cell adhesion and migration, and facilitates epithelial tissue elongation (Chen *et al*., 2005; Deakin and Turner, 2008; Llense and Martin-Blanco, 2008; He *et al*., 2010). RNAi against *Pax* in migrating border cells delays migration and produces elongated cell morphologies (Llense and Martin-Blanco, 2008), similar to the shapes of ttk^{twk} DA-tube cells (Boyle and Berg, 2009). The exquisite spatiotemporal pattern of *Pax* mRNA expression in DA-tube cells, the reduction of *Pax* mRNA expression in ttk^{twk}, and the enhancement of *Pax*-RNAi DA defects in a ttk^{twk}/+ background support a role for Paxillin in DA-tube expansion. Furthermore, the reduced *Pax* mRNA expression following *mirr*-RNAi and the partial suppression of *mirr*-RNAi DA defects following *Pax* over-expression indicate that *Pax* is downstream of *mirr* as well as *ttk69*.

Co-localization of Broad with nascent *Pax* transcripts also raised the possibility that a BTB-mediated interaction between Broad and TTK69 might contribute to *Pax* regulation as well.

How might these TTK69-regulated effectors interact with one another to facilitate DA-tube expansion? My *in situ* hybridization data support a temporal and spatial program of gene regulatory interactions. Although I lack information about protein stability for some of these factors (e.g., Mirror), my genetic studies show that *ttk69* regulated *mirr* mRNA expression, that *mirr* regulated *Pax* mRNA expression, and that *ttk69* also regulated *Rac2* and *shi* mRNA expression. In principle, TTK69 and Mirror could work together to regulate transcription of *Pax*, *Rac2*, and *shi*, so that sufficient levels of these proteins exist at the initiation of, and during, DA-tube expansion. During DA-tube expansion, Paxillin protein may regulate the activity of Rac2, and Rac-related signaling, as it has been shown to do in the *Drosophila* eye and wing (Chen *et al*., 2003). Rac-related signaling could then promote Shibire-mediated recycling of adhesion machinery as it does in the *Drosophila* salivary gland (Pirraglia *et al*., 2006), relaxing the apical constriction in the DA-tube cells and allowing the DA-tube to expand. Notably, this model could help explain the prominent apical-expansion defect that a former graduate student in the lab, Michael Boyle, previously documented in ttk^{twk} (Boyle and Berg, 2009).

Mirror has distinct oogenic roles in DV patterning and epithelial tube expansion

Mosaic analyses with $mirr^{[null]}$ alleles demonstrate that Mirr provides dorsal cues to the egg chamber and embryo (Jordan *et al*., 2000; Zhao *et al*., 2000; Lachance *et al*., 2009), in part by dorsally activating *broad* and repressing *pipe* (Fig 2.10; Fuchs *et al*., 2012; Andreu *et al*., 2012). Since no cell division occurs after S6 (King, 1970), clonal analyses necessarily disrupt

S10 patterning events. Using the *Vm26Aa-GAL4* driver, however, I knocked down *mirr* beginning in S10 and revealed a role for *mirr* beyond DV patterning, a role in tube expansion.

Many lines of evidence support my assertion that Mirror regulates DA-tube expansion downstream of TTK69. First, I showed that *mirr* mRNA expression at S10B is significantly reduced in ttk^{twk} and that the degree of DA-tube expansion depended on the precise level of *mirr* mRNA; I concluded that the S10-expression of *mirr* mRNA in ttk^{twk} was sufficient to pattern the DA-tube cells but was insufficient to activate a tube-expansion program within these cells. Additionally, a second wave of *mirr* expression, which was absent in ttk^{twk}, occurred during later DA-tube expansion (S13-S14). This expression may be important for the terminal widening of the DA paddles at the end of oogenesis. Second, post-patterning, *Vm26Aa*-driven *mirr*-RNAi produced severe, fully penetrant DA defects resembling ttk^{twk}, yet unlike ttk^{twk}, eggshell integrity was normal. This result was consistent with the observation that TTK69 separately regulates DA-tube expansion and eggshell secretion (French *et al.,* 2003) and suggested that Mirror could be important for mediating some TTK69 functions during late oogenesis. Third, under post-patterning RNAi conditions, rates of egg laying and hatching were unaffected: larvae were viable, and displayed normal, ventral-restricted, *pipe*-induced denticle bands. Fourth, distinct *mirr*-RNAi constructs had similar effects, which could be reversed by over-expressing *mirr*. Fifth, the fate of DA-tube cells, assessed by the expression of Broad protein, was unaffected by post-patterning *mirr*-RNAi, as was the case in ttk^{twk} (French *et al.,* 2003). Finally, *Pax* mRNA expression was reduced by *mirr*-RNAi and *Pax* over-expression could suppress these defects. Therefore, I assert that Mirror is an important, TTK69-regulated effector of DA-tube expansion that acts upstream of *Pax*.

Towards a better understanding of TTK69 binding preference

TTK69's DNA binding preference has been a topic of debate since its discovery. The first proposed TTK69 motifs were based on binding interactions with the *fushi tarazu* (*ftz*) promoter (TTATCCG, Harrison and Travers, 1990; TGCNAGGACNT, Brown *et al.,* 1991); or on interactions with both *ftz* and *even-skipped* (*eve*). This knowledge facilitated analysis of TTK69 binding sites in the *tailless* (*tll*) promoter (TCCT; Chen *et al.,* 2002). A weighted TTK69 motif, ascertained through bacterial one-hybrid and DNAseI-footprinting assays, expanded upon the previous TCCT motif (~ttaTCCTg; Kulakovskiy and Makeev, 2009).

The modENCODE ChIP analysis of TTK69 binding in embryos was the first genome-wide, *in vivo* study examining TTK69 binding. Nathaniel Thayer and Martin Tompa used these data to generate a longer motif; its loose nature and slight similarity to previous motifs indicate that DNA-binding by TTK69 is complex, potentially due to variable BTB-mediated protein-protein interactions (Bonchuk *et al.,* 2011).

Since TTK69 could interact with different binding partners in oogenesis and embryogenesis, I viewed the FIMO results conservatively. Nevertheless, with the exception of *lama*, all genes exhibiting RNAi phenotypes possessed at least one FIMO hit in their promoter. Several genes with pronounced reduction in ttk^{twk} expression also possessed promoter enrichment for the TTK69 binding motif: *Arc1* (9 instances), *scramb2* (11), *kat80* (12), and *Cyp18A1* (5), suggesting that TTK69 might have an activating function (Reddy *et al.,* 2010; Rotstein *et al.,* 2011).

TTK69 regulates eggshell and germline gene expression

Consistent with ttk^{twk}'s fragile eggshell phenotype, microarray analysis revealed reduced expression of numerous chorion genes and *Cyp18a1*, an upstream regulator of eggshell gene

expression (Fig 2.10; Tootle *et al*., 2011). CYP18a1 processes the steroid hormone Ecdysone (Guittard *et al*., 2011), a signaling molecule that initiates metamorphosis (reviewed by Andres and Thummel, 1992), and the FC endocycle-to-gene-amplification switch and FC patterning (Sun *et al*., 2008; Boyle and Berg, 2009). Ecdysone is required for anterior FC migration, including centripetal migration and DA-tube formation (Hackney *et al*., 2007); by extension, *Cyp18a1* could function during both migratory events. Alternatively, CYP18a1's role in late oogenesis may be strictly eggshell-related. RNAi against *Cyp18a1* did not affect the DAs or eggshell, but RNAi might not have sufficiently reduced *Cyp18a1* transcripts to cause a visible defect. Nevertheless, ttk^{twk} affects expression of many eggshell genes and an upstream eggshell-gene regulator; I hypothesize that reduced expression of these genes could contribute to the fragile eggshell phenotype of ttk^{twk}.

Finally, TTK69 regulates gene expression in the germline. Since eggs from ttk^{twk} homozygous females are not fertilized, there are no visible ttk^{twk}-associated defects during embryogenesis (French *et al*., 2003). Nevertheless, TTK69 could function in the germline to regulate maternally loaded transcripts.

Where do the "tracks" lead?

I have identified and characterized downstream effectors of TTK69 required for epithelial tube expansion; I showed that *mirr* plays a pivotal role in this process, acting upstream of *Pax*, and I provided corroborating evidence that TTK69 regulates eggshell gene expression. TTK69 also regulates germline gene expression, and expression of stretch-FC-specific genes (*e.g*., *CG7997*) and phagocytosis-associated genes (*e.g*., *Bx, cenB1A, Rac2*). Since stretch-FCs engulf dying nurse cells (Tran and Berg, 2003), it is possible that TTK69 has a regulatory role in nurse-

cell engulfment. Furthermore, the altered expression of genes involved in oxidation-reduction (*e.g.*, *Cyp-9b2, Cyp-12d1, CG31673*) reveals an as yet unexplored protective function for TTK69 late in oogenesis. Clearly we have much to learn about TTK69's role in all ovarian cell types.

TTK69's regulatory function may also be conserved outside of the ovary, and perhaps in other organisms. TTK69 regulates tracheal tube morphogenesis, and, although this process occurs by branching morphogenesis rather than wrapping, as in DA tubulogenesis, TTK69 might regulate similar tube expansion effectors in both contexts. The BTB domain-containing protein, Ribbon, has roles in *Drosophila* tracheal and salivary gland tubulogenesis, and disruption of *ribbon* causes cell defects similar to ttk^{twk} (Shim *et al.,* 2001; Bradley and Andrew, 2001). Since BTB-domain-containing proteins often dimerize or multimerize (Bonchuk *et al.,* 2011), it is possible that TTK69 could interact with Ribbon through its BTB domain, or play a functionally equivalent role to Ribbon, in the ovary. Both TTK69's BTB and DNA-binding domains are conserved (e.g., 218 BLAST hits to the human genome). Indeed, the BTB domain from human Bcl-6 can functionally replace the BTB domain of TTK69 during eye development (Wen *et al.,* 2000). While known functions of *ttk69*-related human genes include B-cell development and immunity, which share features with *Drosophila* innate immunity, functional roles for the vast majority of these TTK69-like proteins are unknown but could include tube morphogenesis. The conservation of TTK69's BTB and DNA-binding domains reveals constraints on TTK69's molecular activity during evolution; in the future we may understand whether this conservation extends into TTK69's regulatory relationships, such as those we have studied in *Drosophila*.

Chapter III

Dynamin-mediated endocytosis is required for tube closure, cell intercalation, and biased apical expansion during epithelial tubulogensis in the *Drosophila* ovary

– Summary –

For metazoans to attain a complexity beyond a few hundred cells and support differentiated tissues, multicellular, epithelial tubes are indispensable. To identify and characterize the cellular behaviors and molecular mechanisms required for the morphogenesis of epithelial tubes (*i.e.,* tubulogenesis), I have turned to the *D. melanogaster* ovary. Here, epithelia surrounding each developing egg chamber pattern, form, and extend paired, unelaborated epithelial tubes in the absence of cell division or apoptosis: the dorsal appendage (DA) tubes. This genetically tractable system lets me assess the relative contributions that coordinated changes in cell shape, adhesion, orientation, and migration make to basic epithelial tubulogenesis. I find that Dynamin, a conserved and critical regulator of endocytosis and the cytoskeleton, serves a key role in DA tubulogenesis. I demonstrate that Dynamin is required for distinct aspects of DA tubulogenesis: DA-tube closure, DA-tube-cell intercalation, and biased apical-luminal expansion. I provide evidence that Dynamin promotes these processes by facilitating endocytosis of cell-cell and cell-matrix adhesion complexes, and I find that precise levels and sub-cellular distribution of E-Cadherin and specific Integrin subunits impact DA tubulogenesis. Thus, my studies identify novel morphogenetic roles (*i.e.,* tube closure and biased apical expansion), and expand upon established roles (*i.e.,* cell intercalation and adhesion remodeling), for Dynamin in tubulogenesis.

– Introduction –

Epithelial tubes perform numerous critical functions in metazoan physiology, and these functions often depend on specific tube morphologies. The fidelity of epithelial tube morphogenesis (*i.e.,* tubulogenesis) during development is therefore essential. Errors in these morphogenetic programs can result in harmful, even fatal, developmental defects, and mis-regulation is associated with metastatic cancers (Wallingford *et al.,* 2005; Andrew and Ewald, 2010; Ray and Niswander, 2012; Iruela-Arispe and Beitel, 2013).

Tubulogenesis typically involves tube formation, tube elongation, and tube elaboration; each of these three events requires tight regulation of cell adhesion and cell polarity. The formation of a tube lumen from a polarized epithelium can be achieved through several mechanisms, including wrapping, which produces a tube parallel to the original epithelial sheet. At the cellular level, these tissue behaviors require apical constriction, basal nuclear positioning and, in the case of wrapping, the formation of new cell-cell adhesions to close the tube. Once formed, the elongation of the tube lumen is achieved through oriented cell shape-change, rearrangement, proliferation, recruitment, and migration. Elaboration of a tube lumen can be simple or even unnecessary, if the terminal tube morphology is also simple, or it can be highly complex and require intricate bifurcation, side branching, or clefting, events that can be either programmed or stochastic (Andrew and Ewald, 2010; Iruela-Arispe and Beitel, 2013). Relative to the cellular behaviors that drive tube formation, less is known about the mechanisms that regulate tube elongation and elaboration: How do epithelia achieve specific tube morphologies following tube formation, and what genes, molecules, and mechanisms are responsible for these cellular behaviors?

To address these questions I have turned to the *Drosophila* ovary, to study the formation of epithelial tubes involved in synthesizing the dorsal respiratory appendages (DAs) of the eggshell (reviewed by Berg, 2005). DA tubulogenesis exhibits many features that make it particularly attractive as a model for epithelial tube formation and elongation. First, this process is simple: a) each DA-tube primordium is composed of <100 cells of two primary types; b) once patterned, DA-tube cells do not divide, die, or recruit new cells during DA-tube elongation; and c) DA-tubes are branchless and do not elaborate beyond bending and flattening the lumen into a shape resembling a hockey stick. Second, DA morphology reveals the shape of the terminal DA-tube lumen and reflects any defects that may have occurred during DA tubulogenesis. Finally, the fly ovary is genetically tractable, easily accessible via dissection, and readily amenable to microscopy; furthermore, each ovary contains a distribution of all egg-chamber stages, providing a wealth of tubulogenic material for analysis of fixed or living tissue. These features have facilitated the study of DA-tube-cell patterning (*e.g.,* Tzolovsky *et al.,* 1999; Ward and Berg, 2005; Yakoby *et al.,* 2008; Boslair Lachance *et al.,* 2009; Boyle and Berg, 2009; Andreu *et al.,* 2012; Fuchs *et al.,* 2012), DA-tube formation (Dorman *et al.,* 2004; Osterfield *et al.,* 2013), and DA-tube elongation (Dorman *et al.,* 2004; Boyle *et al.,* 2010; Peters *et al.*, 2013). Thus, the *Drosophila* ovary provides an ideal system for understanding how the regulation of cell shape, rearrangement, adhesion, and migration contribute to epithelial tube formation and elongation.

DA tubulogenesis occurs during the late stages of oogenesis (S10—S14), shortly after the follicle cell (FC) epithelium that encases each cluster of germ cells receives signals that pattern two dorsal primordia of DA-forming cells (S10B; Fig 3.1A). This patterning relies on the intersection of epidermal growth factor receptor (EGFR) and bone morphogenetic protein (BMP) pathways within the FC epithelium of each egg chamber, providing a combinatorial

framework for establishing precise spatial and temporal gene-expression patterns (summarized in Yakoby *et al.,* 2008). By S10B, each DA primordium contains two major cell types: *broad*-expressing "roof" FCs that form the outward-facing roof of the DA tube, and *rhomboid*-expressing "floor" FCs that seal off the floor of the DA tube (Dorman *et al.,* 2004; Ward and Berg, 2005). At the end of S10B, roof FCs initiate apical constriction from the anterior to posterior as the floor FC hinge begins to buckle. In S11, roof FC apices constrict down to their smallest size while floor FCs dive underneath the roof cells, flip their apical-basal orientation, and zipper together to seal the DA-tube (Dorman *et al.,* 2004; Osterfield *et al.,* 2013). This wrapping process, which resembles primary vertebrate neurulation, forms each of the rudimentary DA tubes (S11; Fig 3.1B). Once each DA tube is formed, DA-tube cells rearrange, expand, and migrate over the adjacent, squamous, stretch FCs towards the anterior end of the egg chamber, and interactions between the physically apposed stretch FCs and floor FCs of the DA tube facilitate tubulogenesis (S12—13; Fig 3.1C-D; Tran and Berg 2003; Dorman *et al.,* 2004). Throughout this process (S11—S14), the FCs, which are oriented with their basal faces out and apical faces in, secrete eggshell protein into the DA-tube lumens to form the DAs of the eggshell (Fig 3.1E).

While characterizing the transcriptional regulation of DA-tube elongation, I discovered that Tramtrack69 regulates the expression of *shibire* (*shi*, Poodry *et al.,* 1973; *shi* encodes *Drosophila* Dynamin, van der Bliek and Meyerowitz, 1991) in FCs at the transition from tube formation to tube expansion (Peters *et al.,* 2013). Dynamin has known roles in other morphogenetic contexts (*e.g.,* Pirraglia *et al.,* 2006; Pirraglia *et al.,* 2010; Fabrowski *et al.,* 2013; Gomez *et al.,* 2012); Rodriguez-Fraticelli *et al.,* 2014; Lepage *et al.,* 2014; Lee and Harland, 2010; Ogata *et al.,* 2007; Bogdanovic *et al.,* 2012; Lee *et al.,* 2014; Gray *et al.,* 2005) and

functional RNAi studies indicate that Dynamin promotes DA elongation (Peters *et al.,* 2013). Therefore, I decided to delve deeper into Dynamin's role in DA tubulogenesis.

Dynamin is a large GTPase that is best known for its ability to self-assemble into multimeric rings around the necks of clathrin-coated membrane pits and, through enhanced GTP hydrolysis provided by this conformation, to exert the mechanical force necessary for vesicle scission during endocytosis (Chappie *et al.,* 2011; Chappie and Dyda 2013). However, the role of Dynamin is not limited to clathrin-mediated endocytosis, and extends to a wide variety of cellular processes including alternative endocytic pathways and intracellular budding (Furgeson and Camilli, 2012), regulation of actin and microtubule dynamics (Sever *et al.,* 2013), centrosome cohesion (Thompson *et al.,* 2004), and apoptosis (Soulet *et al.,* 2006).

Here, I explore the role of Dynamin in DA tubulogenesis, and I demonstrate that disruption of Dynamin function in DA-tube cells leads to defects in DA-tube closure, DA-tube-cell rearrangement, and planar-polarized apical membrane expansion during DA-tube elongation. Furthermore, I provide evidence that Dynamin promotes these movements by regulating endocytosis. Consistent with this claim, I observe mis-localized both E-cadherin and Integrin following Dynamin disruption, and present functional data consistent with a model in which Dynamin promotes DA-tube elongation through endocytic remodeling of cellular adhesions.

– Materials and Methods –

Drosophila strains

I used the following strains, which are available from the Bloomington Stock Center (BL) or the Vienna Drosophila Resource Center, VDRC (V), and are described in FlyBase (http://flybase.bio.indiana.edu/): *UAS-shi[K44A]* (dominant negative Dynamin; BL5811), *UAS-mCD8::GFP* (negative control; BL5137), *UAS-Rab5[S43N]* (dominant negative Rab5; BL42703), *UAS-mCherry* RNAi (RNAi negative control; BL35785), *UAS-Rab5* RNAi (BL34832), *UAS-AP50* RNAi (BL28040), *UAS-shotgun* RNAi (E-Cadherin RNAi; V27082), *UAS-myospheroid* RNAi (*βPS*-Integrin RNAi; V29619), *br[69B08]-GAL4* (BL39481). The following strains were gifts: *w*; brL-GAL4; tub-gal80[ts]/TM3* (S. Shvartsman), *w**; ; *20XUAS-TTS-shi[1]* (temperature-sensitive Dynamin; Pfeiffer *et al.,* 2012, via A. Sustar), *y* w**; *shg::GFP* (endogenous E-Cadherin::GFP; Huang *et al.,* 2009, via M. Osterfield), *y* w**; *EGFP::Rab5*/*CyO* (endogenous EGFP::Rab5) and *y* w**; *UASP-shi::YFP* (Dynamin::YFP; Fabrowski *et al.,* 2013, via S. De Renzis), *w**; ; *UAS-shg::GFP* (E-Cadherin::GFP; Oda and Tsukita 1999, via S. Hou), *w**; ; *UAS-βPS-Integrin(mys), UAS-PS1-Integrin(mew)* and *w**; ; *UAS-βPS-Integrin(mys), UAS-PS2-Integrin(if)* (Beumer *et al.,* 1999; Beumer *et al.,* 2002, via K. Broadie), and *P{GawB}A90* (*A90-GAL4*; Gustafson and Boulianne 1996, via G. Boulianne). The *Vm26Aa-GAL4* driver is described in Peters *et al.,* 2013. To visualize floor cells, I used *y* w **; *P{w+mC=Rho(ve)-lacZ.0.7}* (*rhomboid-lacZ* reporter; Ip *et al.,* 1992).

Immunostaining

Ovary immunostaining was as described (Ward and Berg, 2005; Zimmerman *et al.,* 2013), except that permeabilizations were performed with 2% Triton in PBT (PBS + 0.1%

Tween). Antibodies used were rabbit anti-β-galactosidase (pre-adsorbed 1:500, 1:10,000 final dilution; Cappel), rabbit anti-GFP (1:200, Molecular Probes), mouse anti-BR-core (1:250, 25E9.D7-concentrate, Developmental Studies Hybridoma Bank, DSHB; Emery *et al.,* 1994), rat anti-α-E-cadherin (1:50, DCAD2-concentrate, DSHB; Oda *et al.,* 1994), mouse anti-α-Spectrin (1:50, 3A9-concentrate, DSHB; Dubreuil *et al.,* 1987), mouse anti-β-PS-Integrin (1:50, CF.6G11-concentrate, DSHB; Brower *et al.,* 1984), mouse anti-β-Catenin (1:50, N2 7A1-concentrate, DSHB; Peifer *et al.,* 1992), rabbit anti-Dynamin (1:100, Ab 2074, via M. Ramaswami; Estes *et al.,* 1996) and goat anti-mouse Alexa Fluor 488-, 555-, and 647-conjugated antibodies (1:500, Molecular Probes). Imaging was performed on either a Zeiss 510 or Leica SP8X scanning confocal microscope (immunostaining, live imaging), or a Nikon Microphot FXA (eggshells). Images were processed using Helicon Focus (Helicon Soft Ltd.) and FIJI (ImageJ-based, NIH; Schneider *et al.,* 2012).

Tissue-specific expression: GAL4-UAS

I crossed *GAL4*-bearing virgin females to *UAS*-bearing males at 25°C, or at 18°C if the *GAL4-UAS* combination resulted in lethality at 25°C. To collect eggs, I mated female progeny from these crosses to w^{1118} males at 30°C in the presence of wet yeast, to optimize *GAL4* expression and egg production. After >24 hr at 30°C, I collected eggs over successive 8-12-hr periods on apple juice/agar plates, then rinsed, pooled, and mounted the eggs in Hoyer's medium (van der Meer, 1977). If a *GAL4-UAS* combination perturbed egg-laying, I dissected ovaries, fixed in 4% para-formaldehyde for 20 min, dissociated ovaries, and either proceeded with immunostaining, or eggshell preparation in Hoyer's medium. For some over-expression assays, to evaluate more moderate defects and determine which features were most sensitive to

perturbation, I collected eggs from flies kept at 25°C or 28°C. In addition to qualitative descriptions, I evaluated DA defects using a three-tiered scoring system (N = normal DAs or DAs with mild defects, M = moderate DA defects, S = severe DA defects), counting a minimum of 100 eggs (mean = 312 eggs). Moderate defects included rough/feathered DA shape, a difference in DA length within the DA pair, wide DA paddles, shafts, or bases, and short DAs that extended past the micropyle. Severe DA defects included short and/or wide DAs that did not extend past the micropyle, fused DAs, or a combination of moderate defects.

Quantitative cytology

To quantify the dimensions of Broad-expressing roof FC primordia (Fig 3A-K), I made the following measurements using FIJI (ImageJ). For anterior-posterior (AP) length, I made a maximum-intensity XY projection of each egg chamber and measured the length from the most anterior to the most posterior roof FC nucleus. For dorsoventral (DV) width, which occurs along a curved surface, I made a 3D projection of each egg chamber around the Y axis, rotated the projection to view the egg chamber head on, and measured the circumferential distance from the most dorsal to the most ventral roof FC nucleus in each primordium (inset in Fig 3.3K). For each condition at each stage, I measured a minimum of 10 primordia (mean = 12 primordia), and for AP:DV ratios I only used primordia for which I could obtain both AP and DV measurements.

To quantify the apical dimensions and surface area of anterior and posterior roof FC apices (Fig 3.3L-W), I made the following measurements using FIJI (ImageJ). For anterior and posterior roof FC apices, I chose ~3 non-adjacent cells in the front 1/3 or rear 1/3 of each roof FC primordium, respectively (Fig 3.3 L-U), and I only measured apices for which I could achieve a view perpendicular to the apical plane. For each apical surface, I measured AP and

DV lines that intersected at their midpoints and at the center of the apical surface (inset in Fig 3.3V), and I traced the outline of the apical surface and measured the area (inset in Fig 3.3W). For each condition at each stage, I measured a minimum of 20 apices (mean = 47 apices).

For statistical analyses, I compared means using ANOVA and Tukey's posthoc tests.

Live imaging

I dissected ovaries from flies raised at 30°C in Schneider's medium (S2 cell culture medium; Sigma), equilibrated to 30°C, and combed the ovarioles apart. I then carefully squeezed individual S10B egg chambers out of their ovariole muscle sheaths to avoid complications from muscle contractions during live imaging. Once liberated, I transferred these S10B egg chambers to fresh 30 °C S2 medium in a coverslip-bottomed 35mm culture dish (MatTek Corp.) that had already been positioned on an inverted-objective, scanning confocal microscope. During subsequent steps, the temperature of the medium was allowed to fall to room temperature, ~22°C. I brushed the egg chambers into the center of the coverslip, soaked and sank a small (~1cm x 1cm) piece of Kimwipe into the S2 medium and positioned it over the egg chambers like a blanket. I placed a small (>1cm diameter) brass washer over the Kimwipe such that it surrounded, but did not lie on top of, the egg chambers. This weight provided just enough downward force on the egg chambers to keep them in place without crushing them, a precaution that was particularly necessary because DA-tube elongation is a forceful process, and DA-tube cells will easily push an unanchored egg chamber away from the coverslip. Once anchored, I selected the best S10B or S11 dorsal- or dorsolateral-oriented egg chamber, and collected Z-stacks for 10 hours at 15-minute time intervals. I subsequently processed the movies in Imaris (Bitplane, Oxford Instruments).

– Results –

Expression of dominant-negative Dynamin in DA-tube cells disrupts DA tubulogenesis

To characterize Dynamin's role in promoting DA tubulogenesis, I disrupted its function by expressing dominant-negative, GTP-hydrolysis-defective forms of Dynamin (*shibire[1ts]* (functional at 25°C, DN at 30°C) van der Bliek and Meyerowitz 1991; *shibire[K44A]* (always DN), van der Bliek *et al.,* 1993) in the DA-tube cells using the *GAL4-UAS* system (Brand and Perrimon, 1993). I targeted DA-tube cells with the *brL-GAL4* driver (*broad Late* enhancer, Fuchs *et al.,* 2012). At 25 ^{o}C, I determined that GAL4-driven expression of CD8::GFP is restricted to roof and floor cells; at 30 ^{o}C, I determined that CD8::GFP expression was also detectable in nearby anterior FC types (centripetal, midline, and stretch FCs) and main-body FCs posterior and ventral to the DA primordia (Fig 3.1A, B, C, and D*)*. This expanded expression pattern included all cell types that contribute to DA tubulogenesis (roof, floor, and stretch FCs), and was therefore favorable. To assess DA defects, I scored eggshell DAs as either normal (N), moderately defective (M) or severely defective (S), and represented the proportions of each category (Fig 3.1; see methods).

DAs of *brL>CD8::GFP* eggs were slightly shorter than those of wild type but exhibited the expected wild-type DA morphology: a narrow stalk connected to a widened, anterior paddle (Fig 3.1E). These control eggs displayed minimal DA defects at 25 ^{o}C and 30 ^{o}C (Fig 3.1E and F). DAs of *brL>shi[1ts]* eggs were indistinguishable from controls at 25 ^{o}C, indicating that moderate over-expression of functional Dynamin does not disrupt DA-tube morphogenesis (Fig 3.1G). At 30 ^{o}C, a temperature at which *shi[1ts]*-encoded Dynamin acts as a semi-dominant negative (van der Bliek et a., 1993), the eggs exhibited shorter, wider DAs with moderate

penetrance and expressivity (Fig 3.1H). The DA defects of *brL>shi[K44A]* (dominant negative) eggs produced at 25 ^{o}C were similar in frequency and severity to those of *brL>shi[1ts]* eggs at 30 ^{o}C (compare Fig 3.1H with Fig 3.1I). At 30 ^{o}C, *brL>shi[K44A]* eggs displayed DA defects of substantially higher severity and penetrance (Fig 3.1J), supporting the hypothesis that the degree of *shi[K44A]*'s disruptive effect depends on expression level (Moline *et al.,* 1999). These DAs were short, wide, and flat, had rough, irregular edges, and were either closer together than controls (Fig 3.1J, red arrowheads) or had become fused (Fig 3.1J, magenta arrowhead). In addition, the eggs themselves were shorter, indicating either incomplete nurse-cell dumping or a defect in egg-chamber elongation [Mahajan-Miklos and Cooley, 1994; Horne-Badinovac and Bilder, 2005]. Taken together, these results support my previous observation that Dynamin is required in the FCs for DA-tube elongation and indicate that *shi[K44A]* expression is an effective and penetrant tool for disrupting Dynamin function in FCs. Furthermore, the dramatically widened DA bases and frequent DA fusions suggested that Dynamin could also play a role earlier, in DA-tube formation.

Since at 30 ^{o}C the *brL-GAL4* driver expresses in all FC types that contribute to DA tubulogenesis, I wanted to determine whether all or just some of these FC types require Dynamin. At that time, I was mentoring a summer undergraduate, Kamsi Odinammadu, and this became his summer research project. To restrict expression to DA-tube cells specifically, he used *br*[*69B08]-GAL4 (*Jenett *et al., 2012)*, which drives expression specifically in roof and floor cells (data not shown and personal communication from N. Yakoby), even at 30 ^{o}C (Fig 3.1K and L). Control *br*[*69B08]-GAL4>CD8::GFP* eggs displayed a much higher proportion of DA defects than control *brL>CD8::GFP* eggs, but these baseline defects were primarily associated with DA length, not width or shape (compare Fig 3.1F with 1O). The DAs of

Fig 3.1. (**A-D**) Control *brL >CD8::GFP* egg chambers raised at 30°C, stained for Broad protein (roof FC nuclei – yellow, yellow arrows), DNA (DAPI – blue). All subsequent images are shown with the anterior facing left, and dashed white lines indicate dorsal midlines. (**E-J**) Laid eggs from control *brL >CD8::GFP* (**E, F**), *brL >shi[1ts]* (**G, H**), or *brL >shi[K44A]* (**I, J**) females, raised at either 25 ˚C (**E-I**) or 30 ˚C (**F-J**). In **E**, the parts of a wild-type DA are labeled (paddle, stalk, base). Numbers indicate percentages of normal or mildly defective (N), moderately defective (M), and severely defective (S) DAs; yellow numbers indicate the category of egg being shown. The number of eggs scored for each condition is shown in the lower left of each panel. Red arrowheads indicate abnormally wide DAs, orange brackets indicate abnormally wide DA bases, magenta arrowheads indicate DA fusions, and magenta brackets indicate fused DA bases. (**K, L**) Control *br[69B08] >CD8::GFP* egg chambers raised at 30 °C, stained for DNA (DAPI – blue). (**M, N**) Control *A90 >CD8::GFP* egg chambers raised at 30 °C, stained for DNA (DAPI – blue). (**O, P**) Laid eggs from control *br[69B08] >CD8::GFP* (O) or *br[69B08] >shi[K44A]* (P) females raised at 30 ˚C. (**Q, R**) Laid eggs from control *A90 >CD8::GFP* (Q) or *A90 >shi[K44A]* (R) females raised at 30 ˚C. Scale bars = 100 μm.

Figure 3.1. FC expression of dominant-negative Dynamin disrupts DA tubulogenesis

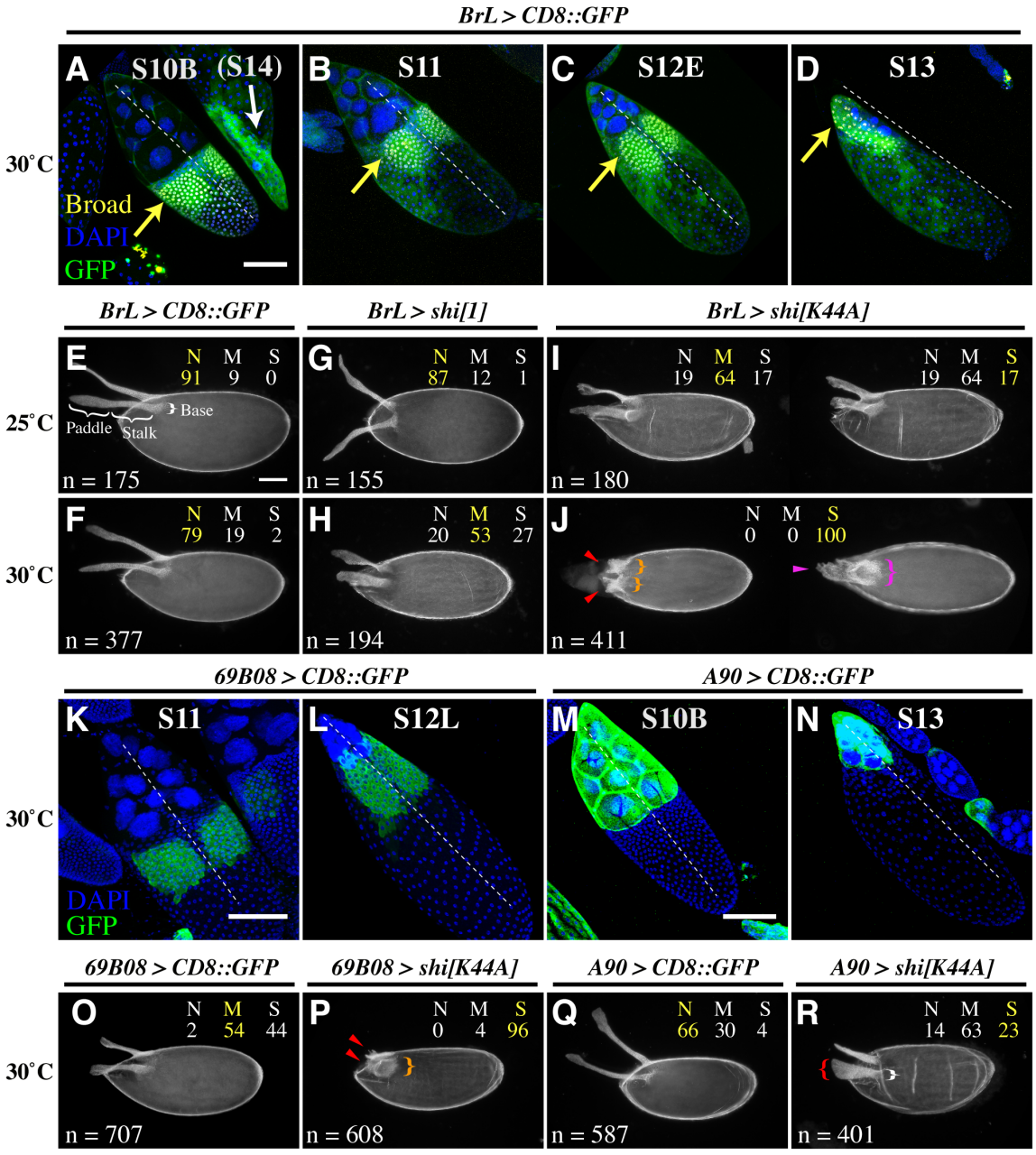

br[*69B08*]>*shi[K44A]* eggs, on the other hand, were stunted, wide, and irregular in shape (Fig 3.1P, red arrowheads), like those of *brL>shi[K44A]* eggs (Fig 3.1J, red arrowheads). Despite these similarities in DA morphology, fewer DA fusions occurred in *br*[*69B08*]>*shi[K44A]* eggs; this difference may be due to expression of Gal4 in midline cells with *brL-GAL4* but not with *br*[*69B08]-GAL4* (compare Fig 3.1A, B, C, and D with K and L). These results demonstrate that the DA-tube cells themselves (*i.e.,* roof and floor FCs) require functional Dynamin for DA tubulogenesis.

Kamsi next tested whether Dynamin function in stretch FCs is required for DA tubulogenesis using the *A90-GAL4* driver (Fig 3.1M and N), since I observed highest *shibire* expression in stretch FCs (Peters *et al.,* 2013). DAs of *A90>shi[K44A]* eggs were indeed shorter and wider than DAs of control *A90>CD8::GFP* eggs, but their smooth edges suggested that DA-tube integrity had been maintained. Furthermore, DA bases were narrow, distinct, and resembled controls, suggesting that DA-tube closure was successful (compare Fig 3.1Q with 1R). These results demonstrate that the stretch FCs, as well as DA-tube cells, require Dynamin function for DA tubulogenesis, but that Dynamin's function in stretch FCs is distinct from its role in the DA-tube cells: it does not appear to influence DA-tube formation or DA-tube integrity, but instead restricts tube width and promotes tube length.

Dynamin is required in the floor FCs for DA-tube closure

The formation of the DA tube requires the cooperative actions of two distinct, juxtaposed cell types: roof FCs and floor FCs (Dorman *et al.,* 2004, Ward and Berg 2005, Osterfield *et al.,* 2013). The wide and often fused DAs exhibited by *brL>shi[K44A]* eggs suggested that Dynamin could be required for DA-tube formation as well as elongation. To test this hypothesis,

I used *brL-GAL4* to drive expression of either *CD8::GFP* or *shi[K44A]*, and I compared floor FC morphology (*rhomboid-lacZ* marker – *rho-lacZ*) throughout DA tubulogenesis (S11—S14; Fig 3.2). I found no obvious differences between control *brL>CD8::GFP* and *brL>shi[K44A]* egg chambers during S10B, indicating that *brL>shi[K44A]* expression did not affect DA-tube patterning (data not shown), or during S11, when DA tubulogenesis begins (compare Fig 3.2A to F). By early S12, the first differences between *brL>CD8::GFP* and *brL>shi[K44A]* egg chambers were apparent: whereas control floor FCs had sealed together to complete tube formation (Fig 3.2B; orange arrow), the floor FC hinge in Dynamin[DN] egg chambers remained open (Fig 3.2G). By late S12, control roof FCs had continued to intercalate, and the floor FCs had shortened along their apical-basal axes and were migrating anteriorly over the dying nurse cells (Fig 3.2C). As a result, the distance between the two primordia increased along the dorsal midline, especially near the DA bases. These movements proceeded through S13 (Fig 3.2D) and S14 (Fig 3.2E), with the DA tube remaining sealed throughout this time (orange arrows), until the floor FCs were arranged in two rows along the AP axis and had adopted the shape of the finished DA tube (Fig 3.2E). In contrast, roof FCs in *brL>shi[K44A]* egg chambers did not intercalate correctly between S12—S14, the floor FCs did not change shape or move anteriorly around the nurse cell nuclei. Furthermore, the two primordia stayed in contact along the dorsal midline, and the DA tubes remained unsealed (Fig 3.2G, H, I, J, orange dotted lines). Indeed, I never observed an instance of DA-tube closure in *brL>shi[K44A]* egg chambers from S12—S14 (n = 95). Interestingly, I observed cytoplasmic protrusions on the leading edges of *brL>shi[K44A]* floor FCs in S14, indicating that the floor cells

Fig 3.2. (**A-J**) Anterior views of S11—S14 control *brL >CD8::GFP* (**A-F**) vs. *brL >shi[K44A]* (**G-L**) egg chambers, stained for DNA (DAPI – blue), Broad protein (roof-FC nuclei – red), and β-galactosidase produced by *rhomboid-lacZ* (floor FCs – yellow or white). Each panel also includes an orange tracing of floor FC outlines for a single DA tube, with orange dotted lines indicating an open DA tube and orange arrows indicating a sealed DA tube. Note that while control DA tubes have closed by S12E (**B**) and remain closed (**C-E**), dominant-negative-Dynamin-expressing DA tubes fail to close (**G-J**), although floor-FC leading edges still attempt anterior migration (inset in **J**). Scale bar = 50 μm.

Figure 3.2. FC expression of dominant-negative Dynamin disrupts DA-tube closure

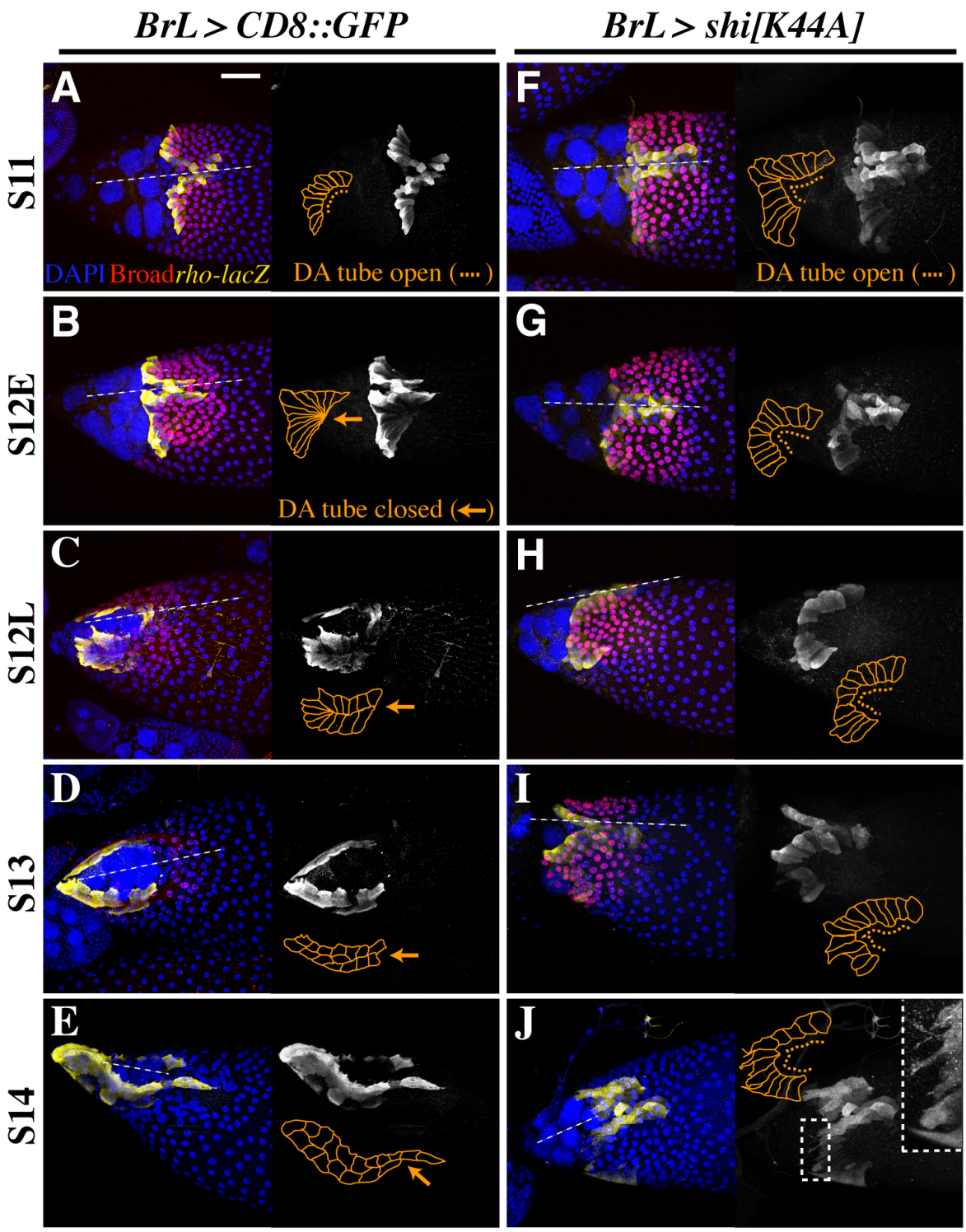

were still attempting to migrate in an anterior direction (inset in Fig 3.2J). Together, these data revealed a dramatic failure of DA-tube formation in *brL>shi[K44A]* egg chambers and demonstrated that Dynamin plays a critical role in DA-tube closure and roof-FC intercalation.

As the floor FCs and overlying roof FCs failed to move out over the stretch FCs during S12—S14, I also noted that the remnant nurse-cell nuclei failed to fully degrade by S14 (Fig 3.2J). Since stretch FCs may help remove the nurse cells by engulfment (Cummings and King 1970; Nezis *et al.,* 2000; Jenkins *et al.,* 2013), the failure of nurse-cell degradation could mean that stretch FCs require Dynamin for this process. Nevertheless, since floor FCs seal up the DA tube before moving out over the stretch FCs (Fig 3.2B), and because I did not observe eggshell defects consistent with DA-tube closure defects in *A90>shi[K44A]* eggs (stretch FC-specific, Fig 3.1R), it is unlikely that the stretch FCs play a direct role in the early events of DA-tube closure.

Dynamin is required for roof-FC intercalation during DA-tube elongation

To reveal cellular behaviors that could explain the eggshell defects I observed upon *brL>shi[K44A]* expression, and to determine whether *brL>shi[K44A]* expression affected the viability of DA-tube cells, I examined DA tubulogenesis live using an E-Cadherin::GFP knock-in strain (Huang *et al.,* 2009). I compared control egg chambers that also expressed *brL-GAL4* (Movies 3.1 and 3.2) to Dynamin[DN] egg chambers expressing both endogenous E-Cadherin::GFP and *brL>shi[K44A]* (Movies 3.3 and 3.4). In control egg chambers, roof-cell apical constriction and DA-tube formation were quickly followed by intercalation and dramatic, anterior DA-tube elongation (Movies 3.1 and 3.2). Between 7-9 hours after DA-tube formation, I observed significant eggshell secretion, indicating that my culturing conditions were not

affecting egg chamber viability (Movie 3.2). In E-Cadherin::GFP *brL>shi[K44A]* egg chambers, apical constriction occurred normally as in controls, but in contrast to controls, the DA tubes did not narrow and elongate along the DV axis; each patch remained wide and appeared disorganized, reflecting the DA-tube-formation defects I saw in fixed tissue (Fig 3.2; Movies 3.3 and 3.4). Roof-cell apical expansion occurred at the expected time, but DA-tube-cell apices did not properly intercalate, and DA-tube elongation was severely impaired and disordered (Movies 3.3 and 3.4). In some cases, I observed DA-tube fusions resulting from a loss of distinction between DA-tube cells and midline cells (Movie S4); these phenotypes were consistent with DA fusions I observed in laid eggs (Fig 3.1J). Importantly, eggshell secretion occurred at a time comparable to controls (compare Movie 3.2 to 3.3 or 3.4). Interestingly, I also noted altered behavior of E-Cadherin in *brL>shi[K44A]* egg chambers; E-cadherin accumulated in apical "blobs", which appeared prior to and during eggshell secretion (Movies 3.3 and 3.4). These live-imaging data demonstrated that *brL>shi[K44A]* expression did not affect FC viability or eggshell secretion but did affect E-Cadherin behavior, and suggested that defects in DA-tube-cell intercalation might underlie the observed DA-tube elongation defects.

Prior to DA tubulogenesis, each roof FC primordium is wider along the DV axis than it is along the AP axis; during DA-tube elongation, the primordia shrink in width and extend in length as the roof FCs intercalate (Dorman et al. 2004; Ward and Berg 2005). To ascertain the underlying mechanisms that contribute to Dynamin[DN]- associated tube-elongation defects, I tested whether *brL>shi[K44A]* expression affected roof FC patterning or intercalation (Broad protein stains; Fig 3.3A-K).

I first asked whether disrupting Dynamin function had any effect on roof-FC patterning. I compared the number of BR-positive nuclei in *brL>CD8::GFP* control and *brL>shi*[K44A] egg

Fig 3.3. (**A-J**, **L-U**) Anterior views of S10B—S13 control *brL >CD8::GFP* (**A-E**, **L-P**) vs. *brL >shi[K44A]* (**F-J**, **Q-U**) egg chambers, stained for Broad protein (roof-FC nuclei – green **A-E**, magenta **F-J**), and E-Cadherin (FC apices – **L-U** white). Broad and E-Cadherin stains were administered on the same egg chamber (*e.g.,* **A** and **L**, **F** and **Q**). The number of egg chambers scored for each condition is shown in the lower right of panels **A-J**. (**L-U**) Full-sized images (left) are accompanied by enlarged insets of roof-FC apices (right), and labeled A (anterior) or P (posterior) if the enlargement is split. In enlarged panels, representative examples of anterior (red or orange) or posterior (blue or cyan) apices are outlined, and the total number of apices compared for each condition is indicated. (**K, V**) Mean AP length : DV width ratios, ± standard error, for roof-FC primordia (**K**) or roof-FC apices (**V**) as a function of stage (S10B—S13). (**W**) Mean surface area, ± standard error, for roof-FC apices as a function of stage (S10B—S13). Insets in K, V, and W indicate how AP length, DV width, or apical surface area were measured (see also methods); asterisks indicate statistical differences (* = $p<0.05$, ** = $p<0.001$, and asterisk color indicates which value was greater (green vs. magenta, red vs. orange, blue vs. cyan)). Colors are consistent between images (**A-J**, **L-U**) and charts (**K**, **V**, **W**). Scale bars = 50 μm.

Figure 3.3. FC-expression of dominant-negative Dynamin disrupts roof FC intercalation and anterior-biased apical expansion

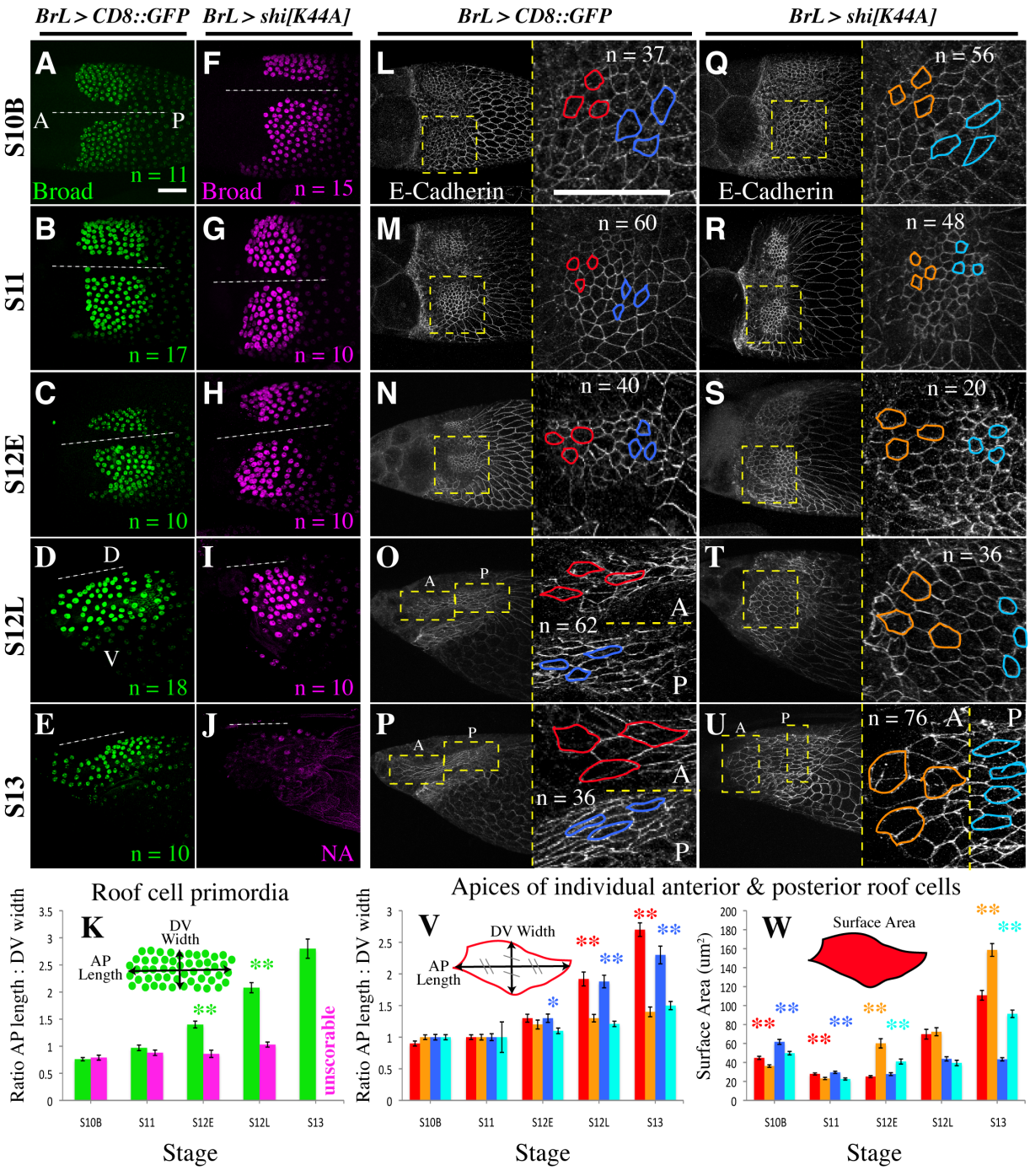

chambers between S10B—S12 (once patterned, the number of BR nuclei remain constant; Ward and Berg 2005). I found no significant difference ($p>0.1$) between the number of BR-positive nuclei in *brL>CD8::GFP* control egg chambers (67 nuclei per primordium, n=49) and *brL>shi[K44A]* egg chambers (65 nuclei per primordium, n=35), indicating that *brL>shi[K44A]* does not affect roof FC patterning as revealed by BR protein expression.

To compare the dimensions of the roof-FC primordia, I measured the ratio of AP length to DV width in control and *brL>shi[K44A]* roof-FC primordia from stages 10B—S13 (see methods and schematic in Fig 3.3K). As expected, I observed that roof FCs in S10B control *brL>CD8::GFP* egg chambers were positioned on either side of the dorsal midline and that the DV width was greater than the AP length (AP:DV ratio=0.8, Fig 3.3A, first green bar in Fig 3.3K). By S11, the AP:DV ratio was 1; by the end of S12, it had increased to 2.1; and by the end of S13, roof FC primordia were 2.8 times longer than they were wide, indicating substantial roof-FC reorganization during DA-tube expansion (Fig 3.3B, C, D, and E, green bars in Fig .33K). In *brL>shi[K44A]* egg chambers, the roof-FC primordia at S10B resembled controls, with similar position and AP:DV character (AP:DV ratio=0.8, Fig 3.3F, first magenta bar in Fig 3.3K), but during S11—S14, the roof-FC nuclei remained relatively static and did not reorganize along the AP axis (Fig 3.3G, H, I, and J, magenta bars in Fig 3.3K, green asterisks indicate $p<0.001$). I could not measure roof-FC primordia dimensions in S13 and older *brL>shi[K44A]* egg chambers because the BR signal was too weak and variable (Fig 3.3J and K). This apparent early loss of Broad protein in S13 *brL>shi[K44A]* egg chambers could suggest that Dynamin helps maintain Broad nuclear localization. Alternatively, these egg chambers were actually older, but neither nurse-cell death nor DA-tube elongation had proceeded normally. Together, that in addition to

floor FCs requiring Dynamin function during DA-tube formation, roof FCs require Dynamin function to intercalate during DA-tube elongation.

Dynamin is required for AP-biased apical expansion during DA-tube elongation

Concomitant with roof-FC intercalation and DA-tube elongation, the apical surfaces of DA-tube cells expand, increasing the volume of the tube and elongating the tubes toward the anterior of the egg chamber (Dorman *et al.,* 2004; Boyle et al, 2010). To compare the apical membrane morphology and behavior of roof FCs in control and *brL>shi[K44A]* egg chambers, I measured the ratio of apical AP length to apical DV width, as well as apical surface area, for individual roof FCs from S10B—S13. I compared 3 non-adjacent apices in the anterior (Fig 3.3, red vs. orange) and 3 non-adjacent apices in the posterior (Fig 3.3, blue vs. cyan) of each roof-FC primordium (see methods, enlargements in Fig 3.3L, M, N, O, P, Q, R, S, T, U, charts in Fig 3.3V, W). This detailed quantification of roof-FC apical behavior during DA tubulogenesis revealed a striking planar-polarized elongation of roof cells during tube expansion.

In *brL>CD8::GFP* control egg chambers at S10B, at the first initiation of roof-FC apical constriction, anterior apices (45 μm^2) began to constrict slightly before posterior apices (62 μm^2), and both anterior apices (0.9) and posterior apices (1.0) maintained a nearly equivalent AP:DV ratio (Fig 3.3L, V, W; see also Dorman *et al.,* 2004). In S11, constricted anterior (28 μm^2) and posterior (30 μm^2) apices were almost identical in area (Fig 3.3M, W), and the cells maintained an equivalent AP:DV ratio of 1.0 (Fig 3M and V). By early S12, as overlying roof FC nuclei began to rearrange and extend along the AP axis (Fig 3.3C), anterior (25 μm^2) and posterior (28 μm^2) apices remained tightly constricted, but their shapes began to change from hexagonal to

rhomboidal, resulting in an increase in AP:DV ratio (both = 1.3, Fig 3.3N, V, W). By late S12, anterior apices had substantially expanded (70 μm^2) while posterior apices (44 μm^2) had expanded to a lesser degree (Fig 3.3O and W), though again, cell shapes exhibited an equivalent AP:DV ratio of 1.9. These results suggest that both anterior and posterior cells within the primordium expand in an AP-biased direction (Fig 3.3O, V). By S13, the behavior of anterior apices had diverged from that of posterior apices. Anterior apices, which form the DA paddle, had expanded dramatically (111 μm^2), almost 3 times that of posterior apices (40 μm^2), which make the stalk, and the AP:DV ratio of anterior vs. posterior apices was 2.7 vs. 2.3, respectively (Fig 3.3P, U, V, W).

In *brL>shi[K44A]* egg chambers at S10B, as in controls, anterior apices (36 μm^2) began to constrict slightly before posterior apices (50 μm^2), and both anterior apices (1.0) and posterior apices (1.0) maintained equivalent AP:DV ratios (Fig 3.3Q, V, W). Interestingly, both anterior and posterior apical areas were significantly smaller than in controls ($p<0.001$). In S11, constricted anterior (23 μm^2) and posterior (23 μm^2) apices maintained an equivalent AP:DV ratio of 1.0 (Fig 3.3R, V, and W) and were again significantly smaller than controls ($p<0.001$). This smaller apical surface area could be due to *shi[K44A]* over-stimulating the apical constriction machinery, as shown in vertebrate cell culture (Chua *et al.,* 2009), or it could be due to smaller overall egg chamber size. Consistent with the latter possibility, I found that *brL>shi[K44A]* egg chambers were ~5% shorter than controls (482 μm vs 506 μm, n=12, $p<0.05$). By early S12, however, Dynamin[DN] egg chambers had reversed this trend toward tight apical constriction. Anterior apices (1.2) and posterior apices (1.1) had slightly increased in AP:DV ratio (Fig 3.3S and V), as was the case in controls, but unlike controls, anterior (60 μm^2) and posterior (41 μm^2) apices had expanded considerably (Fig 3.3S, W, $p<0.001$). By late S12,

anterior apices (72 μm^2) and posterior apices (40 μm^2) had slowed their expansion and now exhibited surface areas similar to controls (Fig 3.3T, W), but overall, this expansion had occurred without any AP bias; neither anterior nor posterior apices had increased in AP:DV ratio (S12E = 1.2, S12L = 1.3), and both were significantly lower than controls ($p<0.001$). These results revealed a failure of AP-biased expansion in *brL>shi[K44A]* roof FCs (Fig 3.3T, V). By S13, the behavior of anterior apices had diverged from that of posterior apices, and neither resembled controls. Surprisingly, anterior apices had expanded to 159 μm^2, and posterior apices had expanded to 91 μm^2; both values were significantly greater than controls (Fig 3.3U, W, $p<0.001$). The AP:DV ratio of anterior vs. posterior apices was 1.4 vs. 1.5, respectively (Fig 3.3U, V), again representing a significant departure from controls ($p<0.001$), and only a slight AP-biased apical expansion.

In summary, control roof FCs constricted their apices during tube formation at S11, then expanded these surfaces such that cells elongated preferentially on the AP axis during S12—S14. In contrast, disruption of Dynamin function in roof FCs caused cells to constrict their apices to an even greater degree than controls, and then expand these surfaces beyond controls in all directions, with little or no directional bias to the expansion, and without extending the DA tube in an anterior direction.

Dynamin's function in DA tubulogenesis is to promote endocytosis

Other studies have shown that Dynamin's functions include but are not limited to endocytosis (*e.g.,* Sever *et al.,* 2013; Thompson *et al.*, 2004; Soulet *et al.,* 2006). Therefore, I sought to determine whether Dynamin's function in DA tubulogenesis is to facilitate endocytosis. Therefore, I independently disrupted the function of two other well-characterized

endocytic players, Rab5 and AP50, and compared their eggshell phenotypes to those of *brL>shi[K44A]* eggshells (Fig 3.4; distinct data from Fig 3.1). The Rab5 GTPase is a rate-limiting component of the early endocytic pathway (Bucci *et al.,* 1992), and mutant Rab5[S34N] protein (S43N in *D. melanogaster*) acts as a strong dominant negative (Stenmark *et al.,* 1994). At 28 ^{o}C, the *brL>Rab5[S43N*] eggs exhibited a high frequency of severe DA defects (short, broad DAs) compared to controls (Fig 3.4A and C); *brL>shi[K44A]* eggs were similar in phenotype, though the frequency of severe defects was lower (Fig 3.4B). At 30 ^{o}C, the frequency and severity of DA defects on *brL>shi[K44A]* and *brL>Rab5[S43N]* eggs were indistinguishable: DA fusions were frequent (Fig 3.4E and F, magenta arrowheads), and eggshells displayed a similar shortened length compared with controls (Fig 4D, E, and F). In addition, loss of function through expression of *Rab5*-RNAi resulted in a severe and fully penetrant stunted DA phenotype compared to controls (Fig 3.4G and H). The stunted DAs of *brL>Rab5*-RNAi eggs were less broad than those of *brL>Rab5[S43N]* eggs, suggesting that *Rab5*-RNAi expression was weaker and/or less able to produce an effect due to perdurance of Rab5 protein compared to expression of dominant-negative Rab5[S43N] (compare red arrowheads in Fig 3.4F and H).

The AP2-adaptor complex is the primary membrane adaptor for clathrin, and RNAi against AP50 (AP2 subunit μ) is an effective tool for disrupting AP2 function and clathrin-mediated endocytosis (Motley *et al.,* 2003; Boucrot *et al.,* 2010, McMahon and Boucrot, 2011). The DAs of *brL>AP50*-RNAi eggs were wide, had irregular edges, and were sometimes fused (Fig 3.4I, magenta arrowhead), supporting the hypothesis that clathrin-mediated endocytosis facilitates DA-tube morphogenesis. These defects were not as severe or penetrant as those produced by *Rab5*-RNAi, *Rab5[S43N]*, or *shi[K44A]*, perhaps reflecting an incomplete

knockdown of AP50, which can be difficult to fully deplete (Boucrot *et al.,* 2010). Taken together, these results support a role for Dynamin in facilitating clathrin-mediated endocytosis and demonstrate a requirement for endocytosis during DA tubulogenesis.

Dynamin is present both apically and basally in DA-tube cells

To identify potential targets of Dynamin-mediated endocytosis within DA-tube FCs, I examined the localization of endogenous Dynamin protein in DA-tube cells during normal DA tubulogenesis (Fig 3.5). I observed the highest levels of Dynamin protein in the stretch FCs, consistent with previous mRNA expression data (Peters *et al.,* 2013), and this expression increased over the course of DA tubulogenesis (Fig 3.5A, B, C, and D). In DA-tube FCs, Dynamin protein redistributed from lateral membranes to the cytoplasm between S10B—S12 relative to adjacent main body FCs (Fig 3.5A and D), and by S12, the division between DA-tube-FC Dynamin and main-body-FC Dynamin was distinct (Fig 3.5D). Subcellular inspection of DA-tube FCs indicated that Dynamin protein was most prominent at cell apices (Fig 3.5E) and on the basal surface (Fig 3.5F). I also observed unexpected nuclear Dynamin signal, but I reasoned that this apparent sub-cellular distribution was likely due to cross-reactivity of the Dynamin antibody, which was polyclonal and unpurified. To obtain an independent evaluation of Dynamin localization, I drove expression of Dynamin::YFP (*UASp-shi::YFP*; Fabrowski *et al.,* 2014) using the *Vm26Aa-GAL4* driver; *Vm26Aa-GAL4* expresses in all columnar FCs, but because the *UASp-shi::YFP* was designed for germline, not somatic, expression, Dyn::YFP-was only visible in some cells (*i.e.,* mosaic), which afforded me the benefit of being able to visualize Dynamin::YFP in individual cells (Fig 3.5G). This approach confirmed that the highest concentration of Dynamin was present apically and basally in DA-tube cells (yellow

Fig 3.4. (**A-F**) Laid eggs from control *brL >CD8::GFP* (**A, D**), *brL >shi[K44A]* (**B, E**), or *brL >Rab5[S43N]* (**C, F**) females, raised at either 28 ˚C (**A-C**) or 30 ˚C (**D-F**). (**G-I**) Laid eggs from control *brL >mCherry*-RNAi (G), *brL >Rab5*-RNAi (H), or *brL >AP50*-RNAi (I) females, raised at 30 ˚C. Numbers indicate percentages of normal or mildly defective (N), moderately defective (M), and severely defective (S) DAs; yellow numbers indicate the category of egg being shown. The number of eggs scored for each condition is shown in the lower left of each panel. Red arrowheads indicate abnormally wide DAs, orange brackets indicate abnormally wide DA bases, purple arrowheads indicate DA fusions, and purple brackets indicate fused DA bases. Scale bar = 100 μm.

Figure 3.4. Defects associated with FC expression of dominant-negative Dynamin are consistent with a disruption in endocytosis.

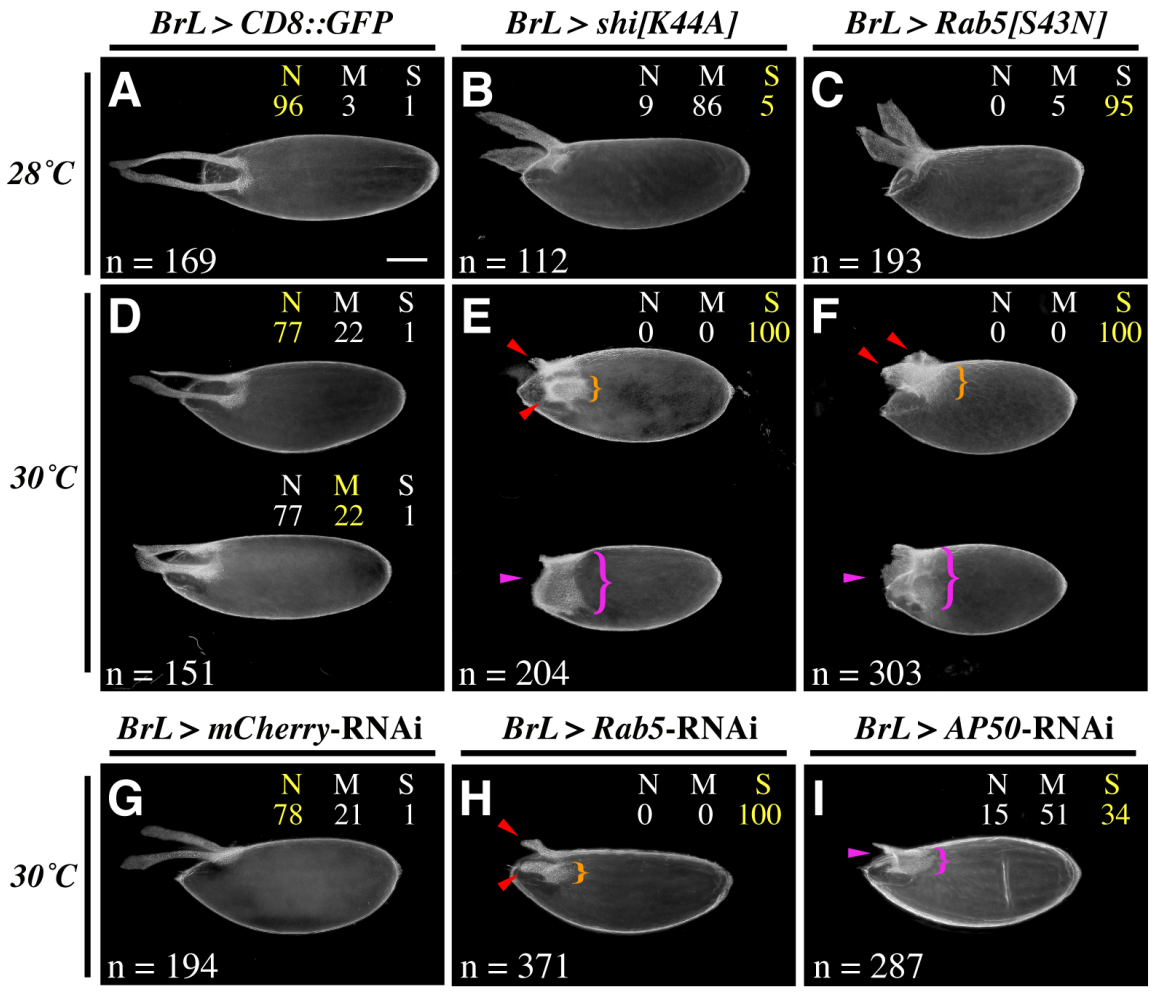

Fig 3.5. (**A-F**) Wild-type egg chambers stained for α-Spectrin (FC outlines – cyan), Dynamin (white), and/or DAPI (DNA – blue). From S10B (**A**) through S11 (**B**) and S12E (**C, D**), Dynamin protein in DA-tube FCs redistributes from FC membranes, and stretch-FC Dynamin levels increase dramatically. By S12L, the highest levels of Dynamin protein are visible at FC apices (**E**) and bases (**F**). Nuclear staining is non-specific. (**G, H**) *Vm26Aa-GAL4>UASp-shi::YFP* S12E egg chamber, in which Dyn::YFP (yellow) expression is mosaic due to the *P*-element promoter present in the UAS construct, stained for Actin (Phalloidin – red), and Dynamin (magenta). In **G**, which is an end-on, cross-sectional view of an egg chamber, yellow arrowheads indicate highest levels of Dyn::YFP at apices and bases of apically constricted DA-tube FCs, and the purple arrowhead indicates more uniform Dyn::YFP in basally constricted midline FCs. In **H**, which is a magnified view of the basal surface of DA-tube cells, dotted lines indicate FCs expressing high Dyn::YFP, and white-outlined arrowheads indicate co-localization of endogenous Dynamin protein and Dyn::YFP. Scale bars = 50 μm.

Figure 3.5. Dynamin protein behavior in DA-tube FCs during DA tubulogenesis.

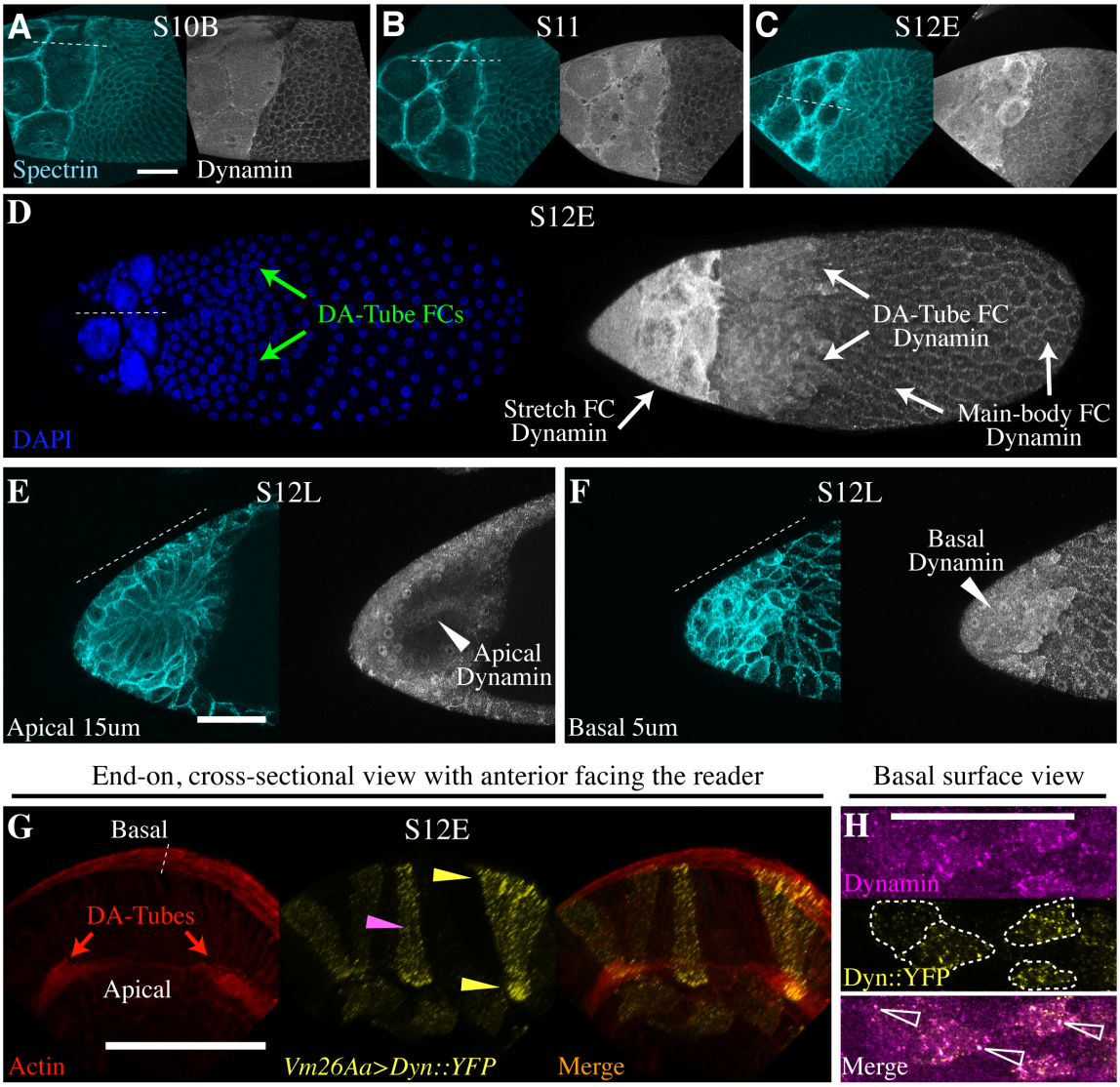

arrowheads), in contrast to nearby midline cells (pink arrowhead) or main body FCs (data not shown), and the absence of nuclear Dyn::YFP indicated that the Dynamin antibody did recognize a non-specific target(s) (Fig 3.5G). To verify that the Dynamin antibody recognized Dynamin, I stained *Vm26Aa>shi::YFP* egg chambers for Dynamin; I observed co-localization of Dynamin antibody with Dyn::YFP (Fig 3.5H, white arrowhead outlines). Together, these observations led us to hypothesize that Dynamin might be functioning both apically and basally to promote DA tubulogenesis.

Interestingly, and consistent with previous unpublished observations from our lab, midline FCs basally constricted during DA tubulogenesis such that they resembled apico-basally inverted DA-tube FCs (Fig 3.5G, pink arrowhead). Consistent with this observation, I noted high basal E-Cadherin in midline FCs (see also James *et al.,* 2002) relative to adjacent DA-tube FCs, and basal βPS-Integrin appeared to be relatively excluded (Fig 3.6A). Furthermore, basal midline-FC E-Cadherin co-localized with another AJ-component, β-Catenin (Fig 3.6B). These observations, along with the preferred apical and basal localization of Dynamin protein in DA-tube FCs, suggested that the endocytic remodeling of both apical and basal adhesions could be important for DA-tubulogenesis.

E-Cadherin- and Integrin-based adhesions display altered localization when Dynamin function is disrupted

I reasoned that apically localized Dynamin could be required for remodeling apical, E-Cadherin-based, cell-cell adhesions, a critical step for morphogenetic events involving cell intercalation and convergent extension (Ulrich *et al.,* 2005; Langevin *et al.,* 2005; Pirraglia *et al.,* 2006, Nishimura and Takeichi, 2009). Therefore, I compared E-Cadherin localization in

brL>CD8::GFP control and *brL>shi[K44A]* egg chambers at S12, early in DA-tube expansion, and at S13, late in DA-tube expansion (Fig 3.7). At S12, in DA-tube cells of control egg chambers, E-Cadherin was visible in the cytoplasm (Fig 3.7B, B') and outlining apical membranes (Fig 3.7B'). In DA-tube cells of S12 *brL>shi[K44A]* egg chambers, cytoplasmic E-Cadherin was greatly reduced (Fig 3.7D D'), and membrane-associated E-Cadherin was primarily apical (Fig 3.7D'). At S13 in control DA-tube cells (Fig 3.7E, F E', F'), cytoplasmic E-cadherin remained punctate (Fig 3.7F), while apical, membrane-associated E-Cadherin was higher than during S12 (compare Fig 3.7F' to B'). In contrast, DA-tube cells of S13 *brL>shi[K44A]* egg chambers had less cytoplasmic, punctate E-Cadherin than controls (compare Fig 3.7H to F), and apical E-Cadherin was more uniformly distributed along membranes than in controls (compare Fig 3.7H' to F'). In summary, *brL>shi[K44A]* egg chambers displayed weaker cytoplasmic E-Cadherin localization compared to controls, more uniform, apical, membrane-associated E-Cadherin than in controls, and these effects were more pronounced with time. These data show that disrupting Dynamin function alters E-Cadherin localization in FCs, particularly DA-tube cells, and are consistent with Dynamin functioning to remodel apical, E-Cadherin-based adhesions during DA tubulogenesis.

Conversely, I reasoned that basally localized Dynamin could be required for endocytic turnover of basal, Integrin-based adhesions, a critical step for morphogenetic events involving cell migration and tissue elongation (He *et al.,* 2010; Dong *et al.,* 2011; Huttenlocher *et al.,* 2011; Bogdanovic *et al.,* 2012). Therefore, I compared the localization of βPS-Integrin (encoded by *myospheroid*) in *brL>CD8::GFP* control and *brL>shi[K44A]* egg chambers during DA-tube expansion (S12—S13; Fig 3.7). In DA-tube cells of control egg chambers, βPS-Integrin was present on the basal surface and in basal puncta (Fig 3.7J and N), and sub-basally on lateral

Fig 3.6. (**A**) Basal projection of a S11 *brL > CD8::GFP* egg chamber stained for DAPI (**A**), E-Cadherin (**A´**), and βPS-Integrin (**A´´**). White (**A´**) or magenta (**A´´´**) brackets indicate high basal E-Cadherin in midline FCs; white dotted bracket (**A´´**) indicates low basal βPS-Integrin in midline FCs. (**B**) Basal projection of a *brL > CD8::GFP* egg chamber stained for DAPI (**B**), E-Cadherin (**B´**), and β-Catenin (**B´´**). White arrowhead (**B´´´**) indicates basal co-localization of the AJ components E-Cadherin and β-Catenin. Scale bar = 100 μm.

Figure 3.6. Midline FCs display inverted adhesion-molecule localization relative to DA-tube FCs.

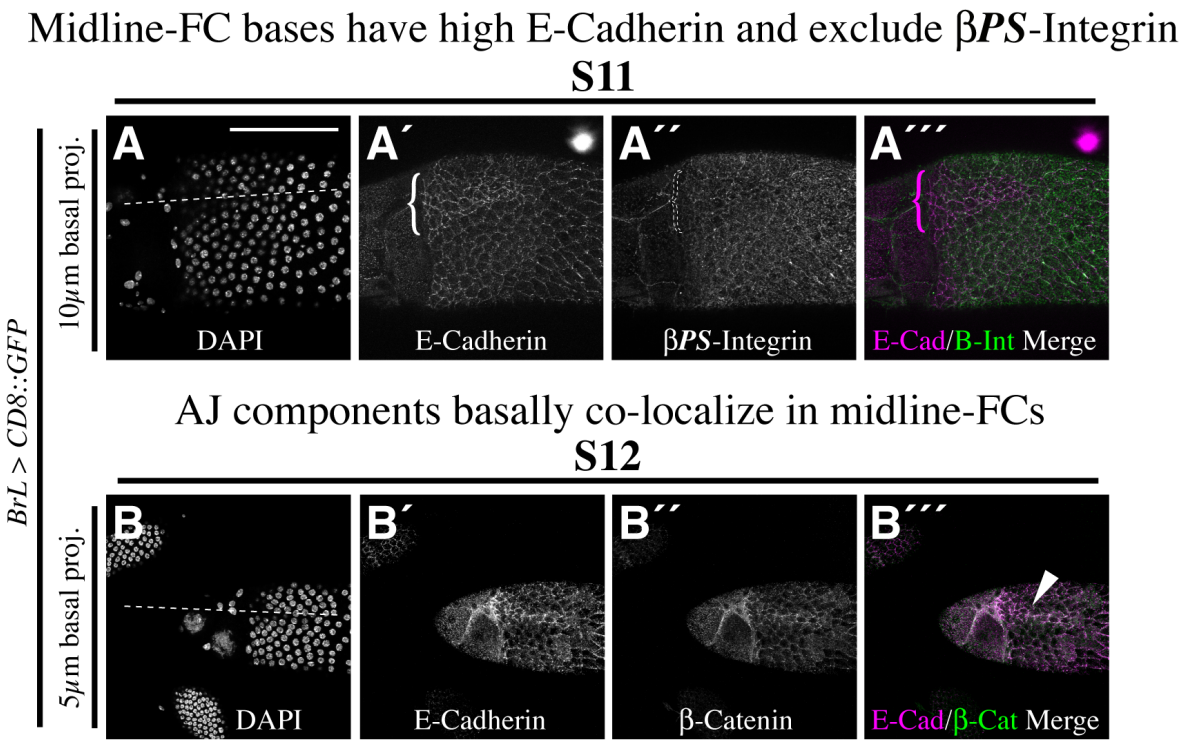

Fig 3.7. (**A-P**) Anterior views of S12 and S13 control *brL >CD8::GFP* (**A-B´**, **E-F´**) vs. *brL >shi[K44A]* (**C-D´**, **G-H´**) egg chambers, stained for E-Cadherin (encoded by *shotgun* – **A-H´**) and βPS-Integrin (encoded by *myospheroid* – **I-P´**). Diagrams to the left indicate the approximate Z-dimension used for either apical or basal projections, with green indicating basal, orange indicating apical, blue indicating roof FCs, red indicating floor FCs, and magenta indicating the roof-FC—main-body-FC boundary. For each E-Cadherin or βPS-Integrin full-sized image (left), there is an enlarged view (right). Arrowheads indicate cytoplasmic puncta details, arrows indicate membrane-associated details, and colors correspond with colors in the diagram (*e.g.*, blue color points out a roof FC feature, orange color points out an apical feature, green color points out a basal feature). Scale bars = 50 μm.

Figure 3.7. FC expression of dominant-negative Dynamin alters E-Cadherin and βPS-Integrin localization.

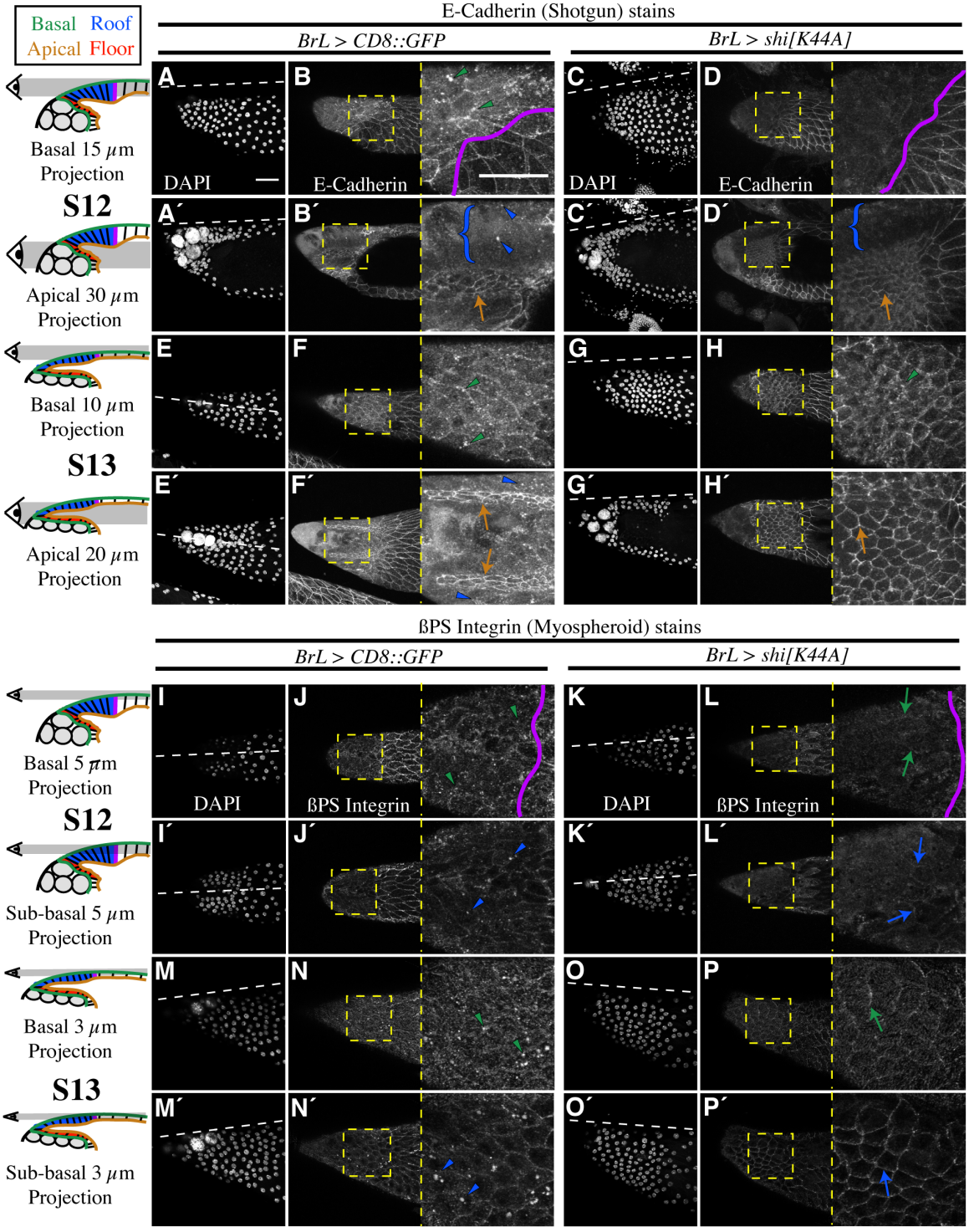

membranes and in large, cytoplasmic puncta (Fig 3.7J' and N'). In DA-tube cells of *brL>shi[K44A]* egg chambers, I observed βPS-Integrin on the basal surface as in controls, but the pattern appeared more ordered; basal puncta were less conspicuous, and cell outlines were more prominent than controls (compare Fig 3.7J and N to L and P). βPS-Integrin was also more uniform along sub-basal, lateral membranes than controls, and the large, cytoplasmic puncta were not visible (compare Fig 3.7J' and N' to L' and P'). In summary, S12 and S13 *brL>shi*[K44A] egg chambers displayed more-ordered basal βPS-Integrin, more-uniform sub-basal βPS-Integrin on lateral membranes, and less-punctate basal and cytoplasmic βPS-Integrin than controls, and these effects were progressive. These data demonstrate that disrupting Dynamin function alters βPS-Integrin localization in DA-tube FCs and are consistent with Dynamin functioning in the turnover of basal, Integrin-based adhesions during DA-tube migration and elongation.

Altering the behavior of Cadherin- and Integrin-based adhesions demonstrates that the regulation of adhesion molecules is essential for DA tubulogenesis

Disrupting Dynamin function alters the level and sub-cellular distribution of E-Cadherin (Fig 3.7, Movies 3.3 and 3.4) and βPS-Integrin (Fig 3.7), particularly during DA- tube expansion, suggesting that the regulation of both apical and basal adhesive turnover could be an important function of Dynamin. Thus, individually disrupting E-Cadherin- and βPS-Integrin-based adhesions could reveal their separate contributions to DA-tube expansion. To this end, I used *brL-GAL4* to drive the expression of loss-of-function and over-expression constructs and compared the resulting eggshell DA defects to controls (Fig 3.8).

First, I assessed the effects of adhesion-component knockdown. DAs of *brL>E-Cadherin*-RNAi eggs were dramatically reduced in length and located further back on the egg relative to controls (Fig 3.8A and B). DAs and DA bases were wider than controls and exhibited both detached chorion particles (white arrow in Fig 3.8B) and gaps in eggshell deposition (posterior region of DAs in right egg, Fig 3.8B), consistent with loss of cell-cell adhesion and aberrant eggshell secretion. Despite these defects, I did not observe an increased frequency of DA-fusion in *brL>E-Cadherin*-RNAi eggs relative to controls. Knockdown of *β-Integrin-ν*, an infrequently used *Drosophila* Integrin subunit (FlyBase: Graveley *et al.,* 2011), resulted in only modest defects, such as thinner DAs (Fig 3.8C), whereas knockdown of *βPS-Integrin (myospheroid)*, the most commonly used *Drosophila* β-Integrin, resulted in dramatically stunted DAs that had a kinked shape reminiscent of DAs with distinct stalks and paddles (left egg in Fig 3.8D). Occasionally (~5%), these DAs were fused (right egg in Fig 3.8D). These results demonstrate that E-Cadherin and βPS-Integrin are both required for DA-tube elongation, but E-Cadherin is important for maintaining DA-tube integrity and uniform eggshell secretion, whereas βPS-Integrin is important for migration and could help maintain DA-tube separation.

To test whether levels of adhesion-component expression were important for DA tubulogenesis, I assessed the effects of over-expression. Over-expression of E-Cadherin produced some defects similar to E-Cadherin knockdown: DAs of *brL>E- Cadherin::GFP* eggs were shorter and wider, distinctly formed (*i.e.,* not fused), and placed more posteriorly on the eggshell. However, the integrity of the DA-tubes was not grossly affected, as I observed relatively smooth DA-edges, uniform eggshell secretion, and no notable increase in DA-fusions (Fig 3.8E and F). On the other hand, DAs of *brL>βPS-Integrin—αPS1-Integrin* and *brL>βPS-Integrin—αPS2-Integrin* eggs were distinctly different from those of *brL>E-Cadherin::GFP*

Fig 3.8. (A-H) Laid eggs from control *brL > mCherry*-RNAi (A), *brL > E-Cadherin* RNAi (B), *brL > β-Integrin-v* RNAi (C), *brL > βPS-Integrin* RNAi (D), *brL > CD8::GFP* (E), *brL >E-Cadherin*::GFP (F), *brL > βPS-Integrin, PS1-Integrin* (G), and *brL > βPS-Integrin, PS2-Integrin* (H) females, raised at 30 ˚C. Numbers indicate percentages of normal or mildly defective (N), moderately defective (M), and severely defective (S) DAs; yellow numbers indicate the category of egg being shown. The number of eggs scored for each condition is shown in the lower left of each panel. Red arrowheads indicate abnormally wide DAs, orange brackets indicate abnormally wide DA bases, purple arrowheads indicate DA fusions, and purple brackets indicate fused DA bases. In panel B, note that small globs of DA-eggshell material have become detached from the primary eggshell (white arrow). Scale bar = 100 μm.

Figure 3.8. Regulation of E-Cadherin and specific Integrin levels are essential for DA tubulogenesis

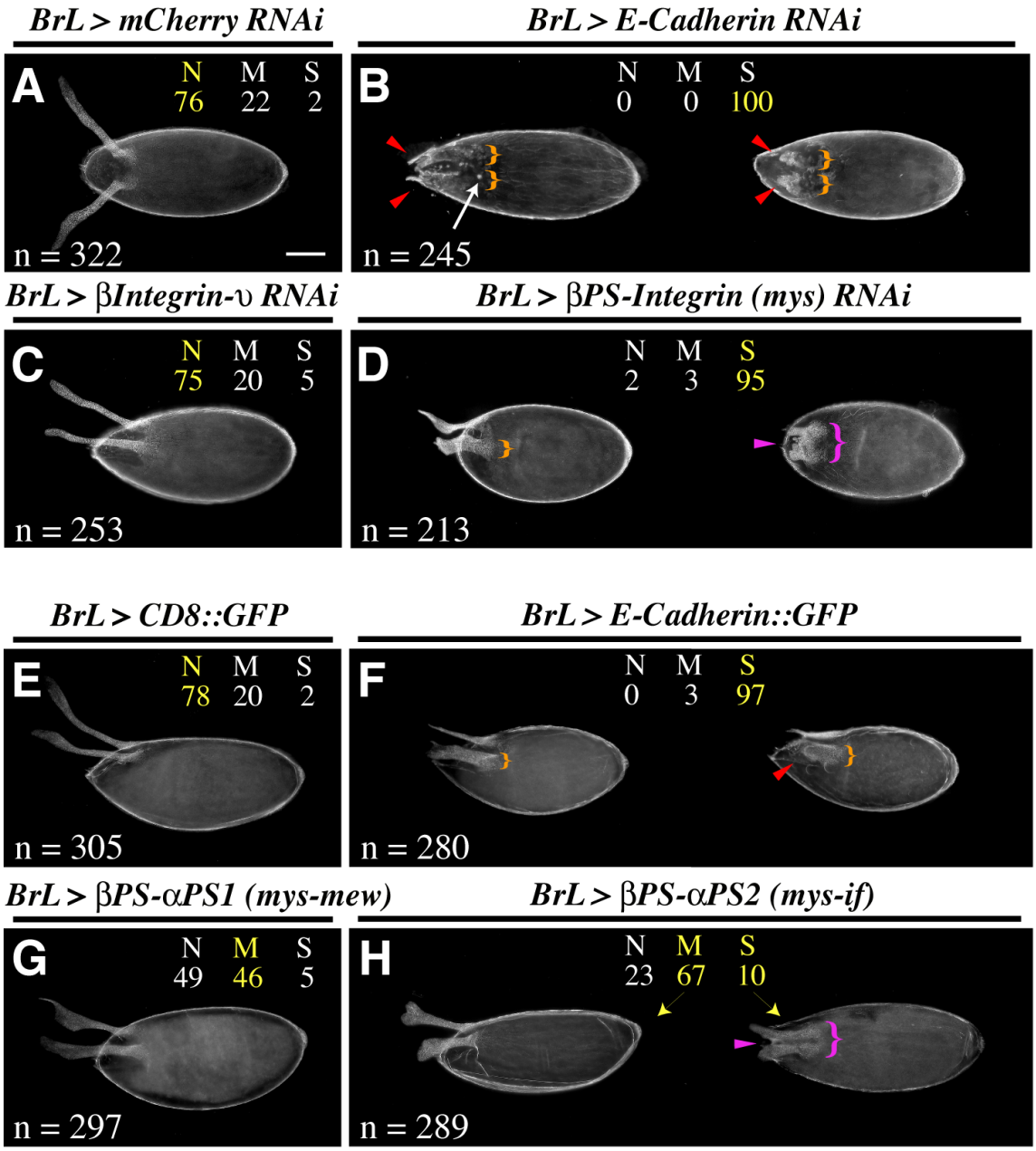

Fig 3.9. Basal (A-B), apical (C-D), and full (E) projections of control *brL > CD8::GFP* (A, C) or *brL >E-Cadherin*::GFP (B, D ,E) S13 egg chambers, stained for DAPI (A-E), E-Cadherin (A´-E´), and β-Catenin (A´´-D´´). In C and D, projections have been brightened to allow the autofluorescence of the DAs to be visualized (outlined in red dotted lines). White arrowheads (A´´´, B´´´, C´´´, D´´´) indicate co-localization of AJ components E-Cadherin and β-Catenin, and white arrow with question mark (D´´´) indicates the relative absence of apical AJ components. Magenta arrowhead in E´´´indicates aggregated, endogenous E-Cadherin following overexpression of E-Cadherin::GFP. Scale bar = 100 μm.

Figure 3.9. E-Cadherin overexpression mis-localizes AJ components from DA-tube-FC apices.

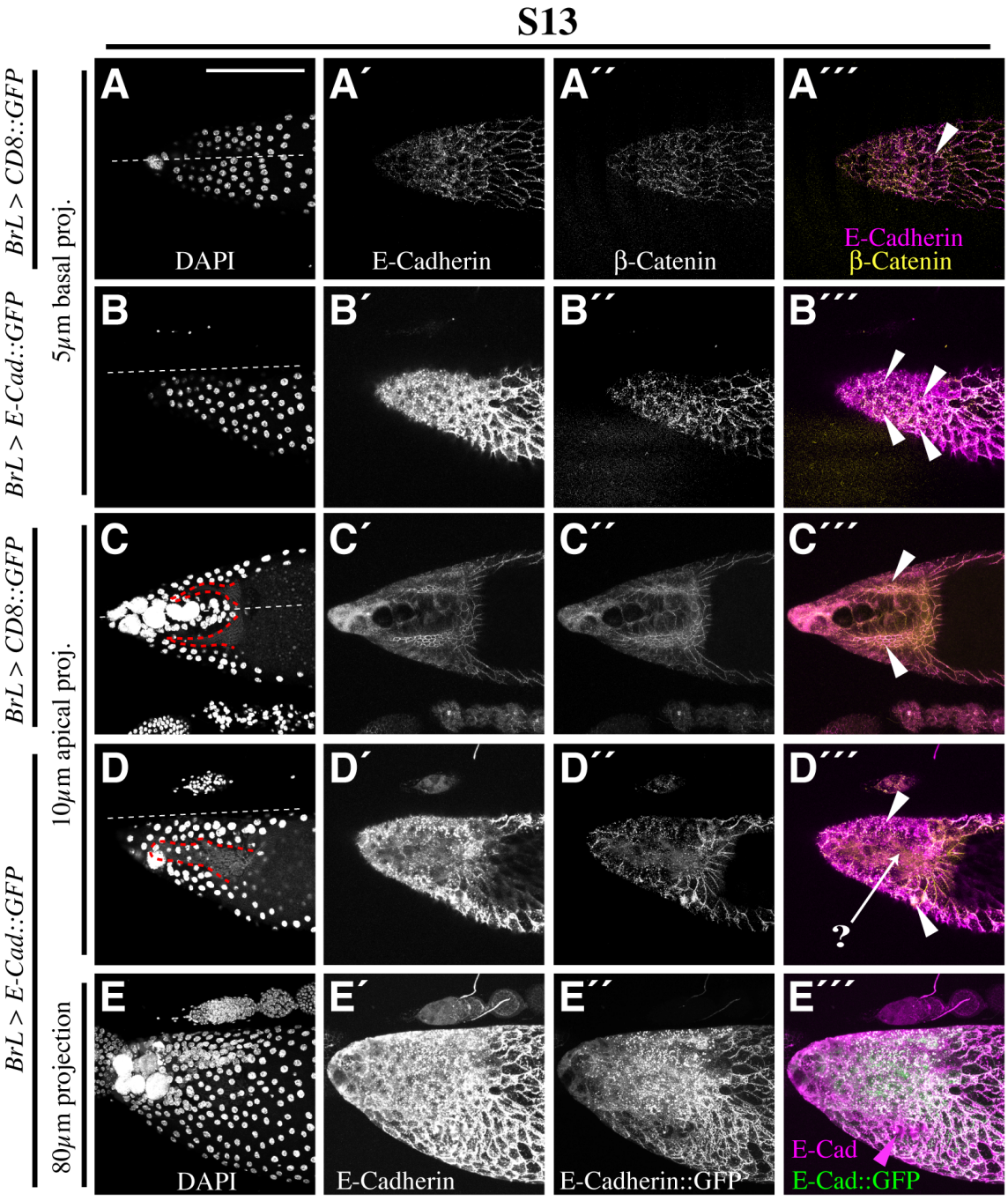

eggs: DA borders were less roughened, DA paddles were wide and more prominent, and DA bases were occasionally fused (Fig 3.8G and H). Interestingly, DA defects were significantly more severe and penetrant with the βPS-Integrin—αPS2-Integrin combination (Fig 3.8H), suggesting that these complexes could be the more important Integrin-subunit combination for DA tubulogenesis. Taken together, these results demonstrate regulation of E-Cadherin and Integrin levels affects DA tubulogenesis, and that altering the behavior of E-Cadherin- and Integrin-based adhesions causes distinct defects.

For E-Cadherin::GFP over-expression, I asked whether endogenous adherens-junction (AJ) components were being altered (Fig 3.9). Intriguingly, over-expression of E-Cadherin::GFP disrupted the apical localization of both endogenous E-Cadherin and endogenous β-Catenin (Fig 3.9D′′′, white arrow) and redistributed these proteins to the basal cytoplasm (Fig 3.9B′′′, D′′′, white arrowheads). Furthermore, over-expressed E-Cadherin::GFP, which appeared both on membranes and in cytoplasmic puncta (Fig 3.9E′′), caused massive overall buildup of membrane-associated E-Cadherin (Fig 3.9E′) and aggregation of endogenous E-Cadherin (Fig 3.9E′′′, magenta arrowhead). Together, these results suggest an underlying mechanism whereby disrupting E-Cadherin levels and localization could impact apical AJ integrity and DA tubulogenesis.

– Discussion –

Since its discovery and characterization as a critical regulator of clathrin-mediated endocytosis, Dynamin has been indispensably linked to a myriad of cellular processes, particularly those involving membrane remodeling and cytoskeletal regulation (Ferguson and Camilli, 2012). As this study demonstrates, Dynamin-mediated endocytosis can be a major driving force in tissue morphogenesis (*e.g.,* the elongation of an epithelial tube). I identify novel roles for Dynamin in DA-tube closure and DA-tube elongation, and these roles impact DA-tube length, shape, and position on the eggshell. I show that Dynamin is required both within DA-tube cells and in adjacent FC types that contribute to DA tubulogenesis, and I find that Dynamin serves to facilitate endocytosis in this context. My data support the hypothesis that DA-tube-cell intercalation and directionally biased apical expansion are required for DA-tube elongation, and Dynamin promotes these processes through the spatial and temporal modulation of cellular adhesions (Fig3.10).

Towards a complete understanding of tube cell behavior during DA tubulogenesis

DA tubulogenesis is an elegant system for understanding how cell shape change, adhesion, and migration contribute to epithelial tubulogenesis, unencumbered by complications presented by cell division and apoptosis (Dorman *et al.,* 2004; Berg 2005; Osterfield *et al.,* 2013). Recently, Osterfield and colleagues characterized the cellular events of DA-tube formation in precise detail, asserting that a pattern of line tensions along apical cell-cell edges is sufficient to drive tube formation (Osterfield *et al.,* 2013). Although this model remains to be tested, it offers an elegant and plausible explanation for cell behaviors during DA-tube

Fig 3.10. Dynamin-mediated endocytosis is essential for DA tubulogenesis. To the left are tracings and schematics representing the wild type (functional Dynamin), in which DA tubulogenesis proceeds normally. To the right are tracings and schematics representing the cellular and molecular defects associated with a loss of Dynamin function, following expression of Dynamin[DN] protein, which dramatically perturbs multiple aspects of DA tubulogenesis.

Figure 3.10. Model for Dynamin's role in DA tubulogenesis.

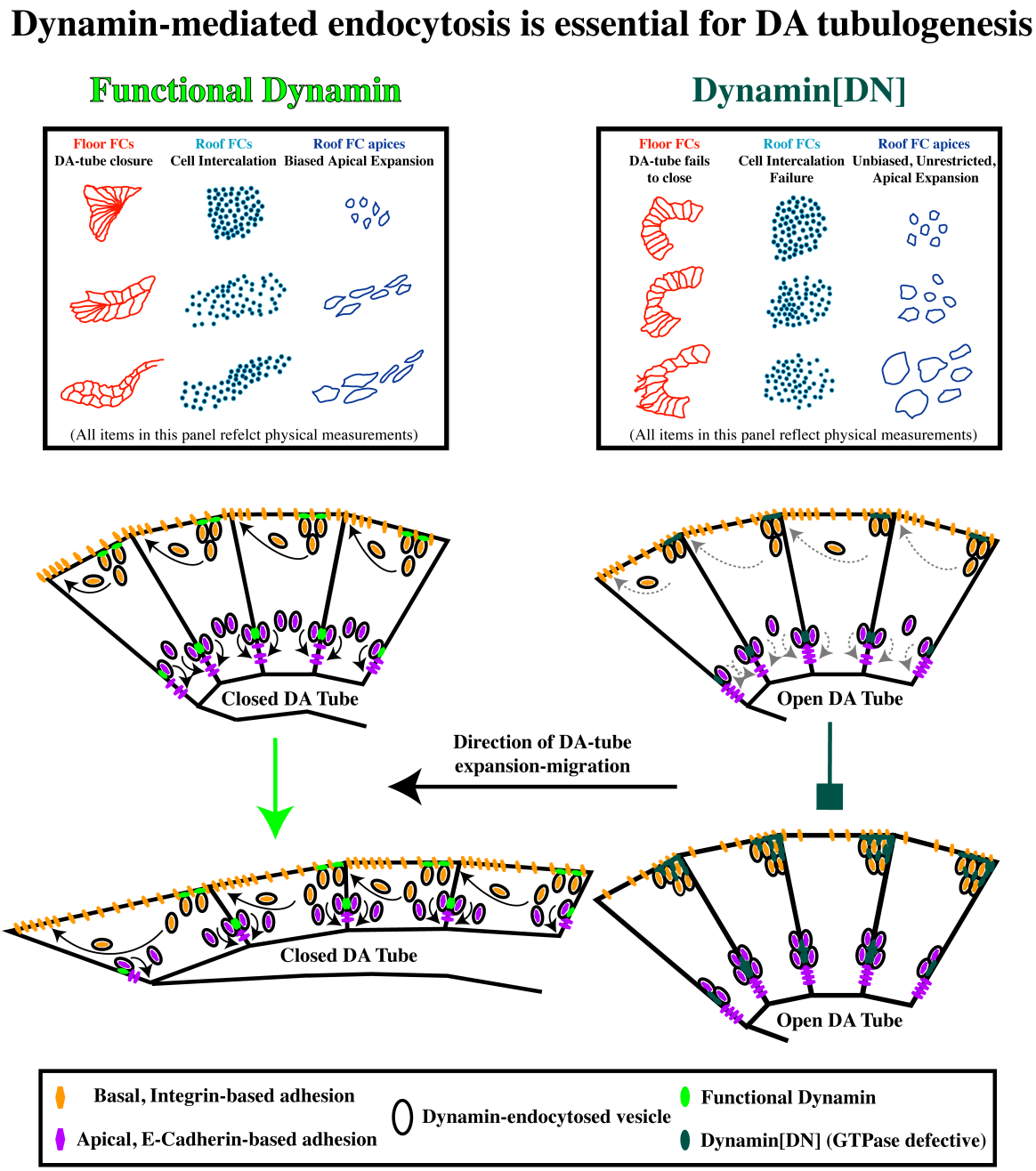

formation, the first stage of DA tubulogenesis. Herein, I identify a requirement for Dynamin in DA-tube formation, and I complement the previous characterization of DA-tube formation with a precise analysis of DA-tube elongation, documenting the spatially and temporally regulated intercalation of roof FCs and biased expansion of roof-FC luminal apices. I demonstrate that between S12—S14, roof FCs intercalate such that each primordium experiences an ~3-fold reduction in DV width and an ~3-fold extension in AP length, and this roof-FC intercalation is accompanied by a rapid expansion of luminal apices with a nearly 3-fold anterior to lateral bias. Additionally, I highlight temporal and terminal differences in apical surface-area regulation of anterior roof FCs, which secrete the wider DA paddles, with respect to posterior roof FCs, which secrete the narrower DA stalks. I propose that these directed intercalation and apical expansion behaviors in roof FCs are necessary for DA-tube elongation, since in their absence, DA tubes are uniformly short and wide. To complete this picture of DA-tube elongation, a precise, quantified characterization of floor-FC behavior during DA-tube elongation will be required, for it is clear that the floor FCs are essential for interactions between migrating DA-tube cells and their stretch FC substrate, and for the proper shaping of the DA tubes (Tran and Berg 2003; Dorman *et al.,* 2004; Boyle *et al.,* 2010). Finally, my work suggests that the regulated behavior of adjacent FC types, such as midline FCs, impacts DA tubulogenesis, and understanding the contributions of these FC types will require further characterization, modeling, and testing.

Distinct cellular movements of DA tubulogenesis require the GTPase activity of Dynamin

Analysis of eggshell morphology and FCs in fixed and living egg chambers expressing GTPase-defective Dynamin in FCs (*brL>shi[K44A]*) indicate that Dynamin's GTPase activity is

required during distinct steps of DA tubulogenesis. It remains to be seen whether any other functions of Dynamin protein, other than its GTPase activity, contribute to DA tubulogenesis. In either case, the GTPase requirements for Dynamin are not just for general FC maintenance, since *brL>shi[K44A]*-expressing egg chambers complete oogenesis and eggshell secretion on a similar timescale to controls.

First, the invariant failure of DA-tube closure following *brL>shi[K44A]* expression, visualized by floor-FC morphology, indicates a critical role for Dynamin in sealing off the DA tubes. This assertion is supported by the dramatically widened DAs and DA bases on *brL>shi[K44A]* eggshells.

Second, the frequent DA fusions on *brL>shi[K44A]* eggshells, and the loss of morphological distinction between midline and DA-tube FCs following *brL>shi[K44A]* expression, indicate that one function of Dynamin is to maintain DA-tube separation. One possibility is that Dynamin could keep the DA-tube-FC primordia distinct by differentially localizing adhesive proteins in midline vs. DA-tube FCs. Alternatively, it could simply be that simultaneous DA-tube elongation and midline-FC migration keeps the DA-tubes separate by maintaining a midline buffer of cells between the DA tubes; when Dynamin function is disrupted, DA-tube FCs remain in place while midline FCs move forward, and there are no cells left in between the DA-tubes to keep them separate.

Third, the short and wide DAs of *brL>shi[K44A]* eggshells, and the failure of roof-FC intercalation and biased apical expansion following *brL>shi[K44A]* expression, indicate that Dynamin is required in DA-tube FCs for DA-tube elongation. Not only does disrupting Dynamin function in DA-tube FCs result in a failure of directionally biased apical expansion, but it also increases the rate and terminal extent of apical expansion, suggesting that precise

regulation of Dynamin activity is critical during DA-tube elongation. The similar DA defects observed following *brL>shi[K44A]* and *br*[*69B08*]*>shi[K44A]* expression indicate that Dynamin is required primarily in DA-tube FCs for DA-tube elongation, but it is not clear what the relative contributions of the roof FCs and floor FCs are in this process. Indeed, the intercalation and apical expansion defects I have documented are roof-FC-specific, but a failure of floor-FC closure could underlie these defects if the floor FCs require Dynamin function to promote intercalation and laterally contain apical expansion, thus driving anterior DA-tube elongation.

Finally, the distinctly different defects observed following *A90>shi[K44A]* expression, and the high levels of Dynamin protein observed in stretch FCs, suggest that Dynamin function in stretch FCs contributes to DA tubulogenesis as well. Dynamin could be required for the interactions between stretch FCs and floor FCs that regulate DA-tube shape. It could also be required for proper engulfment and degradation of nurse cell nuclei, thus indirectly blocking DA-tube elongation.

Understanding the role of Dynamin in each of these processes will require more detailed analysis of fixed tissue, the development of live-imaging tools that can distinguish floor from overlying roof FCs, the identification or production of *GAL4* lines that can drive more limited expression in either roof, floor, or midline cells without adverse effects on DA tubulogenesis, and the generation of Dynamin[DN] constructs that could be activated at sub-cellular locations, potentially even in living tissue.

Dynamin impacts DA tubulogenesis through endocytosis

Although Dynamin's vast repertoire of cellular functions extends beyond endocytosis, my data (disruption of Rab5 activity, *Rab5* knockdown, and *AP-50* knockdown) are consistent

with Dynamin promoting DA tubulogenesis through endocytosis and suggest that it is doing so through a classic, clathrin-mediated pathway (McMahon and Boucrot, 2011). However, Rab5 has been linked to non-clathrin-mediated endocytic processes (Hagiwara *et al.,* 2009; Fabrowski *et al.,* 2013; Diaz *et al.,* 2014), and *AP50*-RNAi expression did not produce as severe defects as Dynamin[DN], Rab5[DN], or *Rab5*-RNAi. Therefore, while my data strongly support a role for Dynamin in promoting DA tubulogenesis via endocytosis, it is not clear whether this function is entirely, or in part, via clathrin-mediated endocytosis, nor can I exclude the possibility that there is a non-endocytic contribution of Dynamin to DA tubulogenesis.

DA tubulogenesis requires a spatiotemporal balance of cellular adhesion

What might be the targets of Dynamin-mediated endocytosis during DA tubulogenesis, and what are the relative contributions of apical endocytosis and basal endocytosis?

? Given the observed bias towards apical and basal localization of Dynamin protein in DA-tube cells undergoing DA tubulogenesis, Cadherin- and Integrin-based adhesions were appealing candidates. E-Cadherin recycling is implicated in a variety of morphogenetic processes, including zebrafish gastrulation, salivary-gland morphogenesis in *Drosophila*, and mouse heart-valve morphogenesis, and in many cases, this requirement has been attributed to clathrin-mediated endocytosis (Ulrich *et al.,* 2005; Pirraglia *et al.,* 2006; Tatin *et al.,* 2013; Goldenberg and Harris, 2013). Likewise, Integrin recycling is a well-documented feature of cell migration and morphogenesis. It has been linked to both clathrin-dependent (Nishimura and Kaibuichi, 2007; Chao and Kunz, 2009; Ezratty *et al.,* 2009; Bogdanovic *et al.,* 2012) and calveolin-dependent endocytosis (Shi and Sottile 2008). In the *Drosophila* salivary gland, PS1-

Integrin (*mew*) plays a key role in budding morphogenesis (Pirraglia *et al.,* 2013). It is intriguing that PS2-Integrin (*if*) appears to be more important in the DA tube, which forms by wrapping.

Consistent with this, and supporting a role for Dynamin in regulating adhesive turnover during DA tubulogenesis, *brL>shi[K44A]* egg chambers exhibited more stable, uniform apical E-Cadherin, more ordered, basal βPS-Integrin, decreased cytoplasmic localization of these proteins, and a temporal progressivity to these effects. My evidence supports a model in which remodeling of cellular adhesions facilitates the cell movements required for DA tubulogenesis (Fig 3.10). I observed inverted apico-basal localization of E-Cadherin vs. βPS-Integrin in DA-tube FCs vs. midline FCs, and these FC types must behave differently during DA-tubulogenesis to prevent DA-tube fusion. I demonstrated that individually altering E-Cadherin and Integrin levels, via both RNAi and overexpression, have dramatic and distinct effects on DA tubulogenesis. Indeed, regulating the balance of cellular adhesion appears to be at the very heart of DA tubulogenesis.

In summary, Dynamin appears to function both apically and basally to regulate the remodeling of cellular adhesions during the cell movements of DA tubulogenesis. Thus, loss of Dynamin's GTPase activity disrupts the neighbor exchange that facilitates tube closure, and the planar-polarized apical expansion and intercalation that accompanies tube elongation (Fig 3.10). Dynamin plays a central role throughout this process of epithelial tube morphogenesis, and we are only beginning to understand the capability and responsibility of this fascinating molecule.

Chapter IV

Conclusions and Future Directions

– Overall conclusions –

Tubulogenesis is a fundamental component of metazoan development and requires the precise regulation of a variety of cellular and molecular processes (*e.g.*, transcriptional regulation, intracellular trafficking, cytoskeletal regulation, adhesion, polarity, cell division), and the solving of a variety of morphogenetic problems. This dissertation addresses two of these problems in particular: 1) How transcription factors equip cells with the tools needed to execute tubulogenesis, and 2) How those tools work mechanistically to drive the coordinated changes in cell behavior required for tubulogenesis. In **Chapter II**, I revealed the unexpectedly wide regulatory influence of the Tramtrack69 transcription factor during late *Drosophila* oogenesis, and I identified several Tramtrack69 effectors that function in epithelial tube cells to facilitate the downstream cell movements of DA tubulogenesis, including the focal adhesion scaffold Paxillin and the mechanical GTPase Dynamin. Finally, I discovered an active, morphogenetic role for the transcription factor Mirror during DA tubulogenesis, which is distinct from its previously described function in DA tube patterning. In **Chapter III**, I focused specifically on the role of Dynamin as tubulogenic effector in the *Drosophila* ovary, and I showed that Dynamin's functions as a regulator of endocytosis in both tube cells and the cells over which they migrate. I demonstrated novel roles for Dynamin in promoting three important cell movements during DA tubulogenesis (*i.e.,* tube closure, cell intercalation, biased apical expansion), and I proposed that Dynamin facilitates these movements by regulating cell-cell and cell-matrix adhesion dynamics.

– Conclusions of Chapter II –

Our lab first described functions for the zinc finger Tramtrack69 transcription factor during late oogenesis in promoting eggshell synthesis and DA-tube elongation (French *et al*., 2003), and we subsequently elaborated on these findings by demonstrating that Tramtrack69 regulates DA-cell shape and interacts with Notch and Ecdysone (Boyle *et al*., 2009). These findings both intrigued and inspired me because they supported active roles for a transcription factor during morphogenesis, not just during the establishment of cell fate prior to morphogenesis. Therefore, I set out to identify the tubulogenic effectors of Tramtrack69 in the ovary through microarray-based gene expression profiling, *in situ* hybridization, and follicle cell-specific RNAi. The results of these efforts were both successful and informative, and reflect the major findings of **Chapter II**.

Microarray and *in situ*-based gene expression analysis successfully identified Tramtrack69-regulated genes whose products could accomplish the two previously known functions of Tramtrack69 in late oogenesis: eggshell synthesis and DA-tube elongation. Intriguingly, my efforts also identified a previously unknown role for Tramtrack69 in regulating germline gene expression, which has absolutely no effect on DA tubulogenesis (Boyle *et al*., 2009), but could be important for executing the early events of embryogenesis (Peters *et al*., 2013; see **Chapter II**).

In regard to eggshell synthesis, I discovered that Tramtrack69 promotes the expression of *cyp18A1*, an upstream, master regulator of eggshell synthesis, and at least five known downstream chorion genes that encode specific eggshell proteins (Tootle *et al*., 2011). These results both establish an important link between Tramtrack69 and the known eggshell synthesis program of the *Drosophila* ovary and help explain why there needs to be *tramtrack69* expression

in all columnar, eggshell secreting, follicle cells, and not just the DA-tube cells (Peters *et al.,* 2013; see **Chapter II**).

In regard to DA-tube elongation, I discovered that Tramtrack69 promotes the expression of at least eight genes whose products contribute to DA tubulogenesis: *lamina ancestor*, *CG31918*, *Cp16*, *katanin80*, *Rac2*, *Paxillin*, *Dynamin*, and *mirror*. Of these, perhaps the most unexpected was *mirror*, because *mirror* encodes yet another transcription factor that plays an active role in DA tubulogenesis, and this function is separate from its previously characterized role in establishing DV patterning and DA-tube cell fate. Furthermore, the expression of *mirror*, which is restricted to the DA-tube cells and some adjacent cell types, explains how a transcription factor with expression throughout all of the columnar follicle cells, such as Tramtrack69, can execute specific functions in DA-tube cells, which represent only a subset of the columnar follicle cells. Consistent with Mirror serving to spatially restrict the DA tubulogenic function of Tramtrack69, I demonstrated that Mirror promotes the expression of *Paxillin*, whose expression is strictly, spatially limited to DA-tube cells during DA tubulogenesis, and that this regulatory relationship is indeed important for DA-tube elongation. These efforts demonstrated a novel role for Paxillin in DA-tubulogenesis, and, for that matter, in epithelial tubulogenesis altogether (Peters *et al.,* 2013; see **Chapter II**).

Thus, the major findings of **Chapter II** demonstrated important, morphogenetic roles for two transcription factors beyond establishing cell fate, identified genes with novel, tubulogenic functions, established a regulatory relationship between a morphogenetic transcription factor and a downstream tubulogenic effector that is important for DA tubulogenesis, and highlighted the complexity of Tramtrack69's function in regulating gene expression during late oogenesis. As part of these efforts, I helped develop superior methods for *in situ* hybridization in the

Drosophila ovary and contributed to the establishment of a technique for dual visualization of proteins and RNAs in that tissue (Zimmerman et al. 2013).

– Conclusions of Chapter III –

Chapter II indicated that the known endocytic and cytoskeletal regulator, Dynamin, plays an important role in DA tubulogenesis. Therefore, characterizing the function of Dynamin during DA tubulogenesis became the focus of the second half of my graduate research, and the results of these efforts represent the major findings of **Chapter III**.

By inhibiting Dynamin's GTPase activity in all cell types that contribute to DA tubulogenesis, I demonstrated an essential, newly described role for Dynamin's GTPase function during DA tubulogenesis. Without Dynamin function in the follicle cells, DA tubes fail to properly close and elongate, and this failure produces dramatically shortened, wide DA tubes. Importantly, I demonstrated via live imaging that disruption of Dynamin function specifically affects DA tubulogenesis without generally affecting cell viability or function, as affected cells survive to complete eggshell synthesis at the very end of oogenesis. Dynamin's most well characterized cellular function is to facilitate endocytosis, but this role is by no means the only demonstrated function of Dynamin. However, independent disruption of other known components of the endocytosis pathway, via expression of dominant negatives and RNAi, indicated that Dynamin promotes DA tubulogenesis through facilitating endocytosis. Interestingly, independent disruption of Dynamin function either in DA-tube cells or in the stretch cells over which the DA-tube cells migrate disrupted DA tubulogenesis, but in different ways. Most notably, I did not observe DA-tube closure defects when I disrupted Dynamin

function specifically in the stretch cells, as I did when I disrupted its function specifically in the DA-tube cells (Peters and Berg, submitted; see **Chapter III**).

Once I established an essential role for Dynamin during DA tubulogenesis, I then demonstrated that Dynamin is required for three key features of DA tubulogenesis: DA-tube closure, DA-tube-cell intercalation, and DA-tube-cell biased apical-luminal expansion. The occurrence of biased apical-luminal expansion during DA tubulogenesis was previously undocumented, and my research now provides a quantitative, cytological characterization of this process. A requirement for Dynamin in epithelial tube closure has not been previously described. A requirement for Dynamin-mediated endocytosis during epithelial cell intercalation has been previously described in the *Drosophila* trachea (Shaye *et al.,* 2008; Warrington *et al.,* 2013) and salivary gland (Pirraglia *et al.,* 2006; Pirraglia *et al.,* 2010), but not during DA tubulogenesis. Finally, others have demonstrated roles for Dynamin in regulating apical constriction (Chua *et al.,* 2009) and apical spreading (Fabrowski *et al.,* 2013), but I report here a newly described role in biased apical expansion during tubulogenesis (Peters and Berg, submitted; see **Chapter III**).

In many developmental contexts, particularly involving cell intercalation, Dynamin-mediated endocytosis is required for removal and turnover of apical, cell-cell, E-Cadherin-based adhesions (Harris, 2012; Walck-Shannon and Hardin, 2013). Dynamin-mediated endocytosis is also required for removal and turnover of basal, cell-matrix, Integrin-based adhesions (He *et al.,* 2010; Dong *et al.,* 2011; Huttenlocher *et al.,* 2011, Bogdanovic *et al.,* 2012). My findings suggest that DA tubulogenesis employs both of these mechanisms simultaneously for DA-tube elongation, supporting and expanding upon a conserved, morphogenetic role for Dynamin in modulating cell adhesion (Peters and Berg, submitted; see **Chapter III**).

Thus, the major findings of **Chapter III** demonstrated a requirement for Dynamin-mediated endocytosis in DA tubulogenesis, both in DA-tube cells and their migratory substrate, showed that Dynamin facilitates specific cell movements during DA tubulogenesis, and highlighted the importance of endocytic modulation of cell-cell and cell-matrix adhesions during epithelial morphogenesis and tubulogenesis.

Future Directions
– Transcriptional regulation of tubulogenic networks –

Tramtrack69 and tubulogenesis

My research represented the first attempt to identify and characterize the genes downstream of Tramtrack69 in the *Drosophila* ovary, with the goal of identifying downstream effectors of epithelial tubulogenesis (Peters *et al.,* 2013; see **Chapter II)**. While those efforts were fruitful, they were by no means exhaustive, and they raised several important questions. Does Tramtrack69 act as a transcriptional repressor, activator, or both? What are Tramtrack69's roles in the germline, the stretch cells, and the main-body follicle cells? How do these roles differ from its functions in the DA-tube cells? Could new technologies be employed for a more directed identification of Tramtrack69's tubulogenic effectors, versus its roles in eggshell synthesis or germline effectors? Does Tramtrack69 regulate a similar complement of tubulogenic effectors during other tubulogenic events in *Drosophila* development?

First, does Tramtrack69 act as a repressor, activator, or both? Only a handful of direct targets of Tramtrack69 have been identified and validated (*e.g., even-skipped*, *fushi tarazu, tailless*) (Harrison and Travers 1990; Read *et al.,* 1992; Chen *et al.,* 2002), and those interactions are strictly repressive and function during embryogenesis. Genome-wide profiling efforts for Tramtrack69 reveal potential targets in 0-12hr embryos (the modENCODE consortium *et al.,* 2012), in S2 cells (Reddy *et al.,* 2010), and during tracheal tubulogenesis (Rotstein *et al.,* 2011), but these targets have not yet been extensively validated to determine whether regulation by Tramtrack69 is direct, and therefore if Tramtrack69 interactions are activating or repressive. The Tramtrack69-regulated, tubulogenic effectors that I identified in **Chapter II** were all positively

regulated by Tramtrack69, and though I did not demonstrate whether those interactions were direct or indirect, my work suggests that Tramtrack69 could have direct activating and repressing activity. I could potentially address this question by generating germline null clones of *tramtrack69* during oogenesis, as in Boyle *et al.,* 2009, allowing these eggs to be fertilized, and allowing the embryos to develop, if they were viable. I could then select genes directly bound by Tramtrack69 during embryogenesis (the modENCODE consortium *et al.,* 2012), and compare expression levels between wild type and *tramtrack69* null embryos by *in situ* hybridization or qRT-PCR. Down-regulated expression of normally Tramtrack69-bound genes would indicate a direct, activating interaction. Conversely, up-regulated expression of normally Tramtrack69-bound genes would indicate a direct, repressive interaction. I could validate Tramtrack69-binding using a gel-shift assay, alter the binding site to show that it disrupts binding, also via gel shift assay, and show that disrupting the binding site alters the expression *in vivo*.

Unfortunately, independent analyses of Tramtrack69 binding sites have not agreed upon a universal, predictive, consensus-binding sequence for Tramtrack69 (Harrison and Travers 1990; Brown *et al.,* 1991; Chen *et al.,* 2002; Kulakovskiy and Makeev, 2009). My collaborative work with Nathaniel Thayer and Martin Tompa identified a probable Tramtrack69 binding sequence in embryos based on modENCODE data (Peters *et al.,* 2013; **Chapter II**), but this sequence was quite flexible and was not the only binding sequence identified in the analysis (data not shown). Furthermore, a search for this binding sequence within promoters of genes in my dataset indicated that many Tramtrack69-regulated genes had binding sequences, many Tramtrack69-regulated genes did not, and many non-Tramtrack69-regulated genes had binding sites. This incoherency is possibly due to the fact that Tramtrack69 contains a Bric-a-brac—Tramtrack—Broad (BTB) protein-protein interaction domain that potentially allows it to interact, in dimers or

multimers, with over 50 BTB-domain containing transcription factors in *Drosophila* (Zollman *et al.,* 1994; Bonchuck *et al.,* 2011). There is no longer a good antibody available for Tramtrack69, but a transgenic tagged Tramtrack69 was developed and used for the modENCODE project, and this tool enables ChIP experiments in the ovary that could, along with my expression data, indicate whether the interactions between Tramtrack69 and the tubulogenic effectors that I identified were direct, and, if so, whether they were activating or repressive. Additionally, tagged Tramtrack69 could facilitate IP pull-downs to determine whether Tramtrack69 was interacting with other BTB-domain-containing transcription factors during DA tubulogenesis.

Second, how could my findings and new technologies be employed for a more directed identification of Tramtrack69's tubulogenic effectors versus its eggshell synthesis or germline effectors? Though my research efforts with the *tramtrack*^{twk} mutant successfully identified several of Tramtrack69's tubulogenic effectors in the ovary (Peters *et al.,* 2013; **Chapter II**), I could significantly improve on several features of the analysis if I wanted to identify more effectors, in a more temporally or spatially focused way. For transcriptional profiling, I could employ RNA-Seq instead of microarrays, a technology that has tremendously improved since I began graduate school, to get a more complete and quantitative perspective on the Tramtrack69-regulated transcriptional landscape. With the dissection and manipulation skills that have come with seven years of practice, I could easily temporally restrict my analysis by separating and profiling specifically staged egg chambers. On the other hand, I could spatially restrict my analysis through labeling and purification of specific cell types. Since cell purification was first employed for transcriptional profiling in the *Drosophila* ovary by flow cytometry (Bryant *et al.,* 1999) and magnetic bead purification (Wang *et al.,* 2006), our lab has improved and optimized a follicle-cell purification protocol to the point that even mass spectrometry and proteomic

profiling is possible (Zimmerman *et al.,* in preparation). If I were to express CD8::GFP only in DA-tube cells using the Br^{69B08}-GAL4 driver, in both wild type and *tramtrack*^{fwk} backgrounds, I could rapidly and effectively purify DA-tube cells, and use them for either transcriptional or proteomic comparative profiling. Additionally, in a wild-type background, transcriptional or proteomic profiling of all DA-tube cells, just DA-floor cells, the stretch cells, the whole columnar epithelium, the whole follicular epithelium, and the germline (*i.e.*, any ovarian cell type for which there exists a specific GAL4-driver) would augment our understanding of DA tubulogenesis and provide a valuable resource for the *Drosophila* research community.

Finally, does Tramtrack69 regulate a similar complement of tubulogenic effectors during other tubulogenic events in *Drosophila* development? Since null mutants of *tramtrack69* die during early embryogenesis (Xiong and Montell 1993), addressing this question would require either tissue-specific RNAi, clonal analysis, or, ideally, some method for creating a conditional tramtrack69 "null" only in the tissue of interest. As it turns out, such a technology now exists in *Drosophila* as an elaboration upon the CRISPR/Cas9 system, which has taken the developmental biology world by storm over the last three years (Jinek *et al.,* 2012). Last year, this technique was adapted for conditional mutagenesis in *Drosophila* using the GAL4-UAS system. In multiple contexts (*e.g.,* adult cuticle, adult wing, female ovary, male testis), for multiple genes, when GAL4 was used to express Cas9, when two guide RNAs were used to target a given locus, and when the temperature was raised from 25°C to 28°C, over 90-95% of organs or tissues displayed a complete loss-of-function phenotype (Xue *et al.,* 2014). I could use this technology to remove the *tramtrack69* locus from any tubulogenic context in *Drosophila* for which there are tissue-specific GAL4 drivers and for which the cells are diploid or have near-normal DNA

content. This approach would likely not work during DA tubulogenesis because the follicle cells have dramatically amplified genomes, but that possibility remains to be tested.

Mirror and tubulogenesis

The same questions that my research raised for Tramtrack69 apply, at least in part, to Mirror. Prior to my research, I knew that Mirror established DV patterning of the DA tubes, but I did not know that it directly facilitated DA tubulogenesis. I discovered that Mirror promotes DA tubulogenesis downstream of Tramtrack69, and I proposed that this role might be how Tramtrack69 spatially restricts its tubulogenic function to DA-tube cells, because *mirror* expression is restricted to those cells and not throughout the columnar epithelium like *tramtrack69* (Peters *et al.,* 2013; see **Chapter II)**.

The question of whether Mirror acts as a repressor, activator, or both has already been answered. Mirror has been shown to be a direct repressor of *pipe* (Andreu *et al.,* 2012), but also a direct activator of *broad* (Fuchs *et al.,* 2012). Thus, Mirror can serve as both a transcriptional activator and repressor. Unlike Tramtrack69, Mirror possesses a canonical and predictive binding sequence (Fuchs *et al.,* 2012). Since I showed that Mirror is downstream of Tramtrack69, I could use this binding sequence to identify genes within my Tramtrack69 data whose promoters have a Mirror binding site (Bailey *et al.,* 2009), with the goal of enriching for genes involved in DA tubulogenesis.

I could employ similar technologies and approaches for identifying Tramtrack69 tubulogenic effectors to identifying Mirror tubulogenic effectors, or for that manner the effectors of any tubulogenic transcription factor. Since the *mirror* RNAi phenotype is so severe and penetrant, I could simultaneously express CD8::GFP and either *mirror* RNAi or control RNAi in

DA-tube cells, purify DA-tube cells using our lab's magnetic bead purification protocol, and subject the cells to comparative transcriptional or proteomic profiling..

Conservation of tubulogenic networks

There is tremendous diversity of epithelial tube morphology and specialized functions within *Drosophila* alone. There are unelaborated epithelial tubes, transient epithelial tubes, and intricately branched epithelial tubes. Despite this diversity, there is a shared arsenal of cell shape-changes and movements that facilitate these tubulogenic events, and the molecular mechanisms underlying these cell shape-changes and movements are likely conserved (Lubarsky and Krasnow 2003; Andrew and Ewald 2010; Maruyama and Andrew 2012; Iruela-Arispe and Beitel 2014). In *Drosophila*, I would begin to assess the conservation of downstream tubulogenic mechanisms by comparing the transcriptional or proteomic profiles for tubes undertaking similar kinds of cell movements. For instance, I could use cell purification to compare transcriptional or proteomic profiles between cells of the DA-tubes, salivary glands, trachea, hindgut, ventral furrow, etc., and look for common, up-regulated genes, proteins, or pathways. I could also compare the regulatory profiles of tubulogenic transcription factors that facilitate similar tubulogenic cell movements, such as cell intercalation and tube elongation. For example, I could use RNAi or CRISPR/Cas9 and cell purification to remove *tramtrack69* or *mirror* from DA-tube cells, *ribbon* or *huckebein* from salivary glands or the trachea, and *STAT92E* from the embryonic hindgut, purify the mutagenized tube cells and control tube cells, identify differentially expressed genes or proteins, and determine whether there are any similar trends in downstream transcript or protein levels that might indicate conserved, *Drosophilid*, tubulogenic effectors.

There is perhaps a more important question than whether networks of downstream tubulogenic effectors are conserved across different tubulogenic contexts in *Drosophila*: Are downstream tubulogenic networks conserved outside of *Drosophila*, and across evolutionarily diverse metazoans? If a core set of tubulogenic effectors, whose general molecular function is conserved, can be identified in, say, *Drosophila*, then these genes could be disrupted in tubulogenic contexts in other metazoans, and the results could be compared. I could use the GAL4-UAS system to drive RNAi or dominant negatives in *Xenopus* (Hartley *et al*., 2002), zebrafish (Halpern *et al*, 2008), or mouse (Lewandowski 2001), or I could use other, established gene disruption methods, such as morpholino injection. In principle, the same kinds of CRISPR/Cas9 mutagenesis experiments that I proposed to conditionally mutagenize transcription factors in *Drosophila* could be used to conditionally mutagenize potential, conserved, downstream tubulogenic effectors in other organisms, and determine whether these gene products are required to execute conserved, tubulogenic mechanisms and cell movements.

Future Directions
– Molecular effectors of epithelial tubulogenesis –

The focal adhesion scaffold Paxillin

Paxillin is a conserved molecular scaffold that assembles regulatory and structural components on the intracellular side of Integrin-based focal adhesions, where it helps regulate changes in cell adhesion and activity of the Rho GTPases. Therefore, Paxillin is considered to be very important for Integrin-mediated cell migration (Deakin and Turner 2008). My research in the *Drosophila* ovary demonstrated that there is a wave of Paxillin expression strictly within the DA-tube cells at the onset of DA-tube elongation, that both Tramtrack69 and Mirror promote this expression of Paxillin, and that this expression of Paxillin promotes DA tubulogenesis *tramtrack69* (Peters *et al*., 2013; see **Chapter II**). As a tubulogenic role for Paxillin had not previously been described, this result raised at least three important questions: 1) How vital is Paxillin for DA tubulogenesis? 2) Since Paxillin is a complicated molecule, what features of Paxillin are essential for DA tubulogenesis? 3) Is the tubulogenic function of Paxillin conserved in *Drosophila* and across metazoans?

First, how important is Paxillin for DA tubulogenesis? My early attempts to answer this question were limited by availability of disruption tools. My RNAi assays targeting *Paxillin* revealed a role for Paxillin in DA tubulogenesis, but the phenotypes were relatively weak and variable compared to, for instance, *tramtrack69* or *mirror* RNAi. I attempted to use imprecise P-element excision to generate a *Paxillin* null allele that I could use for clonal analysis, but my initial efforts were unsuccessful, and this project took a backseat to my research on Dynamin. Now, with the availability of CRISPR/Cas9 technology, I could quite effectively design flanking

guide RNAs and employ them in transgenic flies to generate a stable *Paxillin* null allele. If there were any problem with viability in the *Paxillin* null mutant, as there very well might be, I could use the *Paxillin* null to generate negatively (Xu and Rubin, 1993) or positively (Lee and Luo, 2001) marked mosaic clones in the follicle cells. CRISPR/Cas9 conditional mutagenesis might also be useful here. I could use the already integrated guide RNA sequences from generating the stable *Paxillin* null, a DA-tube-cell-specific GAL4, and UAS-Cas9 to mutagenize *Paxillin* only in DA-tube cells prior to DA-tube elongation. Though this technique would not eliminate Paxillin protein already present in the follicle cells prior to the conditional mutagenesis, it would determine how important the late, specific wave of *Paxillin* expression in DA-tube cells is for DA-tube elongation, if the Paxillin locus could be efficiently removed from these cells.

What features of Paxillin are important for DA-tubulogenesis? Paxillin is a complicated molecular scaffold that performs many functions, and it is not itself an enzyme. This complexity does not make it easy to, for example, design a dominant negative Paxillin. If I successfully demonstrated a key role for Paxillin in DA-tubulogenesis using *Paxillin* null alleles, then I could use the CRISPR/Cas9 system again to target and remove specific domains of Paxillin, either in a stable mutant or in a conditional manner. This approach would be limited by the availability of appropriate guide RNA sequences within the Paxillin locus, but the same types of analysis could be performed on these mutants as for null mutants, and this domain analysis could implicate specific regulatory and structural functions of Integrin-based adhesions, of which Paxillin is a key player, in DA-tubulogenesis.

Finally, is the tubulogenic function of Paxillin conserved in *Drosophila*, and across metazoans? To address this question, I would use similar approaches and tools as described above. First, if a *Paxillin* null were viable in *Drosophila*, and if it caused a dramatic defect in

DA tubulogenesis, I would examine other tubulogenic contexts in the *Paxillin* null mutant to determine whether they were also disrupted. If viability were an issue for the stable *Paxillin* null mutant, I would generate mosaic clones using MARCM or conditional *Paxillin* null mutants with tissue-specific drivers and compare any resulting tubulogenic defects to those in DA tubulogenesis. If these efforts were productive, I could then extend this analysis to other metazoan model systems by using CRISPR/Cas9 to generate stable or conditional *Paxillin* alleles (CRISPR/Cas9 has been shown to work in >20 tested model systems and plants; Harrington *et al.,* 2014)

The mechanical GTPase Dynamin

Dynamin is a conserved, mechanical GTPase that undergoes a conformational shape change upon GTP hydrolysis. When Dynamin molecules oligomerize and cooperatively hydrolyze GTP, this hydrolysis can provide the force necessary for vesicle scission during endocytosis or in other contexts where cell membranes need to be bent and pinched (Ferguson and Camillie 2012; Chappie and Dyda 2013). Dynamin's function is not limited to endocytosis, but during DA-tubulogenesis, I have shown that Dynamin promotes the endocytosis of apical, cell-cell and basal, cell-matrix adhesions, both of which appear to be important for DA-tube closure, DA-tube-cell intercalation, and biased apical expansion (Peters and Berg, submitted; **Chapter III**). My research on Dynamin raises a number of interesting questions about Dynamin's involvement in DA-tubulogenesis and in tubulogenesis in general: 1) Do other features of Dynamin, other than its GTPase activity, have roles during DA tubulogenesis? 2) What are the relative contributions of apical endocytosis and basal endocytosis to DA tubulogenesis? 3) What mechanism underlies the biased apical expansion that I observed and

characterized during DA-tube elongation? 4) Is the tubulogenic function of Dynamin conserved in *Drosophila*, and across metazoans?

First, do other features of Dynamin, other than its GTPase activity, have roles during DA tubulogenesis? For instance, are previously demonstrated interactions between Dynamin's plekstrin homology (PH) domain and lipids of the plasma membrane, or its Proline-rich-domain (PRD) with the SH3-domains of actin-binding proteins, such as cortactin, required for DA tubulogenesis? To address this question, I could remove or disrupt specific domains of Dynamin, and compare those effects to the expression of Dynamin[DN], or to a homozygous Dynamin null, which would also need to be generated. Dynamin[DN] is a well-accepted and characterized tool for disrupting Dynamin function, and it may be the case that all of Dynamin's functions require a functional GTPase domain. However, it would be both intriguing and potentially groundbreaking if a non-GTPase-requiring function were to be identified.

Second, what are the relative contributions of apical endocytosis and basal endocytosis to DA tubulogenesis? Another, slightly different way to approach this would be to ask what are the relative contributions of cell-cell adhesion endocytosis versus cell-matrix adhesion endocytosis to DA tubulogenesis? This question is difficult to address because use of a *Dynamin* null allele, or expression of a Dynamin[DN], affects Dynamin's function throughout the cell. I have come up with two ideas as to how I could address this question, and both of these ideas would involve the generation of new transgenic tools. The first idea would involve expressing a Dynamin[DN] protein that could be directed to, and tethered to, a specific region or target within the cell. For instance, with a flexible protein linker, I could directly fuse Dynamin[DN] to the cytoplasmic domain of E-Cadherin, which might inhibit endocytosis of E-Cadherin-based cell-cell adhesions. This transgene could have adverse effects throughout development if stably integrated and

ubiquitously expressed, or it could cause defects related to E-Cadherin over-expression if expressed in a tissue-specific manner, but a way to get around both of these would be to use a FLP-out method to express the construct in mosaic clones (Pignoni and Zipursky 1997). Alternatively, Dynamin[DN] could be tethered to a different, apically-localizing protein, and this localized dominant-negative function might specifically distinguish the contribution of apical endocytosis from that of cell-cell adhesion endocytosis. I could also employ this technique basally by fusing Dynamin[DN] to a component of the Integrin-based adhesions, such as Paxillin. I previously showed that Paxillin over-expression does not dramatically affect DA-tubulogenesis (Peters *et al.,* 2013; **Chapter II)** and that Paxillin localization is primarily basal (personal observations), and so a conditionally expressed, Dynamin[DN]-Paxillin fusion might be a useful tool for specifically disrupting basal endocytosis of cell-matrix adhesions during DA tubulogenesis.

The second idea is a little more abstract, but by no means implausible. It would involve the creation of a light-activated or light-uncaged Dynamin[DN] that could be stably or conditionally expressed, and then, during live imaging, selectively activated or uncaged in a specific part of the cell. Light-activated small GTPases, such as Rac, have already been used successfully in the *Drosophila* ovary for localized activation and inhibition (Wang *et al.,* 2010). Similarly, caged molecules that can be uncaged following exposure to specific wavelengths of light have already been developed, though it can be more difficult to employ these tools in biological tissues (Ellis-Davies 2007). The clear advantages of using light activated or uncaged Dynamin[DN] is its precise temporal and spatial specificity, but such tools could still diffuse within the cell, and could affect other parts of the cell than those intended or targeted. Another method which could address both the problems of over-expressing a Dynamin[DN]-fusion and a

diffusion of a light-activated or -uncaged molecule would be to replace the sequence for the targeting molecule of interest (*e.g.*, E-Cadherin, Integrin, Paxillin) with a sequence for a Dynamin[DN] fusion in which the Dynamin[DN] is initially caged or inactive. The Dynamin[DN] could then be conditionally activated or uncaged by light at the appropriate time.

Third, what mechanism underlies the biased apical expansion that I observed and characterized during DA-tube elongation? There are several possible answers to this question. One possibility is suggested by the observation that the DA-tube fails to close when Dynamin[DN] is expressed in DA-tube cells. Perhaps the closed DA-tube in wild type serves to spatially confine the DA-tube cells along the DV axis, like a trough constricting the flow of water. Thus, when the DA-tube cells expand apically, they can only do so along the AP axis, and the bias of the apical expansion is more of a passive effect of expanding within a constrained surface. Another possibility is that Dynamin is facilitating the biased localization of a protein, or proteins, in a planar orientation across the epithelium, and that biased apical expansion is an active process in the DA-tube cells. Examination of E-Cadherin protein localization did not indicate a bias towards DV or AP cell surfaces, but there are many other proteins that have been shown to localize in a planar fashion in epithelial cells and to be important for morphogenesis and tissue elongation. For instance, during germ band elongation in *Drosophila*, Myosin II and filamentous actin localize to AP surfaces, and E-Cadherin, Armadillo/β-catenin, and Bazooka/PAR3 localize to DV surfaces to facilitate AP elongation of the tissue (Bertet *et al.,* 2004; Zallen and Wieschaus, 2004; Blankenship *et al.,* 2006; Zallen, 2007). Components of the Frizzled/PCP pathway are also known to localize with planar bias, both in stable tissues and, to varying degrees, during morphogenesis (Zallen, 2007). Dynamin facilitate the planar localization of any of these components, and so examining candidate protein localization in DA-

tube cells, and comparing those localizations to those in Dynamin[DN]-expressing DA-tube cells, may help determine whether this biased apical expansion is an active process.

Finally, is the tubulogenic function of Dynamin conserved in *Drosophila*, and across metazoans? Based on what I have discussed previously, I have already essentially answered how I could approach this question. In *Drosophila*, I could express Dynamin[DN] in other tubulogenic contexts using tissue specific drivers, or I could conditionally mutagenize *Dynamin* in those tissues. In other model systems, I could express Dynamin[DN] (mutation of the corresponding, conserved serine residue in the GTPase domain of Dynamin creates a Dynamin[DN] in human cells (Chua *et al.,* 2009), and potentially in any metazoan Dynamin) using tissue-specific drivers, or use CRISPR/Cas9 conditional mutagenesis to remove the *Dynamin* locus in specific tubulogenic contexts, document the effects, and determine whether Dynamin was serving a conserved, tubulogenic function.

Future Directions

– A last thought for the road –

Live imaging of floor cell morphogenesis using of the *rho-lacZ* reporter

During my graduate research, I have frequently used the *lacZ* reporter system as a marker for specific cell types (*e.g.*, the *rhomboid-lacZ* marker to visualize floor cells of the DA tube). It has always bothered me that this system traditionally worked only in fixed tissue, where the product of the *lacZ* gene, β-galactosidase, can be stained for with an antibody. Recently, I began to think, "What if someone were to create a tool to allow all these *lacZ* reporter lines, which developmental biologists use in fixed tissue, to be used to mark living cells?" All all that one would need would be a fluorescent molecule that could bind β-galactosidase and, upon that binding, change its behavior. As fate would have it, I wasn't the first to think of this idea, and another research group had already successfully generated and tested a chromogenic β-galactosidase substrate (DDAOG; Tung *et al.,* 2004). As *Drosophila* egg chambers are readily cultured in S2 medium, to which a compound like DDAOG could be added. If this addition did not have a toxic effect, then the treated medium could be used in conjunction with the *rhomboid-lacZ* reporter to visualize live DA-floor cell morphogenesis, which has not been previously possible. Our lab has previously attempted to make stable, fluorescent, transgenic lines that mark the floor cells for live imaging, but they do not provide sufficiently early expression to be useful. The *rhomboid-lacZ* reporter, however, is readily visible in floor cells after S10B in fixed tissue, and so would likely be an excellent tool for live imaging if it could be successfully used in conjunction with a compound like DDAOG. This technique would potentially provide valuable new insight into the morphogenetic behavior of this fascinating cell type.

References

Adler, P. N., Krasnow, R. E. and Liu, J., 1997. Tissue polarity points from cells that have higher Frizzled levels towards cells that have lower Frizzled levels. Curr. Biol. 7, 940–949.

Amos, W. B. and White, J. G., 2003. How the confocal laser scanning microscope entered biological research. Biol. Cell 95, 335–342.

Anderson, J. M. and Van Itallie, C. M., 2009. Physiology and function of the tight junction. . Cold Spring Harb Perspect Biol. 1, 1–16.

Andres, A. J. and Thummel, C. S., 1992. Hormones, puffs and flies: The molecular control of metamorphosis by ecdysone. Trends Genet. 8, 132–138.

Andreu, M. J., González-Pérez, E., Ajuria, L., Samper, N., González-Crespo, S., Campuzano, S. and Jiménez, G., 2012. Mirror represses *pipe* expression in follicle cells to initiate dorsoventral axis formation in *Drosophila*. Development 139, 1110–1114.

Andrew, D. J. and Ewald, A. J., 2010. Morphogenesis of epithelial tubes: Insights into tube formation, elongation, and elaboration. Dev. Biol. 341, 34–55.

Arakaki Y., Kawai-Toyooka H., Hamamura Y., Higashiyama T., Noga A., Hirono, M., Olson, B. J. S. C. and Nozaki, H., 2013. The simplest integrated multicellular organism unveiled. PLoS ONE 8, 1–8.

Araújo, S. J., Cela, C. and Llimargas, M., 2007. Tramtrack regulates different morphogenetic events during *Drosophila* tracheal development. Development 134, 3665– 3676.

Assemat, E., Bazellieres, E., Pallesi-Pocachard, E., Le Bivic, A. and Massey-Harroche, D., 2008. Polarity complex proteins. Biochim. Biophys. Acta. 1778, 614–630.

Atkey, M. R., Lachance, J. B., Walczak, M., Rebellow, T. and Nilson, L. A., 2006. Capicua regulates follicle cell fate in the *Drosophila* ovary through repression of *mirror*. Development 133, 2115–2123.

Bailey, T. L., Boden, M., Buske, F. A., Frith, M., Grant, C. E., Clementi, L., Ren, J.,Li, W. W. and Noble, W. S., 2009. MEME SUITE: tools for motif discovery and searching. Nucleic Acids Res. 37, W202–W208.

Baonza, A., Murawsky, C. M., Travers, A. A. and Freeman, M., 2002. Pointed and Tramtrack69 establish an EGFR-dependent transcriptional switch to regulate mitosis. Nat. Cell Biol. 4, 976–980.

Beitel, G. J. and Krasnow, M. A., 2000. Genetic control of epithelial tube size in the *Drosophila* tracheal system. Development 127, 3271–3282.

Berg, C. A., 2005. The *Drosophila* shell game: patterning genes and morphological change. Trends Genet. 21, 346–355.

Berg, C. A., 2008. Tube formation in *Drosophila* egg chambers. Tissue Eng. Part A. 14, 1479–1488.

Bertet, C., Sulak, L. and Lecuit, T., 2004. Myosin-dependent junc- tion remodelling controls planar cell intercalation and axis elongation. Nature 429, 667–671.

Beumer, K. J., Rohrbough, J., Prokop, A., and Broadie, K., 1999. A role for PS integrins in morphological growth and synaptic function at the postembryonic neuromuscular junction of *Drosophila*. Development 126, 5833–5846.

Beumer, K. J., Matthies, H. J., Bradshaw, A., and Broadie, K., 2002. Integrins regulate DLG/FAS2 via a CaM kinase II-dependent pathway to mediate synapse elaboration and stabilization during postembryonic development. Development 129, 3381–3391.

Bhat, M. A., Izaddoost, S., Lu, Y., Cho, K. O., Choi, K. W., Bellen, H. J., 1999. Discs Lost, a novel multi-PDZ domain protein, establishes and maintains epithelial polarity. Cell 96, 833–845.

Bilder, D., Li, M. and Perrimon, N., 2000. Cooperative regulation of cell polarity and growth by *Drosophila* tumor suppressors. Science289, 113–116.

Bilder, D. and Perrimon, N., 2000. Localization of apical epithelial determinants by the basolateral PDZ protein Scribble. Nature 403, 676–80.

Blankenship, J. T., Backovic, S. T., Sanny, J. S., Weitz, O. and Zallen, J. A., 2006. Multicellular rosette formation links planar cell polarity to tissue morphogenesis. Dev. Cell 11, 459–470.

Bloor, J. W. and Kiehart, D. P., 2001. Zipper non-muscle myosin-II functions downstream of PS2 Integrin in *Drosophila* myogenesis and is necessary for myofibril formation. Dev. Biol. 239, 215–228.

Bogdanovic, O., Machin-Delfino, M., Nicolas-Perez, M., Gavilan, M. P., Gago-Rodriguez, I., Fernandez-Minan, A., Lillo, C., Rios, R. M., Wittbrodt, J., and Martinez-Morales, J. R., 2012. Numb/Numbl-Opo antagonism controls retinal epithelium morphogenesis by regulating integrin endocytosis. Dev. Cell 23, 782–795.

Bonchuk, A., Denisov, S., Georgiev, P. and Maksimenko, O., 2011. *Drosophila* BTB/POZ domains of '*ttk* group' can form multimers and selectively interact with each other. J. Mol. Biol. 412, 423–436.

Bosclair Lachance, J. F., Lomas, M. F., Eleiche, A., Kerr P. B. and Nilson, L. A., 2009. Graded Egfr activity patterns the *Drosophila* eggshell independently of autocrine feedback. Development 136, 2893–2902.

Botto, L. D., Moore, C. A., Khoury, M. J. and Erickson, J. D., 1999. Neural-tube defects. New Engl. J. Med. 341, 1509–1519.

Boucrot, E., Saffarian, S., Zhang, R., and Kirchhausen, T., 2010. Roles of AP-2 in Clathrin-mediated endocytosis. PLoS One 5, 1–12.

Boyle, M. J. and Berg, C. A., 2009. Control in time and space: Tramtrack69 cooperates with Notch and Ecdysone to repress ectopic fate and shape changes during *Drosophila* egg chamber maturation. Development 136, 4187–4197.

Boyle, M. J., French, R. L., Cosand, A. K., Dorman, J. B., Kiehart, D. P. and Berg, C. A., 2010. Division of labor: Subsets of dorsal-appendage-forming cells control the shape of the entire tube. Dev. Biol. 346, 68–79.

Bradley, P. L. and Andrew, D. J., 2001. *ribbon* encodes a novel BTB/POZ protein required for directed cell migration in *Drosophila melanogaster*. Development 128, 3001– 3015.

Brand, A. H. and Perrimon, N., 1993. Targeted gene expression as a means of altering cell fates and generating dominant phenotypes. Development 118, 401–415.

Brand, A. H. and Perrimon, N., 1994. Raf acts downstream of the EGF receptor to determine dorsoventral polarity during *Drosophila* oogenesis. Mech. Develop. 8, 629–639.

Brower, D., Wilcox, M., Piovant, M., Smith, R. J., and Reger, L. A., 1984. Relatedcell-surface antigens expressed with positional specificity in *Drosophila* imaginal discs. Proc. Natl. Acad. Sci. 81, 7485–7489.

Brown, J. L., Sonoda, S., Ueda, H., Scott, M. P. and Wu, C., 1991. Repression of the *Drosophila fushi tarazu* (*ftz*) segmentation gene. EMBO J. 10, 665–674.

Brown, M. C. and Turner, C. E., 2004. Paxillin: Adapting to change. Physiol. Rev. 84, 1315–1339.

Bryant, Z., Subrahmanyan, L., Tworoger, M., LaTray, L., Liu, C., Li, M., van denEngh, G. and Ruohola-Baker, H., 1999. Characterization of differentially expressed genes in purified *Drosophila* follicle cells: toward a general strategy for cell type-specific developmental analysis. Proc. Natl. Acad. Sci. USA 96, 5559–5564.

Bucci, C., Parton, R. G., Mather, I. H., Stunnenberg, H., Simons, K., Hoflack, B., and Zerial, M., 1992. The small GTPase Rab5 functions as a regulatory factor in the early endocytic pathway. Cell 70, 715–728.

Buechner, M., 2002. Tubes and the single *C. elegans* excretory cell. Trends Cell Biol. 12, 479–484.

Cabernard, C. and Affolter, M., 2005. Distinct roles for two receptor tyrosine kinases in epithelial branching morphogenesis in *Drosophila*. Dev. Cell 9, 831–842.

Caussinus, E., Colombelli, J. and Affolter, M., 2008. Tip-cell migration controls stalk-cell intercalation during Drosophila tracheal tube elongation. Curr. Biol. 18,1727–1734.

Chao, W., and Kunz, J., 2009. Focal adhesion disassembly requires clathrin-dependent endocytosis of integrins. FEBS Lett. 583, 1337–1343.

Chappie, J. S., Mears, J. A., Fang, S., Leonard, M., Schmid, S. L., Milligan, R. A., Hinshaw, J. E., and Dyda, F., 2011. A pseudoatomic model of the dynamin polymer identifies a hydrolysis-dependent power stroke. Cell 147, 209–222.

Chappie, J. S., and Dyda, F., 2013. Building a fission machine – structural insights into dynamin assembly and activation. J. Cell Sci. 126, 2773–2784.

Chen, C. K., Kühnlein, R. P., Eulenberg, K. G., Vincent, S., Affolter, M. and Schuh, R., 1998. The transcription factors KNIRPS and KNIRPS RELATED control cell migration and branch morphogenesis during *Drosophila* tracheal development. Development 125, 4959–4968.

Chen, Y.-J., Chiang, C.-S., Weng, L.-C., Lengyel, J. A. and Liaw, G.-J., 2002. Tramtrack69 is required for the early repression of *tailless* expression. Mech. Develop. 116, 75–83.

Chen, G.-C. Turano, B. Ruest, P. J. Hagle, M. Settleman, J. and Thomas, S. M., 2005. Regulation of Rho and Rac signaling to the actin cytoskeleton by Paxillin during *Drosophila* development. Mol. Cell. Biol. 25, 979–987.

Chen, Y. and Schüpbach, T., 2006. The role of brinker in eggshell patterning. Mech. Dev. 123, 395–406.

Cheshire, A. M., Kerman, B. E., Zipfel, W. R., Spector, A. A. and Andrew, D. J., 2008. Kinetic and mechanical analysis of live tube morphogenesis. Dev. Dyn. 237, 2874–2888.

Cheung, L. S., Schüpbach, T. and Shvartsman, S. Y., 2011. Pattern formation by receptor tyrosine kinases: analysis of the Gurken gradient in *Drosophila* oogenesis. Curr. Opin. Genet. Dev. 21, 719–725.

Chua, J., Rikhy, R., and Lippincott-Schwartz, J., 2009. Dynamin 2 orchestrates the global actomyosin cytoskeleton for epithelial maintenance and apical constriction. PNAS 106, 20770–20775.

Chung, M. I., Nascone-Yoder, N. M., Grover, S. A., Drysdale, T. A. and Wallingford, J. B., 2010. Direct activation of Shroom3 transcription by Pitx proteins drives epithelial morphogenesis in the developing gut. Development 137, 1339–1349.

Greene, N. D., Stanier, P. and Copp, A. J., 2009. Genetics of human neural tube defects. Hum. Mol. Genet. 18, 113–129.

Cummings, M.R. and King, R.C. (1970) Ultrastructural changes in nurse and follicle cells during late stages of oogenesis in *Drosophila melanogaster*. Z. Zellforsch. Mikrosk. Anat. 110, 1–8.

Davidoff, M. J., Petrini, J., Damus, K., Russell, R. B. and Mattison, D., 2002. Neural tube defect-specific infant mortality in the United States. Teratology 66 Suppl 1, S17–22.

Deakin, N. O. and Turner, C. E., 2008. Paxillin comes of age. J. Cell. Sci. 121, 2435– 2444.

Delva, E, Tucker, D. K. and Kowalczyk, A. P., 2009. The desmosome. Cold Spring Harb. Perspect. Biol. 1, 1–19.

Deng, W. M. and Bownes, M., 1997. Two signalling pathways specify localised expression of the Broad-Complex in *Drosophila* eggshell patterning and morphogenesis. Development 124, 4639–4647.

Deng, W. M., Schneider, M., Frock, R., Castillejo-Lopez, C., Gaman, E. A., Baumgartner, S. and Ruohola-Baker, H., 2003. Dystroglycan is required for polarizing the epithelial cells and the oocyte in *Drosophila*. Development 130, 173–184.

Denholm, B., Sudarsan, V., Pasalodos-Sanchez, S., Artero, R., Lawrence, P., Maddrell, S., Baylies, M. and Skaer, H., 2003. Dual origin of the renal tubules in *Drosophila*: mesodermal cells integrate and polarize to establish secretory function. Curr. Biol. 13,1052–1057.

Diaz, J., Mendoza, P., Ortiz, R., Diaz, N., Leyton, L., Stupack, D., Quest, A. F. G., and Torres, V. A., 2014. Rab5 is required in metastatic cancer cells for Caveolin-1- enhanced Rac1 activation, migration and invasion. J. Cell Biol. 127, 2401–2406.

Dietzl, G., Chen, D., Schnorrer, F., Su, K., Barinova, Y., Fellner, M., Gasser, B., Kinsey, K., Oppel, S., Scheiblauer, S., Couto, A., Marra, V., Keleman, K. and Dickson, B. J., 2007. A genome-wide transgenic RNAi library for conditional gene inactivation in *Drosophila*. Nature 448, 151–156.

Dong, B., Deng, W., and Jiang, D., 2011. Distinct cytoskeleton populations and extensive crosstalk control *Ciona* notochord tubulogenesis. Development 138, 1631–1641.

Dorman, J. B., James, K. E., Fraser, S. E., Kiehart, D. P. and Berg, C. A., 2004. *bullwinkle* is required for epithelial morphogenesis during *Drosophila* oogenesis. Dev. Biol. 267, 320–341.

Dubreuil, R., Byers, T. J., Branton, D., Goldstein, L. S. and Kiehart, D. P., 1987. *Drosophila* spectrin I. Characterization of the purified protein. J. Cell Biol. 105, 2095– 2102.

Edgar, R., Domrachev, M., and Lash, A. E., 2002. Gene Expression Omnibus: NCBI gene expression and hybridization array data repository. Nucleic Acids Res. 30, 207–210.

Ellis-Davies, G. C. R., 2007. Caged compounds: photorelease technology for control of cellular chemistry and physiology. Nat. Methods 4, 619–628.

Elul, T., Koehl, M. A. and Keller, R., 1997. Cellular mechanism underlying neural convergent extension in *Xenopus laevis* embryos. Dev. Biol. 191, 243–258.

Emery, I. F., Bedian, V. and Guild, G. M., 1994. Differential expression of Broad-Complex transcription factors may forecast tissue-specific developmental fates during *Drosophila* metamorphosis. Development 120, 3275–3287.

Estes, P. S., Roos, J., van der Bliek, A., Kelly, R. B., Krishnan, K. S., Ramaswami, M., 1996. Traffic of dynamin within individual *Drosophila* synaptic boutons relative to compartment-specific markers. J Neurosci. 16, 5443–5456.

Etemad-Moghadam, B., Guo, S. and Kemphues, K. J., 1995. Asymmetrically distributed PAR-3 protein contributes to cell polarity and spindle alignment in early *C. elegans* embryos. Cell 83, 743–752.

Ezratty, E. J., Bertaux, C., Marcantionio, E. E., and Gunderson, G. G., 2009. Clathrin mediates integrin endocytosis for focal adhesion disassembly in migrating cells. J. Cell Biol. 187, 733–747.

Fabrowski, P., Necakov, A. S., Mumbauer, S., Loeser, E., Reversi, A., Streichan, S., Briggs, J. A. G., and De Renzis, S., 2013. Tubular endocytosis drives remodelling of the apical surface during epithelial morphogenesis in *Drosophila*. Nat. Commun. 4, 1–12.

Fankhauser, G., 1945. Maintenance of normal structure in heteroploid salamander larvae, through compensation of changes in cell size by adjustment of cell number and cell shape. J. Exp. Zool. 100, 445–455.

French, R. L., Cosand, A. K. and Berg, C. A., 2003. The *Drosophila* female sterile mutation *twin peaks* is a novel allele of *tramtrack* and reveals a requirement for TTK69 in epithelial morphogenesis. Dev. Biol. 253, 18–35.

Fuchs, A., Cheung, L. S., Charbonnier, E., Shvartsman, S. Y. and Pyrowolakis, G., 2012. Transcriptional interpretation of the EGF receptor signaling gradient. Proc. Natl. Acad. Sci. USA 109, 1572–1577.

Furger, A., O'Sullivan, J. M., Binnie, A., Lee, B. A. and Proudfoot, N. J., 2002. Promoter proximal splice sites enhance transcription. Genes Dev. 16, 2792–2799.

Furgeson, S. M., and De Camilli, P., 2012. Dynamin, a membrane-remodeling GTPase. Nat. Rev. Mol. Cell Biol. 13, 75–88.

Furuse, M., 2010. Molecular basis of the core structure of tight junctions. Cold Spring Harb. Perspect. Biol. 2, 1–16.

Garrod, D. and Chidgey, M., 2007. Desmosome structure, composition and function. Biochim. Biophys. Acta. 1778, 572–587.

Gates, J., 2012. *Drosophila* egg chamber elongation: insights into how tissues and organs are shaped. Fly 6, 213–227.

Ghiglione, C., Carraway, K. L., Amundadottir, L. T., Boswell, R. E., Perrimon, N., Duffy, J. B., 1999. The transmembrane molecule kekkon 1 acts in a feedback loop to negatively regulate the activity of the *Drosophila* EGF receptor during oogenesis. Cell 96, 847–856.

Gillespie, D. E. and Berg, C. A., 1995. Homeless is required for RNA localization in *Drosophila* oogenesis and encodes a new member of the DE-H family of RNA-dependent ATPases. Genes Dev. 9, 2495–2508.

Godt, D., Couderc, J. L., Cramton, S. E. and Laski, F. A., 1993. Pattern formation in the limbs of *Drosophila*: *bric à brac* is expressed in both a gradient and a wave-like pattern and is required for specification and proper segmentation of the tarsus. Development 119, 799–812.

Godt, D. and Tepass, U., 1998. *Drosophila* oocyte localization is mediated by differential cadherin-based adhesion. Nature 395, 387–391.

Goldenberg, G. and Harris, T. J. C, 2013. Adherens junction distribution mechanisms during cell- cell contact elongation in *Drosophila*. PLoS One 8, 1–14.

Gomez, J. M., Wang, Y. and Riechmann, V., 2012. Tao controls epithelial morphogenesis by promoting Fasciclin 2 endocytosis. J. Cell Biol. 199, 1131–1143.

Gonzalez-Reyes, A., Elliott, H. and St. Johnston, D., 1995. Polarization of both major body axes in *Drosophila* by *gurken-torpedo* signaling. Nature 375, 654–658.

Gosens, I., den Hollander, A. I., Cremers, F. P. and Roepman, R., 2008. Composition and function of the Crumbs protein complex in the mammalian retina. Exp. Eye Res. 86, 713–726.

Goto, T., Davidson, L., Asashima, M. and Keller, R., 2005. Planar cell polarity genes regulate polarized extracellular matrix deposition during frog gastrulation. Curr. Biol. 15, 787–793.

Graveley, B. R., May, G., Brooks, A. N., Carlson, J. W., Cherbas, L., Davis, C. A., Duff, M., Eads, B., Landolin, J., Sandler, J., Wan, K. H., Andrews, J., Brenner, S. E., Cherbas, P., Gingeras, T. R., Hoskins, R., Kaufman, T., Celniker, S. E. (2011.4.13). The *D. melanogaster* transcriptome: modENCODE RNA-Seq data for dissected tissues http://www.modencode.org/Celniker.shtml

Gray, N. W., Kruchten, A. E., Chen, J. and McNiven, M. A., 2005. A dynamin-3 spliced variant modulates the actin/cortactin-dependent morphogenesis of dendritic spines. J. Cell Sci. 118, 1279–1290.

Griffin-Shea, R., Thireos, G. and Kafatos, F. C., 1982. Organization of a cluster of four chorion genes in *Drosophila* and its relationship to developmental expression and amplification. Dev. Biol. 91, 325–336.

Guillot, C. and Lecuit, T. 2013. Mechanics of epithelial tissue homeostasis and morphogenesis. Science 340, 1185–1189.

Guioli, S., Sekido, R. and Lovell-Badge, R., 2007. The origin of the Mullerian duct in chick and mouse. Dev. Biol. 302, 389–398.

Guittard, E., Blais, C., Maria, A., Parvy, J., Pasricha, S., Lumb, C., Lafont, R., Daborn, P. and Dauphin-Villemant, C., 2011. CYP18A1, a key enzyme of *Drosophila* steroid hormone inactivation, is essential for metamorphosis. Dev. Biol. 349, 35–45.

Guo, M., Bier, E., Jan, L. Y. and Jan, Y. N., 1995. *tramtrack* acts downstream of *numb* to specify distinct daughter cell fates during asymmetric cell divisions in the *Drosophila* PNS. Neuron 14, 913–925.

Guo, S. and Kemphues, K., 1995. *par-1*, a gene required for establishing polarity *in C. elegans* embryos, encodes a putative Ser/Thr kinase that is asymmetrically distributed. Cell 81, 611-620.

Guruharsha, K. G., Rual, J., Zhai, B., Mintseris, J., Vaidya, P., Vaidya, N., Beekman, C., Wong, C., Rhee, D. Y., Cenaj, O., McKillip, E., Shah, S., Stapleton, M., Wan, K. H., Yu, C., Parsa, B., Carlson, J. W., Chen, X., Kapadia, B., VijayRaghavan, K., Gygi, S. P., Celniker, S. E., Obar, R. A. and Artavanis-Tsakonas, S., (2011). A protein complex network of *Drosophila melanogaster*. Cell 147, 690–703.

Gustafson, T. and Wolpert, L., 1963. The cellular basis of morphogenesis and sea urchin development. Int. Rev. Cytol. 15, 139–214.

Gustafson, K., and Boulianne, G. L., 1996. Distinct expression patterns detected within individual tissues by the GAL4 enhancer trap technique. Genome 39, 174–182.

Hackney, J. F., Pucci, C., Naes, E. and Dobens, L., 2007. Ras signaling modulates activity of the *ecdysone* receptor EcR during cell migration in the *Drosophila* ovary. Dev. Dyn. 236, 1213–1226.

Hagiwara, M., Shirai, Y., Nomura, R., Sasaki, M., Kobayashi, K., Tadokoro, T., and Yamamoto, Y., 2009. Caveolin-1 activates Rab5 and enhances endocytosis through direct interaction. Biochem. Biophys. Res. Commun. 378, 73–78.

Haigo, S. L. and Bilder, D., 2011. Global tissue revolutions in a morphogenetic movement controlling elongation. Science 331, 1071–1074.

Hall, A., 2005. Rho GTPases and the control of cell behaviour. Biochem. Soc. Trans. 33, 891–895.

Halpern, M. E., Rhee, J., Goll, M. G., Akitake, C. M., Parsons, M. and Leach, S. D., 2008. Gal4/UAS transgenic tools and their application to zebrafish. Zebrafish 5, 97–110.

Hardin, J. D. and Cheng, L.Y., 1986. The mechanisms and mechanics of archenteron elongation during sea urchin gastrulation. Dev. Biol. 115, 490–501.

Harrington, M. J., Hong, E. and Brewster, R., 2009. Comparative analysis of neurulation: first impressions do not count. Mol. Reprod. Dev. 76, 954–965.

Harrison, M. M., Jenkins, B. V., O'Connor-Giles, K. M. and Wildonger, J., 2014. A CRISPR view of development. Genes Dev. 28, 1859–1872.

Harrison, S. D. and Travers, A. A., 1990. The *tramtrack* gene encodes a *Drosophila* finger protein that interacts with the *ftz* transcriptional regulatory region and shows a novel embryonic expression pattern. EMBO J. 9, 207–216.

Hartley, K. O., Nutt, S. L. and Amaya, E., 2002. Targeted gene expression in transgenic *Xenopus* using the binary Gal4-UAS system. PNAS 99, 1377–1382.

He, L., Wang, X., Tin, H. A. U. and Montell, D. J., 2010. Tissue elongation requires oscillating contractions of a basal actomyosin network. Nat. Cell Biol. 12, 1133–1142.

Hinton, H. E., 1959. Plastron respiration in the eggs of *Drosophila* and other flies. Nature 184, 280–81.

Hinton, H. E., 1960. The chorionic plastron and its role in the eggs of the *muscinae* (*Diptera*). Q J Microsc. Sci. 101, 313–332.

Hinton, H. E., 1969. Respiratory systems of insect egg shells. Ann. Rev. Entomol. 14, 343–68.

Holtfreter, J., 1939. Bewebeaffinitat, ein Mittel der embryonalen Formbildung. Arch. Exp. Zellforsch. 23, 169–209.

Townes, P. and Holtfreter, J., 1955. Directed movements and selective adhesion of embryonic amphibian cells. J. Exp. Zool. 128, 53–120.

Hong, Y., Dong, W., Zhang, X., Liu, W., Chen, Y.-J., and Huang, J. 2015. An evolutionarily conserved polybasic motif mediates the plasma membrane targeting of Lgl and its regulation by hypoxia. 56th Annual Drosophila Research Conference. #112.

Horne-Badinovac, S., and Bilder, D., 2005. Mass Transit: epithelial morphogenesis in the *Drosophila* egg chamber. Dev. Dyn. 232, 559–574.

Hsouna, A., Lawal, H. O., Izevbaye, I., Hsu, T. and O'Donnell, J. M., 2007. *Drosophila* dopamine synthesis pathway genes regulate tracheal morphogenesis. Dev. Biol. 308, 30–43.

Huang, J., Zhou, W., Dong, W., Watson, A. M., and Hong, Y., 2009. Directed, efficient, and versatile modifications of the *Drosophila* genome by genomic engineering. Proc. Natl. Acad. Sci. 106, 8284–8289.

Hung, T. J. and Kemphues, K., 1999. PAR-6 is a conserved PDZ domain-containing protein that colocalizes with PAR-3 in *Caenorhabditis elegans* embryos. Development 126, 127–135.

Huttenlocher, A., and Horwitz, A. R., 2011. Integrins in cell migration. Cold Spring Harb Perspect Biol. 3, 1–16.

Hyodo-Miura, J., Yamamoto, T. S., Hyodo, A. C., Iemura, S., Kusakabe, M., Nishida, E., Natsume, T. and Ueno, N., 2006. XGAP, an ArfGAP, is required for polarized localization of PAR proteins and cell polarity in *Xenopus* gastrulation. Dev. Cell 11, 69–79.

Ip, Y.T., Park, R.E., Kosman, D., Bier, E., and Levine, M., 1992. The *dorsal* gradient morphogen regulates stripes of *rhomboid* expression in the presumptive neuroectoderm of the *Drosophila* embryo. Genes Dev. 6, 1728–1739.

Iruela-Arispe, M. L., and Beitel, G. J., 2013. Tubulogenesis. Development 140, 2851–2855.

Irvine, K. D., and Wieschaus, E., 1994. Cell intercalation during *Drosophila* germband extension and its regulation by pair-rule segmentation genes. Development 120, 827–841.

Isaac, D. D. and Andrew, D. J., 1996. Tubulogenesis in *Drosophila*: a requirement for the *trachealess* gene product. Genes Dev. 10, 103–117.

Jaffe, A. B. and Hall, A., 2005. RHO GTPASES: Biochemistry and Biology. Ann. Rev. Cell Dev. Biol. 21, 247–269.

James, K. E, Dorman, J. E., and Berg, C. A., 2002. Mosaic analyses reveal the function of *Drosophila* Ras in embryonic dorsoventral patterning and dorsal follicle cell morphogenesis. Development 129, 2209–22.

James, K. E. and Berg, C. A., 2003. Temporal comparison of Broad-complex expression during eggshell-appendage patterning and morphogenesis in two *Drosophila* species with different eggshell-appendage numbers. Gene Exp. Patterns 3, 629–634.

JayaNandanan, N., Mathew, R. and Leptin, M., 2014. Guidance of subcellular tubulogenesis by actin under the control of a synaptotagmin-like protein and Moesin. Nat. Commun. 5, 1–10.

Jenett, A., Rubin, G. M., Ngo, T-T. B., Shepherd, D., Murphy, C., Dionne, H., Pfeiffer, B. D., , *et al.,* 2012. A GAL4-driver line resource for *Drosophila* neurobiology. Cell Reports 2, 991–1001.

Jenkins, V. K., Timmons, A. K., and McCall, K., 2013. Diversity of cell death pathways: Insight from the fly ovary. Trends Cell Biol. 23, 567–574.

Jin, J. and Petri, W. H., 1993. Developmental control elements in the promoter of a *Drosophila* vitelline membrane gene. Dev. Biol. 156 557–565.

Jinek, M.,. Chylinski, K., Fonfara, I., Hauer, M, Doudna, J. A. and Charpentier, E., 2012. A programmable dual-RNA-guided DNA endonuclease in adaptive bacterial immunity. Science 337, 816–821.

Johansen, K. A., Iwaki, D. D. and Lengyel, J. A., 2003. Localized JAK/STAT signaling is required for oriented cell rearrangement in a tubular epithelium. Development 130, 135–145.

St. Johnston, D. and Ahringer, J., 2010. Cell polarity in eggs and epithelia: parallels and diversity. Cell 141, 757–774.

Jordan, K. C., Clegg, N. J., Blasi, J. A., Morimoto, A. M., Sen, J., Stein, D., McNeill, H., Deng, W. M., Tworoger, M. and Ruohola-Baker, H., 2000. The homeobox gene *mirror* links EGF signalling to embryonic dorso-ventral axis formation through Notch activation. Nat. Genet. 24, 429–433.

Jordan, K. C., Hatfield, S. D., Tworoger, M., Ward, E. J., Fischer, K. A., Bowers, S. and Ruohola-Baker, H., 2005. Genome wide analysis of transcript levels after perturbation of the EGFR pathway in the *Drosophila* ovary. Dev. Dyn. 232, 709–724.

Jürgens, G., Wieschaus, E., Nüsslein-Volhard, C. and Kluding, H., 1984. Mutations affecting the pattern of the larval cuticle in *Drosophila* melanogaster II. Zygotic loci on the third chromosome. Roux's Arch. Dev. Biol. 193, 283–295.

Kagesawa, T., Nakamura, Y., Nishikawa, M., Akiyama, Y., Kajiwara, M., Matsuno, K., 2008. Distinct activation patterns of EGF receptor signaling in the homoplastic evolution of eggshell morphology in genus *Drosophila*. Mech. Dev. 125, 1020–1032.

Kamei, M., Saunders, W. B., Bayless, K. J., Dye, L., Davis, G. E. and Weinstein, B. M., 2006. Endothelial tubes assemble from intracellular vacuoles *in vivo*. Nature 442, 453–456.

Keller, R., Davidson, L., Edlund, A., Elul, T. Ezin, M., Shook, D. and Skoglund, P., 2000. Mechanisms of convergence and extension by cell intercalation. Philos. Trans. R. Soc. Lond. B Biol. Sci. 355, 897–922.

Keller, R., 2002. Shaping the vertebrate body plan by polarized embryonic cell movements. Science 298, 1950–1954.

Keller, R., 2006. Mechanisms of elongation in embryogenesis. Development 133, 2291–2302.

Keller, R., 2012. Developmental biology. Physical biology returns to morphogenesis. Science 338, 201–203.

Kerman, B. E., Cheshire, A. M., Myat, M.M. and Andrew, D. J., 2008. Ribbon modulates apical membrane during tube elongation through Crumbs and Moesin. Dev. Biol. 320, 278–288.

King, R. C., 1970. Ovarian development in *Drosophila melanogaster*. Academic Press, Inc. NY.

Klebes, A., Sustar, A., Kehris, K., Li, H., Schubiger, G. and Kornberg, T. B., 2005. Regulation of cellular plasticity in *Drosophila* imaginal disc cells by the Polycomb group, trithorax group and *lama* genes. Development 132, 3753–3765.

Kominami, T. and Takata, H., 2004. Gastrulation in the sea urchin embryo: a model system for analyzing the morphogenesis of a monolayered epithelium. Dev. Growth Differ. 46, 309–326.

Knust, E., Tepass, U. and Wodarz, A., 1993. *crumbs* and *stardust*, two genes of *Drosophila* required for the development of epithelial cell polarity. Dev. Suppl. 261–268.

Knust, E., 1994. Control of epithelial cell polarity in *Drosophila*. Trends Genet. 10, 275–280.

Kulakovskiy, I. V. and Makeev, V. J., 2009. Discovery of DNA motifs recognized by transcription factors through integration of different experimental sources. Mol. Biophysics 54, 667–674.

Langevin, J., Morgan, M. J., Rossé, C., Racine, V., Sibarita, J., Aresta, S., Murthy, M., Schwarz, T., Camonis, J., and Bellaiche, Y., 2005. *Drosophila* exocyst components Sec5, Sec6, and Sec15 regulate DE-Cadherin trafficking from recycling endosomes to the plasma membrane. Dev. Cell 9, 365–376.

Lecuit, T. and Lenne, P. F., 2007. Cell surface mechanics and the control of cell shape, tissue patterns and morphogenesis. Nat. Rev. Mol. Cell Biol. 8, 633–644.

Lecuyer, E., Parthasarathy, N. and Krause, H. M., 2007. Fluorescent *in situ* hybridization protocols in *Drosophila* embryos and tissues. in: Dahmann, C. (Ed.), Methods in Molecular Biology. Humana Press, Inc., Totowa, NJ, pp. 289–302.

Lee, J. Y. and Harland, R. M., 2010. Endocytosis is required for efficient apical constriction during *Xenopus* gastrulation. Curr. Biol. 20, 253–258.

Lee, M. Y., Skoura, A., Park, E. J., Landskroner-Eiger, S., Jozsef, L., Luciano, A. K., Murata, T., Pasula, S., Dong, Y., Bouaouina, M., Calderwood, D. A., Ferguson, S. M., De Camilli, P. and Sessa, W. C., 2014. Dynamin 2 regulation of integrin endocytosis, but not VEGF signaling, is crucial for developmental angiogenesis. Development 141, 1465–1472.

Lembong, J., Yakoby, N. and Shvartsman, S. Y., 2008. Spatial regulation of BMP signaling by patterned receptor expression. Tissue Eng. Part A, 14, 1469–1477.

Lembong, J., Yakoby, N. and Shvartsman, S. Y., 2009. Pattern formation by dynamically interacting network motifs. PNAS USA 106, 1469–1477.

Lenard, A., Ellertsdottir, E., Herwig, L., Krudewig, A., Sauteur, L., Belting, H. G. and Affolter, M., 2013. *In vivo* analysis reveals a highly stereotypic morphogenetic pathway of vascular anastomosis. Dev. Cell 25, 429–506.

Lepage, S. E. and Bruce, A. E, 2014. Dynamin-dependent maintenance of epithelial integrity is essential for zebrafish epiboly. Bioarchitecture 4, 31–34.

Leptin, M. and Grunewald, B., 1990. Cell shape changes during gastrulation in *Drosophila*. Development 110, 73–84.

Lewandowski, M., 2001. Conditional control of gene expression in the mouse. Nat. Rev. Genet. 2, 743–755.

Llense, F. and Martín-Blanco, E., 2008. JNK signaling controls border cell cluster integrity and collective cell migration. Curr. Biol. 18, 538–544.

Llimargas, M. and Casanova, J., 1999. EGF signalling regulates cell invagination as well as cell migration during formation of tracheal system in *Drosophila*. Dev. Genes Evol. 209, 174–179.

Fregoso Lomas, M., Hails, F., Lachance, J. F. and Nilson, L. A., 2013. Response to the dorsal anterior gradient of EGFR signaling in *Drosophila* oogenesis is prepatterned by earlier posterior EGFR activation. Cell Rep. 4, 791–802.

Lubarsky, B. and Krasnow, M. A., 2003. Tube morphogenesis: making and shaping biological tubes. Cell 112, 19–28.

Lützelschwab, R., Klämbt, C., Rossa, R. and Schmidt, O., 1987. A protein product of the *Drosophila* recessive tumor gene, *l (2) giant gl*, potentially has cell adhesion properties. EMBO J 6, 1791–1797.

Maeda, Y., Davé, V. and Whitsett, J. A., 2007. Transcriptional control of lung morphogenesis. Physiol. Rev. 87, 219–244.

Mahajan-Miklos, S. and Cooley, L., 1994. Intercellular cytoplasm transport during *Drosophila* oogenesis. Dev. Biol. 165, 336–351.

Maier, P., Rathfelder, N., Maeder, C. I., Colombelli, J., Stelzer, E. H. K., and Knop, M., 2008. The SpoMBe pathway drives membrane bending necessary for cytokinesis and spore formation in yeast meiosis. EMBO J. 27, 2363–2374.

Margolis, B. and Borg, J. P., 2005. Apicobasal polarity complexes. J. Cell Sci. 118, 5157–5159.

Marmion, R., Jevtic, M., Springhorn, A., Pyrowolakis, G., Yakoby, N., 2013. The *Drosophila* BMPRII, *wishful thinking*, is required for eggshell patterning. Dev. Biol. 375, 45–53.

Martin, A. C., Kaschube, M. and Wieschaus, E. F., 2009. Pulsed contractions of an actin-myosin network drive apical constriction. Nature 457, 459–499.

Martin, A. C. and Goldstein, B., 2014. Apical constriction: themes and variations on a cellular mechanism driving morphogenesis. Development 141, 1987–1998.

Maruyama, R. and Andrew, D. J., 2012. *Drosophila* as a model for epithelial tube formation. Dev. Dyn. 241, 119–135.

McLean, P. F. and Cooley, L., 2013. Protein equilibration through somatic ring canals in *Drosophila*. Science 340, 1445–1447.

McMahon, H. T., and Boucrot, E., 2011. Molecular mechanism and physiological functions of clathrin-mediated endocytosis. Nat. Rev. Mol. Cell Biol. 12, 517–533.

McNeill, H., Yang, C. H., Brodsky, M., Ungos, J. and Simon, M. A., 1997. *mirror* encodes a novel PBX-class homeoprotein that functions in the definition of the dorsal-ventral border in the *Drosophila* eye. Genes Dev. 11, 1073–1082.

Mechler, B. M., McGinnis, W. and Gehring, W. J., 1985. Molecular cloning of *lethal(2)giant larvae*, a recessive oncogene of *Drosophila* melanogaster. EMBO J 4, 1551–1557.

Medioni, C. and Noselli, S., 2005. Dynamics of the basement membrane in invasive epithelial clusters in *Drosophila*. Development 132, 3069–3077.

Metzger, R. J., Klein, O. D., Martin, G. R. and Krasnow, M. A., 2008. The branching programme of the mouse lung. Nature 453, 745–750.

Mirouse, V., Christoforou, C. P., Fritsch, C., St. Johnston, D. and Ray, R. P., 2009. Dystroglycan and perlecan provide a basal cue required for epithelial polarity during energetic stress. Dev. Cell. 16, 83–92.

Moline, M. M., Southern, C., and Bejsovec, A., 1999. Directionality of Wingless protein transport influences epidermal patterning in the *Drosophila* embryo. Development 126, 4375–4384.

Montell, D. J., 2001. Command and control: regulatory pathways controlling invasive behavior of the border cells. Mech. Dev. 105, 19–25.

Moore, C. J. and Winder, S. J., 2010. Dystroglycan versatility in cell adhesion: a tale of multiple motifs. Cell Commun. Signal. 8, 1–12.

Motley, A., Bright, N. A., Seaman, M. N. J., and Robinson, M. S., 2003. Clathrin-mediated endocytosis in AP-2–depleted cells. J. Cell Biol. 162, 909–918.

Myat, M. M. and Andrew, D. J., 2000. Fork head prevents apoptosis and promotes cell shape change during formation of the *Drosophila* salivary glands. Development 127, 4217–4226.

Myat, M. M. and Andrew, D. J., 2002. Epithelial tube morphology is determined by the polarized growth and delivery of apical membrane. Cell 111, 879–891.

Nakamura, Y. and Matsuno, K., 2003. Species-specific activation of EGF receptor signaling underlies evolutionary diversity in the dorsal appendage number of the genus *Drosophila* eggshells. Mech. Dev. 120, 897–907.

Nakamura, Y., Kagesawa, T., Nishikawa, M., Hayashi, Y., Kobayashi, S., Niimi, T. and Matsuno, K., 2007. Soma-dependent modulations contribute to divergence of *rhomboid* expression during evolution of *Drosophila* eggshell morphology. Development 134, 1529–1537.

Niepielko, M. G., Y. Hernáiz-Hernández, Y. and Yakoby, N., 2011. BMP signaling dynamics in the follicle cells of multiple *Drosophila* species.. Dev. Biol. 354, 151–159.

Niepielko, M. G., Ip, K., Kanodia, J. S., Lun, D. and Yakoby, N., 2012. The evolution of BMP signaling in *Drosophila* oogenesis: a receptor-based mechanism. Biophys. J. 102, 1722–1730.

Niepielko, M. G., Marmion, R. A., Kim, K., Luor, D., Ray, C. and Yakoby, N., 2014. Chorion Patterning: A window into gene regulation and *Drosophila* species-relatedness.. Mol. Biol. Evol. 31, 154–164.

Niepielko, M. G., and Yakoby, N., 2014. Evolutionary changes in TGF-alpha distribution underlie morphological diversity in *Drosophila* eggshells. Development, 141, 4710–4715.

Nishimura, T. and Takeichi, M., 2009. Remodeling of the adherens junctions during morphognesis. Curr. Top. Dev. Biol. 89, 33–54.

Nelson, J. W., 2009. Remodeling epithelial cell organization: Transitions between front–rear and apical–basal polarity. Cold Spring Harb. Perspect. Bio. 1, 1–19

Nelson, K. S., Furuse, M. and Beitel, G. J., 2010. The *Drosophila* Claudin Kune-kune is required for septate junction organization and tracheal tube size control. Genetics 185, 831–839.

Neuman-Silberberg, F. S. and Schüpbach, T., 1993. The *Drosophila* dorsoventral patterning gene *gurken* produces a dorsally localized RNA and encodes a TGF alpha-like protein. Cell 75, 165–174.

Nezis, I.P. *et al.,* 2000. Stage-specific apoptotic patterns during *Drosophila* oogenesis. Eur. J. Cell Biol. 79, 610–620.

Nilson, L. A. and Schüpbach, T., 1999. EGF receptor signaling in *Drosophila* oogenesis. Curr. Top. Dev. Biol. 44, 203–243.

Ninomiya, H., Elinson, R. P., and Winklbauer, R., 2004. Antero-posterior tissue polarity links mesoderm convergent extension to axial patterning. Nature 430, 364–367.

Oda, H., Uemura, T., Harada, Y., Iwai, Y., and Takeichi, M., 1994. A *Drosophila* homolog of cadherin associated with armadillo and essential for embryonic cell-cell adhesion. Dev. Biol. 165, 716–726.

Oda, H., and Tsukita, S., 1999. Nonchordate classic cadherins have a structurally and functionally unique domain that is absent from chordate classic cadherins. Dev. Biol. 216, 406–422

Oda, H. and Takeichi, M., 2011. Evolution: structural and functional diversity of cadherin at the adherens junction. J. Cell Biol. 193, 1137–1146.

Odell, G. M., Oster, G., Alberch, P. and Burnside, B., 1981. The mechanical basis of morphogenesis. I. Epithelial folding and invagination. Dev. Biol. 85, 446–462.

Ogata, S., Morokuma, J., Hayata, T., Kolle, G., Niehrs, C., Ueno, N. and Cho, K. W., 2007. TGF-beta signaling-mediated morphogenesis: modulation of cell adhesion via cadherin endocytosis. Genes Dev. 21, 1817–1831.

Orvis, G. D. and Behringer, R. R., 2007. Cellular mechanisms of Müllerian duct formation in the mouse. Dev. Biol. 306, 493–504.

Osterfield, M., Du, X., Schüpbach, T., Wieschaus, E., Shvartsman, S. Y., 2013. Three-dimensional epithelial morphogenesis in the developing *Drosophila* egg. Dev. Cell 24, 400–410.

Osterfield, M., Schüpbach, T., Wieschaus, E., and Schvartsman, S. Y., 2015. Diversity of epithelial morphogenesis among *Drosophilid* eggshells. Development (in press).

Parks, S. and Spradling, A., 1987. Spatially regulated expression of chorion genes during *Drosophila* oogenesis. Genes Dev. 1, 497–509.

Paul, S. M., Ternet, M., Salvaterra, P. M. and Beitel, G. J., 2003. The Na+/K+ ATPase is required for septate junction function and epithelial tube-size control in the *Drosophila* tracheal system. Development 130, 4963–4974.

Peifer, M., McCrea, P. D., Green, K. J., Wieschaus, E., and Gumbiner, B. M., 1992. The vertebrate adhesive junction proteins Catenin and Plakoglobin and the *Drosophila* segment polarity gene *armadillo* form a multigene family with similar properties. J. Cell Biol. 118, 681–691.

Perez, S. E. and Steller, H., 1996. Molecular and genetic analyses of *lama*, an evolutionarily conserved gene expressed in the precursors of the *Drosophila* first optic ganglion. Mech. Dev. 59, 11–27.

Peri, F., Bökel, C. and Roth, S., 1999. Local Gurken signaling and dynamic MAPK activation during *Drosophila* oogenesis. Mech. Dev. 81, 75–88.

Peri, F. and Roth, S., 2000. Combined activities of Gurken and Decapentaplegic specify dorsal chorion structures of the *Drosophila* egg. Development 127, 841–850.

Peters, N. C., Thayer, N. H., Kerr, S. A., Tompa, M., and Berg, C. A., 2013. Following the 'tracks': Tramtrack69 regulates epithelial tube morphogenesis in the *Drosophila* ovary through Dynamin, Paxillin, and the homeobox protein Mirror. Dev. Biol. 378, 154–169.

Pfeiffer, B.D., Truman, J. W., and Rubin, G. M., 2012. Using translational enhancers to increase transgene expression in *Drosophila.* Proc. Natl. Acad. Sci. U.S.A. 109, 6626–6631.

Pielage, J., Stork, T., Bunse, I. and Klämbt, C., 2003. The *Drosophila* cell survival gene discs lost encodes a cytoplasmic Codanin-1-like protein, not a homolog of tight junction PDZ protein Patj. Dev. Cell 5, 841–851.

Pirraglia, C., Jattani, R. and Myat, M. M., 2006. Rac function in epithelial tube morphogenesis. Dev. Biol. 290, 435–446.

Pirraglia, C., Walters, J., Ahn, N., and Myat, M. M., 2013. Rac1 GTPase acts downstream of αPS1βPS integrin to control collective migration and lumen size in the *Drosophila* salivary gland. Dev. Biol. 377, 1–21.

Pocha, S. M. and Montell, D. J., 2014. Cellular and molecular mechanisms of single and collective cell migrations in *Drosophila*: themes and variations. Annu. Rev. Genet. 48, 295–318.

Poodry, C. A., Hall, L. and Suzuki, D. T., 1973. Developmental properties of *shibire* ts-1: A pleiotropic mutation affecting larval and adult locomotion and development. Dev. Biol. 32, 373–386.

Popodi, E., Minoo, P., Burke, T., and Waring, G. L., 1988. Organization and expression of a second chromosome follicle cell gene cluster in *Drosophila*. Dev. Biol. 127, 248–256.

Queenan, A. M., Ghabrial, A. and Schüpbach, T., 1997. Ectopic activation of *torpedo*/*Egfr*, a *Drosophila* receptor tyrosine kinase, dorsalizes both the eggshell and the embryo. Development 124, 3871–3880.

Ray, H. J. and Niswander, L., 2012. Mechanisms of tissue fusion during development. Development 139, 1701–1711.

Read, D., Levine, M. and Manley, J. L., 1992. Ectopic expression of the *Drosophila tramtrack* gene results in multiple embryonic defects, including repression of *even-skipped* and *fushi tarazu*. Mech. Develop. 38, 183–195.

Reddy, B. A., Bajpe, K. P., Bassett, A., Moshkin, Y. M., Kozhevnikova, E., Bezstarosti, K., Demmers, J. A. A., Travers, A. A. and Verrijzer, C. P., 2010. *Drosophila* transcription factor Tramtrack69 binds MEP1 to recruit the chromatin remodeler NuRD. Mol. Cell. Biol. 30, 5234–5244.

Reich, A., Sapir, A. and Shilo, B., 1999. Sprouty is a general inhibitor of receptor tyrosine kinase signaling. Development 126, 4139–4147.

Reiter, J. F., Kikuchi, Y. and Stainier, D. Y., 2001. Multiple roles for Gata5 in zebrafish endoderm formation. Development 128, 125–135.

Rittenhouse, K. R., and Berg, C. A., 1995. Mutations in the *Drosophila* gene *bullwinkle* cause the formation of abnormal eggshell structures and bicaudal embryos. Development 121, 3023–3033.

Rodriguez-Fraticelli, A. E. and Martin-Belmonte, F., 2014. Picking up the threads: extracellular matrix signals in epithelial morphogenesis. Curr. Opin. Cell Biol. 30, 83–90.

Roth, S., Neuman-Silberberg, F. S., Barcelo, G., Schüpbach, T., 1995. cornichon and the EGF receptor signaling process are necessary for both anterior-posterior and dorsal-ventral pattern formation in *Drosophila*. Cell 81, 967–978.

Rotstein, B., Molnar, D., Adryan, B. and Llimargas, M., 2011. Tramtrack is genetically upstream of genes controlling tracheal tube size in *Drosophila*. PLoS ONE 6, 1–13.

Rozario, T. and DeSimone, D. W., 2010. The extracellular matrix in development and morphogenesis: a dynamic view. Dev. Biol. 341, 126–140.

Ruohola-Baker, H., Grell, E., Chou, T. B., Baker, D., Jan, L. Y., Jan, Y. N., 1993. Spatially localized rhomboid is required for establishment of the dorsal-ventral axis in *Drosophila* oogenesis. Cell 73, 953–965.

Sapir, A., Schweitzer, R. and Shilo, B. Z., 1998. Sequential activation of the EGF receptor pathway during *Drosophila* oogenesis establishes the dorsoventral axis. Development 125, 191–200.

Sawyer, J. M., Harrell, J. R., Shemer, G., Sullivan-Brown, J., Roh-Johnson, M. and Goldstein, B., 2010. Apical constriction: a cell shape change that can drive morphogenesis. Dev. Biol. 341, 5–19.

Schindelin, J., Arganda-Carreras, I., Frise, E., Kaynig, V., Longair, M., Pietzsch, T., Preibisch, S., Rueden, C., Saalfeld, S., Schmid, B., Tinevez, J. Y., White, D. J., Hartenstein, V., Eliceiri, K., Tomancak, P. and Cardona, A., 2012. Fiji: an open-source platform for biological-image analysis. Nat Methods 9, 676–682.

Schneider, M., Khalil, A. A., Poulton, J., Castillejo-Lopez, C., Egger-Adam, D., Wodarz, A., Deng, W. M. and Baumgartner, S., 2006. Perlecan and Dystroglycan act at the basal side of the *Drosophila* follicular epithelium to maintain epithelial organization. Development 133, 3805–3815.

Schneider, C. A., Rasband, W. S. and Eliceiri, K. W., 2012. NIH Image to ImageJ: 25 years of image analysis. Nat. Methods 9, 671–675.

Schüpbach, T., 1987. Germ line and soma cooperate during oogenesis to establish the dorsoventral pattern of eggshell and embryo in *Drosophila melanogaster*. Cell 49, 699–707.

Schnorr, J. D. and Berg, C. A., 1996. Differential activity of Ras1 during patterning of the *Drosophila* dorsoventral axis. Genetics 144, 1545–1557.

Sever, S., Chang, J., and Gu, C., 2013. Dynamin Rings: Not Just for Fission. Traffic 14, 1194–1199.

Shi, F., and Sottile, J., 2008. Caveolin-1-dependent β1 integrin endocytosis is a critical regulator of fibronectin turnover. J. Cell Sci. 121, 2360–2371.

Shim, K., Blake, K. J., Jack, J. and Krasnow, M. A., 2001. The *Drosophila ribbon* gene encodes a nuclear BTB domain protein that promotes epithelial migration and morphogenesis. Development 128, 4923–4933.

Simakov, D. S., Cheung, L. S., Pismen, L. M., Shvartsman, S. Y., 2012. EGFR-dependent network interactions that pattern *Drosophila* eggshell appendages. Development 139, 2814–2820.

Solnica-Krezel, L. and Sepich, D. S., 2012. Gastrulation: making and shaping germ layers. Annu. Rev. Cell Dev. Biol. 28, 687–717.

Soulet, F., Schmid, S. L., and Damke, H., 2006. Domain requirements for an endocytosis-independent, isoform-specific function of dynamin-2. Exp. Cell. Res. 312, 3539–3545.

Spradling, A. C., 1993. Developmental genetics of oogenesis, in: The Development of *Drosophila melanogaster* (Bate, M., Martinez Arias, A. (Eds.), Cold Spring Harbor Press, Cold Spring Harbor, NY, pp. 1–70.

Steinberg, M. S., 1970. Does differential adhesion govern self-assembly processes in histogenesis? Equilibrium configurations and the emergence of a hierarchy among populations of embryonic cells. J. Exp. Zool. 173, 395–433.

Steinberg, M. S., 1978. Cell-Cell Recognition (A. S. G. Curtis (Ed.)), Society for Experimental Biology Symposium 32, Cambridge Univ. Press, Cambridge, pp. 25–49.

Stenmark, H., Parton, R. G., Steele-Mortimer, O., Lütcke, A., Gruenberg, J., and Zerial, M., 1994. Inhibition of rab5 GTPase activity stimulates membrane fusion in endocytosis. EMBO J. 13, 1287–1296.

Stern, C., 2004. Gastrulation: From Cells to Embryo (Stern, C. (Ed.)), Cold Spring Harbor Laboratory Press, Cold Spring Harbor, NY.

Sun, J., Smith, L., Armento, A. and Deng, W. M., 2008. Regulation of the endocycle/gene amplification switch by Notch and ecdysone signaling. J. Cell Biol. 182, 885–896.

Suzuki, A. and Ohno, S., 2006. The PAR-aPKC system: lessons in polarity. J. Cell Sci. 119, 979–987.

Sweeton, D., Parks, S., Costa, M. and Wieschaus, E., 1991. Gastrulation in *Drosophila*: the formation of the ventral furrow and posterior midgut invaginations. Development 112, 775–89.

Tabuse, Y., Izumi, Y., Piano, F., Kemphues, K. J., Miwa, J. and Ohno, S., 1998. Atypical protein kinase C cooperates with PAR-3 to establish embryonic polarity in *Caenorhabditis elegans*. Development 125, 3607–3614.

Tada, M. and Heisenberg, C.-P., 2012. Convergent extension: using collective cell migration and cell intercalation to shape embryos. Development 139, 3897–3904.

Tatin, F., Taddei, A., Weston, A., Fuchs, E., Devenport, D., Tissir, F., and Makinen, T., 2013. Planar Cell Polarity Protein Celsr1 Regulates Endothelial Adherens Junctions and Directed Cell Rearrangements during Valve Morphogenesis. Dev. Cell 26, 31–44.

Tepass, U. and Knust, E., 1993. *Crumbs* and *stardust* act in a genetic pathway that controls the organization of epithelia in *Drosophila* melanogaster. Dev. Biol. 159, 311–326.

The modENCODE Consortium, Roy, S., Ernst, J., Kharchenko, P. V., Kheradpour, P., Negre, N., Eaton, M. L., Landolin, J. M., Bristow, C. A., Ma, L. *et al.,* 2010. Identification of functional elements and regulatory circuits by *Drosophila* modENCODE. Science 330, 1787–1797.

Thompson, H. M., Cao, H., Chen, J., Euteneur, U., and McNiven, M. A., 2004. Dynamin 2 binds γ-tubulin and participates in centrosome cohesion. Nat. Cell Biol. 6, 335–342.

Throckmorton, L. H., 1962. Throckmorton: The problem of phylogeny in the genus *Drosophila*, in: Studies in Genetics II (Wheeler, M. R. (Ed)), Univ. Texas Publ., Austin, TX, 207–343.

Tootle, T. L., Williams, D., Hubb, A., Frederick, R. and Spradling, A., 2011. *Drosophila* eggshell production: Identification of new genes and coordination by Pxt. PLoS ONE 6, 1–12.

Tran, D. H. and Berg, C. A., 2003. Bullwinkle and Shark regulate dorsal-appendage morphogenesis in *Drosophila* oogenesis. Development 130, 6273–6282.

Tung, C. H., Zeng, Q., Shah, K., Kim, D. E., Schellingerhout, D. and Weissleder, R., 2004. *In vivo* imaging of beta-galactosidase activity using far red fluorescent switch. Cancer Res. 64, 1579–1583

Turner, C. E., Glenney, J. R. and Burridge, K., 1990. Paxillin: A new Vinculin-binding protein present in focal adhesions. J. Cell Biol. 111, 1059–1068.

Twombly, V., Blackman, R. K., Jin, H., Graff, J. M., Padgett, R. W. and Gelbart, W. M., 1996. The TGF-beta signaling pathway is essential for *Drosophila* oogenesis. Development 122, 1555–1565.

Tzolovsky, G., Deng, W. M., Schlitt, T. and Bownes, M., 1999. The function of the *broad*-complex during *Drosophila melanogaster* oogenesis. Genetics 153, 1371–1383.

Ulrich, F., Krieg, M., Schotz, E., Link, V., Castanon, I., Schnabel, V., Taubenberger, A., Mueller, D., Puech, P., and Heisenberg, C., 2005. Wnt11 Functions in Gastrulation by Controlling Cell Cohesion through Rab5c and E-Cadherin. Dev. Cell 9, 555–564.

van der Bliek, A. M., and Meyerowitz, E. M., 1991. Dynamin-like protein encoded by the *Drosophila shibire* gene associated with vesicular traffic. Nature 351, 411–414.

van der Bliek, A. M., Redelmeier, T. E., Damke, H., Tisdale, E. J., Meyerowitz, E. M., and Schmid, S. L., 1993. Mutations in human Dynamin block an intermediate stage in coated vesicle formation. J. Cell Biol. 122, 553–563.

van der Meer, J. M., 1977. Optical clean and permanent whole mount preparation for phase-contrast microscopy of cuticular structures of insect larvae. Dros. Inf. Serv. 52, 160.

Walck-Shannon, E. and Hardin, J., 2014. Cell intercalation from top to bottom. Nat. Rev. 15, 34–48.

Wallingford, J. B., Fraser, S. E. and Harland, R. M., 2002. Convergent Extension: The molecular control of polarized cell movement during embryonic development. Dev. Cell 2, 695–706.

Wallingford, J. B., 2005. Neural tube closure and neural tube defects: Studies in animal models reveal known knowns and known unknowns. Am. J. Med. Genet. 135C, 59–68.

Waslh, E. P. and Brown, N. H., 1998. A screen to identify *Drosophila* genes required for integrin-mediated adhesion. Genetics 150, 791–805.

Wang, X., Bo, J., Bridges, T., Dugan, K. D., Pan, T., Chodosh, L. A. and Montell, D. J., 2006. Analysis of cell migration using whole-genome expression profiling of migratory cells in the *Drosophila* ovary. Dev. Cell 10, 483–495.

Wang, X., He, L., Wu, Y. I., Hahn, K. M. and Montell, D. J., 2010. Light-mediated activation reveals a key role for Rac in collective guidance of cell movement *in vivo*. Nat. Cell. Biol. 12, 591–597.

Ward, E. J. and Berg, C. A., 2005. Juxtaposition between two cell types is necessary for dorsal appendage tube formation. Mech. Dev. 122, 241–255.

Wasserman, J. D. and Freeman, M., 1998. An autoregulatory cascade of EGF receptor signaling patterns the *Drosophila* egg. Cell 95, 355–364.

Watson, C. J. and Khaled, W. T., 2008. Mammary development in the embryo and adult: a journey of morphogenesis and commitment. Development 135, 995–1003.

Wen, Y., Nguyen, D., Li, Y. and Lai, Z., 2000. The N-terminal BTB/POZ domain and C-Terminal sequences are essential for Tramtrack69 to specify cell fate in the developing *Drosophila* eye. Genetics 156, 195–203.

Wilk, R., Weizman, I. and Shilo, B. Z., 1996. *trachealess* encodes a bHLH-PAS protein that is an inducer of tracheal cell fates in *Drosophila*. Genes. Dev. 10, 93-102.

Wilson, P. D. and Goilav, B., 2007. Cystic disease of the kidney. Annu. Rev. Pathol. 2, 341–368.

Wolpert, L., Tickle, C. and Martinez Arias, A., 2010. Principles of Development. Oxford University Press, USA. Ch. 8: Cell Differentiation and Stem Cells, Fig. 15.

Woods, D. F. and Bryant, P. J., 1991. The discs-large tumor suppressor gene of *Drosophila* encodes a guanylate kinase homolog localized at septate junctions. Cell 66, 451–464.

Wu, V. M. and Beitel, G. J., 2004. A junctional problem of apical proportions: epithelial tube-seize control by septate junctions in the *Drosophila* tracheal system. Curr. Opin. Cell Biol. 16, 493-499.

Xue, Z., Wu, M., Wen, K., Ren, M., Long, L., Zhang, X. and Gao, G., 2014. CRISPR/Cas9 mediates efficient conditional mutagenesis in *Drosophila*. G3 4, 2167–2173.

Yakoby, N., Bristow, C. A., Gong, D., Schafer, X., Lembong, J., Zartman, J. J., Halfon, M. S., Schüpbach, T., and Shvartsman, S. Y., 2008. A combinatorial code for pattern formation in *Drosophila* oogenesis. Dev. Cell 15, 725–737.

Yakoby, N., Lembong, J., Schüpbach, T., and Shvartsman, S. Y, 2008. *Drosophila* eggshell is patterned by sequential action of feedforward and feedback loops. Development 135, 343–351.

Yan, S. J., Zartman, J. J., Zhang, M., Scott, A., Shvartsman, S. Y., Li, W. X., 2009. Bistability coordinates activation of the EGFR and DPP pathways in *Drosophila* vein differentiation. Mol. Syst. Biol. 5, 1–7

Zallen, J.A., and Wieschaus, E., 2004. Patterned gene expression directs bipolar planar polarity in *Drosophila*. Dev. Cell 6, 343–355.

Zallen, J. A., 2007. Planar polarity and tissue morphogenesis. Cell 129, 1051–1063.

Zartman, J. J., Yakoby, N., Bristow, C. A., Zhou, X., Schlichting, K., Dahmann, C., and Shvartsman, S. Y., 2008. Cad74A is regulated by BR and is required for robust dorsal appendage formation in *Drosophila* oogenesis. Dev. Biol. 322, 289–301.

Zartman, J. J., Kanodia, J. S., Yakoby, N., Schafer, X., Watson, C., Schlichting, K., Dahmann, C. and Shvartsman, S. Y., 2009. Expression patterns of cadherin genes in *Drosophila* oogenesis. Gene Exp. Patterns 9, 31–36.

Zartman, J. J., Cheung, L. S., Niepielko, M. G., Bonini, C., Haley, B., Yakoby, N. and Shvartsman, S. Y., 2011. Pattern formation by a moving morphogen source. Phys. Biol. 8, 1–20.

Zhao, D.,Woolner, S. and Bownes, M., 2000. The Mirror transcription factor links signalling pathways in *Drosophila* oogenesis. Dev. Genes Evol. 210, 449–457.

Zimmerman, S. G., Peters, N. C., Altaras, A. E., Berg, C. A., 2013. Optimized RNA ISH, RNA FISH and protein-RNA double labeling (IF/FISH) in *Drosophila* ovaries. Nat. Protoc. 8, 2158–2179.

Zimmerman, S. G., Merrihew, G., Sustar, A., MacCoss, M. and Berg, C. A., in preparation.

Zollman, S. Godt, D., Privé, G. G., Couderc, J. L. and Laski, F. A., 1994. The BTB domain, found primarily in zinc finger proteins, defines an evolutionarily conserved family that includes several developmentally regulated genes in *Drosophila*. Proc. Natl. Acad. Sci. USA 91, 10717–10721.

Vita

Nathaniel Clement Peters was born on August 2, 1984 to James Robert Peters and Cheri Bedell Peters in in Chattanooga, Tennessee. As a child, he became fascinated with the natural world, met his hero, Sir David Attenborough at age 6, and decided at that time to become a biologist. In high school, his biological interests expanded from the macroscopic to include the microscopic. He received a BA in Biology from Claremont McKenna College, received a post-baccalaureate research fellowship at the NIH/NIDDK, and, most recently, received a PhD in Molecular and Cellular Biology from the University of Washington. In addition to his interests in molecular and cellular biology, which focus primarily on developmental biology and the exquisitely intricate process of cellular morphogenesis, he has a profound interest in birds. He and his father have birded in 49/50 US states, and his North American life list currently stands at 664 species. From birds to bugs to Broad-expressing tube cells, he is and will always be a lover of biology.